

2001-01-04

# Dry Chemical Fire Suppression System Discharge Modeling and Testing

Robert Mark Eber  
*Worcester Polytechnic Institute*

Follow this and additional works at: <https://digitalcommons.wpi.edu/etd-dissertations>

---

## Repository Citation

Eber, R. M. (2001). *Dry Chemical Fire Suppression System Discharge Modeling and Testing*. Retrieved from <https://digitalcommons.wpi.edu/etd-dissertations/3>

This dissertation is brought to you for free and open access by [Digital WPI](#). It has been accepted for inclusion in Doctoral Dissertations (All Dissertations, All Years) by an authorized administrator of Digital WPI. For more information, please contact [wpi-etd@wpi.edu](mailto:wpi-etd@wpi.edu).

DRY CHEMICAL FIRE SUPPRESSION SYSTEM DISCHARGE  
MODELING AND TESTING

By

Robert Mark Eber

A Dissertation

Submitted to the Faculty

of the

WORCESTER POLYTECHNIC INSTITUTE

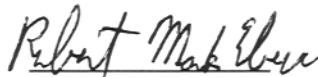
in partial fulfillment of the requirements of the

Degree of Doctor of Philosophy

in

Fire Protection Engineering

By



January 2001

APPROVED:



Professor Robert G. Zalosh, Major Advisor

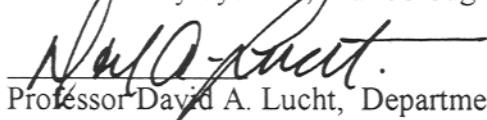


Professor Mark W. Richman, Co-Advisor



Dr. Erdem A. Ural, Co-Advisor

Fenwal Safety Systems, Marlborough, MA



Professor David A. Lucht, Department Head

## ABSTRACT

An engineering method has been developed for calculating the blowdown of agent from a pressurized dry chemical fire suppression system supply cylinder, and the flow rate of agent through a piping delivery system. Its goal is to provide the means to determine the blowdown time and agent delivery capabilities of pre-engineered and simple engineered systems.

The method is based on the treatment of the two-phase powder-gas flow as an equivalent fluid with thermodynamic properties that account for agent composition and the relative proportions of agent and gas propellant. The mixture is treated as compressible, and the expansion in the supply tank is assumed isentropic. A key assumption in the model is that the agent (powder) mass fraction remains constant, in both the tank and delivery system.

Laboratory tests were conducted to examine the validity of the model and its assumptions. Simple systems were discharged to measure pressures in the cylinder and nozzle inlet during discharge, and the mass of agent discharged. A 0.43 cubic foot cylinder containing 0-25 lbm of either sodium bicarbonate or monoammonium phosphate, pressurized at up to 300 psig of nitrogen, was discharged, either alone, or with an 8-foot length of piping and a single nozzle.

For the cylinder by itself, gas alone pressurized to 300 psig discharged in 1.5 seconds, while 25 lbm of sodium bicarbonate agent pressurized to 300 psig discharged in 5.2 seconds with 0.10 lbm of agent remaining in the cylinder after discharge. There was no significant difference in the discharge times or residual masses in the cylinder after discharge between the sodium bicarbonate and monoammonium phosphate agents.

For a cylinder-pipe-nozzle system, gas-alone discharges pressurized to 300 psig took 7 seconds, while 25 lbm of sodium bicarbonate agent pressurized to 300 psig discharged in 26 seconds with 0.64 lbm of residual agent in the cylinder after discharge.

Predictions generated by the model were compared with test results. Cylinder alone gas-only discharge model predictions agreed well with test data for the full duration of tests using a discharge coefficient of 0.380 to characterize the gas flow through the dip tube / valve assembly; a simple isentropic analytical model gave a good prediction using a discharge coefficient of 0.430. Gas-solids predictions using a discharge coefficient of 0.500 agreed well with test data up to the observed inflection point near the end of discharge. This inflection point is caused by the agent in the cylinder reaching the bottom of the dip tube, resulting in reduced flow of agent from the cylinder, and thus reducing the mass fraction of the flow.

Cylinder-pipe-nozzle model discharge predictions for gas-only discharges agreed well with test data for the full duration of tests using a discharge coefficient of 0.470 for the 0.173-inch diameter nozzle used in the testing. Model predictions agreed well with the gas-solids mixture test data up to the inflection point, using a discharge coefficient of 0.999.

The constant mass fraction assumption results in residual agent mass predictions of 2.0 lbm or more after discharge. Test data shows 0.6 lbm or less of residual. This residual discrepancy, and the presence of the inflection point observed in solids-gas tests, suggests that the constant mass fraction assumption is not adequate to accurately model agent discharge from the cylinder.

Using an appropriate discharge coefficient, the model can be used to determine approximate discharge times for simple systems.

## ACKNOWLEDGEMENTS

Earning a Ph.D. is much like running for public office or being in a popular musical group – no one does it alone. Behind the student there are a great number of people whose support is crucial to the student’s success; yet who seldom receive the credit they deserve.

A large number of people deserve mention for directly or indirectly making it possible for me to successfully complete this dissertation. They fall into several categories:

### Academic:

- My academic and dissertation advisor, Professor Robert G. Zalosh – his advice and guidance were critical to the success of this project, his friendship important to maintaining my determination to finish the job, and his insistence on “holding my feet to the fire” taught me the importance of persistence in the research process;
- Co-advisors Professor Mark Richman of the Mechanical Engineering Department at WPI, and Dr. Erdam Ural of Fenwal Safety Systems, Inc., who contributed their expertise and experience to the resulting success of the project;
- The faculty and staff of the Center for Firesafety Studies at WPI, contributing ideas, support, and oftentimes contributed to keeping the “ship of state” on course;

- Technicians working in the Fire Protection Engineering (FPE) laboratories, in particular Patricia Beaulieu, whose expertise with laboratory equipment, procedures, and software made the test discharge program go smoothly;
- And my fellow students, whom I bounced a lot of ideas off of. Your patience and support has meant a lot to me over the course of my studies, and I greatly appreciate being accepted as “one of the students.”

Corporate:

- Kidde-Fenwal, Inc., including Joseph Senecal, Richard Lupien, and Erdam Ural, who generously supplied dry chemical fire suppression system hardware, extinguishing agent powder, system information, and test data;
- Kidde-International, Inc., who supplied information on preliminary analytical and experimental efforts, useful in the process of validating the work described in this dissertation.

And others...

- My parents and siblings, who waited a long time for this to happen, and whom I got to see a lot of while transitioning between my home in Delaware and Worcester,
- My family, including my spouse Patricia, and sons Colin and Alaric, who had to keep things going on the home front while I was away at school, and who sacrificed much to make this Ph.D. happen;
- Toastmasters International, including Greater Newark Area Toastmasters (#1833, Newark, Delaware) and in particular Central Toastmasters (#2277, Worcester, Massachusetts) – from whom I learned a great deal about the art

and science of public speaking, giving me the confidence to go forward when presentations were called for. They also provided me a home away from home, strongly supported my efforts, and gave me a great deal of strength to carry the project to completion. Their comments and criticisms have significantly improved my public speaking, and their friendship has enabled me to grow as a person.

- Finally, if one thing has enabled me to keep on going no matter what, it has been my love of music. While my musical tastes are eclectic, in particular the music of ABBA has been a source of comfort and inspiration.

I'm sure there are others that I've forgotten to mention – if so, the fault is mine, and I offer them my thanks, as well, for their support, encouragement, and guidance.

This material is based upon work supported by the National Science Foundation under Grant No. 9256999.

Any opinions, findings, and conclusions or recommendations expressed in this material are those of the author and do not necessarily reflect the views of the National Science Foundation.



# TABLE OF CONTENTS

ACKNOWLEDGEMENTS.....	iv
TABLE OF CONTENTS .....	vii
TABLE OF FIGURES .....	x
TABLE OF TABLES .....	xiii
NOMENCLATURE.....	xiv
CD ROM CONTENTS.....	xxiv
1.0 Introduction.....	1
2.0 Problem Statement.....	5
3.0 Literature Survey.....	10
3.1 Full System Development.....	10
3.2 Systems Modeling.....	13
3.3 Solid Phase Influence on Pipe Friction – Drag Reduction.....	28
3.4 Pipe Network Components.....	49
3.5 Mixture Behaviors.....	53
3.6 Summary.....	56
4.0 Theoretical Model.....	65
4.1 Selection of Agent/Gas Model.....	65
4.2 Assumptions.....	66
4.2.1 Quasi-Steady-State.....	66
4.2.2 Constant Mass Fraction.....	67
4.2.3 Further Assumptions.....	68
4.3 Generalized One-Dimensional Analyses – Constant Mass Fraction.....	68
4.3.1 Physical Equations and Definitions.....	69
4.3.1.1 State Equation.....	70
4.3.1.2 Sound Velocity Definition.....	71
4.3.1.3 Mach Number Definition.....	71
4.3.1.4 Mass Conservation Equation.....	72
4.3.1.5 Energy Conservation Equation.....	72
4.3.1.6 Linear Momentum Conservation Equation.....	73
4.3.2 Solution of Differential Equations.....	75
4.4 Component Development.....	80
4.4.1 Mixture Isentropic Relations.....	81
4.4.2 Cylinder.....	83
4.4.3 “START” – Cylinder Exit.....	88
4.4.3.1 Simplified Isentropic Discharge Model.....	90
4.4.3.2 Simplified Isothermal Discharge Model.....	94
4.4.4 Sudden Contractions.....	96
4.4.4.1 Compressible Flow.....	97
4.4.4.2 Incompressible Flow.....	100
4.4.5 Sudden Expansions.....	102
4.4.5.1 Compressible Flow.....	103
4.4.5.2 Incompressible Flow.....	106

4.4.6	Nozzles.....	107
4.4.7	Pipes.....	118
4.4.7.1	Compressible Flow.....	126
4.4.7.2	Incompressible Flow.....	127
4.4.8	Summary.....	128
5.0	Computer Program – Implementation of the Theoretical Model.....	135
5.1	General Approach.....	136
5.2	Data-structural Representation.....	137
5.2.1	Dry Chemical System Component Representation.....	137
5.2.2	Other Data Structures.....	147
5.3	Computational Procedures.....	147
5.3.1	Solution Technique – General.....	148
5.3.1.1	Theoretical Model Solution Technique.....	148
5.3.2.1	Computational Model Solution Technique.....	149
5.3.2	Solution Technique – Components.....	153
5.3.2.1	START – Cylinder Exit.....	154
5.3.2.2	Sudden Contractions.....	157
5.3.2.3	Sudden Expansions.....	159
5.3.2.4	Pipes.....	161
5.3.2.5	Nozzle Throats.....	164
5.3.2.6	Source Cylinder (TANK, TWO_TANK).....	169
5.3.3	Modeling of Flow Conditions – Choking.....	171
5.4	“Zero” Routine.....	173
5.5	Newton-Raphson and Richmond Iteration Algorithms.....	176
5.6	Bulirsch-Stoerr Numerical Integration Algorithm.....	177
5.7	Run-Time Characteristics.....	179
6.0	Illustration of Procedure.....	181
6.1	Input File Description.....	212
7.0	Testing.....	218
7.1	General Approach.....	218
7.2	Test Descriptions.....	219
7.2.1	WPI Tests.....	219
7.2.1.1	Nozzle Flow Tests.....	219
7.2.1.2	Cylinder-Alone Tests.....	223
7.2.1.3	Cylinder-Pipe-Nozzle Tests.....	231
7.2.1.4	Additional Equipment.....	233
7.2.2	Kidde International UK Tests.....	236
7.2.3	Corn Starch Tests.....	236
7.2.4	Vendor System Tests.....	237
7.3	Test Materials.....	237
7.4	Test Results.....	243
7.4.1	WPI Tests.....	243
7.4.1.1	Cylinder-Alone Tests.....	243
7.4.1.2	Cylinder-Pipe-Nozzle Tests.....	255
7.4.2	Kidde International UK Tests.....	273
7.4.3	Corn Starch Tests.....	273

7.4.4	Vendor System Tests.....	276
8.0	Comparison of Test Results To Model Predictions.....	277
8.1	WPI Tests.....	277
8.1.1	Cylinder-Alone Tests.....	277
8.1.2	Cylinder-Pipe-Nozzle Tests.....	284
8.2	Kidde International UK Tests.....	293
8.3	Corn Starch Tests.....	296
8.4	Vendor System Tests.....	300
8.5	Assessment of Model Sensitivities and Accuracy.....	301
8.5.1	Material Parameters.....	302
8.5.2	Cylinder Parameters.....	305
8.5.3	Network Component Parameters.....	307
8.5.4	Other Parameters.....	312
8.5.5	Model Accuracy.....	315
9.0	Conclusions and Recommendations.....	319
9.1	Conclusions.....	319
9.2	Recommendations.....	322
10.0	Appendices.....	325
10.1	“Zero” Code.....	325
10.2	Pipe Cross-Sectional Integrations.....	325
10.2.1	Fluid-Only Momentum Equation Derivation.....	326
10.2.2	Ural Momentum Equation Derivation.....	328
10.2.3	Ahmadi Momentum Equation Derivation.....	329
10.2.4	Summary.....	333
10.3	Particle Acceleration to Gas Velocity.....	334
10.4	Influence Coefficients.....	337
10.5	Station_list, Station_list_node Classes Listing (classes.h).....	346
10.6	Data Structure Listing (data1.h).....	354
10.7	Kidde International (UK) Memo (Spring).....	356
11.0	Bibliography.....	364

## TABLE OF FIGURES

Figure 2.1 Typical Dry Chemical Fire Suppression System (Source: Kidde-Fenwal (1994)).	6
Figure 3.1 Comparison of Choi & Chung Analyses with Results of Melville & Bray Analyses and Boothroyd Data.	34
Figure 3.2 Loading Ratio Vs. Mach Number.	62
Figure 4.1 Control Volume Definition (Source: Shapiro (1953), Vol. I, p. 221).	70
Figure 4.2 Simple Cylinder / Exit Schematic.	83
Figure 4.3 Sudden Contraction (Source: John & Haberman (1988), p. 180).	97
Figure 4.4 Sudden Expansion (Source: John & Haberman (1988), p. 179).	103
Figure 4.5 Typical Nozzles (Source: Kidde-Fenwal (1994)).	109
Figure 4.6 More Nozzles.	110
Figure 4.7 Sketch of Differential Element of Variable Area Piping (Source: Emanuel (1986)).	112
Figure 5.1 Typical Object Oriented Design Hierarchical Relationship for Dry Chemical Fire Suppression System.	140
Figure 5.2 Typical Double-Linked List.	142
Figure 5.3 Double-Linked List for Pressure Transducer and Piping System.	146
Figure 5.4 START Node - Flow Chart.	156
Figure 6.1 Experimental Test PNS-1 - Model Representation of Configuration.	181
Figure 6.2 Input File for Configuration of Figure 6.1 and Figure 5.2.	186
Figure 6.3 Output File enode_00.txt - Source Tank Predicted Behavior.	189
Figure 6.4 Output File enode_01.txt - START Predicted Behavior.	194
Figure 6.5 Output File enode_02.txt - SUDDEN CONTRACTION Predicted Behavior.	198
Figure 6.6 Output File enode_03.txt - PIPE Predicted Behavior.	202
Figure 6.7 Output File enode_04.txt - Nozzle THROAT Predicted Behavior.	206
Figure 6.8 Test PNS-1 - Predicted Pressure Response of Components.	210
Figure 6.9 Test PNS-1 - Predicted Mass Flow Response of Components.	210
Figure 6.10 Test PNS-1 - Mach Number Response of Piping Network Components.	211
Figure 6.11 Typical Input File - Dual Chains (Pressure Transducer).	216
Figure 7.1 Nozzle Flow Test - Configuration Schematic.	220
Figure 7.2 Nozzle Discharge Coefficient Versus Corrected Measured Mass Flow.	223
Figure 7.3 Cylinder Assembly Tests – Schematic.	224
Figure 7.4 IND 25/21 Cylinder.	225
Figure 7.5 IND 25/21 Cylinder - Basic Dimensions.	226
Figure 7.6 Valve Assembly.	227
Figure 7.7 Dip Tubes.	228
Figure 7.8 Manual Trigger Mechanism.	229
Figure 7.9 WPI Dry Chemical Cylinder Alone Discharge Test Configuration.	230
Figure 7.10 Cylinder-Pipe-Nozzle Test Configuration.	232
Figure 7.11 Deflector Assembly.	233
Figure 7.12 Pressure Transducers.	235
Figure 7.13 Sodium Bicarbonate and Monoammonium Phosphate Agents.	238

Figure 7.14 Sodium Bicarbonate Without Flow Additives. ....	239
Figure 7.15 Fill Level of Cylinder - Test PNM-2. ....	242
Figure 7.16 Test G-7 - Pressure Vs Time. ....	245
Figure 7.17 Test P-6 - Pressure Vs Time. ....	246
Figure 7.18 Test P-7 - Pressure Vs Time. ....	246
Figure 7.19 Test M-1 - Pressure Vs. Time. ....	247
Figure 7.20 Test M-2 - Pressure Vs Time. ....	247
Figure 7.21 Typical Gas-Liquid Multi-Phase Cylinder Discharge. ....	251
Figure 7.22 Comparison of Discharge Tests G-7 and P-6. ....	252
Figure 7.23 Comparison of Discharge Tests P-6 and P-7. ....	253
Figure 7.24 Comparison of Discharge Tests P-7 and M-1. ....	254
Figure 7.25 Test PG-1 - Pressure Vs Time. ....	257
Figure 7.26 Test PG-2 - Pressure Vs Time. ....	258
Figure 7.27 Test PNS-1 - Pressure Vs Time. ....	258
Figure 7.28 Test PNS-2 - Pressure Vs Time. ....	259
Figure 7.29 Test PNS-3 - Pressure Vs Time. ....	259
Figure 7.30 Test PNS-4 - Pressure Vs Time. ....	260
Figure 7.31 Test PNM-1 - Pressure Vs Time. ....	260
Figure 7.32 Test PNM-2 - Pressure Vs Time. ....	261
Figure 7.33 Pipe/Nozzle Effects on Discharge Time (Gas Only Tests). ....	265
Figure 7.34 Initial Cylinder Pressure Effects on Discharge Time (Tests PG-1 and PG-2 - Gas Only). ....	266
Figure 7.35 Pipe Network Component Effects on Discharge (Tests P-6, PNS-1, PNS-2 - Sodium Bicarbonate Agent). ....	267
Figure 7.36 Cylinder Dip Tube Length Effects on Discharge Time (Tests PNS-1, PNS-4). ....	269
Figure 7.37 Agent Effect on Discharge Time (Tests PNS-1, PNM-1). ....	270
Figure 7.38 Flow Additives Effect on Discharge (Tests PNS-1, PNS-3). ....	271
Figure 7.39 Discharge Test F-9 - Pressure Vs Time. ....	274
Figure 7.40 Discharge Test F-10 - Pressure Vs Time. ....	275
Figure 7.41 Discharge Test F-11 - Pressure Vs Time. ....	275
Figure 8.1 Test G-7 - Models Vs Discharge Test Response. ....	277
Figure 8.2 Test P-6 - Model Vs Discharge Test Response, $C_d = 0.500$ . ....	278
Figure 8.3 Test P-6 - Model Vs Discharge Test Response, $C_d = 0.380$ . ....	278
Figure 8.4 Test P-6 - Model - Mass Remaining in Cylinder. ....	279
Figure 8.5 Test P-7 - Model Vs Discharge Test Response. ....	279
Figure 8.6 Test M-1 - Model Vs Discharge Test Response. ....	280
Figure 8.7 Test M-2 - Model Vs Discharge Test Response. ....	280
Figure 8.8 Test PG-1 - Comparison of Model Prediction and Test Data. ....	285
Figure 8.9 Test PG-2 - Comparison of Model Prediction and Test Data. ....	285
Figure 8.10 Test PNS-1 - Comparison of Model Prediction and Test Data. ....	286
Figure 8.11 Test PNS-1 - Model - Mass Remaining in Cylinder. ....	286
Figure 8.12 Test PNS-2 - Comparison of Model Prediction and Test Data. ....	287
Figure 8.13 Test PNM-1 - Comparison of Model Prediction and Test Data. ....	287
Figure 8.14 Test PNM-2 - Comparison of Model Prediction and Test Data. ....	288
Figure 8.15 Test PNM-2 - Comparison of Predicted and Actual Residual Levels. ....	291

Figure 8.16 Test UK-F6 - Comparison of Model Prediction and Test Data. ....	294
Figure 8.17 Test UK-F7 - Comparison of Model Prediction and Test Data. ....	294
Figure 8.18 Comparison of Predicted and Actual Agent Remaining in Cylinder, Kidde International - Test UK-F7.....	296
Figure 8.19 Test F-9 - Comparison of Model Prediction and Test Data.....	297
Figure 8.20 Test F-10 - Comparison of Model Prediction and Test Data.....	298
Figure 8.21 Test F-11 - Comparison of Model Prediction and Test Data.....	298
Figure 8.22 Variance in Time to Unchoke as a Function of Gas Parameter Changes...	303
Figure 8.23 Variance in Time to Unchoke as a Function of Solids Parameter Changes. .....	304
Figure 8.24 Variance in Time to Unchoke as a Function of Cylinder Parameter Changes. .....	306
Figure 8.25 Variance in Time to Unchoke as a Function of START Parameter Changes. .....	308
Figure 8.26 Variance in Time to Unchoke as a Function of Pipe Length Change. ....	308
Figure 8.27 Variance in Time to Unchoke as a Function of Pipe and Sudden Contraction Changes.....	309
Figure 8.28 Variance in Time to Unchoke as a Function of Nozzle Changes.....	309
Figure 8.29 Variance in Time to Unchoke as a Function of Mass Fraction Changes....	313
Figure 8.30 Variance in Time to Unchoke as a Function of Program Time Step Changes. .....	313
Figure 10.1 Standard Text Book Pipe Momentum Conservation – Schematic. ....	326

## TABLE OF TABLES

Table 3.1 Effect of particles on turbulence (data from Tsuji & Shiomi (1984), presented in Hestroni (1989)).....	45
Table 4.1 General One-Dimensional Analysis – Equation Matrix. ....	76
Table 4.2 General One-Dimensional Analysis – Solutions (Influence Coefficients). ....	78
Table 4.3 Equations for Parameter Calculations for Cylinder. ....	129
Table 4.4 Equations for Parameter Calculations for START Node.....	130
Table 4.5 Equations for Parameter Calculations for Sudden Contraction.....	131
Table 4.6 Equations for Parameter Calculations for Sudden Expansion.....	132
Table 4.7 Equations for Parameter Calculations for Nozzle Throat. ....	133
Table 4.8 Equations for Parameter Calculation for Pipe. ....	134
Table 7.1 Results of Nozzle Calibration Experiments .....	221
Table 7.2 Powder Material Properties. ....	240
Table 7.3 Gas Material Properties.....	243
Table 7.4 Cylinder-Alone Discharge Tests. ....	245
Table 7.5 Cylinder-Pipe-Nozzle Test Summary. ....	256
Table 7.6 Powder Weights and Their Distribution After Discharge Testing. ....	264
Table 7.7 Summary of Discharge Tests Performed at Kidde International (UK).....	273
Table 7.8 Summary of Available Corn Starch Tests.....	274
Table 8.1 Comparison of Predicted and Actual Cylinder Powder Residual Mass - WPI Tank-Pipe-Nozzle Tests. ....	290
Table 8.2 Comparison of Predicted and Actual Cylinder Powder Residual Mass - Corn Starch Tests. ....	299

## NOMENCLATURE

### English:

- A Cross-sectional area ( $\text{ft}^2$ ),  
linear algebra  $n \times n$  matrix (square).
- a Replacement variable,  
speed of sound,  
function of radius ratio.
- B Linear algebra  $n \times m$  matrix.
- b Replacement variable,  
replacement variable, influence coefficients.
- C Coefficient,  
constant value,  
integration constant.
- c Replacement variable, influence coefficients,  
solid phase specific heat ( $\text{BTU}/\text{lbm}\text{-}^\circ\text{R}$ ).
- D Particle diameter (microns),  
pipe diameter (ft).
- d Diameter (ft),  
differential,  
replacement variable, influence coefficients.
- e Replacement variable,  
replacement variable, influence coefficients.
- F Force,



	projected pipe areas in pipe branches.
$F^*$	Froude number.
$F_r$	Froude number.
FS	Full scale.
f	Body force per unit mass, dummy variable - definition of barred (normalized) variables, unspecified function, pipe friction factor, replacement variable.
fd1	Iteration algorithm variable.
fd2	Iteration algorithm variable.
g	Replacement variable.
$g_c$	Gravitational constant (lbm-ft/lbf-sec <sup>2</sup> ).
h	Enthalpy (BTU/lbm), iteration interval, replacement variable, variable.
$I_1, I_2$	Area integrals defined by <b>Michaelides (1984)</b> .
I.D.	Inside Diameter (ft.).
K	Sudden contraction / expansion loss factor.
k	Kinetic energy, pipe roughness factor.
$\tilde{k}$	Turbulent wavenumber.

L	Length (ft).
l	Characteristic length (ft).
M	Mach number, mass in cylinder (lbm).
m	Linear algebra matrix – number of columns, weak function of total solids concentration.
$\dot{m}$	Mixture mass flow (lbm/sec).
$m_{\dot{}}$	Mixture mass flow (lbm/sec).
n	Exponential variable, linear algebra matrix - number of rows or columns.
O.D.	Outside diameter (ft.).
P	Unspecified function, pressure (psi).
PVC	Poly-vinyl chloride.
p	Pressure (psi).
Q	Unspecified function.
R	Ideal gas law constant (ft-lbm/lbf-°R). radius (ft).
Re	Reynolds number.
r	Radial distance, radial direction (cylindrical coordinates).
T	Temperature (°R).
t	Time (sec),

	stress.
$t^*$	Particle relaxation time (sec).
$U$	Averaged flow velocity (ft/sec).
$u$	Velocity (ft/sec).
$u^*$	Dimensionless velocity ( $= u/V^*$ ).
$u'$	RMS fluid velocity (ft/sec).
$\sqrt{u'}/U$	Turbulence intensity (%).
$V$	Volume ( $\text{ft}^3$ ), velocity (ft/sec).
$V^*$	Shear velocity (ft/sec).
$v'$	RMS particle velocity (ft/sec).
$V_{Dc}$	Volts, direct current.
$V_{\text{dot}}$	Volumetric flow ( $\text{ft}^3/\text{sec}$ ).
$v$	Integration replacement variable, velocity (ft/sec).
$w'$	Relative velocity between two particles with zero separation (ft/sec).
$x$	Linear algebra matrix – $n \times 1$ matrix (vector), pipe location (ft.). variable.
$y$	Variable, radial direction in pipe.
$Z$	Compressibility factor.
$z$	Axial direction in pipe,

axial direction in pipe (cylindrical coordinates),  
compressibility factor.

Greek:

- $\beta$  Function of solids / gas density ratio and  $\psi$ .
- $\Delta$  Differential.
- $\delta$  Differential,  
ratio of solid phase specific heat capacity to gas specific heat capacity at constant pressure.
- $\varepsilon$  Pipe roughness factor,  
turbulent energy dissipation rate.
- $\phi$  Mixture solids mass fraction,  
angle of slanted surface of differential area piping with x-axis.
- $\Gamma$  Viscous stress (fluid or mixture).
- $\gamma$  Specific heat ratio,  
function of total solids concentration.
- $\eta$  Boundary layer coordinate ( $= \ln(y/y_0)$ ).
- $\lambda$  Friction factor.
- $\mu$  Kinematic viscosity.
- $\nu$  Dynamic viscosity ( $= \mu/\rho$ ).
- $\theta$  Mixture volume fraction ( $= \rho\phi/\rho_D$ ),  
angular direction in pipe (cylindrical coordinates),  
angle of pipe in branch,  
dimensionless particle relaxation time.

$\rho$	Density (lbm/ft <sup>3</sup> ).
$\rho^*$	Dimensionless density (= $f(\eta)$ ).
$\tau$	Sheer stress, non-dimensional time in Cheoweth & Paolucci analyses.
$\psi$	Function of Reynolds number.
$\zeta$	Pipe elbow loss variable ( <b>Ito (1960)</b> ).

Superscript:

f	Fluctuation,  fluid,  laminar fluid.
fT	Turbulent fluid.
S	Superficial.
T	Turbulent.
~	Turbulent flow mass-weighted ensemble average.
^	Averaged value.

Miscellaneous:

$\nabla$	Del operator.
$\partial$	Partial differential.
$\Sigma$	Summation operator.
$\leftarrow$	Replacement operator.

Subscript:

0	Stagnation condition, Outermost diameter of inside of pipe (pipe I.D.).
1	Cylinder exit reference.
0,1,2,3	Constant subscripts, locations.
a	Ambient, gas only.
c	Cylinder reference.
cyl	Cylinder reference.
D	Discharge, Solid phase.
d	Solid phase.
e	Eddy.
f	Fluid (gas) phase.
G	Gas phase.
G-cyl	Gas phase in the source cylinder.
g	Gas phase.
i	Direction in coordinate system.
j	Direction in coordinate system.
m	Gas phase.
new	Current calculation cycle.
old	Immediately previous calculation cycle.
P	Constant pressure.

p	Constant pressure, particle.
pg	Friction factor multiplier subscript.
r	Radial direction.
s	Solid phase, surface.
T	Stagnation condition.
t	Throat, stagnation condition.
v	Constant volume.
w	Wall.
w-g	For gas alone.
w-i	For individual solid alone.
w-p	For solids alone.
w-pg	For full mixture.
z	Axial direction.
$\theta$	Angular direction.
#	Location reference.
*	Throat reference.
‘	Friction factor augmentation multiplier denotation, first differential.
“	Second differential.

Notes:

1. All variables are in British units, unless otherwise specified.
2. (t) indicates variable is a function of time; (0) indicates variable at time = 0 seconds.
3. In Ural/Ahmadi analyses, barred variables indicate values averaged as a result of integration across the cross-sectional area of a pipe.
4. In Chenowith & Paolucci analysis, barred variables are non-dimensionalized by division by corresponding value at initial time, unless otherwise noted in text.





## CD ROM Contents

The CD-Rom included with this document contains a number of important support documents, as well as source files, and sample files for running the program DryRun documented herein. There are three main directories:

Flowcharts – contains flowchart Figures 5.5 through 5.8 – too big to get onto a single page. Copies are in three sub-directories – jpg files, tif files, and sdr files. The lattermost is a format used by the flowcharting program SmartDraw™, available on the Web. The jpg and tif files can be read and printed using any software capable of interpreting these graphical formats.

DryRun – contains program file source code, executable, and support files generated by Borland's C++ compiler. The source files: classes.h, data1.h, classes.cpp, DryRun.exe, zero.h, zero.cpp. These source files are all in text format, and can be read and printed by any program capable of handling ASCII text files.

Samples – contains input files, and output files used to model several of the test discharges described in this document. As labeled.

## 1.0 Introduction.

Commercial dry chemical fire suppression systems are currently pre-engineered, i.e. they are designed, tested, and certified for specific discharge piping, nozzles, and source tank sizes and pressures. The relatively few certified designs have restricted dry chemical system use to a few established applications such as dip tanks and spray paint booths. This situation is in contrast to virtually every other type of fire suppression agent, for which an approved methodology exists to do site and application specific engineering designs.

Computer simulation programs have been developed for several different types of fire suppression systems. Due to the extensive use of water sprinkler systems in buildings, a number of commercial codes are available to analyze sprinkler system hydraulics. These codes generally give good results, enabling a designer to quickly produce a sprinkler design whose hydraulic acceptability can be readily demonstrated. In fact, almost all sprinkler systems for large industrial and commercial buildings are now designed with hydraulic computer code calculations to demonstrate compliance with NFPA 13 requirements for discharge flow rates at a prescribed number of operating sprinklers.

A more recent development is the computer simulations of Halon replacement gaseous suppression system discharges (**Forsell *et al* (1995)**, **Bird *et al***). These programs implicitly include turbulent two-phase liquid-gas flow considerations such as turbulent energy dissipation, gas-liquid phase interactions, etc..., and empirical prescriptions for gas-liquid separations at pipe junctions. These codes simulate the depressurization of the liquefied gas and nitrogen in the source tank(s), two-phase flow

pressure losses and phase separations in the delivery system piping, and flow through the discharge nozzle(s). The codes make design of a system relatively simple, and some have been verified (by independent certifying organizations) via comparison with discharge test data for a wide variety of suppression gases and piping networks.

The primary obstacle in the way of developing a generalized engineering design method for dry chemical systems is the absence of a suitable calculation technique to simulate the discharge of powdered agent from the pressurized cylinder, piping, and nozzles. Design tools, for the most part, have been limited to vendor proprietary in-house programs. These programs are usually of empirical origin, and not readily amenable to revision, upgrading, or use by the engineering design community. Vendors design pre-engineered systems either with these proprietary codes, or by extensive testing of systems, adjusting physical hardware until acceptable results are achieved. Vendor manuals for pre-engineered systems (**Kidde-Fenwal (1994)**, **Ansul (1995)**) carefully prescribe design limits for their pre-engineered systems; so long as application designers stay within the established limits, the system so-designed is guaranteed to perform acceptably. Drawbacks to these procedures include the labor and time required for developing new programs for new systems or new agents or making even small changes to already developed systems; and more importantly, the inability of the customer; i.e. the facility owner/operator, to engineer a site-specific system.

The development of more general design software has been limited by the complex nature of the underlying phenomena. As described in Section 3.0, two-phase, particulate-gas flow, in general, has been an active field of research, but the completed research encompasses only some of the many possible flow regimes. There are very few

published results in the regions of interest for dry chemical fire suppression systems; i.e. high Reynolds number, compressible flow through branching pipe networks, with high solids particle concentrations. Thus, there isn't any firm theoretical basis for modeling of dry chemical fire suppression systems (much less software implementing such modeling), and there is hardly any applicable published test data to validate theoretical predictions.

Modeling of proposed engineering systems enables the designer to determine the adequacy of the design to meet its intended purposes, and to discover critical issues in the proposed design. In addition, design and development costs are significantly reduced if proposed designs are tested in a simulation model, rather than in labor-intensive and time-consuming full-scale testing. Furthermore, the impact of changes to a proposed system is more easily examined through a simulation than through repeated full-scale tests.

Although the limited capability to design more general engineered dry chemical systems is due in part to the limitations of fire suppression technology<sup>1</sup>, the current lack of a code capable of designing a dry chemical delivery system is a much more immediate barrier. A further barrier is the lack of a code utilizing a simple modeling approach. A number of field models exist, such as Fluent™ and TASCflow™, some with multiphase capabilities. However, these multiphase capabilities are limited to “dilute” flows, with mass fractions sufficiently low as to limit the influence of the solids on mixture flow. Furthermore, these codes tend to be complicated to use and understand, and require long run times and large memory capacities to model even simple compartment scenarios, much less pipe networks. While, with the right theoretical underpinnings, field models

could model high load high velocity gas/solids pipe flow, their use would be limited to experimental research.

A simpler approach, utilizing enough of the physics of the problem to predict configuration performance with acceptable accuracy would be of greater practical applicability than a full-featured field model. On the one hand, the user would end up with less insight as to the behavior of particular portions of the system, losing detailed information, for example, on exact locations of solids accumulations, or exact information on solids distributions at all points of a system. However, the details of system behavior during discharge lost by pursuing a simple approach generally add little to the ability of a designer to develop a working application. As a result, the virtues of a simpler implementation (faster program execution, lower memory requirements, rapid ability to test alternative solutions, etc...) outweigh the details lost by choosing a simple approach. Ultimately, the important question is whether or not the physics of a two-phase gas/solids flows in a dry chemical system will allow the implementation of a “simple” approach.

Thus, research was undertaken with the aim of developing the basis for a general engineering method for the calculation of dry chemical fire suppression system performance, and implementation of that engineering method in software.

---

<sup>1</sup> Laboratory testing to better understand dry chemical fire suppression fundamental phenomena was started at the Naval Research Labs in 1996 (**Sheinson (1996)**).

## 2.0 Problem Statement.

The objectives of this dissertation were:

- to examine previously-developed mathematical models of two-phase gas-solids vessel blow down and pipe flow, and either select a previously developed model of a two-phase gas-solids material, or develop a model from scratch, for future development.
- to use the previously-selected material model to develop a mathematical model simulating the discharge of a source cylinder containing dry chemical fire suppression agent and a carrier gas (usually nitrogen) , through a valve and dip tube assembly integral to the cylinder design, through a simple downstream network consisting of piping, fittings, and a single nozzle.
- to compare model calculations with system discharge test data and revise the model where necessary.
- to determine the positive points, and drawbacks, of the material representation and the system simulation developed from that representation.
- to provide a computer code, based on the model, that will facilitate design calculations for simple single-nozzle systems.

A typical system used by at least one vendor is shown in Figure 2.1.

Piping Limitations Total Flooding System IND-50/IND- 45

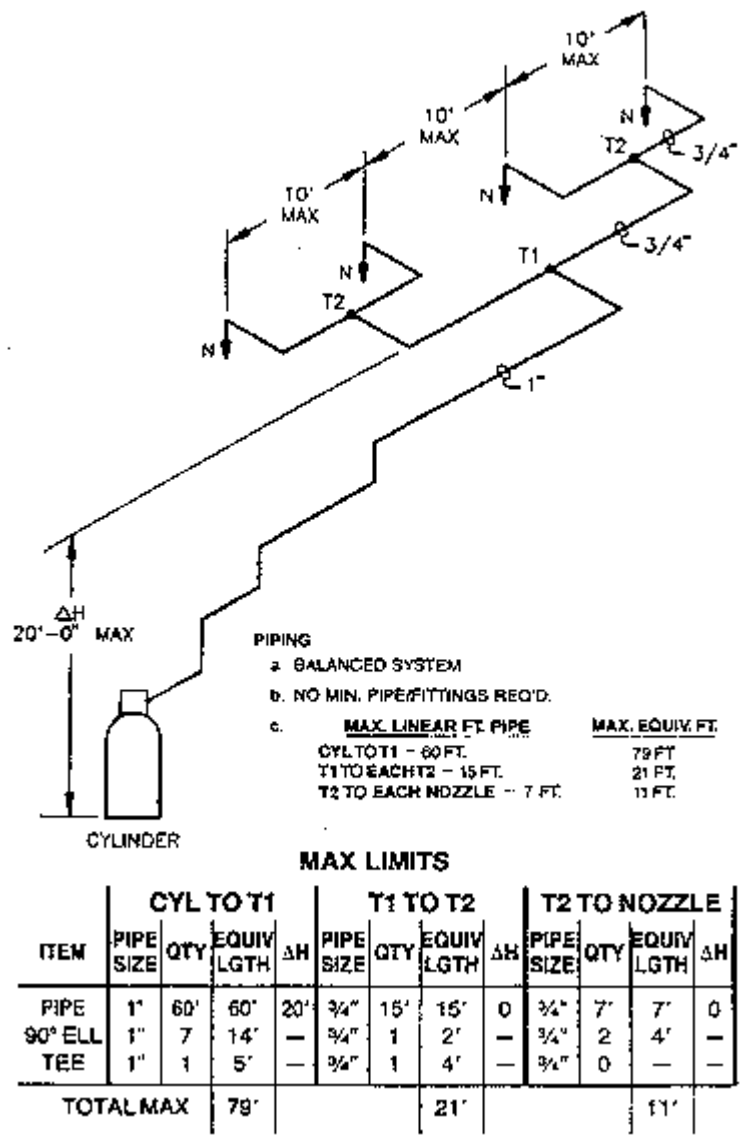


Figure 2.1 Typical Dry Chemical Fire Suppression System (Source: Kidde-Fenwal (1994)).

Source tanks for the system illustrated often contain from 21 to 25 pounds of agent, pressurized to 360 PSIG with nitrogen, with total discharge times required (NFPA 17 (1998)) to be specified by the manufacturer (for the illustrated system, less than 25



seconds when attached to pipe networks with nozzles at the downstream end of the piping). Typical extinguishing agents include sodium bicarbonate and monoammonium phosphate. The formulation of these agents is generally proprietary to the individual vendors, but usually contain small amounts of additives, such as zinc stearate, to enhance flow characteristics of the powder. The particle size range of the agents is between 10 and 100 microns.

The simple system considered in these studies consists of a single nitrogen pressurized storage cylinder, a multi-segment piping network, and a single discharge nozzle. The agents considered were sodium bicarbonate and monoammonium phosphate, assumed to contain additives, and in the 10-100 micron particle diameter range; typical of those used in the industry. An initial pressure of 300 psig and initial temperature of 530 °R were assumed, modeling a “cold day” discharge (“standard day” (70 °F) pressure is 360 psig). Maximum loads of 25 lbm sodium bicarbonate, and 21 lbm of monoammonium phosphate were assumed. The source cylinder, pipes, and nozzle used are typical of what is installed in systems in the field, with the exception of using a clear Lexan™ pipe, so that mixture flow phenomena could be observed and videotaped.

Underwriters Laboratory Standards regulating dry chemical systems include (but are not necessarily limited to) **UL 299 (2000)**, **UL 711 (2000)** and **UL 1254 (1999)**. NFPA standards include (but are not necessarily limited to) **NFPA 10 (1998)** and **NFPA 17 (1998)**. The only specified requirements in these Standards for discharge times are:

- Total flooding systems, required to achieve design concentration of agent in no more than 30 seconds, and

- Hand hose line systems, required to contain enough agent to permit effective use for a minimum of 30 seconds.

Other systems are required to fully extinguish test fires as specified under conditions specified in the standards. However, discharge times are to be specified by a system's manufacturer; this includes pre-engineered systems.

The primary objective of the modeling was to calculate the cylinder depressurization time and any agent holdup in the various pipe segments and nozzle. Model input parameters were to include the quantity, particle size distribution, and physical properties of suppressant, the storage container gas pressure, physical properties, and volume, and the piping/nozzle sizes and hydraulic characteristics. The model and computer code to be developed were to include the following features:

- Implementation of conservation equations for two-phase gas-solid compressible turbulent flow, including boundary and initial conditions.
- Determination of the significance of interparticle collisions and powder flow characteristics on mixture discharge time.
- User ability to examine output data graphically, or in tabular form.
- Object-oriented code design, to obtain the maximum flexibility in terms of implementation, alteration, and future maintenance/upgrading.
- Documentation and examples of program use and features.

The model developed to simulate the discharge of the single nozzle system is described in Section 4.0 and the corresponding computer code in Section 5.0. Test data generated and compared with predictions made by the model are described in Sections

7.0 and 8.0. Virtues and failings of the developed model were also examined as part of the studies.

### **3.0 Literature Survey.**

Multiphase flows have found increasing applications in commerce and industry. Some of the earliest attempts to understand and utilize such flows are in the coal industry, where transport of pulverized coal in slurries, especially to boilers, requires accurate information to design and control the flow processes. Any application where bulk solids may be moved pneumatically utilizes multiphase flows to facilitate processing of materials. In fire suppression systems, a number of multi-phase flow system models have been successfully developed, including models for CO<sub>2</sub>, and halon replacement agents such as FM-200. These suppression system models utilize gas-liquid systems, including distinctive phenomena such as changes of phase, and dissolving and undissolving of gases in the models, phenomena affecting the energy content, physical properties, and flow characteristics of the agent/gas mixture as it passes through the delivery system. While dry chemical systems do not undergo phase changes during delivery, they exhibit complex behaviors that are affected by a number of factors, including turbulence, agent and carrier physical properties, physical properties of the delivery system, particle sizes, and proportions of agent and carrier (“loading factors”). The complexities involved in adequately accounting for these and other phenomena of interest when developing models have often resulted in an over-reliance on empirical data and experimental system development.

#### **3.1 Full System Development.**

Dry chemical suppression systems have generally been designed through trial and error methods. **Cholin (1969)** discussed development of an early version of a dry

chemical suppression system in this manner, describing extensive testing before an acceptable delivery system was developed. Cholin's development goals were to:

- minimize travel time (which was divided into displacement of air in the pipe prior to agent delivery, delivery of agent, and blowdown after agent is exhausted).
- have sufficient agent to meet delivery requirements.
- have sufficient carrier gas to achieve pressures able to maximize the amount of agent delivered.
- deal successfully with agent/carrier separations after passage through bends in the piping.

Cholin obtained experimental results with measured flows of 7500 ft/min (125 ft/sec) for a system pressured to 350 psi with nitrogen, delivering 175 pounds of Purple K agent through a piping network with initial inside diameter of 2 ½ inches. (Note: current manufacturers, per UL listings, list systems in terms of mass of agent, rather than in terms of cylinder capacity. A number of design options make an exact comparison difficult, including manifolded several cylinders of smaller capacity together, and systems (such as manufactured by Ansul) in which agent and carrier gas are housed in separate cylinders, mixed only during discharge.) No indication was given as to the exact sizing of the nozzles used. Tests with the cylinder and no piping network or nozzle(s) discharged in 4.5 seconds, with approximately 1 lbm residual. Full scale tests were conducted to extinguish 20-foot square pans containing approximately 250 gallons of heptane, with 2 nozzles, and the source cylinder 110 feet and 6 elbows away. The ambient temperature was -40 °F, giving an equivalent cylinder pressure of 280 psi. The tests were outdoors, with winds up to 35 miles per hour. For the full tank-cylinder-

nozzles system, piping travel time ranged from 1 to 2 ½ seconds, with a discharge time from 6 to 12 seconds. Extinguishment time was from 4 to 8 seconds, with 30 to 60 second preburns. Unfortunately, cylinder pressure was not measured or recorded during discharge.

As part of the Underwriters Laboratories (UL) certification process (**UL 1254(1999)**), the Factory Mutual approval process, and verification of compliance with the provisions of NFPA 17 (**NFPA 17(1998)**) for pre-engineered dry chemical fire suppression delivery systems, tests are conducted pre-engineered system manufacturers. The purposes of these tests are to see that, within the design limitations allowed for, that a system performs as expected, and to see that the system, as designed, is able to extinguish fires within areas the system is designed to protect. As part of these tests, variations in system designs are also tested to verify system performance characteristics. Tests include standard equipment sold by the manufacturer as part of these systems, such as source cylinder(s), valving and nozzles, and piping of the type prescribed by the manufacturer. Data collected from these tests include discharge times, powder delivered by the system, residual powder in system components, and success or failure of the discharge to extinguish fires. No transient pressure information is recorded in these tests. How the discharge time is measured is up to the manufacturer. Kidde-Fenwal determines discharge times by sound cues listened for by test technicians, timing the discharge with stop watches. The tests, configurations, and generated data are considered proprietary by a system's manufacturer.

UL (**UL 711 (2000)**, **UL 1254(1999)**) and NFPA17 (**NFPA 17(1998)**) requirements specify discharge times only for total flooding systems (design agent

concentrations must be reached in no more than 30 seconds), and hand hose line systems (must have enough agent to be effective for 30 seconds). Discharge and extinguishment times, particularly for pre-engineered systems, are to be specified by the manufacturer.

The system described in **Cholin (1969)**, while lacking some of the refinements of current systems, resembles many of the systems in use or available today. Agent loads can range from as low as 25 lbm to as high as 1000 lbm. Available agents include (but are not limited to) sodium bicarbonate based, ammonium phosphate based and potassium bicarbonate based. Piping can be up to 3 inches ID, or whatever size is capable of delivering agent in the desired time. UL listings (example: **UL (1999)**) show a fairly wide range of sizes and options that are available for various applications.

### **3.2 Systems Modeling.**

The complications in modeling gas-solids multiphase flows as opposed to single-phase flows were summarized by **Sharma & Crowe (1978)**. One of the major difficulties lies in how to treat the solid and gas phases. In development of models of the materials, a gas would normally be modeled as Eulerian (continua), while the solid powder would seem to be better modeled as Lagrangian (particulate). One approach to dealing with the two phases in the flow is to develop an Eulerian model combining the gas and solid phases into single continua, merging properties of the two phases in some manner to define mixture properties. Sharma & Crowe noted that, if behaviors of the individual phases were the primary objective, that the "single continua" approach would make it almost impossible to determine behaviors of individual phases. It becomes difficult, for example, to determine the meaning of "particle density" at a point, and

defining “average” velocity for particle distributions is difficult when the distinction between particles and carrier gas is blurred.

**Drew (1971)** was noted to have implemented a single continua approach, defining composite averages by integral averaging over space and time, a viable approach provided that sufficient space and time for a stationary average are allowed for. While sufficiently long continual operation of an apparatus could justify utilization of properties averaged over time, local behaviors of the different phases are, as noted above, lost in this approach. Whether these lost behaviors represent insurmountable difficulties depends on the intended goals of model development. If the aim is to develop a model to predict overall system performance, treating the mixture as a single continua results in a simpler model, despite the loss of some details of system behavior.

A second complication noted by Sharma & Crowe concurred with observations by Boothroyd, namely the coupling effect between the gaseous and solid particle phases. Both momentum and energy couplings are of relevance to dry chemical systems. Accurate modeling of highly loaded gas-solids multiphase flows requires the modeling of interactions between particles and carrier fluid, as well as interactions among particles and between particles and surrounding structures. If a composite continua approach is to be implemented, some means needs to be established for arriving at properties of the mixture. Transport phenomena between phases that result in irreversible losses, such as energy losses resulting from momentum exchanges, also need to be included in the approach. In addition, phenomena such as interparticle collisions, particle drag, particle entrainment, and wall friction should be considered.



Prior approaches described by Sharma & Crowe included assumptions of dynamic and thermal equilibrium between phases (equilibrium solution), corresponding to solutions with single phases and composite properties. Other solutions modeled aerodynamic particle drag, but included no effect of particles on the gas flow. Sharma & Crowe noted that such highly idealized models had not proven highly reliable up to the time of their paper. They also noted that many of the modeling efforts up to the time of their paper were semi-empirical, with correlations based on limited experimental data.

Sharma & Crowe proposed an alternative to a composite material approach, dividing a pipe into a series of segments, treating each segment (or "cell") as a control volume (Figure 3), and applying basic compressible flow conservation equations to a series of "cells" (in their paper, a Venturi tube was modeled). Particle/gas interactions were modeled through source terms in the equations. The computational model, CONVAS, implemented mass, momentum, and energy balances on a series of cells modeling a pipe. All analyses were done subsonically for gas/solids mixtures, and neglected particle/particle collisions, and particle/wall interactions.

Comparisons with data generated by **Faber (1953)** showed good agreement between CONVAS and measured pressure drops. One of the more interesting results of pressure drop predictions using CONVAS was the sensitivity of pressure drops to particle size. For low solids loading ratios (on the order of 1 to 2), flows with particle sizes less than 30 microns in size were predicted to have significantly larger pressure drops than flows with particles larger than 30 microns.

**Özbelge (1983)** implemented a mathematically simplified approach, involving the solution of separate momentum equations for gas and solid phases for dilute flow in a

vertical pipe, developing a Fortran implementation solution for turbulent upward flowing gas/solids mixtures. Özbelge's assumptions included:

- “dilute” flows, although test printouts indicate load ratios as high as 14.6 were achieved. Note also that drag coefficients for “relatively dense” and “dilute” flows were included in the model.
- gas phase flows not affected by solid particles for dilute flows (it is unclear if interactions are considered for “higher” loading conditions).
- gas phase obeys the Ideal Gas Law.
- neglect of buoyancy effects.
- radial symmetry of flow parameters.
- fluid and solid densities and velocities do not vary much in the axial direction in fully developed flows, so that averaging of these values in the axial direction is justified.
- linear variation of pressure with axial distance.

Özbelge developed an iterative 1-D incompressible algorithm using an initial guess for drag velocity as the basis for calculations of average fluid velocity, voidage (gas volume fraction), average solids velocity, solids density, drag (slip) velocity, external forces on particles, and calculated solids loading ratio (weight of solid particles divided by weight of gas). The code was validated against data of **Hairu & Molstad (1949)**, with a reported error margin of  $\pm 10\%$ , for particle diameters of 30-500 microns and pipe diameters of 0.007-0.018 m. Calculations were also done using data from studies by **Depew (1960)**, and as a basis for heat transfer calculations reported in **Özbelge & Somer (1982)**. The results of these calculations were reported as “very

close”, but there was no indication of the actual closeness of the algorithm results to actual data.

**Durst, Milojevic, & Schönung (1984)** compared the Eulerian and Lagrangian flow representations. Compressible flow equations were derived for a two-fluid representation to solve two-phase gas/solids pipe flow problems, both from the Eulerian and Lagrangian points of view. Particle/particle interactions, and turbulence effects were not included in the models. The results of the analyses were partial differential equations that were discretized and solved with implicit difference schemes, yielding similar results when applied to two simple cases - vertical pipe flow, and a sudden expansion in vertical pipe flow. For the Eulerian approach the primary parameters of interest turned out to be large particle accelerations/decelerations, non-uniform distribution of the solid phase (denoted in the paper as non-uniform “void fraction distribution”), high solids volume fractions, and mixtures of particle sizes. For the Lagrangian approach, the primary parameters of interest turned out to be choice of the number of particle starting locations, large particle accelerations/decelerations, high solids volume fractions, and mixtures of particle sizes. The main difference in the two approaches was in the treatment of the solid phase.

Durst, Milojevic, & Schönung's analyses suggested that there were advantages and disadvantages to each approach. The Lagrangian approach gave better predictions of particle behavior, and with smaller time steps in the solution implementation, yielded better predictions in situations with high velocity gradients. The Lagrangian approach was also less subject to particle discretization errors, even with a relatively coarse fluid grid. While recommended for multi-sized particle scenarios, the Lagrangian approach

solution technique had convergence problems, particularly when particle loadings were high. The Eulerian approach was found superior for scenarios with high solids volume fractions (denoted as “void fractions” in the paper), and numerical diffusion problems with were found to be avoidable by the use of a suitable higher order difference scheme. The Eulerian approach also excelled in its simulation of particle turbulent mixing processes, thus influencing momentum and energy transfers. Note that, for test runs utilizing the Eulerian and Lagrangian equations, loading ratios were low (between 0.1 and 2.0 (a solids mass fraction range of 0.09 to 0.667), with solids volume fractions at the inlet to the modeled pipe ranging from  $4 \times 10^{-4}$  to 0.2. Pipe diameters were 0.1 and 0.2 inches in diameter, with lengths ranging from 1 to 15 inches. Gas pipe Reynolds numbers ranged from  $2.5 \times 10^4$  to  $8 \times 10^4$ .

**Doss (1985)** developed a one-dimensional incompressible gas/solids flow model in a variable area duct, such as a Venturi tube. Doss reviewed several previously developed analytical models involving ducts, nozzles, and/or Venturi tubes, and noted a number of approaches and limitations. He developed a 1-D steady state two-phase multiparticle model, including particle/particle interactions. Model solution output parameters included gas pressure and velocity, particle velocity, volume fraction, and average density of the mixture. The developed model treated the gaseous phase as Eulerian, while treating the particles as Lagrangian. Particle/wall interactions were modeled after the results of work by **Pfeffer *et al* (1966)**. The resulting  $2n + 2$  equations were then solved using a standard integration routine for a set of ordinary differential equations (Doss used a fourth-order modified Runge-Kutta algorithm). The effects of turbulence did not seem to be considered in the Doss model.

Doss reached several conclusions; among them, the pressure drop in the Venturi tubes was sensitive to the particle sizes and size distribution. Single particle sizes are a poor substitute for the actual particle distribution to be encountered; attempts to come up with a single particle diameter equivalent to the particle sizes and size distribution actually encountered resulted in both over- and underpredictions of pressure losses compared to losses predicted using the actual size and size range. Furthermore, particle/particle interactions need to be included in the particle momentum equation in models treating the gas and solids as distinct phases. Omission of these phenomena results in overpredictions of pressure recovery in the Venturi tube, and deviations of the predicted values from observed values increases with increasing load ratio. Doss' model agreed well with the Venturi data of **Faber (1953)**. Analysis of the pressure recovery predictions showed that for gas-only situations, or light loading, the diffuser section of the Venturi was highly effective, its effectiveness was lost as the loading ratio increased.

**Soo (1989)** developed a series of models of multiphase flow, sufficiently generic to model a number of mixtures, including gas/solid and gas/liquid systems. Initially, he develops a "two-fluid" set of equations covering the phases, generating conservation equations and interface balance equations. With initial and boundary conditions, the equation set is closed; however, the lack of information regarding interface areas between phases, including area sizes and locations, makes practical application of this solution difficult, if not impossible. Soo further develops a set of equations based on space- and then time-averaging techniques, to average out phase properties and turbulent fluctuations. The resulting set of equations, like before, is solvable, but like before, still requires unavailable information on phase interfaces to be able to generate a solution.

Ultimately, Soo generates a set of one-dimensional equations applicable to dilute flows, including terms for both the gaseous and solid phases. Soo finishes with discussion of issues involving “dense” flows, with special emphasis on fluidized beds. Soo’s combined equations give some insights as to otherwise unaccounted for terms that ought to be included in whatever analytical solution is derived, but are of limited use due to the interface area issues, and the apparent applicability of many of his equations to dilute flow (with no indication as to their applicability to dense flows, such as experienced by dry chemical systems.)

**Ahmadi & Ma (1990a, 1990b)** presented a comprehensive general model of both compressible and incompressible turbulent solids/gas multiphase flows. The authors developed comprehensive global conservation laws for each phase, applying ensemble averaging to the integral form of the equations, and then applied the divergence theorem to develop local forms of the equations. Constitutive equations were also developed, with turbulence modeling similar to the k- $\epsilon$  model. Particle-particle collisions similar to previous work of the authors were included in the modeling. **Ahmadi & Ma (1990b)** described an application of the theory developed in **Ahmadi & Ma (1990a)**, examining the behavior in simple incompressible shear flows involving a “dense” mixture, comparing the results predicted by the theory favorably with experimental data.

A recent approach using a simplified composite mixture was used in **Chenoweth & Paolucci (1990)**. The authors derived equations to model the compressible flow of a gas/solids multiphase mixture between two finite volume vessels, based on earlier work by Chenoweth. While not the first model to incorporate compressible flow, it follows from **Heinrich (1942)** and **Tangren *et al* (1949)** in combining compressible flow

principles with a composite approach to modeling the gas/solids mixture. The mixture consisted of an ideal gas, and solid particles having constant density. Homogeneous equilibrium (constant solids mass fraction) two-phase mixtures were examined, and an isentropic expansion of the mixture gas in the source tank was assumed. Stagnation conditions in the tank(s) were assumed, with a connection between tanks with negligible length and volume. As part of the analysis, considerable discussion was devoted to the difficulty in determining the speed of sound in the mixture, and of the effect of the mixture (and its corresponding loading ratio) on the time to discharge a cylinder.

As Chenoweth & Paolucci note in their paper, the combination into a single mixture of two or more phased materials, with potentially non-uniform distribution of the phases, can make determination of the speed of sound complicated. Since, for a discharging system, the speed of sound is critical to determining flow characteristics throughout the system, it is crucial to have a meaningful formulation for the parameter. A number of other investigators besides Chenoweth & Paolucci, such as **Soo (1989)** have shown that, as a result of inertia of the solid particles, the speed of sound for a mixture is always less than that for a gas by itself. As a result, choking of a discharging mixture takes place at a lower velocity than for a discharging gas. Inasmuch as the gas portion of the mixture takes longer to discharge when part of a mixture, the time for a gas/solids mixture to discharge (as measured by the time it takes for the gas phase in the source cylinder to reach ambient) is longer than that for a gas-only discharge. A number of investigators have derived expressions for the speed of sound, many of which are only applicable to gas-liquid multiphase flows. **Marble (1970)** discussed limiting conditions and derived several expressions, all for dilute flows. **Heinrich (1942)** derived a

formulation for the speed of sound for a homogeneous mixture undergoing isentropic expansion. **Tangren *et al* (1949)** rederived the same expression, based on temperature, the mixture mass loading ratio, and the mixture volumetric loading ratio (the experimental work was done using a gas/water mixture.) Chenoweth & Paolucci use Heinrich and Tangren *et al*'s formulations of the speed of sound in a gas/solid mixture, described below. Soo's derivation resulted in a formulation that included the effects of turbulent dissipative processes, but excluded flow velocities, in the calculation of the speed of sound.

Chenoweth & Paolucci treat the gas as ideal (with compressibility factor  $Z$  equal to 1). The thermodynamic and physical properties of the gas/solid mixture were defined in a manner analogous to property definitions given by **Heinrich (1942)** and **Tangren *et al* (1949)**. These parameters were also used by **Rudinger (1965)** and by **Fan & Zhu (1998)** to define mixture properties in gas/solids multiphase flows. The model assumes 1) that particle sizes are small enough so that there is no thermal lag between particles and the surrounding gas – i.e., gas and particles are at the same temperature; and 2) the solid phase contributes nothing to the mixture (and gas) pressure. Rudinger determined that for the pressure contributions to be negligible (i.e., less than 1% of the pressure), that particle sizes must satisfy the condition

$$D \geq 0.0192 \left[ \left( \frac{d}{\rho_0} \right) \frac{(1-f)}{f} \right]^{-1/3} \quad (3.1)$$

where  $D$  is the particle diameter in microns,  $d$  is the particle density,  $\rho_0$  is the gas density at standard temperature and pressure, and  $\phi$  is the solid mass fraction. For a sodium bicarbonate mixture with nitrogen at 300 psig, 530 °R, with a particle density of 137.38



lbm/ft<sup>3</sup>, D is calculated as 0.0173 microns. Since the bulk of the particles in the solid agent mixtures examined in this research are in the 10.0 to 100.0 micron diameter range, the condition for treating the particle contribution to pressure is easily met for dry chemical systems.

The mixture density ( $\rho$ ) was defined as:

$$\rho = \left[ \frac{1-\phi}{\rho_G} + \frac{\phi}{\rho_d} \right]^{-1} = (1-\theta)\rho_G + \theta\rho_d \quad (3.2)$$

The particle volume fraction ( $\theta$ ) was related to the solid mass fraction by:

$$\theta = \phi\rho/\rho_d \quad (3.3)$$

The gas law for the carrier gas phase was:

$$P_G = Z_G \rho_G R_G T_G \quad (3.4)$$

The mixture gas constant ( $R$ ) was related to the carrier gas constant by:

$$R = (1-\phi)R_G \quad (3.5)$$

The mixture compressibility ( $Z$ ) was defined by:

$$Z = \frac{Z_G}{1-\theta} = \frac{1}{1-\theta} \quad (3.6)$$

The mixture gas law was

$$P = Z\rho RT \quad (3.7)$$

The lattermost equality resulted from the treatment of the carrier gas as ideal.

The mixture specific heat ratio ( $\gamma$ ) was defined as:

$$\gamma = \gamma_G \left[ \frac{1-\phi(1-\delta)}{1-\phi(1-\delta\gamma_G)} \right] \quad (3.8)$$

where  $\delta$  was

$$\mathbf{d} = \frac{c}{c_{PG}} \quad (3.9)$$

The mixture specific heat at constant pressure ( $c_p$ ) was

$$c_p = \mathbf{f}c + (1-\mathbf{f})c_{PG} \quad (3.10)$$

and the mixture specific heat at constant volume ( $c_v$ ) was

$$c_v = \mathbf{f}c + (1-\mathbf{f})c_{vG} \quad (3.11)$$

Chenowith & Paolucci noted that, if  $\delta \ll 1$  or  $\phi\delta \ll 1$ ,  $\gamma \rightarrow \gamma_G$ , while the mixture became isothermal ( $\gamma \rightarrow 1$ ) when  $\gamma_G \rightarrow 1$ ,  $\phi \rightarrow 1$  (as is the case for dry chemical systems), or  $\phi\delta \gg 1$ .

The mixture speed of sound ( $a$ ) was defined as

$$a = \frac{a_G}{(1-\theta)} \left[ \frac{\gamma}{\gamma_G} (1-\phi) \right]^{1/2} \quad (3.12)$$

where the adiabatic gas speed of sound ( $a_G$ ) was defined as

$$a_G = (\gamma_G R_G T_G)^{1/2} \quad (3.13)$$

Note that for dry chemical systems, where the solids density is generally much greater than the gas density,

$$(1-\mathbf{f})^{1/2} < (1-\mathbf{q}) \quad (3.14)$$

The impact on the mixture speed of sound can be seen by re-arranging equation (3.12) as:

$$\frac{a_G}{a} = \frac{(1-\mathbf{q})}{\sqrt{(1-\mathbf{f})}} \sqrt{\frac{\mathbf{g}}{\mathbf{g}_G}} \quad (3.15)$$

---

<sup>2</sup> Chenowith & Paolucci (1990), page 1050.

With the square root of  $\gamma/\gamma_G$  close to 1.0, the primary impact on the mixture speed of sound is the ratio between the solids volume fraction and the solids mass fraction. Since equation (3.14) generally holds for dry chemical systems, the result from equation (3.15) is that for dry chemical systems, the mixture speed of sound is less than the speed of sound for a gas-only discharge. As a result, discharges of solid/gas dry chemical mixtures will take longer than for gas-only discharges. Mach 1.0 is used as the choking point dimensionless velocity for the dry chemical discharge model developed herein. However, the mixture velocity at which Mach 1.0 is reached is lower than the velocity for a gas alone.

Chenoweth & Paolucci listed three isentropic relations for the gas and mixture:

$$T r_G^{-(g-1)} = C_1 \quad (3.16)$$

$$P r_G^{-g} = C_2 \quad (3.17)$$

and

$$P T^{-g/(g-1)} = C_3 \quad (3.18)$$

where  $C_1$ ,  $C_2$ , and  $C_3$  were constant values.

As noted in equations (3.8) and (3.12), Chenoweth & Paolucci's formulations for the speed of sound depended on characteristics of the individual phases in the mixture, and the relative amounts of each phase present. The relative amounts of solid and gaseous phases are represented by the solids mass fraction ( $\phi$ ), and indirectly by the solids volume fraction ( $\theta$ ), which in turn is also dependent on  $\phi$ . If the extreme case of  $\theta \rightarrow 0$  ( $\phi \rightarrow 0$ ) is considered, then the speed of sound  $a \rightarrow a_G$ , the speed of sound for gas alone. As noted earlier, particle inertia results in a slower speed of sound, resulting in

choking at a lower velocity, and thus a lower mass flow, than for a gas-only flow. As a result, as the levels of solids in the mixture increase (and the solids mass and volume fractions rise), the maximum velocity of flow through a choke point decreases, resulting in reduced volumetric flows, and ultimately in longer blow down times compared to gas-only discharges.

Chenoweth & Paolucci derived an equation for the discharge of a gas/solids mixture from a pressure vessel in terms of the solids particle mass fraction from a basic mass balance of flow out of the vessel. While their study involved flow from one vessel to another, the discharge mass balance equation is also applicable to discharges from a vessel to the surrounding environment. Their model has been adapted for this investigation. Special attention was given to dilute mixtures and isothermal modeling. No test data was presented to validate analytical findings.

The methodology suggested by **Ahmadi & Ma (1990a, 1990b)** was applied to gas/solids flow in a vertical duct by **Cao & Ahmadi (1995)**. Ahmadi & Ma's technique is applied in an isothermal, incompressible form to analyze turbulent flow using a two-equation low Reynolds number turbulence model. Both dilute and dense flows were analyzed, and solved using a semi-implicit finite difference technique, utilizing a time marching forward scheme and iterating from an initial guess until a steady solution is achieved. The governing equations were presented in numerical form, and the general solution steps were presented. Flow predictions were compared with pipe flow data in **Tsuji *et al* (1989)**, and **Miller & Gidaspow (1992)**. A model for gravity-driven high-loading flows was also developed; however, there was no experimental data for model validation. The particle sizes modeled and compared were in the millimeter range.

Conclusions reached by Cao & Ahmadi included:

“1. The fluctuation energies of gas and particulate phases strongly affect the behavior of two-phase turbulent flow.

2. In addition to the interaction momentum supply, the interaction fluctuation energy supply is important and must be accounted for in the analysis of two-phase flow.

3. For pressure gradient-driven two-phase gas-solid flows, the gas velocity is larger than the particle velocity. As a result the momentum is continuously supplied from the gas phase to the particulate phase. The effect of gravity is secondary and leads only to a small difference in the mean relative slip between particle and gas velocities (See Appendix 10.3.)

4. For a mass loading ratio of 0.6 or larger, the particulate fluctuation energy and its collisional production are important and affect the dynamic behavior of two-phase flows. ...

5. The gas phase velocity profile becomes more flat due to the presence of particles. The larger the mass loading ratio, the flatter the mean air velocity profile becomes. The particle velocity profile is generally flat in most of the duct and exhibits a large slip at the wall.

...

8. For both dilute and dense flows, the energy production of particulate and fluid phases is larger than their energy dissipation in most parts of the flow region except near the wall and channel centerline regions. There is a significant energy dissipation because of fluid-particle interactions.

...

10. The model reduces to the kinetic theory of granular material in the limit of dense collisional flows....”<sup>3</sup>

### **3.3 Solid Phase Influence on Pipe Friction – Drag Reduction.**

While there has been a great deal of industrial interest in multiphase flows as related to bulk transport of relatively “large” particles (greater than 100 microns in diameter), there has been little work done prior to the 1960’s to examine the behavior of pneumatically transported particles of 100 microns or less (**Babcock & Wilcox, Hawes et al (1964)**). While prior investigators found that pneumatic system efficiency increased with decreased particle size (with agglomeration effects limiting the minimum particle size), and smaller particles were more effective in heat transfer than large particles, research on the behaviors of small particle, multiphase gas-solids flows was limited in scope.

**Boothroyd (1966, 1969)** established a distinct flow regime for particle flows in the 1-100 micron range in the late 1960's and early 1970's. **Boothroyd (1966)** used an experimental apparatus to measure pressure drops in clear PVC, Perspex or glass tubes ranging from 1 to 3 inches in size, carrying a mixture of air and free-flowing zinc powder. Particle sizes were no larger than 40 microns in diameter, with the largest percentage of particles approximately 10-14 microns in diameter. The overall solids/gas mass flow ratios ranged between 0.1 and 17 inclusive (low for dry chemical systems), and Reynolds numbers were in the range  $10^4$  to  $10^5$ . Air flow rates ranged from 20 ft/sec for the 3-inch tubing, to a maximum of 140 ft/sec in the 1-inch tubing.

---

<sup>3</sup> **Cao & Ahmadi (1995)**, page 1225-1226.

One results from these studies was the observation of reduced drag for the 1-inch pipes, for load ratios ranging from approximately 0.5 to 2.0. For these relatively low solids/gas loading ratios, for pipe sizes in the range of dry chemical systems, the mixture friction factor tended to drop off, becoming less than the friction factor for gas alone. One implication of this reduction was the existance of a distinct minimum friction factor ratio, in the vicinity of loading ratios between 1 and 2.2 (the loading ratio is defined as the ratio of the mass of solids to the mass of gas in a give volume.) For loads above 2.0, friction increased, but at a lower level than would have occurred if the region with reduced friction had not occurred. There was also a distinct difference between the pressure drop experienced by a single-phase fluid and that experienced by a solids-gas mixture. The pipe friction factor was dependent in part on flow turbulence, which was influenced by the presence and quantities of particles in the gaseous carrier, with mixture friction factors significantly different from friction factors for gas alone. Both turbulent dissipation and generation (taking place near pipe walls) were affected.

Boothroyd's results also suggested that pipe flow losses were dependent on the pipe Reynolds number, the solids loading ratio, and time scale ratio (defined as  $= \rho_f D^2 / \rho_p d^2 Re$ , where  $\rho_f$  is the fluid density,  $\rho_p$  the solids density,  $D$  the tube diameter, and  $d$  the particle diameter.) The dependence on Reynolds number was weaker than the dependence on loading ratio or time scale ratio. Furthermore, while some electrostatic effects were noted, these were limited in extent, due to a buildup of a layer of particles on the inside tube surfaces, resulting in eventual interior tube surfaces identical in composition to the solids being transported.

A plotting of data from Boothroyd's research, with additional data from other investigators, suggested that the presence of small particles (100 microns or less in diameter) has a significant influence on pipe/mixture friction. Friction was influenced by mixture turbulence, which in turn was influenced by the presence of particles. Hestroni (discussed below) examined the influence of particle size on mixture turbulence. Research by **Ewing *et al* (1989, 1992, 1994, 1995)** has since shown that dry chemical agents are most effective in extinguishing fires at particle sizes less than 100 microns. The maximum particle size at which an agent is at its maximum effectiveness varies with differing agents, but all maximum sizes are less than 100 microns. The results of the Boothroyd's studies indicated that dry chemical system models cannot treat either of the two phases as having any kind of behavior independent of the other phase. (One example would be the one-way model, in which the fluid influences particles, but particles do not influence fluid behavior. Another example: for solids with particle sizes greater than 100 microns, losses for each phase can be calculated separately, and added together. This is not possible for solids with particle sizes less than 100 microns.) Furthermore, to correctly calculate pipe flows, a determination must be made of how the pipe friction factor changes with the addition of the solids. Boothroyd's dimensional analysis suggested the primary influence on friction factor of the loading ratio and time scale, with a lesser influence by the Reynolds number.

In a later publication, **Boothroyd (1969)** used momentum and heat transfer equations to determine dimensionless parameters that could be used to correlate experimental data. The intent of the work described was to develop a small set of dimensionless parameters, since conventional dimensional analyses yielded a set of eight



parameters, too large a set for correlation purposes. For fine particles the previously developed set of parameters (Reynolds number, loading ratio, and time scale ratio) were found to assure kinematic and dynamic similarity of the particles. By writing an equation for two systems, one defined in terms of simple ratios to the other system, dimensionless parameters of importance to the correlation of experimental data were determined. Particle interactions were ignored. Evaluation of these equations confirmed the dependence of frictional pressure drop on the aforementioned set of parameters. Boothroyd found that while relatively large particles had little influence on turbulence generation at the walls, small particles tended to follow large eddy motion, and stabilize the smaller eddies. As a result, for solids with particles less than 100 microns in diameter, such as dry chemical systems, pipe frictional pressure losses from the solids and gaseous portions of the flow cannot be assessed separately and added together. Interactions between particles and the gaseous flows must also be included in the analysis. Boothroyd also determined that relevant parameters for frictional momentum transfer in a pipe for fine particles should include electrostatic charges (the exact influence of charges depends on system grounding and frequency /regularity of usage). Further issues include two-phase flow turbulence mechanics, particle agglomeration, and electrostatic charge transfer at separating surfaces. For instance, agglomeration effects, to which fine particles are particularly prone, will affect the average particle size, and thus mixture flow properties. Boothroyd further commented that if consideration of particle collisions and cohesion become important in an analysis, that some of his findings might not be applicable to the analysis.

**Choi & Chung (1983)** analyzed incompressible gas/solids multiphase pipe flow in wall-bounded turbulent pipe flow to determine the influence of the solid particle phase on mixture velocity and the friction encountered in a pipe. Their work, built on the work of several previous investigators, was intended to be an analytical approach to estimating the effect of multiple phases on turbulent flow behavior in pipes. It was further intended to extend mixing length theory to being capable of calculating turbulent flow for gas/solids mixtures at low loading ratios, and relatively small particle sizes.

**Abramovich (1971)** assumed that the solids, by exerting drag on the fluid phase, reduce the turbulent fluctuating velocity. His results showed that finer particles had a greater effect on decreasing turbulence than relatively coarse particles, consistent with the results of **Sharma & Crowe (1983)**. However, his formulation of the ratio of stress in a mixture to that of stress in a single fluid,

$$\frac{\Gamma}{\Gamma_0} = \left( 1 + \frac{\bar{r}_p}{\rho} \right)^{-1} \quad (3.19)$$

was found by **Melville & Bray (1979)** to be inconsistent.

**Owen (1969)** estimated the ratio of turbulent energy dissipation in a mixture of fluid and fine particles to the dissipation for a single fluid alone to be

$$1 + \frac{\bar{r}_p}{\rho} \quad (3.20)$$

where  $\bar{r}_p$  was the mass of particles per unit volume, and  $\rho$  was the fluid density (i.e., so that the ratio

$$\frac{\bar{r}_p}{r} \tag{3.21}$$

was the loading ratio.)

Choi & Chung developed a model of the influence of solid particles on a multiphase mixture in turbulent pipe flow, extending and modifying a gas/solids turbulent round jet model developed by **Melville & Bray (1979)**. Choi & Chung applied their analysis to a scenario of turbulent multiphase pipe flow. Their analysis is based on a “two-fluid” model, treating the particles as a hypothetically continuous fluid (“secondary” fluid), intermixed with the gaseous phase (“primary” fluid). Choi & Chung developed new virtual laminar and eddy viscosity models, and numerically integrated their equations to obtain velocity profiles and skin friction factors. Results compared favorably with experimental data from **Boothroyd (1966)**. Reynolds-averaged mass and momentum balance equations were developed in cylindrical coordinates, using the assumption that particle sizes were small enough, and gas velocities fast enough so that the mean velocity of the particles was approximately equal to that of the gas. The equations were closed at the first order level using Boussinesq eddy viscosity models. Interactions between particles and fluid were accounted for in the models for the eddy viscosities of the primary and secondary fluids, and the laminar kinematic viscosity of the secondary fluid.

Choi & Chung compared their analytical formulations to test data from several investigators. Comparison of their results to those of **Melville & Bray (1979)** and **Boothroyd (1966)** are shown in Figure 3.1.

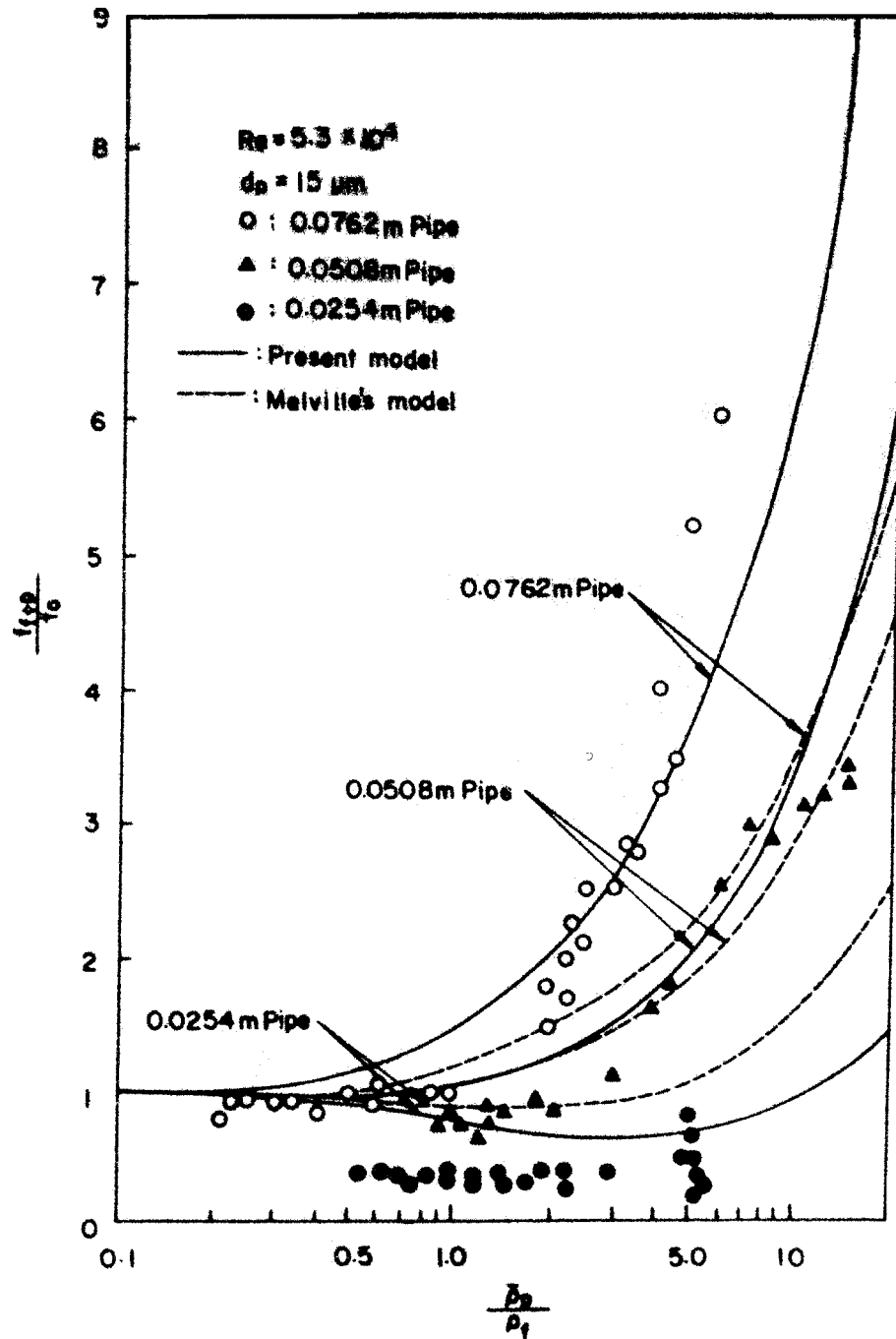


Figure 3.1 Comparison of Choi & Chung Analyses with Results of Melville & Bray Analyses and Boothroyd Data.

Results were generated for 1- (0.0254 m), 2- (0.0508 m) and 3-inch (0.0762 m) pipes, with a pipe-based Reynolds number of  $5.3 \times 10^4$ , and zinc powder with average diameters

of 15  $\mu\text{m}$  diameter. While the results were generally better than those of Melville & Bray, the model over-predicts the 3-inch pipe data by about 3%, and the 1-inch pipe is underpredicted by about 5%. Choi & Chung's model showed the same tendency towards drag reduction noted by the experimental results of Boothroyd, for small load ratios and pipe diameters.

Choi & Chung also compared their analytical results to those predicted by Melville & Bray using data from **Barth (1962)**, plotting the mixture friction factor versus the square root of Froude number, on a logarithmic scale. Results in these circumstances show an excellent correlation between Barth's data and the Choi & Chung model, and almost no correlation whatsoever to the Melville & Bray model.

Choi & Chung further compared the interaction of particles with turbulent flow, finding that for a given Reynolds number and loading ratio, the predominant source of additional wall friction in the flow was due to particles in the 15-micron diameter and less size range. They also noted that an increase in pipe diameter had a similar effect to reduction in particle diameter, so that the ratio of particle size to pipe diameter (a dimensionless parameter), rather than just pipe diameter itself, might be a better way to represent friction factor variation, rather than pipe diameter alone.

Velocity profiles showed variations as a function of loading ratio for two different pipe sizes. Three-inch pipes showed virtually no change in velocity across the pipe diameter for loadings ranging from zero (gas alone) to 20. For the 1-inch diameter pipe, centerline velocities increased by 1.4 ft/sec when the load ratio increased from 0 to 20, while wall velocities decreased by as much as 4 ft/sec for the same change in solids loading. Particle/particle interactions were not accounted for in this model, and the

concentration of particles in the mixture was assumed uniform over the cross-sectional area of the pipe.

Results of Choi & Chung's analyses suggested that the mixture laminar kinematic viscosity of the solid phase is implicitly a function of the gas Reynolds number, relative particle size, and loading ratio. They observed that 1) the mixture friction factor increases as the ratio of particle size to pipe diameter decreases, 2) if the relative particle size is large and the loading ratio low, the mixture friction factor can be smaller than that of the gas alone (consistent with Boothroyd's observations), and 3) friction factor augmentation is logarithmically linear with the Froude number. Note that, particularly for the third observation, that flows were relatively dilute; the observed relations may not hold for a dense mixture of solid particles and gas.

The pipe flow analyses of **Choi & Chung (1983)** were further extended by **Chung *et al* (1986)**, whose analysis of turbulent dilute gas/solids flow in a Venturi tube assumed negligible relative velocity between the solids and gaseous phases. **Chung *et al*** argued that in developing flows, the relative velocity is not zero, and that the time scale ratio varies dependent on location; thus Stokesian drag is important and must be accounted for. Their model extended the incompressible two-fluid model of **Choi & Chung (1983)**, with relative velocity and turbulent kinetic energy budgeting. While **Chung *et al*** retained the secondary fluid (solids) kinematic eddy viscosity proposed by **Choi & Chung**, for the primary fluid (gas) kinematic eddy viscosity, they used the model of **Elghobashi & Abou-Arab (1983)**, derived from a  $k$ - $\epsilon$  energy balance. Numerical computations utilized the forward marching technique of **Patankar & Spalding (1967)**.

Chung *et al* claimed that the advantages of their technique over particle trajectory models, such as the PSI-Cell model of **Crowe *et al* (1977)** include:

- not needing empirical information about interactive momentum and energy exchanges between fluid and particles.
- having momentum wall friction losses naturally incorporated into the computations.
- having more detailed information about particles in the flow fields, easier extension to multi-dimensional recirculating geometries.
- easier extension to more sophisticated turbulent energy modeling such as k- $\epsilon$  modeling, or algebraic Reynolds stress modeling.

The modeling in this paper included flows with particle diameters in the 1-80 micron range, with loading up to a ratio of 7. Comparisons with analytical results were made with data from several investigators. Comparison of predicted pressure drops between the CONVAS predictions of **Sharma & Crowe (1978)** and the Chung *et al* model showed good agreement for a loading ratio of 1 for particles in the 10-80 micron diameter range, and for a loading ratio of 2, in the 30-80 micron diameter range. Comparisons of the predicted pressure drops of CONVAS and the current model with experimental data of **Farber (1953)** show excellent agreement between the data and predictions of the two models for loading ratios up to 5, with good agreement for ratios from 5 to 7. A comparison of pressure drops for loading ratios from 0 to 1.6 between CONVAS, the present model, an equilibrium flow model, a two-dimensional model of Lee & Crowe, and experimental data from **Lee & Crowe (1982)** shows Chung *et al*'s model comes closest to matching Lee & Crowe's data (with Lee & Crowe's two-dimensional model also coming very close.) As a result, the combination of the k- $\epsilon$

primary fluid eddy viscosity model of Chung *et al*, combined with the secondary fluid (solids) eddy viscosity model of Choi & Chung gives a good fit to experimental data for relatively dilute flows.

**Michaelides (1984)** treated the gas/solid mixture as a single-phase incompressible fluid with variable time-averaged local density. A one-dimensional isothermal model using the Navier-Stokes equations in cylindrical coordinates was developed. For more or less constant boundary conditions, two length scales are present, one significantly longer than the other. Since changes in the fluid properties in the longitudinal direction are more gradual than in the transverse direction, most derivatives in the longitudinal direction, with the exception of the pressure differential, were neglected. As a result, the flow is treated as one-dimensional, with flow in the axial direction. The analyses assumed a vertical pipe; the main difference between that and a horizontal pipe is in the body force term carried in the vertical pipe equation. Particle/particle and particle/wall interactions were not included in the model, which was developed for steady state conditions. As part of the analyses, Michaelides develops a two-phase friction factor, based on flow conditions, including the Froude number based on the shear velocity. Michaelides's model represents, with the addition of particle interactions, possibly the simplest model that could be developed for a field model approach.

As part of his analysis, Michaelides defines the average velocity and mass flux in a pipe flow as:

$$\bar{u} = \frac{2}{r_0^2} \int_0^{r_0} ur \, dr = V^* I_1 \quad (3.22)$$

and



$$G = \frac{2}{r_0^2} \int_0^{r_0} u r r dr = V^* r_G I_2 \quad (3.23)$$

where  $V^*$  is the shear velocity, defined by

$$\mathbf{t}_w \approx \mathbf{t}(y_0) = \mathbf{r}_G V^{*2} \quad (3.24)$$

where  $y_0$  is the width of the viscous sub-layer, which is very small in comparison to the pipe radius  $r_0$ . With some manipulation, the integrals  $I_1$  and  $I_2$  are:

$$I_1 = -\frac{1}{r_0^2} \int_0^{r_0} \frac{du^*}{dr} r^2 dr \quad (3.25)$$

and

$$I_2 = -\frac{1}{r_0^2} \int_0^{r_0} \frac{d(u^* r^*)}{dr} r^2 dr \quad (3.26)$$

where  $u^* = u/V^*$ , and

$$\mathbf{r}^* = \mathbf{r}^*(\mathbf{h}) = (1 + \mathbf{g} e^{h-h_0})^m \quad (3.27)$$

where  $\gamma$  and  $m$  are functions of the total solids concentration, with  $m$  a weak function of the concentration, varying between 0.4 and 0.6.  $\eta$  is a boundary layer coordinate, defined as  $\eta = \ln(y/y_0)$ . Michaelides defines a superficial velocity for the gas as

$$V_G^s = \frac{\dot{m}_G}{r_G A} \quad (3.28)$$

where  $A$  is the cross-sectional area of the pipe. He also defines the Froude number as

$$F^* = \frac{V^*}{\sqrt{g r_0}} \quad (3.29)$$

and the discharge density  $\rho_d$  as  $\rho_G I_2 / I_1$ . Using the Fanning equation and equation (3.25)

and (3.26), the following results:

$$\frac{dp_f}{dz} = \frac{2f \mathbf{r}_d \bar{u}^2}{D} = \frac{2f \mathbf{r}_G V^{*2} I_1 I_2}{D} \quad (3.30)$$

The wall shear stress  $\tau_w$  is

$$\mathbf{t}_w = \frac{1}{4} \frac{dp_f}{dz} D = \frac{1}{2} f \mathbf{r}_G V^{*2} I_1 I_2 \quad (3.31)$$

with the friction factor  $f = 2/I_1 I_2$ . A friction factor  $f_m$  is defined based on the work of other investigators, such as **Pfeffer et al (1966)**:

$$\mathbf{t}_w = \frac{1}{2} f_m \mathbf{r}_G (V_G^{s2}) \quad (3.32)$$

where  $f_m$  is described as the factor yielding the same shear  $\tau_w$  with the multiphase system when multiplied by the kinetic energy of the gas phase if that phase were alone in the pipe. Equating equation (3.31) with equation (3.32) and using the relationship between  $f$  and  $I_1$  and  $I_2$ , the result is:

$$f_m = f \left( \frac{V^*}{V_G^s} \right)^2 I_1 I_2 = 2 \left( \frac{F^{*2} r_0 g}{V_G^{s2}} \right) \quad (3.33)$$

Thus, as with Choi & Chung, Michaelides calculates a mixture friction factor based on flow conditions and the Froude number.

**Doss & Srinivasan (1986)** discussed the calculation of the wall friction factor for gas solid mixtures. Expressions for particle/wall friction for both single and multiple species of solids in a gas carrier in terms similar to those for gas/wall friction were reported.

The approach used by Doss & Srinivasan was to work through the conservation of momentum equation for one-dimensional flow along a horizontal axis of particles of a given solid species, and a mixture of gas and one or more types of solid particles. The

wall stress variables for the two momentum equations were  $\tau_{w-pi}$ , and  $\tau_{w-pg}$  for the single species and full mixtures, respectively. The shear stress for a single species is

$$\mathbf{t}_{w-pg} = \mathbf{f}_p \mathbf{t}_{w-p} + (1 - \mathbf{f}_p) \mathbf{t}_{w-g} \quad (3.34)$$

where  $\phi$  is the solids volume fraction, and

$$\mathbf{t}_{w-g} = \frac{1}{2} f_g \mathbf{r}_g u_g^2 \quad (3.35)$$

$$\mathbf{t}_{w-p} = \frac{1}{2} f_p \mathbf{r}_p u_p^2 \quad (3.36)$$

and

$$\mathbf{t}_{w-pg} = \frac{1}{2} f_{pg} \mathbf{r}_g u_g^2 \quad (3.37)$$

with  $f$  being the friction factor.  $f_{pg}$  is an equivalent friction factor yielding the shear stress  $\tau_{w-pg}$  for the mixture when multiplied by the kinetic energy of the gas alone.  $f_g$  is assumed to be the same as for a gas-only situation, with differences caused by changes in the turbulent structure accounted for in the particle-wall stress term.

The eddy viscosity approach suggested by **Julian & Dukler (1965)** found a simple relation for dilute-phase transport:

$$\frac{f_{pg}}{f} = (1 + Z)^{0.3} \quad (3.38)$$

where  $Z$  is the solids/gas loading ratio.

A relation based on application of the Reynolds analogy, recognizing the analogous behavior of momentum and heat transfer rates, can be applied if the mixture is assumed to behave as a homogeneous fluid, and an accurate relation for the heat transfer

coefficient of the mixture is available. **Pfeffer *et al* (1966)** presented the following relation for dilute flows:

$$\frac{f_{pg}}{f_g} = 1 + 4.0(R_N^{-0.32})Z \quad (3.39)$$

where  $R_N$  is the gas Reynolds number.

Due to the complexity and variability of phenomena involved in gas/solids flows, it was suggested by **Rose & Barnach (1957)** that the mixture friction factor could be a function of non-dimensional variables. The empirical relation they developed was:

$$f_{pg} = f_g + bZ \quad (3.40)$$

where

$$b = \frac{\rho}{8} \left( \frac{r_p}{r_g} \right)^{1/2} \psi \quad (3.41)$$

with  $\psi$  a function of Reynolds number. However, there has been considerable disagreement on the value of  $\psi$ .

Testing was planned to validate the calculations, determining by collection of velocity and pressure drop data which of the approaches and friction stress formulas fit the data best.

Given the results of previous investigators, indicating a dependence on Reynolds number, solids loading and the time scale, for the current modeling effort, the Reynolds analogy was tentatively selected as a means of altering the gas-only friction factor to account, to some extent, for effects of the solid phase in the mixture during discharge. However, there is presently no analyses or experimental data to validate the selected model for use for dense, high velocity flows.

**Hestroni (1989)** discussed the interactions between particles and turbulence, comparing the levels of turbulence to relaxation time (the time to accelerate a particle at rest to within approximately 63% of the fluid's velocity) and particle sizes. Hestroni examined data from **Ruck & Makiola (1989)** (among others), finding a clear distinction between fluid responses to particles based on particle size. The particle relaxation time, the time for a particle at rest to be accelerated to ~63% of the fluid velocity, is calculated as

$$t^* = \frac{d^2 \rho_p}{18 \nu_f \rho_f} \quad (3.42)$$

where  $\nu_f$  is the fluid kinematic viscosity,  $d$  is the particle diameter,  $\rho_p$  is the particle density, and  $\rho_f$  is the fluid density. This formulation is strictly correct only in the Stokes regime, where  $Re_p < 1$ ; for larger Reynolds numbers, the drag coefficient is larger than predicted by Stokes' Law, resulting in overpredictions of relaxation time using this formulation. The turbulent eddy characteristic time is calculated as:

$$t_e = \frac{l_e}{u_e} = \frac{2p}{\tilde{k} u_e} \quad (3.43)$$

where  $l_e$  is the eddy characteristic length,  $u_e$  is the eddy characteristic velocity, and  $\tilde{k}$  is the wavenumber. Particles with relaxation times smaller than the turbulent eddy characteristic time did not contribute to the overall turbulence, and tended to increase the rate of turbulent energy dissipation. Particles with relaxation times greater than the eddy characteristic time tended to increase turbulence, by vortex shedding of the particles, thus removing more of the available energy in the system to create the additional turbulence.

. Hestroni defined a particle Reynolds number as:

$$\text{Re}_p = \frac{(u_f - u_p)d}{\mathbf{n}_f} \quad (3.44)$$

where  $u_f$  is the fluid velocity, and  $u_p$  is the particle velocity, such that when this value is relatively small (less than 110), no vortex shedding occurs, whereas for larger values, shedding always occurred, with a transition range between the two extremes where some shedding could occur. Experimental data from **Tsuji & Morikawa (1982)** found that for “small” particles, with  $d = 200 \mu\text{m}$  and  $\text{Re}_p \approx O(0.10)$ , mainstream turbulence was always suppressed. In situations with “large” particles, with  $d = 300 \mu\text{m}$  and  $\text{Re}_p \approx O(1000)$ , mainstream turbulent intensity was always increased. Effects were mixed for particles with  $d = 500 \mu\text{m}$  and  $\text{Re}_p \approx O(100)$ , with turbulence towards the centerline of the pipe increased, and decreased close to the pipe walls. As a result, the particle Reynolds number is useful in determining whether a given particle size dissipates or increases turbulence. Note that Hestroni’s discussions were not particularly directed towards pressurized blow down systems. In the case of dry chemical systems, the experimental data discussed in Sections 7.0 and 8.0 show a decrease in flow rate, based on the blow down time, with the introduction of powder, and as the mass of powder in the cylinder increases, for approximately the same initial pressurization. A rough calculation of the particle Reynolds number for typical dry chemical systems, using powder data and assuming powder flow lagging in velocity only by approximately 1 foot per second, results in a calculated  $\text{Re}_p$  of  $\sim 2440$ . This is in the range where the particles can be expected to increase turbulence, thus removing more useful energy from the blow down than gas alone would be expected to remove. The difference in particle and gas velocities has to be less than 0.1 foot per second to approach the range where the particles would

tend to reduce turbulence. The experimental data shows a significant increase in blow down time (and corresponding reduction in flow rates) with the addition of powder to the cylinder. .

Hestroni also discussed the experimental data of **Tsuji & Shiomi (1984)**, which showed a distinct difference in flow and turbulence effects based on the relative particle loading of the mixture. Tsuji & Shiomi used plastic spheres of 3 mm diameter in air, with loading ratios of 0.6, 2.3, and 3.4 (mass fractions of 0.375, 0.697 and 0.773 respectively). Some of the results are summarized in Table 3.1.

Loading Ratio (Solids mass fraction)	0 (0)	0.6 (0.375)	2.3 (0.697)	3.4 (0.773)
Relative Velocity (m/s)	-	7.4	6.2	5.9
Particles' Velocity (m/s)	-	4.7	5.3	6.0
Particle Reynolds Number $Re_p$	-	1388	1164	1106
Drag on a particle ( $N \times 10^5$ )	-	10.3	7.2	6.5
Energy spent on particle drag ( $J \times 10^3$ )	-	5.6	12	13
Energy dissipation of turbulence ( $J \times 10^3$ )	20	40	50	71
Excess dissipation of turbulence ( $J \times 10^3$ )	-	20	30	51

**Table 3.1 Effect of particles on turbulence (data from Tsuji & Shiomi (1984), presented in Hestroni (1989)).**

Drag was calculated using a drag coefficient of 0.45. Energy calculations were based on transport of particles through a unit length of pipe. The relative velocity is the difference between particle and gas velocities. The “excess dissipation” is the amount of energy dissipated by turbulence due to the presence of the solid particles, above the amounts of energy dissipated in the gas-only flow. As can be seen in the Table, the concentration of particles in the mixture can have a significant impact on flow and energy characteristics

of a discharging mixture, even for relatively dilute mixtures. As the particle concentration increases, the particle Reynolds number decreases, resulting in a relative decrease in turbulent intensity, and an increase in the energy taken up by the turbulent flow.

**Han *et al* (1991)** continued the work described in **Choi & Chung (1983)** and **Chung *et al* (1986)**. The authors here applied Lumley's drag reduction model (**Lumley (1976)**) to a two-fluid pipe compressible flow model similar to those described in **Choi & Chung (1983)** and **Chung *et al* (1986)**. Lumley had suggested that "...because particles have inertia, they cannot follow the smallest scale motions of the turbulence,"<sup>4</sup> resulting further in increased losses in the fluid phase due to differences in motion of the two media, resulting further in damping of small scale turbulence and increasing the viscous sublayer thickness. Lumley further noted that there was also a counterbalancing effect, resulting in the decrease in drag occurring over only a narrow range of loadings. On the basis of these observations, Lumley developed a drag-reduction model which was tested by **Han *et al* (1991)**, with the analytical results compared to previously described data gathered by **Boothroyd (1966, 1969)**. The analysis here did not include interparticle collisions, and used a relatively dilute mixture. The solution technique implemented the same forward marching approach used by **Chung *et al* (1986)**, developed by **Patankar & Spalding (1967)**.

The results of Han *et al*'s analysis agreed well with the experimental data of **Boothroyd (1966)**. For loading ratios from 0.1 to 10, there was good agreement between Boothroyd's mixture friction factor data, pressure drop data, and Han *et al*'s model. The

---

<sup>4</sup> **Han *et al* (1991)**, page 130.



model matched well the dip in the friction factor due to drag reduction phenomena (and pressure drop) for the 1-inch diameter pipe, and generally matched test data well for 1, 2 and 3-inch ID pipes. The principal factors Han *et al* found to be contributing to viscous sub-layer thickness were the particle relaxation time, Kolmogoroff time scale, and the loading ratio. For relatively small particle sizes, particle distribution across the pipe radius are more even at loading ratios up to 10, than for lower loading ratios. One consequence of this is generally larger particle concentrations near the wall for “high” loading ratios. An exception to this is at the loading ratio of 1.0, where the particle concentration drops off the farther from the centerline one goes, only to increase dramatically close to the wall. Han *et al* were not able to explain this phenomenon. Han *et al* also noted that, as the ratio of particle diameter to pipe diameter increased, drag was reduced significantly. As a result, one could select a combination of loading ratio and the ratio of particle diameter to pipe diameter to maximize drag reduction. The authors further noted that as particle sizes decreased, and the loading ratio increased, the pressure drop due to gravity became a predominant factor in the overall pressure drop.

Results by Hestroni and other investigators have suggested that the exact impact of particles in the mixture depends on solids loading and particle size. Later work by **Hishida *et al* (1992)** independently confirmed these findings. Hishida *et al* experimented with sheer between two parallel flows of differing velocities, creating a mixing layer between the two flows. Glass particles with diameters of 42, 72, and 135  $\mu\text{m}$  were used, with the two flows at 4 m/s and 13 m/s. A three-beam laser Doppler velocimeter was used for simultaneous two-component measurements of the solid and gas phases. As Hestroni suggested, Hishida *et al* found that the ability of particles to follow the turbulent

motion of the fluid phase (i.e., whether the particles would add to or reduce turbulence) depended on the ratio of particle relaxation time to the eddy characteristic time scale. Ratioing the two results in the dimensionless Stokes number ( $St$ ). Hishida *et al* found that for the  $St > 4$ , particle motion is independent of the fluid turbulent flow, and that particle dispersion was almost completely unaffected by the turbulence. In the range of  $2.5 < St < 4$ , particle eddy diffusivity increases rapidly with decreasing Stokes number. For  $0.5 < St < 2.5$ , particles tend to disperse more rapidly than what would be expected from the turbulence alone. These results correspond to those reported by Hestroni, where the larger Stokes number, corresponding to larger particle sizes, tend to increase turbulence, whereas situations with Stokes numbers  $< 1.0$ , corresponding to smaller particles, tend to dissipate turbulence.

Drag reduction phenomena is discussed in some detail in **Fan & Zhu (1998)**. The effect of this reduction of drag and friction for load ratios between 0.5 and 2.0, increasingly pronounced as pipe diameters reduce below 3 inches ID, for particles of 200  $\mu\text{m}$  or less is quite pronounced, and has been noted by a number of investigators, as noted above. The causes of the phenomena are not clearly understood, but seem to be linked to a number of factors associated with particle motion near the pipe walls, including particle spin, deposition, agglomeration, and electrostatics. While drag reduction manifests itself for dilute flows, it must be accounted for in the mathematical representation of mixture friction to allow for correct calculation of mixture friction at higher loads. Fan & Zhu offer a formulation for the ratio of wall shear stress for mixtures to wall shear stress for gas alone for dilute flows (where the averaged distance between particles is 10 particle diameters or more):

$$\frac{f_{pg}}{f_g} = 1 + \frac{4m_{dot}}{f_g \sqrt{\rho}} \frac{\sqrt{u'^2}}{U} \left[ 1 + \frac{\text{Re}}{7.2} \frac{r_p}{r_g} \frac{d_p}{D_d} \frac{\sqrt{u'^2}}{U} \right]^{-1/2} \quad (3.45)$$

where  $\tau_{gp}$  is the wall shear stress for the gas phase,  $\tau_{wp}$  is the shear stress of the solid phase (the two stress treated as additives in the momentum balance equation),  $m_{dot}$  is the mass flux ratio of particles to gas ( $=(\rho_p/\rho_g)(\theta/(1-\theta))$ ),  $(\sqrt{u'^2})/U$  is the turbulence intensity (in percentage points, usually taken as approximately 5%), Re the Reynolds number based on pipe diameter  $D_d$  and averaged flow velocity  $U$ ,  $f$  the gas-alone friction factor,  $d_p$  is the particle diameter,  $\rho_p$  is the particle density, and  $\rho_g$  is the gas density.

### 3.4 Pipe Network Components.

While the bulk of the research to date has been on straight lengths of pipes, some work has been done exploring gas/solids behaviors in other fixtures as well. **Morikawa et al (1978a)** examined experimentally flow behaviors through circular and elliptical pipe bends. Nearly circular polyethylene pellets with a mean diameter of 1.1 mm with loading ratios up to 8 were used, and air velocities ranged from 18 to 29 m/s. Experimental runs were made using piping of 40 mm ID, with an “experimental” bend (circular or elliptical) made of vinyl chloride. The test unit consisted of two straight lengths of pipe, with the test bend in between, with numerous holes in the straight portions, used to measure static pressure. Measurements for gas-only and loaded mixtures were made. The difference in pressure across a bend for the gas-only runs established the pressure loss for the gas phase, while the pressure drop for a given load, minus the pressure drop for the gas alone, gave the pressure loss for the solids in the mixture. Total losses were determined by the calculation of losses without particles and particles separately, and adding the results.

Results for the gas-only runs for circular bends compared well with empirical formulations developed by **Ito (1960)** for water flow:

$$z_a = 0.248a \left( \frac{R}{r} \right)^{0.9} / \text{Re}^{0.2}, \quad \text{Re}(r/R)^2 < 91 \quad (3.46)$$

$$z_a = 0.217a \left( \frac{R}{r} \right)^{0.84} / \text{Re}^{0.17}, \quad \text{Re}(r/R)^2 > 91 \quad (3.47)$$

where R is the radius of curvature of the bend, and  $r = D/2$ , the inside radius of the pipe.  $\zeta_a$  is the pressure loss coefficient for air (or gas) with no particles ( $= \Delta p_{ba}/(0.5 \rho u^2)$ ) in a circular bend, where  $\Delta p_{ba}$  is the pressure drop in the bend,  $\rho$  is the air density, and  $u$  the mean air velocity. ( $\zeta_s$  is the corresponding pressure loss coefficient due to the particles ( $= \Delta p_{bs}/(0.5 \rho u^2)$ ) in a circular bend). Morkiawa *et al* proposed that  $\zeta_s$  be calculated by

$$\frac{z_s}{I_s} = \frac{1.5 \times 10^4}{Fr \left( \frac{R}{r} \right)^{0.2}}, \quad Fr > 30$$

where Fr is the Froude number, and  $\lambda_s$  is the pressure loss due to the solids, in a straight pipe, and

$$\frac{z_s}{I_s} = 165 (R/r)^{-0.15} \quad (\text{As proposed by Schuchart (1968).})$$

$\alpha$  is defined as

$$a = 0.95 + 17.2 (R/r)^{-1.96}, \quad R/r < 19.7 \quad (3.48)$$

$$a = 1, \quad R/r > 19.7 \quad (3.49)$$

For elliptical bends, good agreement was found if the radius of curvature R was replaced by the bend length divided by the turning angle (here =  $\pi/2$ .)

For a straight length of pipe, Morikawa *et al* found the following empirical formulations for friction factor of the solids contribution to the pressure loss as follows:

$$\text{Upstream of the bend: } I_s = (1.51 + 1.69n) \times 10^{-3} \quad (3.50)$$

$$\text{Downstream of the bend: } I_s = (2.06 + 1.75n) \times 10^{-3} \quad (3.51)$$

where  $n$  is the loading ratio (ranging from 0 to 8 in the experimentation), and  $\lambda_s$  is the solids friction factor, defined through the equation for the total pressure drop,  $\Delta p = \Delta p_a + \Delta p_s$ , with

$$I_a = \frac{\Delta p_a}{\Delta L} \bigg/ \frac{\rho u^2}{2D} \quad (3.52)$$

$$I_s = \frac{\Delta p_s}{\Delta L} \bigg/ \frac{\rho u^2}{2D} \quad (3.53)$$

$\rho$  is the air density,  $\Delta L$  is the pipe length over which  $\Delta p_a$  or  $\Delta p_s$  is measured,  $u$  is the air velocity, and  $D$  is the pipe ID.

Based on experimental results, Morikawa *et al* proposed the following empirical equation for the solids friction factor in a circular bend:

$$\frac{z_s}{I_s} = \frac{1.5 \times 10^4}{F_r (R/r)^{0.2}}, \quad F_r > 30 \quad (3.54)$$

with  $\lambda_s$  the value for the straight pipe upstream of the bend. As with other investigators, the solids friction factor here was found to be a function of the Froude number.

Morikawa *et al* also noted that the numerator is dependent in part on properties of the solid particles, such as the terminal velocity; however, limitations of the described work to only one kind of particle made a determination of the relationship of the numerator to these factors impossible as of the writing of the paper.

Results for the elliptical bend resulted in an almost identical empirical equation to equation (3.54). The best results were found substituting the radius of curvature of the short radius, rather than either the radius of curvature of the long radius, or the ratio of bend length to turning angle, for the radius of curvature  $R$  in equation (3.54).

The behavior of gas/solids flows in branches was examined by **Morikawa *et al* (1978b)**. Particles 1.1 mm in diameter were investigated, with load ratios no greater than 7, and mean air velocity of the incoming length of pipe was 22 m/s. The apparatus consisted of straight lengths of 41 mm ID piping, with a single branch; the angles of the branches relative to the incoming single pipe were variable. Numerous holes for static pressure taps were present in each straight length of pipe. Results of the experimentation found that the solids contribution to the pressure drop in a branch depended in part on the ratio of flow through the particular downstream branch to the flow from the pipe upstream of the branch, and the angles of the pipes downstream of the branch. If one downstream branch continues straight, while the other pipe is at some angle, for flow ratios of 0.72 and less, the solids contribution to the pressure loss is actually negative. In these situations, while the gas velocity slows as it passes through the branch, inertia carries particles along the “straight” downstream branch, resulting in the particles working to increase gas velocity, and slowing down themselves. For flow ratios close to 1.0, the solids contribution to pressure loss is positive, but close to zero – flow velocity and direction are unchanged in this situation.

Solids distribution in the pipes downstream of the branch were found to be independent of both the flow ratio, and the loading ratio in the upstream pipe. A direct relationship, however, was found between the distribution of powder in the branch piping

downstream of a branch and the ratio of the projected area of the downstream pipe at the branch point onto the plane vertical to the axis of the upstream pipe, which in turn was based entirely on the angles of the downstream pipes relative to the upstream pipe:

$$\frac{F_2}{F_1} = \frac{1}{2} \left\{ 1 - \left( \sin \frac{\mathbf{q}_1 - \mathbf{q}_2}{2} / \sin \frac{\mathbf{q}_1 + \mathbf{q}_2}{2} \right) \right\} \quad (3.55)$$

where  $F_1$  and  $F_2$  are the projected areas of the pipe upstream and downstream of the branch, respectively. As a result, while the flow ratio controls the distribution of powder in the piping downstream of a branch (**Lempp (1966), Maeda & Ikai (1976)**), the ratio of projected pipe areas in the vicinity of a branch is the most important factor in powder distribution downstream of a branch for relatively large particles; i.e., for particles of 1.1 mm diameter.

### **3.5 Mixture Behaviors.**

Numerous investigators have concluded that particle/particle interactions are an important part of the solids/gas mixture phenomena. Two important factors in estimating the applicability of reported analyses are the solids loading of the mixture, and whether particle/particle interactions are included in the calculations. Studies have been done for particular ranges of particle sizes; **Williams & Crane (1983)** described analyses of particle collisions as a function of particle concentration, relaxation times, turbulence intensity and scale, and particle size (including collisions between particles of different sizes). Williams & Crane expressed collision rates by a collision coefficient  $C_{12}$  with dimensions  $L^3T^{-1}$ , such that, in a given volume, for two groups of particles of either the same size or different sizes, having number concentrations  $N_1$  and  $N_2$  respectively,  $C_{12}N_1N_2$  is the number of collisions between particles of the two size types per unit time.

Williams & Crane analyzed particle collisions in terms of the relative velocity between particles for particles in the 50-200 micron size range, for relatively “dilute” flows, and assumed that particles do not significantly change the energy spectra of the carrier gas. The collision coefficient itself was calculated by a process divided into two separate phases: diffusion theory to determine the rate of approach of particles, and a kinetic model to evaluate the outcome of a collision event. This is due to the possible particle concentration gradients that may be encountered as particles collide; the effect of non-uniform concentrations can be appreciable for small particles.

If the particles are small enough to follow turbulent motion exactly, the collision rate is a function of the local velocity gradient. **Saffman & Turner (1956)** developed a formula for particles smaller than the Kolmogorov microscale:

$$C_{12} = \left(\frac{\rho}{2}\right)^{1/2} (d_1 + d_2)^2 \left[ \left(1 - \left(\frac{r_G}{r_p}\right)\right)^2 (\mathbf{t}_1 - \mathbf{t}_2)^2 \times 1.3 \left(\frac{\epsilon^3}{\rho_G}\right)^{1/2} + \left(\frac{1}{36}\right) (d_1 + d_2)^2 \left(\frac{\epsilon}{\rho_G}\right) \right]^{1/2} \quad (3.56)$$

where  $d_1$  and  $d_2$  are diameters of two particles,  $\tau$  is the relaxation time of a particle with diameter  $d$  and density  $\rho_p$ ,  $\epsilon$  is the rate of turbulent energy dissipation of the gas,  $\rho_G$  is the gas density, and  $\nu_G$  is the kinematic viscosity of the gas. Larger particles, on the other hand, tend to approach each other from separate eddies with completely random and independent velocities. **Abrahamson (1975)** derived a collision coefficient formula for this extreme:

$$C_{12} = 1.25(d_1 + d_2)^2 (v_1'^2 + v_2'^2)^{1/2} \quad (3.57)$$



where  $v'$  is the root mean square particle velocity, which is related to the root mean square fluid velocity  $u'$  by

$$v' = u' \left( 1 + 1.5te / u'^2 \right)^{-1/2} \quad (3.58)$$

This formulation is valid when

$$d^2 > 15n_G u'^2 \frac{\begin{pmatrix} \mathbf{r}_G \\ \mathbf{r}_p \end{pmatrix}}{\mathbf{e}} \quad (3.59)$$

As of the writing of the paper, no analyses existed for collision coefficients covering the particle size range between the ranges covered by the two formulations, with particular reference to pipe flow. The results of the analysis in the paper give a collision coefficient for a dimensionless particle relaxation time  $\theta$ :

$$C_{12} = \left[ (8\mathbf{p})^{1/2} \left( \frac{18}{4} \right) \mathbf{n}_G L_f \begin{pmatrix} \mathbf{r}_G \\ \mathbf{r}_p \end{pmatrix} \begin{pmatrix} w'_i \\ u'_i \end{pmatrix} (\mathbf{q}_1^{1/2} + \mathbf{q}_2^{1/2})^2 \right] x \quad (3.60)$$

$$\left[ \left( \frac{2}{\mathbf{p}} \right) \tan^{-1} \left\{ \left( \frac{1}{3} \right) \begin{pmatrix} \mathbf{r}_G \\ \mathbf{r}_p \end{pmatrix} \begin{pmatrix} u'_i L_f \\ \mathbf{n}_G \end{pmatrix} \begin{pmatrix} w'_i \\ u'_i \end{pmatrix} \frac{\mathbf{q}_1 \mathbf{q}_2}{(\mathbf{q}_1^{1/2} + \mathbf{q}_2^{1/2})^2} \right\} \right]$$

where

$$\mathbf{q} = \frac{t u'_i}{L_f} \left( = \frac{t}{T_L} \right) \quad (3.61)$$

where  $u'_i$  is the root mean square fluctuating velocity,  $L_f$  is the longitudinal scale,  $T_L$  is the integral time scale, and  $w'_i$  is the relative velocity between two particles with zero separation. Comparison of this formulation with the previous formulations shows the current formulation to predict a coefficient somewhat lower than predicted for the two extreme particle size ranges by the previous analyses. The results of Williams & Crane's analyses suggest that the levels of turbulence intensity and scale will have a significant

effect on collisions; for example, a doubling of turbulence intensity is predicted to increase the collision rate by an order of magnitude. In terms of pipe flows, the results of these analyses suggest that the amount of turbulence in a discharge flow, as well as the relative particle sizes, will have a great impact on the frequency and consequences of particle collisions in a gas/solids multiphase flow.

### **3.6 Summary.**

**Ahmadi & Ma (1990a)** critiqued previously developed models, as appearing to be deficient in one or more of the following respects:

- “1. Particle-particle collisions are generally neglected.
2. Only dilute mixtures are considered.
- ...
4. The interactions of the fluid and particulate phases are only partially considered.
- ...
6. The requirements of the second law of thermodynamics are totally ignored.

In summary, an adequate model for describing two-phase turbulent flows of dense fluid-solid mixtures is not, as yet, available.”<sup>5</sup>

Consideration only of “dilute” flows allows for a simplification of the mathematics of a model, and also allows for reduction or elimination of interactions between the solid and gaseous phases. This simplification is not entirely unreasonable, except for the vagueness of the definition of “dilute”, and the limits of ranges of analyses considered by the various investigators. None of the literature reviewed gave any kind of

---

<sup>5</sup> **Ahmadi & Ma (1990a)**, page 324.

definition of a “dilute” flow, either in terms of solids mass fraction, or solids volume fraction. The importance of the definition of “dilute” is primarily in defining precisely which flows can be treated as “dilute”, and where an investigator feels the “dilute” assumption will not longer be applicable to a given flow scenario. Without test data in the dry chemical flow regime validating any particular model, it is quite possible that a “dilute” model may already exist that is adequate to predict dry chemical blow downs. If such a model already exists, than development of a new model for high loading high Reynolds number regimes may be unnecessary. Without validating data, and without a firm declaration by an investigator as to the limits of applicability of a model, it is risky to adapt any already-existing model to predict blow down behavior in the dry chemical flow regime.

The research described in the literature often assumes dilute flow, allowing the investigator(s) to ignore effects such as particle-particle and particle-gas interactions. The dependence of momentum and energy balances on interparticle collisions depends greatly upon the flow characteristics of the solids flows in the mixture, particularly on the amount of solids in the mixture, and how much difference there is between particle and gas velocities. The impact of collisions (or the neglect of collisions) was not explicitly explored in the current model.

As can be seen in Figure 3.2 below, only one or two reviewed studies even came close either in analytical or experimental ranges to the loading ratios and Reynolds number expected by dry chemical systems. Since most of the investigated systems were analyzed as “dilute,” a representative pipe Reynolds number based on gas flow characteristics only was calculated for each paper examined, with solid/gas loading ratios

also calculated from reported data. Note that, if actual values were reported in a paper, these values were used directly. The system described in Cholin (**Cholin (1969)**) has a loading ratio of approximately 32.0, with a pipe gas Reynolds number:

$$\text{Re} = \frac{(0.0739 \text{ lbm} / \text{ft}^3) \times (125 \text{ fps}) \times (0.208 \text{ ft})}{(3.63 \times 10^{-7} \text{ lbm} / \text{ft} - \text{sec})} = 5.302 \times 10^6$$

using data from Cholin's development data (**Cholin (1969)**). Based on system design information indicating generally smaller pipe diameter, a pipe gas flow Reynolds number of approximately  $7 \times 10^5$  was calculated. Using a mixture density formed of weighted averages of the densities of the mixture components would result in somewhat higher pipe Reynolds numbers than these. In this case, the result would be to increase the calculated pipe Reynolds numbers, driving the plotted points further still from the locus of points in the low loading, low Reynolds number regime. In any event, the high loading ratio of both the Cholin system and modern dry chemical systems compared to those of the bulk of the investigations still serves to separate dry chemical systems from the bulk of the previous investigations examined.

It is unclear, after examining a number of previously-developed theoretical models of gas-solids multiphase flow, whether any of these models could be applied successfully to model dry chemical systems. A number of limiting or simplifying assumptions, such as "dilute" flow are described, but little or no test data was gathered in any of the examined studies to suggest that these models could model high loading high Reynolds number flows. Since only a few "complete" models of gas-solids multiphase flow exist (such as the modeling of Ahmadi), and no models of the behavior of multiple phases in components such as cylinders exist, it is impossible to say whether any of the

proposed simplifications of prior investigators result in models that adequately describe system behavior while simplifying the necessary calculations. For example, almost nothing was found in the literature (other than the general discharge model of **Chenoweth & Paolucci (1990)**) regarding the modeling of a solids/gas mixture discharging from a cylinder. As the research documented herein shows, there is currently limited understanding of what happens in a cylinder between the solid powder and gaseous carrier agent during discharge. Clearly these events were not in any other model investigated.

Some of the restrictions imposed by previous investigators are obviously limiting – for example, limiting consideration only to constant flow conditions in pipe flow, and not considering tank and/or nozzle modeling. This is not to say the previous modeling efforts do not offer useful insights. Examination of the various means of representing the gas/solids mixture, for instance, was necessary to determine limitations of the various models. Furthermore, many of the reviewed papers presented useful insights as to the behavior of mixtures under various conditions, and useful insights as to how to model various phenomena of interest, such as the impact of momentum transfer between phases on the energy balance (not included in the current model.) But without comparison either with test data from regimes of interest, or with models that do cover the regimes of interest, it is impossible to determine whether a previously-developed model is sufficiently robust to be applied to a dry chemical system.

The impact of the imbalance in the Second Law of Thermodynamics equation on model accuracy is not clear. As noted by Arnold *et al* (**Arnold *et al* (1990)**) and Ahmadi & Ma, the models they investigated, while failing to obey the Second Law, failed to

varying degrees – some of the resulting inaccuracies were minor, some major. **Soo (1989)** indicates that for one-dimensional adiabatic flow, entropy should always increase. As a result, the reported imbalance results from the neglect of certain phenomena, or in certain oversimplifying assumptions, resulting in an incomplete model. The impact of this incompleteness will vary from model to model, and the impact of this incompleteness would need to be assessed in each model by determining the source of the inaccuracy, and rerunning the analysis. The model developed in the research documented in this dissertation also currently neglects certain phenomena, such as particle collisions, particle drag, and the energy cost of momentum transfer between phases; the relative size of these losses should be assessed to determine how critical inclusion of these phenomena is for the dry chemical blow down model.

The literature showed significant activity in the development of models of multiphase gas/solid flows. Numerous solutions have been derived, with various amounts of success, for a number of distinct flow regimes for pipe flows. With the exception of Chenweth & Paolucci's development of a simple model of a solids/gas cylinder blowdown, there was nothing found in the literature regarding the modeling or experimental examination of behaviors of cylinders or nozzles. And with the exception of two short papers by **Morikawa et al (1978a, 1978b)**, nothing was found in the literature regarding pipe fittings such as elbows, branches or other fittings. The suitability of any particular research to a problem of interest depends not only on considerations suggested by Ahmadi & Ma and Arnold *et al*, above, but also on how much accuracy and detail is needed in the model.

The literature suggests several potential models, including models with a single continua utilizing a composite of gas and solid properties, models treating each phase as a separate "fluid", and models treating the gas as Eulerian and the solid particles as Lagrangian. The more comprehensive models (such as Ahmadi & Ma) require field model implementations in order to enable all phenomena having a potential influence on system behaviors to be represented. Simpler models (such as Chenoweth & Paolucci) allow for less complex approaches. The primary drawback of simplified models is that the simplified implementation will not allow for the possible influence of omitted phenomena on system behavior, by not allowing for as detailed a representation of the problem and its solution as the field model would allow. The results of "glossing over the some of the details" can include inaccuracies (small or large) in model predictions, and apparent violations of basic laws, such as the Second Law of Thermodynamics. These apparent violations compensate for omissions in other parts of the model, and may result in model predictions that are simultaneously accurate in comparison with test data and in violation of known laws of physics and fluid mechanics.

A comparison of published test data for gas-solids multi-phase to the regimes of interest in dry chemical suppression systems shows a lack of testing at velocities and loading ratios of interest. Figure 3.2 compares Reynolds number versus loading ratio values for gas-solids multiphase flow tests reported by various investigators to calculated values for dry chemical suppression systems as studied herein.

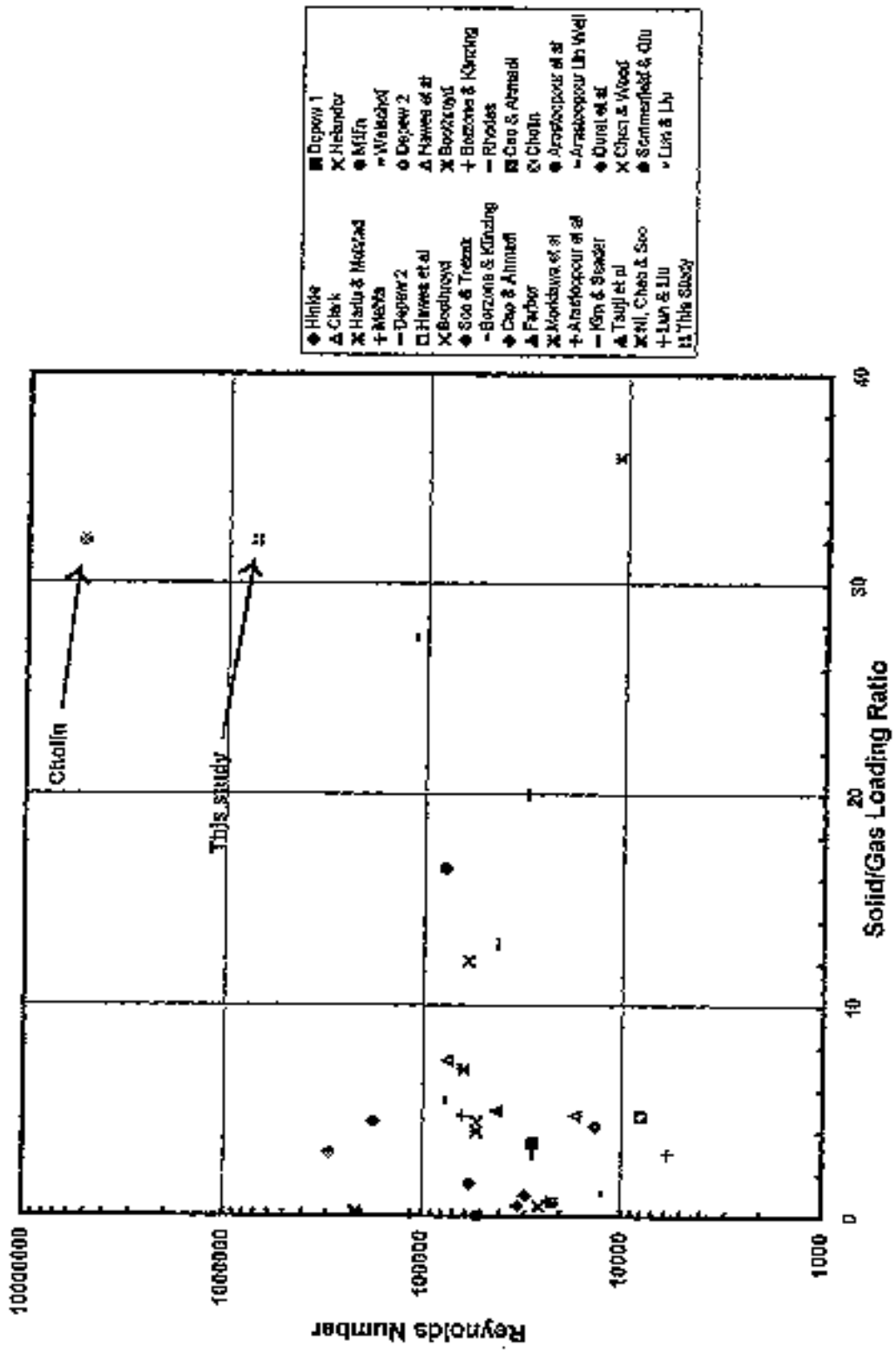


Figure 3.2 Loading Ratio Vs. Mach Number.



Note the “Cholin” point represents one of the few reported studies in the literature of dry chemical systems; making it one of the few published reports with data comparable to work performed in these studies. Most reported studies covered only low velocity, “dilute” (low loading ratio) flows; dry chemical systems tend to be high loading ratio, high velocity flows. As a result, previously reported results can only help validate low-flow/low loading portions of the proposed model. These regimes are far from the normal regimes seen by dry chemical systems, however.

Based on the literature, the relevant parameters in analysis of a dry chemical fire suppression include the physical characteristics of the carrier gas and agent, the particle mass fraction, source tank characteristics (including pressure, temperature and volume), pipe lengths, pipe diameters, pipe internal roughness, system configuration, and the system minimal cross-sectional area. Flow characteristics, such as particle-particle collisions, particle drag, and particle-wall interactions, are also of importance. A model containing enough of the physics of a real discharge system to permit reasonably accurate predictions, while simplifying the representation of those physics to eliminate detailed behavior of limited importance in the general performance behavior of a discharge system, would allow for rapid development of applications without significant loss of performance accuracy. At the very least, a model should follow the Conservation Laws – Mass, Linear Momentum, and Energy. It should also follow other relations, such as the Ideal Gas Law. Some means needs to be found to define mathematically the two phases – either separately or in some sort of composite form. If the flow is treated as a “fluid” flow, analyses similar to those for single fluids should be applicable, resulting in mathematical relations between the various state parameters, such as density,

temperature, pressure, velocity, and parameters describing the relationships between the gaseous and solid phases. If phenomena analogous to those found in single fluids, such as compressibility and choking occur, the behavior of these phenomena need to be incorporated to assure proper model response to system characteristics. If possible, a determination should be made as to how closely the composite material acts in flow situations to a single fluid. The degree to which the composite material behaves like a fluid is the degree to which reasoning about the composite can follow the same lines of reasoning followed for fluid materials.

Outputs from a model need to sufficiently describe the state of each of the components represented in the model. Transient phenomena, such as state variables, and changing driving conditions in the source cylinder, should be available so the user can determine a) the adequacy of the modeled configuration to meet design goals, and b) the quality of the model response – are the answers generated by the model “reasonable”, if not correct? Some configurations modeled may be poorly handled by the model – the user should have enough calculated data available to assess the validity of any answer the model generated.

## **4.0 Theoretical Model.**

### **4.1 Selection of Agent/Gas Model.**

While an Eulerian approach to the modeling of gas-solid multiphase pipe flow allows for a simplified approach in comparison to the more detailed Lagrangian approach, there are still choices to be made in the type of Eulerian approach. Much of the literature favoring the Eulerian approach tends to favor a two-fluid approach, modeling the solids and gas as separate interacting continua. While an approach of this sort, such as presented by **Ahmadi & Ma (1990a)**, allows for a more comprehensive modeling of all phenomena of interest in the pipe flow, it also requires a more complex, comprehensive set of equations to model the flow. Most often, this requires a “field” model, with the volume of interest subdivided into a grid of control volumes, and equations describing the interactions between volumes, to solve a problem, and requires detailed understanding of the phenomena involved, sufficient data and detail to accurately model all the phenomena of interest, and sufficient computer memory and time to generate even a single solution. The current state of the computational art is such that field models, even those specifically designed for special situations, are too complex and time-consuming for general design purposes.

An alternative approach is to treat the flowing materials as a "composite" material, with properties such as density, pressure, etc..., calculated from inputs weighted by such factors as particle volume or mass fractions. While such an approach ignores the interactions between the solids and gas flows, it allows for significant simplification of the modeling process. Instead of having to grapple with unwieldy grids (and their accompanying programming difficulties), one-dimensional pipe flow equations generally

associated with single fluid flows are modified to account for the composite fluid properties and equations of state are used. The main requirement for such an approach is that the model be validated against test data to verify the validity of the simplifying assumptions and modifications.

Based on the results of the literature search, a model was developed using the "composite" property modeling of **Paolucci (1985)** and **Chenoweth & Paolucci (1990)**. The modeling process was broken down into individual components, corresponding to the various subsystems in the model: source tank, pipes, fittings, and nozzle. The breakdown of a typical dry chemical system into these components allowed for a more concentrated approach to problems of each component. Doing the work in the order of tank, pipes, and nozzle also allows for development of "source" flows in a logical order, such that later components do not have to be tested using artificially created inputs - they merely get added to the model already developed, and calculations are then done for the merged model.

## **4.2 Assumptions.**

A number of assumptions were made as part of model development.

### **4.2.1 Quasi-Steady-State.**

Calculations at each time step are assumed to be "quasi-steady-state." An analysis of this sort does not allow for transients, such as pressure "waves", or other changes in the system, to occur as part of the "natural" calculation process. Rather, transient events must be programmed to occur, and such changes are observed in the resulting calculations to occur "suddenly", and affect the entire modeled configuration. No changes are allowed to propagate through a system in some real finite time. The

quasi-steady-state assumption greatly simplifies calculations, although transient effects on the modeled configuration are not included. As an example, changes in a jet flow, in a quasi-steady-state model are reflected instantaneously in all parts of the model, even though, in reality, some finite time will elapse before effects of a change are reflected in other parts of the jet. As another example, changes in the downstream portion of a system discharge, such as pressurization of a pipe, that would reduce the mass flow of components upstream of the pipe, would be modeled in a quasi-steady-state model as affecting the system mass flow instantaneously, rather than over some finite, if very short time. For example, air flowing through an 8-foot pipe has a speed of sound of approximately 1129 ft/sec at ambient temperature. Travel time for a pressure “pulse” or change from the downstream end of the pipe to the upstream end would be approximately 7 milliseconds. Quasi-steady-state modeling with time steps of 1 millisecond would incorrectly model such a pressure change; if the time step were greater than 1 millisecond, a quasi-steady-state assumption would have no problem.

If transient events, such as valve openings/closings, could be incorporated in a model, some of the negative effects of quasi-steady-state modeling can be mitigated. Also, if transients have little or no effect on mass flow rate predictions, they can be safely ignored by using a quasi-steady-state model, resulting in a model simpler to implement.

#### 4.2.2 Constant Mass Fraction.

The Chenowith & Paolucci model, as implemented in this research, assumes that the solids mass fraction ( $\phi$ ) remains constant at all locations at all times. This assumption not only simplifies the mathematical modeling of the flows, but also is consistent qualitatively with the results of system testing, in which residual amounts of agent are

found in the source cylinder. It is also consistent with the supposition of a homogeneous mixture of agent and carrier gas in the supply cylinder and the piping network.

There are several difficulties with this assumption, and its implications. Firstly, while the assumption qualitatively predicts residual powder throughout the suppression system after discharge, it poorly predicts the amounts of residual agent (see discussion, Section 7.5).

#### 4.2.3 Further Assumptions.

All components are assumed axisymmetric. Furthermore, velocities in the radial direction are assumed small enough in comparison to longitudinal velocities that flows may be considered one-dimensional (variable values are averaged over cross-sectional areas.) The gas and particle-gas mixture are treated as “calorically perfect,” with constant specific heats.

The carrier gas is assumed to be “ideal”, with compressibility factor ( $Z_G$ ) equal to 1. Based on compressibility charts for nitrogen close to ambient, this assumption is justified.

Chenowith & Paolucci assume that particle sizes are small enough so that there is no difference in temperature between the gas and solid particles; thus the solid, gas, and mixture temperatures are equal. They also assume that the solid particles contribute nothing to pressure; thus the mixture pressure is equal to the gas pressure.

### **4.3 Generalized One-Dimensional Analyses – Constant Mass Fraction.**

The objectives of theoretical analyses of various components is to derive the means of calculating how state variables change when flows encounter various system

components, what component characteristics are relevant to influencing flow behavior, and how to account for these component characteristics. Some of the components are generally modeled in terms of changing area without friction (nozzles, for instance), and others as constant area with friction effects (pipes, for instance). Components may also be modeled accounting for both area change and friction effects. As a result, while specific modeling may be performed for each component, a more generalized analysis will result in equations that, properly constrained, will result in the same equations that result from individual component analyses. Furthermore, as will be shown below, the generalized analysis is simpler to perform, and no special insights are required for the analyses – manipulating of the equations is entirely mathematical. The resulting equations can be shown, in the limit of zero solids mass fraction, to match the gas dynamics results described in **Shapiro (1953)**, Vol. I.

#### 4.3.1 Physical Equations and Definitions.

The necessary equations to define a general flow situation are described below.

Figure 4.1 shows a control volume definition for the situation analyzed. While this situation resembles that of Figure 8.1 in **Shapiro (1953)**, Vol. I, the two-phase gas-solids analysis applies certain constraints prior to the start of analysis, including adiabatic conditions, no work done by or on the control volume, and no flows extracted from or injected into the control volume.

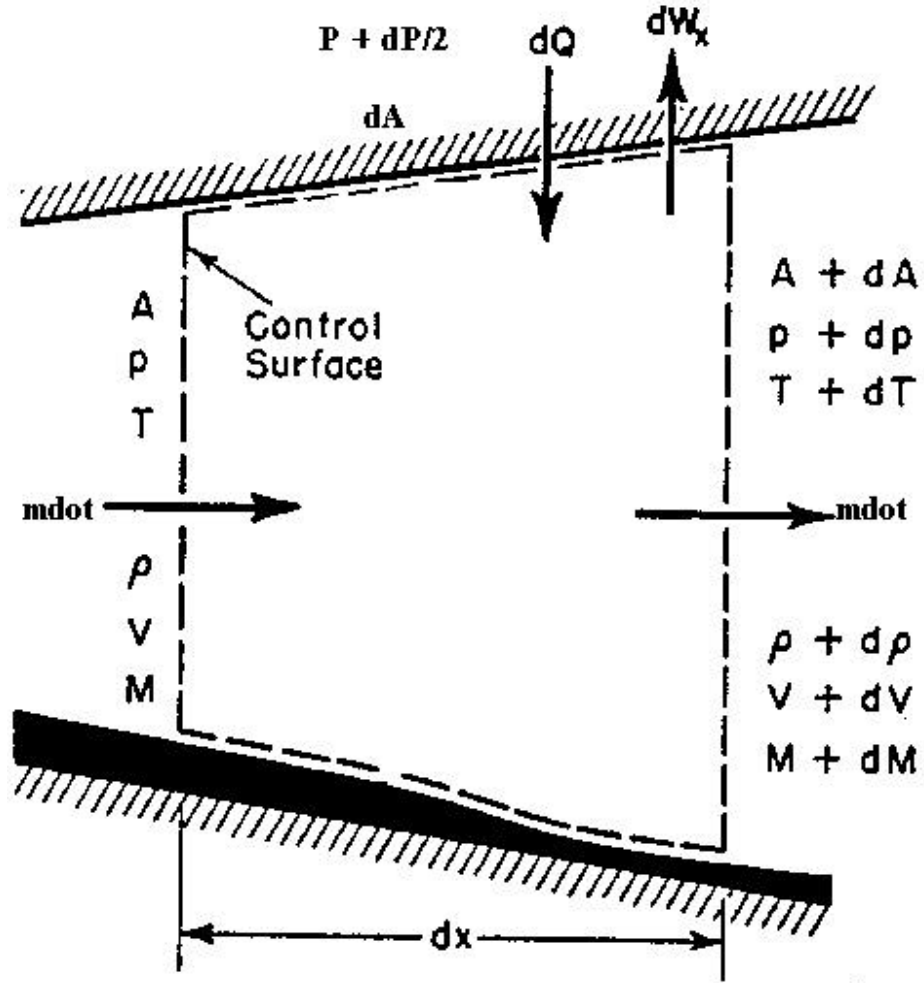


Figure 4.1 Control Volume Definition (Source: Shapiro (1953), Vol. I, p. 221).

#### 4.3.1.1 State Equation.

Combining equations (3.6) and (3.7), the mixture equation of state is:

$$P = \frac{rRT}{(1-q)} = \frac{rRT}{\left(1 - \frac{rf}{r_D}\right)} \quad (4.1)$$

Taking the natural log of both sides yields:

$$\ln(P) = \ln(r) + \ln(T) - \ln(1-q) = \ln(r) + \ln(T) - \ln\left(1 - \frac{rf}{r_D}\right) \quad (4.2)$$



Differentiating and collecting terms:

$$\frac{dP}{P} = \left( \frac{1}{1-q} \right) \frac{d\mathbf{r}}{\mathbf{r}} + \frac{dT}{T} = \left( \frac{1}{1-\frac{\mathbf{r}\mathbf{f}}{\mathbf{r}_D}} \right) \frac{d\mathbf{r}}{\mathbf{r}} + \frac{dT}{T} \quad (4.3)$$

Note: rather than write out the entire definition of the solid volume fraction ( $\theta$ ) (equation (3.3)) each time it appears in an equation, the “ $\theta$ ” symbol for volume fraction will be used, with the understanding that  $\theta = f(\rho)$ , and is thus differentiable whenever differentiation is applied to an equation in which it appears.)

#### 4.3.1.2 Sound Velocity Definition.

Combining equations (3.5), (3.12) and (3.13), the result is:

$$a^2 = \frac{\mathbf{g}RT}{(1-q)^2} \quad (4.4)$$

Taking the natural log of both sides yields:

$$\ln(a^2) = 2\ln(a) = \ln(\mathbf{g}RT) - 2\ln(1-q) \quad (4.5)$$

Differentiating and combining terms gives:

$$\frac{da}{a} = \frac{1}{2} \frac{dT}{T} + \left( \frac{q}{1-q} \right) \frac{d\mathbf{r}}{\mathbf{r}} \quad (4.6)$$

#### 4.3.1.3 Mach Number Definition.

Using equation (4.4) and the definition of Mach number:

$$M^2 = \frac{v^2}{a^2} = \frac{v^2(1-q)^2}{\mathbf{g}RT} \quad (4.7)$$

Taking the natural log of both sides:

$$\ln(M^2) = \ln(v^2) + \ln((1-q)^2) - \ln(\mathbf{g}RT) \quad (4.8)$$

Differentiating and combining terms gives:

$$\frac{dM^2}{M^2} = \frac{dv^2}{v^2} - \frac{dT}{T} - \left( \frac{2q}{1-q} \right) \frac{dr}{r} \quad (4.9)$$

#### 4.3.1.4 Mass Conservation Equation.

The mass conservation equation (continuity equation) is almost identical to that in the standard texts:

$$m_{dot} = r v A C_d \quad (4.10)$$

The discharge coefficient  $C_d$  is a measure of the difference between “ideal” and actual flow. When a component is at the outlet end of a flow system, the discharge coefficient accounts for irreversable losses in the exiting flow, and such phenomena as vena contracta, and has a value less than 1.0. For components within a discharge piping network, the coefficient would have a value of 1.0.

Differentiating:

$$dm_{dot} = v A C_d dr + r A C_d dv + r v C_d dA \quad (4.11)$$

For constant mass flow (quasi-steady state), the left-hand side of equation (4.11) is zero.

Dividing through by the quantity  $\rho v A C_d$ , the result is:

$$0 = \frac{dr}{r} + \frac{dv}{v} + \frac{dA}{A} \quad (4.12)$$

#### 4.3.1.5 Energy Conservation Equation.

For a quasi-steady, adiabatic flow for a “perfect” fluid with no work being done by or on the fluid, and no phase changes either between the solid and gas, or phase changes of the gas itself, the energy conservation equation is:

$$h + \frac{v^2}{2} = \text{constant} \quad (4.13)$$

Substituting the relation for a “perfect” fluid,  $h = h_0 + c_p(T - T_0)$ , and gathering constants:

$$c_p T + \frac{v^2}{2} = \text{constant} \quad (4.14)$$

Substituting the relation  $c_p = (\gamma/(\gamma-1))R$  (**Shapiro (1953)**, p. 78), and differentiating:

$$\left( \frac{gR}{g-1} \right) dT + v dv = 0 \quad (4.15)$$

Dividing through by the coefficient of  $dT$  in equation (4.15), and multiplying each term

by “1”, the result is:

$$\frac{dT}{T} + \frac{v^2 (g-1)}{2gRT} \frac{dv^2}{v^2} = 0 \quad (4.16)$$

Substituting in equations (4.4) and (4.7), the result is:

$$\frac{dT}{T} + \frac{(g-1)M^2}{2(1-q)^2} \frac{dv^2}{v^2} = 0 \quad (4.17)$$

#### 4.3.1.6 Linear Momentum Conservation Equation.

From the control diagram shown in Figure 4.1, the conservation of linear momentum equation is:

$$PA + \left( P + \frac{dP}{2} \right) dA - (P + dP)(A + dA) - \mathbf{t}_w dA_w = m_{dot} ((v + dv) - v) \quad (4.18)$$

where  $dA_w = C dx = \pi D dx$ ,  $A = \pi D^2/4$  and  $m_{dot} = \rho v A = \pi \rho v D^2/4$ . Expanding,

simplifying, and dropping higher order terms:

$$\mathbf{p} \frac{D^2}{4} dP + \mathbf{p} \mathbf{t}_w D dx + \mathbf{p} \mathbf{r} \frac{D^2}{4} v dv = 0 \quad (4.19)$$

The mixture coefficient of friction is related to the Darcy-Weisbach resistance coefficient  $\tau_w$  by:

$$\tau_w = \frac{f r v^2}{8} \quad (4.20)$$

(Roberson & Crowe (1993), page 574). Note that the coefficient of friction here is the coefficient for the combined solids and gaseous phases. As described in Section 3.3, the presence of the solid phase results in increased pipe friction. A number of empirical equations have been derived for determining a multiplier to be applied to the gas-only friction factor to correct for the additional friction; the multiplier equations selectable by the user of the program is discussed in Section 4.4.3.

Using this relation, and dividing through by  $\pi PD^2/4$  results in:

$$\frac{dP}{P} + \frac{r v^2}{P} \frac{dx}{2D} + \frac{r v}{P} dv = 0 \quad (4.21)$$

Rearranging equation (4.1) yields

$$\frac{r}{P} = \frac{(1-q)}{RT} \quad (4.22)$$

Rearranging equation (4.4) results in

$$\frac{(1-q)}{RT} = \frac{g}{a^2 (1-q)} \quad (4.23)$$

Equating equations (4.22) and (4.23) gives

$$\frac{r}{P} = \frac{g}{a^2 (1-q)} \quad (4.24)$$

Substituting equation (4.24) into (4.21) (with a little re-arranging):

$$\frac{dP}{P} + \frac{\mathbf{g}v^2}{a^2(1-\mathbf{q})} \frac{dv}{v} + \frac{\mathbf{g}v^2}{a^2(1-\mathbf{q})} \frac{fdx}{2D} = 0 \quad (4.25)$$

or

$$\frac{dP}{P} + \frac{\mathbf{g}M^2}{2(1-\mathbf{q})} \frac{dv^2}{v^2} + \frac{\mathbf{g}M^2}{(1-\mathbf{q})} \frac{fdx}{2D} = 0 \quad (4.26)$$

#### 4.3.2 Solution of Differential Equations.

The differential form of the aforementioned physical laws and definitions yield 6 equations with 6 dependent differential variables ( $dP/P$ ,  $d\rho/\rho$ ,  $dT/T$ ,  $dM^2/M^2$ ,  $dV^2/V^2$ , and  $da/a$ .) The derived equations, taken to the limit when the solids mass fraction  $\phi \rightarrow 0$ , revert to the same equations generated by Shapiro. The only changes involve either addition of a differential density term to an equation, change of the coefficient of a density differential term already in the equation, or the addition of  $(1-\theta)$  factors to velocities in some of the equations.

While these differential equations do not represent a closed set of equations, if some of the differentials are treated as independent variables, the rest of the variables, treated as dependent variables, may be solved for. Since there are two more variables than equations, two variables must be selected to be independent. Following Shapiro, independent variables are selected that are most easily controlled in practice – in this case physical variables that most readily describe the physical piping network being modeled. As a result, the differential variables based on physical dimensions,  $dA/A$  and  $fdx/2D$  are selected as independent variables; the rest are dependent variables.

Equations (4.3), (4.6), (4.9), (4.12), (4.17) and (4.26) can now be solved for the dependent differential variables as a function of the two independent differential

variables using any convenient method. The equations lend themselves readily to solution through symbolic matrix manipulation. Table 4.1 shows the matrix form of the equations; note that a number of substitution symbols were used to simplify calculations; these substitutions are shown in the Table.

	{←-----x-----→}							
	$\frac{dP}{P}$	$\frac{dr}{r}$	$\frac{dT}{T}$	$\frac{da}{a}$	$\frac{dM^2}{M^2}$	$\frac{dv^2}{v^2}$	$\frac{dA}{A}$	$\frac{fdx}{2D}$
State	1	$-\frac{1}{(1-q)}$	-1	0	0	0	0	0
Sound	0	$-\frac{q}{(1-q)}$	$-\frac{1}{2}$	1	0	0	0	0
Mach Number	0	$\frac{2q}{(1-q)}$	1	0	1	-1	0	0
Mass	0	1	0	0	0	$\frac{1}{2}$	-1	0
Energy	0	0	1	0	0	$\frac{(g-1) M^2}{2 (1-q)^2}$	0	0
Momentum	1	0	0	0	0	$\frac{gM^2}{2(1-q)}$	0	$-\frac{gM^2}{(1-q)}$

{←-----[A]-----→} {←---[B]-----→}

Note:  $\theta = \rho\phi/\rho_D$ ;  $d\theta/\theta = dp/\rho$ .

**Table 4.1 General One-Dimensional Analysis – Equation Matrix.**

This matrix may be solved by hand, or any available symbolic solver may be used. The matrix equation is of the form

$$[A][x] = [B] \tag{4.27}$$

where  $[A]$  is the  $6 \times 6$  coefficient matrix,  $[B]$  is actually two  $6 \times 1$  vectors formed from the two rightmost columns in the table above, and  $[x]$  is the  $6 \times 1$  vector formed from the 6 dependent differentials along the top of the Table. The equation is solved independently for each independent differential variable ( $dA/A$ ,  $fdx/2D$ ), and the two solutions added together to obtain the equation describing each of the dependent differentials in terms of both of the independent differentials.

The general form of the solution is

$$[x] = [A]^{-1} [B] \quad (4.28)$$

where  $[B]$  will be a  $6 \times 1$  vector representing each of the independent differentials, and  $[x]$  the solution vector for each vector  $[B]$ . If  $[B_1]$  is the vector for  $dA/A$ , and  $[B_2]$  the vector for  $fdx/2D$ , and  $[x_1]$  and  $[x_2]$  the solutions corresponding to  $[B_1]$  and  $[B_2]$ , the full solution is

$$[x] = [x_1] + [x_2] = [A]^{-1}[B_1] + [A]^{-1}[B_2] \quad (4.29)$$

For these studies, MatLab™ was used to solve the equations. Table 4.2 shows the solved equations. Like the source equations, taking the limit of these solutions when  $\theta \rightarrow 0$  reverts these solutions to the same equations generated by Shapiro.

	F <sub>1</sub> , coefficient of $\frac{dA}{A}$	F <sub>2</sub> , coefficient of $\frac{fdx}{2D}$
$\frac{dP}{P}$	$\frac{ed}{2c-d+e}$	$-\frac{d(2c+e)}{2c-d+e}$
$\frac{dr}{r}$	$\frac{(-2c+d)}{2c-d+e}$	$\frac{-d}{2c-d+e}$
$\frac{dT}{T}$	$\frac{2ce}{2c-d+e}$	$\frac{2cd}{2c-d+e}$
$\frac{da}{a}$	$\frac{-2bc+bd+ec}{2c-d+e}$	$\frac{(b+c)d}{2c-d+e}$
$\frac{dM^2}{M^2}$	$\frac{-\left(2e+ed+2ec-4bc+2bd\right)}{2c-d+e}$	$\frac{2d(b+c+1)}{2c-d+e}$
$\frac{dv^2}{v^2}$	$-\frac{2e}{2c-d+e}$	$\frac{2d}{2c-d+e}$
Where:		
	$b = \frac{q}{1-q}$	
	$c = \frac{(g-1)}{2} \frac{M^2}{(1-q)^2}$	
	$d = \frac{gM^2}{(1-q)}$	
	$e = \frac{1}{1-q}$	

Note: General solution equation is of the form  $\frac{dn}{n} = F_1 \frac{dA}{A} + F_2 \frac{fdx}{2D}$ , where F<sub>1</sub> and F<sub>2</sub> are the influence coefficients, as shown above, and n is one of the differentiated variables.

**Table 4.2 General One-Dimensional Analysis – Solutions (Influence Coefficients).**

The coefficients are of particular interest; called “influence coefficients” by Shapiro, the values these coefficients take on over the range of values of interest determine how the dependent differential variables behave as a result of changes in the independent variables. As an example, for dP/P, in a constant area pipe with friction, if the influence coefficient of fdx/2D remains negative for all subsonic conditions, the



inference is that, for all subsonic conditions, pressure decreases as flow moves downstream in a straight pipe. The general behaviors predicted for a gas-solids two-phase flow with constant mass fraction may be compared in sign and magnitude to the behaviors predicted by Shapiro for a single-phase fluid. Furthermore, general behaviors of the two-phase mixture may be predicted by the signs and magnitudes of the influence coefficients generated here, and used in the computer modeling process.

Calculated influence coefficients, and their impact on the model developed here, are shown in Appendix 10.4.

It should be noted that the Shapiro influence coefficients show, for most of the differentials, a singularity at Mach 1.0, as a result of the denominator  $1-M^2$  factor in most of the coefficients. In terms of general trends, this indicates that as Mach 1.0 is approached, the coefficients for the dependent differentials go to infinity. As calculated above, the denominator for the influence coefficients calculated using Chenoweth & Paolucci parameters is  $(1-\theta) + M^2(\theta\gamma-1)$ . For the denominator to be zero (i.e.; a singularity), manipulation of this denominator results in:

$$M^2 = (\theta-1)/(\theta \gamma-1) \tag{4.30}$$

For dry chemical mixtures, the mixture specific heat ratio  $\gamma$  is usually very close to 1 ( $\cong$  1.004 for the sodium bicarbonate mixtures tested in this report.) As a result, the ratio is positive, and a Mach number slightly larger than 1.0 results (for an initial  $\theta$  of 0.452,  $M \cong$  1.002). As a result, while the choking Mach number is no longer unity, it remains close to unity for typical mixture parameter values. Further, since the volume fraction is changing with time (due to the decreasing mixture density,) the resulting shifts in the Mach number are negligible. Note that Shapiro, in calculating differentials in the vicinity

of the singularity, recommends using binomial expansions to come up with an approximation that can be integrated and calculated successfully for parameter values close to Mach 1.0. The same procedure can be used here to calculate differentials close to the mixture singularity.

#### **4.4            *Component Development.***

Using the Chenowith & Paolucci equations, and the generalized one-dimensional equations, equations resembling those for single-material fluids may be developed for the calculation of state variables for the various system components considered in these studies. Some of the equations are particular to only one or two components (sudden expansion or contraction loss equations, for instance,) while some calculations are performed identically for each component (particle volume fraction, for instance.) Also, for a number of components, equations for both incompressible and compressible flow conditions were derived. Generally, the incompressible equations were easier to derive and solve for than the equivalent compressible flow equations. The decision as whether to apply compressible or incompressible flow equations is made during program execution, at the moment of application, depending on the flow conditions at and just upstream of the component, as is discussed in Section 4.4.4.2. For the nozzle and starting node (“START”), only compressible flow equations were actively utilized in the model, due to numerical difficulties with some of the incompressible flow calculations.

The component equations used in the model are developed below. General isentropic equations are first derived. Next, equations for the state variables, and other characteristic properties of interest are developed and/or referenced, for both incompressible and compressible flows. In general, mixture densities are first calculated

for each component, given an input Mach number and properties of the component just upstream of the current component, because of the need for the local volume fraction  $\theta$  in the bulk of the equations, which is in turn a function of the local mixture density.

For some components, a set of equations was developed for both compressible and incompressible flows. The incompressible flow equations are used for relatively low Mach number situations; i.e., where the upstream Mach number, the previous local Mach number, and the current guess at the local Mach number are all at or below Mach 0.2. These equations are relatively simpler to solve than those for compressible flow, and should still give the same answers. In the case of the cylinder outlets and nozzles, only compressible flow equations are present and active. For the former, numerical problems were encountered with the incompressible flow equations that did not seem to manifest themselves with the compressible flow equations. For the latter, except close to the end of discharge, nozzle flows are generally at velocities greater than 0.2 Mach.

#### 4.4.1 Mixture Isentropic Relations.

The general form of the isentropic equations for gas-solids mixtures were expressed in equations (3.16), (3.17) and (3.18), where temperature, pressure, and gas density ratios were related to each other. Isentropic ratios may also be expressed as a function of Mach number, specific heat ratio, and (in the case of gas/solids mixtures, solid volume fraction  $\theta$ ); i.e.,

$$\frac{T_0}{T} = 1 + \frac{(g-1)}{2} M^2 \quad (4.31)$$

The equivalent equation for a composite fluid can be derived using the Chenoweth & Paolucci model (Section 3.2). For a calorically perfect gas,

$$h + \frac{v^2}{2} = h_0 \quad (4.32)$$

Substituting in the identity  $h = h_0 + c_p(T - T_0)$  and rearranging:

$$c_p T + \frac{v^2}{2} = c_p T_0 \quad (4.33)$$

Dividing by  $c_p T$ , substituting in the relation  $c_p = (\gamma/(\gamma-1))R$  (**Shapiro (1953)**, p. 78), and using the definitions of speed of sound (equation (4.4)) and Mach number (equation (4.7)), the result is:

$$\frac{T_0}{T} = 1 + \frac{(\mathbf{g}-1)}{2} \frac{M^2}{(1-\mathbf{q})^2} \quad (4.34)$$

From equation (3.16), for the gas density, substituting in equation (4.34), the result is:

$$\frac{\mathbf{r}_{G0}}{\mathbf{r}_G} = \left( 1 + \frac{(\mathbf{g}-1)}{2} \frac{M^2}{(1-\mathbf{q})^2} \right)^{1/(\mathbf{g}-1)} \quad (4.35)$$

(3.17), for the pressure,

$$\frac{P_0}{P} = \left( 1 + \frac{(\mathbf{g}-1)}{2} \frac{M^2}{(1-\mathbf{q})^2} \right)^{\mathbf{g}/(\mathbf{g}-1)} = \left( \frac{T_0}{T} \right)^{\mathbf{g}/(\mathbf{g}-1)} \quad (4.36)$$

An isentropic ratio for the mixture density may also be found, by substituting in local and stagnation forms of the Chenowith & Paolucci relation

$$\mathbf{r}_G = \mathbf{r} \frac{1-\mathbf{f}}{1-\mathbf{q}} \quad (4.37)$$

into equation (4.35). The relation for mixture density is then:

$$\frac{\mathbf{r}_0}{\mathbf{r}} = \frac{(1-\mathbf{q}_0)}{(1-\mathbf{q})} \left( 1 + \frac{(\mathbf{g}-1)}{2} \frac{M^2}{(1-\mathbf{q})^2} \right)^{1/(\mathbf{g}-1)} \quad (4.38)$$

#### 4.4.2 Cylinder.

A sketch of a cylinder, including nomenclature and locations, is shown in

Figure 4.2.

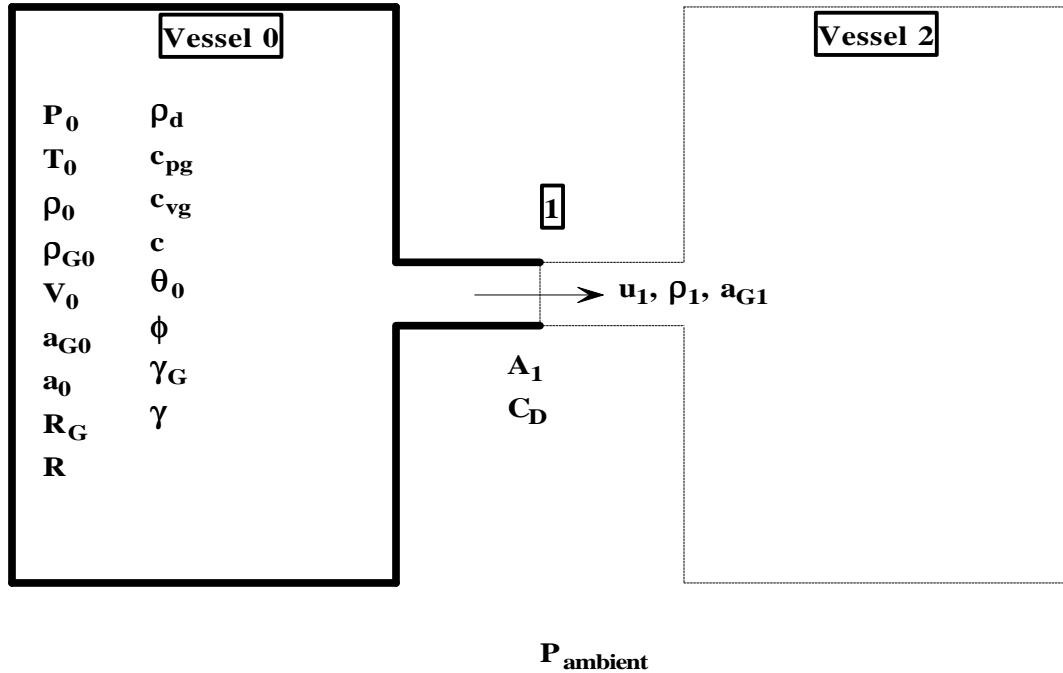


**Figure 4.2 Simple Cylinder / Exit Schematic.**

The mass flux equation, central to determining the discharge time and characteristics of a cylinder, can be derived from basic principals as follows:

The mass balance between a source cylinder and the surrounding environment is:

$$\frac{d(\mathbf{r}_0 V_0)}{dt} = -\mathbf{r}_1 u_1 C_D A_1 \quad (4.39)$$

The size of the cylinder is constant, so  $V_0$  can be removed from the differential:

$$V_0 \frac{d\mathbf{r}_0}{dt} = -\mathbf{r}_1 u_1 C_D A_1 \quad (4.40)$$

**Chenoweth & Paolucci (1990)** defined a non-dimensional time for flow between two cylinders ( $V_0$  the source cylinder, and  $V_2$  the destination cylinder) with a connection of negligible volume and length as:

$$\mathbf{t} = \frac{C_D A_1 a_{G0}(0)}{V_2} (1 + \bar{V}_2) t \quad (4.41)$$

where the barred variable has been normalized relative to its corresponding value in cylinder 0 at time = 0, as shown below:

$$\bar{f}_j = \frac{f_j}{f_0(0)} \quad (4.42)$$

{For dry chemical systems,  $V_2$  may be interpreted as the environment downstream of the delivery system exit. In this situation,  $V_2 \gg V_0$ , so that  $\tau$  becomes

$$\mathbf{t} = \frac{C_D A_1 a_{G0} t}{V_0} \quad (4.43)$$

Defining the differential

$$\frac{d}{dt} = \frac{d\tau}{dt} \frac{d}{d\tau} \quad (4.44)$$

equation (4.41) can be differentiated (the only element varying with time is time), and divide by the differentiated times:

$$\frac{d}{dt} = \frac{C_D A_1 a_{G0}(0)}{V_2} (1 + \bar{V}_2) \frac{d}{d\tau} \quad (4.45)$$

Substituting (4.45) into (4.40) yields:

$$\frac{a_{G0}(0)}{V_2} (1 + \bar{V}_2) V_0 \frac{d\rho_0}{d\tau} = -\rho_1 u_1 \quad (4.46)$$

With some re-arranging, utilizing the definition:

$$\bar{u}_1 = \frac{u_1}{a_{G0}(0)} \quad (4.47)$$

and invoking the definition in (4.42), the result is:

$$\left( \frac{1 + \bar{V}_2}{V_2} \right) V_0 \frac{d\rho_0}{d\tau} = -\rho_1 \bar{u}_1 \quad (4.48)$$

Dividing both sides by  $\rho_0(0)$ :

$$\left( \frac{1 + \bar{V}_2}{V_2} \right) V_0 \frac{d\bar{\rho}_0}{d\tau} = -\bar{\rho}_1 \bar{u}_1 \quad (4.49)$$

Some re-arranging yields:

$$\frac{d\bar{\rho}_0}{d\tau} = -\bar{\rho}_1 \bar{u}_1 \frac{V_2}{(1 + \bar{V}_2)} \frac{1}{V_0} \quad (4.50)$$

But  $V_0$ , the size of cylinder 0, is a constant, so that:

$$\bar{V}_2 = \frac{V_2}{V_0} \quad (4.51)$$

Substituting (4.51) into (4.50) yields:

$$\frac{d\bar{\rho}_0}{d\tau} = -\bar{\rho}_1 \bar{u}_1 \frac{\bar{V}_2}{(1 + \bar{V}_2)} \quad (4.52)$$

The particle volume fraction  $\theta$  is defined by Chenoweth & Paolucci as equation (3.3).

Defining the volume fraction for cylinder 0:

$$\theta_0 = \phi \frac{\rho_0}{\rho_d} \quad (4.53)$$

and for initial conditions in cylinder 0:

$$\theta_0(0) = \phi(0) \frac{\rho_0(0)}{\rho_d(0)} \quad (4.54)$$

Dividing (4.53) by (4.54) yields (invoking the definition of (4.42)):

$$\frac{\overline{\theta_0}}{\overline{\theta_0(0)}} = \overline{\theta_0} = \frac{\overline{\phi}}{\overline{\phi(0)}} \overline{\rho_0} \quad (4.55)$$

By the discussion and assumptions in **Cheoweth & Paolucci (1990)**, the mixture of gas and solid particles in cylinder 0 is homogeneous, such that the particle mass fraction of the original contents of the tank remains constant for mixture leaving the tank, and the remaining mixture within. The particle volume fractions change as mass flows from the cylinder, but the particle mass fraction ratio is assumed to remain constant. As a result,

$$\phi = \phi(0) = \text{constant} \quad (4.56)$$

Thus, (4.55) becomes:

$$\overline{\theta_0} = \overline{\rho_0} \quad (4.57)$$

Substituting (4.57) into (4.52) yields:

$$\frac{d\overline{\theta_0}}{d\tau} = -\overline{\rho_1 u_1} \frac{\overline{V_2}}{(1 + \overline{V_2})} \quad (4.58)$$

the form of the non-dimensional mass flux equation in **Chenoweth & Paolucci (1990)**.

In order to utilize equation (4.58) for the analysis of a single cylinder discharging to the atmosphere, the variable references to a “second” (destination) tank must be eliminated from the equation. This is done in the following manner:

The differential form of the definition for non-dimensional time (4.41) is substituted into (4.58):

$$\frac{d\overline{q_0}}{d\mathbf{t}} = \frac{d\overline{q_0}}{dt} \frac{V_2}{(1 + \overline{V_2})} \frac{1}{C_D A_1 a_{G0}(0)} = -\overline{\mathbf{r}_1 u_1} \frac{\overline{V_2}}{(1 + \overline{V_2})} = -\overline{\mathbf{r}_1 u_1} \frac{V_2}{(1 + \overline{V_2})} \frac{1}{V_0} \quad (4.59)$$

With some re-arranging, (4.59) becomes:



$$\frac{d\bar{q}_0}{dt} = -\bar{r}_1 u_1 \frac{C_D A_1 a_{G0}(0)}{V_0} = -\frac{\bar{r}_1 u_1 C_D A_1}{\bar{r}_0(0) V_0} \quad (4.60)$$

This form of the mass flux equation allows for inclusion of the exit cross-sectional area (including the discharge coefficient), the source cylinder volume, and the speed of sound in the source cylinder gas component at initial conditions.

With the mass flux known from calculation of the mass flow in whatever is downstream of the cylinder, equation (4.60) is used to determine the mass loss for a given time step. Note that, if the cylinder has both an “inlet” and exit, such as with a pressure transducer tap as the “inlet”, and whatever is downstream as an exit, a positive mass flow term is added to the negative mass flowing out the exit; the resulting difference is the change in mass during the time step. With the change in dimensionless mass known, the pressure and temperature may be found from the Chenowith & Paolucci equations:

$$\bar{P}_0 = \bar{q}_0^g \left[ \frac{1 - \bar{q}_0(0)}{1 - \bar{q}_0 \bar{q}_0(0)} \right]^g \quad (4.61)$$

and

$$\bar{T}_0 = \bar{P}_0^{1-(1/g)} \quad (4.62)$$

The cylinder gas density can then be calculated using the gas-only Ideal Gas Law (equation (3.4), and the cylinder mixture density using equation (3.2). Finally, knowing the solids mass in the cylinder at the start of discharge, a simple trapezoidal numerical integration results in the solids mass currently in the cylinder for times after the start of discharge.

#### 4.4.3 “START” – Cylinder Exit.

A “starting” location was established, as a component representing the exit of a cylinder. Depending on the level of detail in the configuration modeled, this may merely represent an outlet orifice, or a number of components (example: cylinder internal dip tube, valve, and exit piping, including any particular features such as elbows, etc....)

An isentropic transition from the cylinder to the piping network was assumed. The stagnation density and temperature are thus identical to those of the component immediately upstream. The local density is iteratively calculated using equation (4.38). The local solids volume fraction is calculated using equation (3.3). The temperature ratio  $T_0/T$  is calculated using equation (4.34), and from this the local temperature  $T$  is calculated. The local pressure is calculated using the mixture Ideal “Gas” Law, equation (4.1). The local speed of sound is calculated using equation (4.4), the gas-only speed of sound from equation (3.13), and the local mixture velocity from equation (4.7). The pressure ratio  $P_0/P$  is calculated from equation (4.36), and from this the local stagnation pressure is determined. The local gas density is calculated using equation (3.4), and the local gas Reynolds number is:

$$\text{Re}_g = \frac{\mathbf{r}_g v D}{\mathbf{m}} \quad (4.63)$$

The mixture Reynolds number is calculated as:

$$\text{Re}_m = \frac{\mathbf{r} v D}{\mathbf{m}} \quad (4.64)$$

In general, friction factors for a given component are calculated and stored in the component immediately upstream of the component representation in the model. The gas-only friction factor is calculated from the gas-only formula

$$f = \left[ 1.14 - 2 \log \left( \frac{e}{D} + \frac{9.35}{\text{Re}_m \sqrt{f}} \right) \right]^{-2} \quad (4.65)$$

(Source: **SFPE (1995)**, page 4-37)

The gas-only friction factor  $f$  is multiplied by a factor that accounted for corrects for the additional friction effects of the solid phase in the flow. Several empirical relations are available (as discussed in Section 3.3); however, all suffer from having been derived from test data for “dilute” flows. As a result, while the standard Moody friction factor has been altered to reflect the two-phase flow, it is highly unlikely that any of the augmentation equations are adequate to model the high loadings experienced by dry chemical fire suppression systems.

Two empirical formulas for determining the friction multiplier accounting for the solids phase are included in the model. Both formulas account for loading and gas Reynolds number. The first, described in **Doss & Srinivasan (1986)** as the “Reynolds Analogy” approach, developed by **Pfeffer *et al* (1966)**, is equation (3.39). The second, equation (3.45), is presented in **Fan & Zhu (1998)**.

The mass flow is calculated using equation (4.10), while the volumetric flow is:

$$V_{dot} = vAC_d \quad (4.66)$$

where the discharge coefficient  $C_d$  is some value less than 1.0 (empirically derived) if the START node exits to the surrounding environment, and = 1.0 if the START node is part of a piping network.

#### 4.4.3.1 Simplified Isentropic Discharge Model.

Based on the choked flow mass flow equation derived in Shapiro, and the modeling of activation time for dry pipe sprinkler system valving (SFPE (1995), Section 4, Chapter 3), a simple equation modeling source cylinder pressure versus time can be derived. This equation can be used to validate the predictive performance of the full computer model for cylinder and exit assembly discharge scenarios (without downstream piping assemblies.)

Combining equation (4.10), and the mixture Ideal “Gas” Law (equation (4.1)), the result is:

$$\frac{m_{dot}(t)}{A} = C_d \mathbf{r}(t) v(t) = \frac{C_d P(t)(1-\mathbf{q}(t))}{RT(t)} v(t) \quad (4.67)$$

where the (t) notation indicates variables that are a function of time. Expanding equation (4.67):

$$\frac{m_{dot}(t)}{A} = \frac{C_d P(t) v(t)(1-\mathbf{q}(t))}{\sqrt{\mathbf{g}RT(t)}} \sqrt{\frac{\mathbf{g}}{R}} \sqrt{\frac{T_0(t)}{T(t)}} \frac{1}{\sqrt{T_0(t)}} \quad (4.68)$$

Since the situation being modeled here consists only of a source cylinder and exit assembly, and flows moving from the cylinder into the exit assembly are assumed isentropic, stagnation temperature and pressure remain constant between the two components. Notations in equation (4.68) of “0” for stagnation conditions may thus be replaced by notations of “cyl”. To simplify the subscript notation, in subsequent equations “0” will represent stagnation conditions at a particular location, while “cyl” will represent conditions in the cylinder (which are stagnation by definition.) If a variable has no subscript, it is either the value at the exit location, or is constant for both

locations ( $\gamma$ , for instance.) For choked conditions in the exit assembly (i.e.; at Mach 1.0 in the exit assembly,) equation (4.36) becomes

$$\frac{P_{cyl}(t)}{P(t)} = \left( \frac{2(1-q(t))^2 + (g-1)}{2(1-q(t))^2} \right)^{g/(g-1)} \quad (4.69)$$

where  $P(t)$  is the local mixture pressure in the exit assembly at time =  $t$ , and  $\theta(t)$  is the local mixture solids volume fraction in the exit assembly at time =  $t$ . Note that for gas only conditions ( $\theta(t) \cong 0$ ), the inverse of equation (4.69) reverts to the form which is a function of the specific heat ratio ( $\gamma_G$ ) only, with a value of 0.5283 for a  $\gamma_G$  of 1.4 (for an ambient pressure of 14.7 psia, the minimum cylinder pressure for choking to occur is 27.83 psia.) For a gas/solids mixture, the inverse of equation (4.69) is no longer constant but for a given mixture, but increases as the solids volume fraction decreases. As long as the ratio of ambient pressure to cylinder pressure for the mixture remains below the critical ratio, flow out of the discharge system will remain choked. The main difference between a gas-only system and a solids/gas mixture is that the critical ratio is no longer a constant value, but dependent on the mixture density, in turn dependent on the mass fraction, and gas density. The results of discharge testing suggest that both the critical and actual pressure ratios increase in magnitude as discharge proceeds, with unchoking occurring when the cylinder pressure drops sufficiently so that the actual pressure ratio matches the critical ratio. For the discharge tests reported in Section 7.0, unchoking generally occurred at a pressure of approximately 25.7 psia.

Equation (4.34) becomes

$$\frac{T_{cyl}(t)}{T(t)} = \frac{2(1-q(t))^2 + (g-1)}{2(1-q(t))^2} \quad (4.70)$$

where  $T(t)$  is the local mixture temperature in the exit assembly at time =  $t$ . Substituting equations (4.69) and (4.70) into equation (4.68), and using the definition of speed of sound (equation (4.4)) and definition of Mach number (equation (4.7)), and resolving and simplifying, the result is:

$$\frac{m_{dot}(t)}{A} = \frac{C_d P_{cyl}(t) M(t)}{\sqrt{T_{cyl}(t)}} \frac{\sqrt{g \left( \frac{T_{cyl}(t)}{T(t)} \right)}}{\sqrt{R \left( \frac{T_{cyl}(t)}{T(t)} \right)}} \frac{1}{\left( \frac{T_{cyl}(t)}{T(t)} \right)^{g/(g-1)}} \quad (4.71)$$

Resolving equation (4.71) at Mach = 1.0 yields:

$$\frac{m_{dot}(t)}{A} = \frac{C_d P_{cyl}(t)}{\sqrt{T_{cyl}(t)}} \sqrt{R \left( \frac{T(t)}{T_{cyl}(t)} \right)^{(g+1)/(g-1)}} \quad (4.72)$$

Substituting equation (4.70) into equation (4.72) results in:

$$\frac{m_{dot}(t)}{A} = \frac{C_d P_{cyl}(t)}{\sqrt{T_{cyl}(t)}} \sqrt{R \left( \frac{2(1-q(t))^2}{2(1-q(t))^2 + (g-1)} \right)^{(g+1)/(g-1)}} \quad (4.73)$$

The isentropic relation between cylinder pressure and cylinder gas density, as a function of time, is:

$$\frac{P_{cyl}(t)}{P_{cyl}(0)} = \left( \frac{\mathbf{r}_{G-cyl}(t)}{\mathbf{r}_{G-cyl}(0)} \right)^g \quad (4.74)$$

or:

$$P_{cyl}(t) = P_{cyl}(0) \left( \frac{\mathbf{r}_{G-cyl}(t)}{\mathbf{r}_{G-cyl}(0)} \right)^g \quad (4.75)$$

Differentiating with respect to time yields:

$$\frac{dP_{cyl}(t)}{dt} = \mathbf{g} P_{cyl}(0) \left[ \left( \frac{\mathbf{r}_{G-cyl}(t)}{\mathbf{r}_{G-cyl}(0)} \right)^{\mathbf{g}-1} \right] \frac{d \left( \frac{\mathbf{r}_{G-cyl}(t)}{\mathbf{r}_{G-cyl}(0)} \right)}{dt} \quad (4.76)$$

With some manipulation and use of equations (4.37) and (4.74), this becomes:

$$\frac{dP_{cyl}(t)}{dt} = \mathbf{g} \frac{P_{cyl}(0)}{\mathbf{r}_{cyl}(0)} (1 - \mathbf{q}_{cyl}(0)) \left[ \left( \frac{P_{cyl}(t)}{P_{cyl}(0)} \right)^{(\mathbf{g}-1)/\mathbf{g}} \right] \frac{d \left( \frac{\mathbf{r}_{cyl}(t)}{(1 - \mathbf{q}_{cyl}(t))} \right)}{dt} \quad (4.77)$$

Differentiating the cylinder mixture density differential on the right-hand side of equation (4.77), substituting the results of the differentiation in to equation (4.77), and simplifying results in:

$$\begin{aligned} \frac{dP_{cyl}(t)}{dt} &= \mathbf{g} \frac{P_{cyl}(0)}{\mathbf{r}_{cyl}(0)} \frac{(1 - \mathbf{q}_{cyl}(0))}{(1 - \mathbf{q}_{cyl}(t))^2} \left[ \left( \frac{P_{cyl}(t)}{P_{cyl}(0)} \right)^{(\mathbf{g}-1)/\mathbf{g}} \right] \frac{d \mathbf{r}_{cyl}(t)}{dt} \\ &= \mathbf{g} \frac{P_{cyl}(0)}{\mathbf{r}_{cyl}(0)} \frac{(1 - \mathbf{q}_{cyl}(0))}{(1 - \mathbf{q}_{cyl}(t))^2} \left[ \left( \frac{P_{cyl}(t)}{P_{cyl}(0)} \right)^{(\mathbf{g}-1)/\mathbf{g}} \right] \frac{m_{dot}}{V_{cyl}} \end{aligned} \quad (4.78)$$

where  $V_{cyl}$  is the source cylinder volume. The mass flow equation (4.73) is now substituted into equation (4.78):

$$\frac{dP_{cyl}(t)}{dt} = -\mathbf{g} \frac{P_{cyl}(0)}{\mathbf{r}_{cyl}(0)} \frac{(1 - \mathbf{q}_{cyl}(0))}{(1 - \mathbf{q}_{cyl}(t))^2} \left[ \left( \frac{P_{cyl}(t)}{P_{cyl}(0)} \right)^{(\mathbf{g}-1)/\mathbf{g}} \right] \frac{C_d A}{V_{cyl}} \frac{P_{cyl}(t)}{\sqrt{T_{cyl}(t)}} \sqrt{\frac{\mathbf{g} \left( \frac{2(1 - \mathbf{q}(t))^2}{2(1 - \mathbf{q}(t))^2 + (\mathbf{g}-1)} \right)^{(\mathbf{g}+1)/(\mathbf{g}-1)}}{R}} \quad (4.79)$$

The minus sign is introduced to indicate that, as a result of the discharge, pressure is lost as time passes, because mass in the cylinder is lost as time passes. Substituting the

isentropic relation between pressure and temperature, dividing through by  $P_{cyl}(0)$ , and simplifying, yields:

$$\frac{d\left(\frac{P_{cyl}(t)}{P_{cyl}(0)}\right)}{dt} = -\frac{gRT_{cyl}(0)}{(1-q_{cyl}(t))^2} \left[\left(\frac{P_{cyl}(t)}{P_{cyl}(0)}\right)^{(3g-1)/2g}\right] \frac{C_d A}{V_{cyl} \sqrt{T_{cyl}(0)}} \sqrt{\frac{g}{R} \left(\frac{2(1-q(t))^2}{2(1-q(t))^2 + (g-1)}\right)^{(g+1)/(g-1)}} \quad (4.80)$$

For a simple cylinder-exit configuration, equation (4.80) can be used to calculate cylinder pressure versus time, to validate computer model results, and to determine the discharge coefficient of the cylinder-exit configuration.

#### 4.4.3.2 Simplified Isothermal Discharge Model.

Analogous to the simplified isentropic discharge equation (4.80), a simplified discharge model may also be derived for isothermal conditions, based on the assumption that temperature change during the discharge is minimal. Use of the computer model has demonstrated that the mixture specific heat ratio  $\gamma$  is close to 1.0, and that temperature change between components and between time steps is minimal, on the order of 5-10 °R at most for a 25 second discharge involving a cylinder, pipe, and nozzle. The model as currently derived assumes isentropic conditions. However, if there is sufficient evidence that the bulk of dry chemical system discharges involve little or no temperature change throughout a configuration or through a discharge, then the model could be re-developed assuming isothermal conditions, resulting in a mathematically simpler model.

The mass flow equation for isothermal conditions is identical to that for isentropic conditions (equation (4.73)). As with the isentropic model, the result of discharging from



the cylinder is a loss in mass of the cylinder contents; thus mass flow will be inserted in derived isothermal equations with a minus sign to account for the mass loss.

The isothermal relationship between cylinder pressure and cylinder gas density, as a function of time, is:

$$\frac{P_{cyl}(t)}{P_{cyl}(0)} = \frac{\mathbf{r}_{G-cyl}(t)}{\mathbf{r}_{G-cyl}(0)} \quad (4.81)$$

or:

$$P_{cyl}(t) = P_{cyl}(0) \frac{\mathbf{r}_{G-cyl}(t)}{\mathbf{r}_{G-cyl}(0)} \quad (4.82)$$

Based on the assumptions of pressure being a function only of the gas phase, and the particle size small enough for temperature to be evenly distributed over both phases, equation (4.37) can be applied to get:

$$\begin{aligned} P_{cyl}(t) &= P_{cyl}(0) \frac{\mathbf{r}_{cyl}(t)/(1-\mathbf{q}_{cyl}(t))}{\mathbf{r}_{cyl}(0)/(1-\mathbf{q}_{cyl}(0))} = \frac{P_{cyl}(0)}{\mathbf{r}_{cyl}(0)} (1-\mathbf{q}_{cyl}(0)) \frac{\mathbf{r}_{cyl}(t)}{(1-\mathbf{q}_{cyl}(t))} \\ &= \frac{P_{cyl}(0)}{M_{cyl}(0)} (1-\mathbf{q}_{cyl}(0)) \frac{M_{cyl}(t)}{(1-\mathbf{q}_{cyl}(t))} \end{aligned} \quad (4.83)$$

Differentiating:

$$\frac{dP_{cyl}(t)}{dt} = \frac{P_{cyl}(0)}{M_{cyl}(0)} (1-\mathbf{q}_{cyl}(0)) \frac{d\left(\frac{M_{cyl}(t)}{(1-\mathbf{q}_{cyl}(t))}\right)}{dt} \quad (4.84)$$

Differentiating the cylinder mixture mass/density differential on the right-hand side of equation (4.84), substituting the results of the differentiation into equation (4.84), and simplifying results in:

$$\frac{dP_{cyl}(t)}{dt} = \frac{P_{cyl}(0)}{M_{cyl}(0)} \frac{(1-\mathbf{q}_{cyl}(0))}{(1-\mathbf{q}_{cyl}(t))^2} \frac{dM_{cyl}(t)}{dt} = \frac{P_{cyl}(0)}{M_{cyl}(0)} \frac{(1-\mathbf{q}_{cyl}(0))}{(1-\mathbf{q}_{cyl}(t))^2} m_{dot} \quad (4.85)$$

The mass flow equation (4.73) is now substituted into equation (4.85):

$$\frac{dP_{cyl}(t)}{dt} = -\frac{P_{cyl}(0)(1-q_{cyl}(0))}{M_{cyl}(0)(1-q_{cyl}(t))^2} \frac{P_{cyl}(t)}{\sqrt{T_{cyl}(t)}} C_d A \sqrt{\frac{g}{R} \left( \frac{2(1-q(t))^2}{2(1-q(t))^2 + (g-1)} \right)^{(g+1)/(g-1)}} \quad (4.86)$$

Using the relationship

$$M_{cyl}(0) = r_{cyl}(0) V_{cyl} = \frac{P_{cyl}(0)(1-q_{cyl}(0))}{RT_{cyl}(0)} V_{cyl} \quad (4.87)$$

and simplifying (isothermal:  $T_{cyl}(t) = T_{cyl}(0) = T_{cyl}$ ), yields:

$$d \left( \frac{P_{cyl}(t)}{P_{cyl}(0)} \right) = -\frac{C_d A}{V_{cyl}} \sqrt{\frac{gRT_{cyl}}{(1-q_{cyl}(t))^4} \left( \frac{P_{cyl}(t)}{P_{cyl}(0)} \right)^2 \left( \frac{2(1-q(t))^2}{2(1-q(t))^2 + (g-1)} \right)^{(g+1)/(g-1)}} \quad (4.88)$$

where the unsubscripted  $\theta$ 's are the solid volume fraction at the cylinder exit. For a simple cylinder-exit configuration, equation (4.88) can be used to calculate cylinder pressure versus time, to validate computer model results, and to determine the discharge coefficient of the cylinder-exit configuration.

#### 4.4.4 Sudden Contractions.

Sudden contractions in a piping network must be handled somewhat differently from other components, since they represent a discontinuity in the physical geometry, and in the contained flows. As a result, differential equations cannot be applied to their analyses. Losses due to the contraction, and the vena contracta phenomena immediately downstream of the physical contraction must be accounted for through a loss formulation related to the ratio of upstream and downstream cross-sectional areas.

Figure 4.3 shows a typical sudden contraction configuration. Losses across discontinuities are generally applied to the side of the configuration with the larger

velocity flow; in this case, losses are applied to the downstream side. Flow equations are derived from application of the conservation laws.

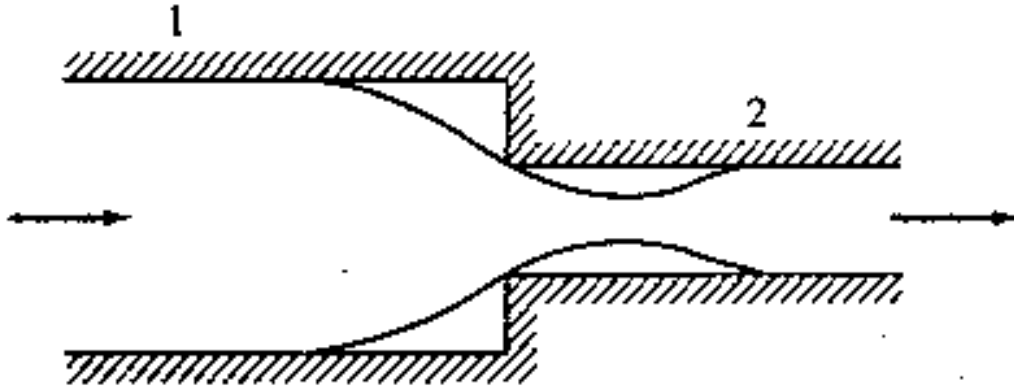


**Figure 4.3 Sudden Contraction (Source: John & Haberman (1988), p. 180).**

#### 4.4.4.1 Compressible Flow.

Referring to Figure 4.3, from equation (4.10), the Conservation of Mass:

$$\mathbf{r}_1 v_1 A_1 C_{d1} = \mathbf{r}_2 v_2 A_2 C_{d2} \quad (4.89)$$

where the discharge coefficient  $C_{d1}$  is = 1.0.  $C_{d2}$  is some value less than 1.0 (empirically derived) if the node exits to the surrounding environment, and = 1.0 if the node is part of a piping network.

The pressure differential across the contraction, accounting for losses through the loss factor  $K$ , is

$$P_1 - P_2 = \frac{\mathbf{r}_2 K v_2^2}{2} \quad (4.90)$$

The loss factor  $K$  can be found in most standard fluid mechanics text books, and is calculated from the relation  $K = 0.50(1.0 - (A_2 / A_1))^2$ .

Since the solution technique described in Section 5.3.2.2 solves for downstream properties in terms of upstream properties, substituting equation (4.89) into equation (4.90) for  $v_2$  results in (with a little re-arranging):

$$P_2 = P_1 - \frac{K}{2} \frac{r_1^2}{r_2} \left( \frac{C_{d1} A_1}{C_{d2} A_2} \right)^2 v_1^2 \quad (4.91)$$

The Conservation of Energy equation for a sudden contraction is:

$$h_1 = h_2 + \frac{K v_2^2}{2} \quad (4.92)$$

Substituting the relation  $h = c_p T$ , solving for  $T_2$ , and substituting equation (4.89) in for  $v_2$ , the result is:

$$T_2 = T_1 - \frac{K v_1^2}{2 c_p} \left( \frac{r_1}{r_2} \right)^2 \left( \frac{C_{d1} A_1}{C_{d2} A_2} \right)^2 \quad (4.93)$$

Using the definitions of speed of sound (4.4) and Mach number (4.7), and dividing through by  $T_1$ , equation (4.93) becomes:

$$\frac{T_2}{T_1} = 1 - \left( \frac{g-1}{2} \right) \frac{K M_1^2}{(1-q_1)^2} \left( \frac{r_1}{r_2} \right)^2 \left( \frac{C_{d1} A_1}{C_{d2} A_2} \right)^2 \quad (4.94)$$

Using the mixture Ideal “Gas” Law (4.1) and the definitions of speed of sound (4.4) and Mach number (4.7), and dividing through by  $P_1$ , equation (4.91) becomes:

$$\frac{P_2}{P_1} = 1 - \frac{K g M_1^2}{2(1-q_1)} \left( \frac{r_1}{r_2} \right) \left( \frac{C_{d1} A_1}{C_{d2} A_2} \right)^2 \quad (4.95)$$

Squaring equation (4.89), and applying the definitions of speed of sound (4.4) and Mach number (4.7), and substituting in equation (4.94), with some re-arranging, the result becomes:

$$M_2^2 = \frac{\left(\frac{\mathbf{r}_1}{\mathbf{r}_2}\right)^2 \left(\frac{C_{d1}A_1}{C_{d2}A_2}\right)^2 \left(\frac{1-\mathbf{q}_2}{1-\mathbf{q}_1}\right)^2 M_1^2}{1 - \left(\left(\frac{\mathbf{g}-1}{2}\right) \frac{M_1^2}{(1-\mathbf{q}_1)^2} \left(\frac{\mathbf{r}_1}{\mathbf{r}_2}\right)^2 \left(\frac{C_{d1}A_1}{C_{d2}A_2}\right)^2 K\right)} \quad (4.96)$$

The ratio of mixture densities across the discontinuity is derived using the mixture Ideal “Gas” Law (4.1). Taking the pressure ratio across the contraction, the result is:

$$\frac{P_2}{P_1} = \frac{\mathbf{r}_2 T_2}{\mathbf{r}_1 T_1} \left( \frac{1-\mathbf{q}_1}{1-\mathbf{q}_2} \right) \quad (4.97)$$

The pressure ratio is also related to the pressure differential equation (4.90):

$$\frac{P_2}{P_1} = \frac{P_1 - \frac{\mathbf{r}_2 K v_2^2}{2}}{P_1} = 1 - \frac{\mathbf{r}_2 K v_2^2}{2P_1} \quad (4.98)$$

Equating equations (4.97) and (4.98):

$$\frac{\mathbf{r}_2 T_2}{\mathbf{r}_1 T_1} \left( \frac{1-\mathbf{q}_1}{1-\mathbf{q}_2} \right) = 1 - \frac{\mathbf{r}_2 K v_2^2}{2P_1} \quad (4.99)$$

Substituting the temperature ratio (4.94) and the pressure difference equation (4.95), the result is:

$$\frac{\mathbf{r}_2}{\mathbf{r}_1} \left( \frac{1-\mathbf{q}_1}{1-\mathbf{q}_2} \right) \left( 1 - \left( \frac{\mathbf{g}-1}{2} \right) \frac{K M_1^2}{(1-\mathbf{q}_1)^2} \left( \frac{\mathbf{r}_1}{\mathbf{r}_2} \right)^2 \left( \frac{C_{d1}A_1}{C_{d2}A_2} \right)^2 \right) = 1 - \frac{K \mathbf{g} M_1^2}{2(1-\mathbf{q}_1)} \left( \frac{\mathbf{r}_1}{\mathbf{r}_2} \right) \left( \frac{C_{d1}A_1}{C_{d2}A_2} \right)^2 \quad (4.100)$$

After some manipulation:

$$\frac{\mathbf{r}_2}{\mathbf{r}_1} = \left( \frac{1-\mathbf{q}_2}{1-\mathbf{q}_1} \right) \frac{\left( 2(1-\mathbf{q}_1)^2 - K(1-\mathbf{q}_1) \mathbf{g} M_1^2 \left( \frac{\mathbf{r}_1}{\mathbf{r}_2} \right) \left( \frac{C_{d1}A_1}{C_{d2}A_2} \right)^2 \right)}{\left( 2(1-\mathbf{q}_1)^2 - K(\mathbf{g}-1) M_1^2 \left( \frac{\mathbf{r}_1}{\mathbf{r}_2} \right)^2 \left( \frac{C_{d1}A_1}{C_{d2}A_2} \right)^2 \right)} \quad (4.101)$$

Equation (4.101) is used to find the local mixture density at the downstream end of the sudden contraction.

The local solids volume fraction is calculated from equation (3.3). The local downstream velocity is calculated from the Conservation of Mass, equation (4.89). The local static temperature is calculated using the temperature ratio, equation (4.94). The local static pressure is calculated using the pressure ratio, equation (4.95). The local speed of sound is found using equation (4.4). The Mach number is determined using equation (4.7). The local stagnation temperature and pressure are determined using the isentropic relations for total-to-local temperature and pressure, equations (4.34) and (4.36) respectively. The local stagnation mixture density is calculated using equation (4.38). The local gas density is calculated using equation (3.4), and the local gas Reynolds number is calculated from equation (4.63), while the local mixture Reynolds number is calculated from equation (4.64). The friction factor is calculated from equation (4.65). The friction factor multiplier was calculated using either equation (3.39) or (3.45). The mass flow was calculated using equation (4.10), while the volumetric flow was calculated using equation (4.66).

#### **4.4.4.2 Incompressible Flow.**

If the Mach numbers at both ends of a sudden contraction are less than 0.2, and the current guess as to a new downstream Mach number is also less than 0.2, flow in the sudden contraction is treated as incompressible. Referring to Figure 4.3, the local mixture density, and stagnation temperature remain constant across the discontinuity. Because of the constant local mixture density, the local solids volume fraction remains constant across the contraction.

For incompressible flow, the local velocity  $v_2$  can be found using the Conservation of Mass (equation (4.89)):

$$v_1 A_1 C_{d1} = v_2 A_2 C_{d2} \quad (4.102)$$

Using the definition of Mach number (equation (4.7)) and equation (4.102), the ratio of upstream to downstream Mach numbers is

$$\frac{M_1}{M_2} = \frac{v_1}{v_2} \frac{a_2}{a_1} = \frac{a_2}{a_1} \frac{A_2 C_{d2}}{A_1 C_{d1}} \quad (4.103)$$

Using the definition of speed of sound (equation (4.4)) and the fact that density remains constant, the ratio of upstream to downstream speeds of sound is

$$\frac{a_2}{a_1} = \frac{\sqrt{gRT_2} (1-q_1)}{\sqrt{gRT_1} (1-q_2)} = \sqrt{\frac{T_2}{T_1}} \quad (4.104)$$

Using the Ideal “Gas” Law for these mixtures (equation (4.1)), the ratio of upstream to downstream temperature is:

$$\frac{T_2}{T_1} = \frac{P_2 (1-q_2)}{P_1 (1-q_1)} \frac{r_1 R}{r_2 R} = \frac{P_2}{P_1} \quad (4.105)$$

Substituting equation (4.105) into (4.104), the results into equation (4.103) and rearranging, the final result is:

$$M_2 = \frac{M_1 A_1 C_{d1}}{A_2 C_{d2} \sqrt{\frac{P_2}{P_1}}} \quad (4.106)$$

Using equation (4.91) and the fact that density remains constant, equation (4.106) becomes:

$$M_2 = \frac{M_1 A_1 C_{d1}}{A_2 C_{d2} \sqrt{1 - \frac{K}{2} \frac{r_1}{P_1} \left( \frac{A_1}{A_2} \right)^2}} v_1^2 \quad (4.107)$$

The local pressure is found using equation (4.90). The local stagnation pressure is found by adding local and local “dynamic” pressures:

$$P_{T2} = P_2 + \frac{r_2 v_2^2}{2} \quad (4.108)$$

The local stagnation density is found from applying the mixture Ideal “Gas” Law (equation (4.1)), and solving for  $\rho_T$ :

$$r_T = \frac{P_T}{R_G (1-f) T_T + \left( \frac{f}{r_D} \right) P_T} \quad (4.109)$$

The local temperature is found from the Ideal “Gas” Law (equation (4.1)). The local speed of sound is found from equation (4.4), and the local Mach number can be confirmed using equation (4.7). The local gas density is calculated using equation (3.4), and the local gas Reynolds number is calculated from equation (4.63), while the local mixture Reynolds number is calculated from equation (4.64). The friction factor is calculated from equation (4.65). The friction factor multiplier was calculated using either equation (3.39) or (3.45). The mass flow was calculated using equation (4.10), while the volumetric flow was calculated using equation (4.66).

#### 4.4.5 Sudden Expansions.

Like sudden contractions, sudden expansions in a piping network must be handled somewhat differently from other components, since they represent a discontinuity in the physical geometry, and in the contained flows. As a result, differential equations cannot



be applied to their analyses. Losses due to the expansion must be accounted for through a loss formulation related to the ratio of upstream and downstream cross-sectional areas.

Figure 4.4 shows a typical sudden expansion configuration. Losses across discontinuities are generally applied to the side of the configuration with the larger velocity flow; in this case, losses are applied to the upstream side. Flow equations are derived from application of the conservation laws, and are similar to those derived for sudden contractions.

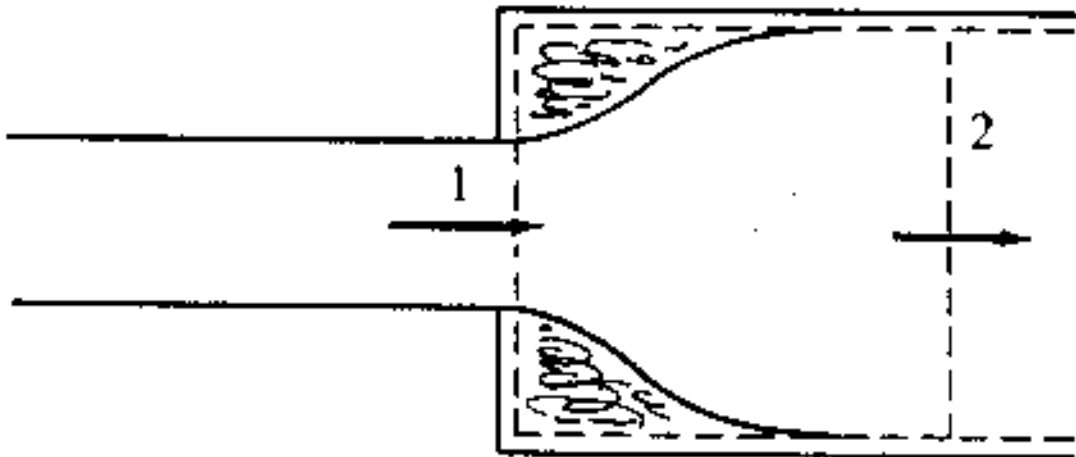


**Figure 4.4 Sudden Expansion (Source: John & Haberman (1988), p. 179).**

#### **4.4.5.1 Compressible Flow.**

Referring to Figure 4.4, from equation (4.10), the Conservation of Mass is calculated using equation (4.89).

The pressure differential across the contraction, accounting for losses through the loss factor  $K$ , is

$$P_1 - P_2 = \frac{\rho_1 K v_1^2}{2} \quad (4.110)$$

where the loss factor  $K$  can be found in most standard fluid mechanics text books, and is defined by the relation  $K = (1.0 - (A_1 / A_2))^2$ .

Since the solution technique described in Section 5.3.2.2 solves for downstream properties in terms of upstream properties, a little re-arranging results in:

$$\frac{P_2}{P_1} = 1 - K \frac{\rho_1 v_1^2}{2P_1} \quad (4.111)$$

The Conservation of Energy equation for a sudden contraction is:

$$h_1 = h_2 + \frac{Kv_1^2}{2} \quad (4.112)$$

Substituting the relation  $h = c_p T$ , and solving for  $T_2$ , the result is:

$$T_2 = T_1 - \frac{Kv_1^2}{2c_p} \quad (4.113)$$

Using the definitions of speed of sound (4.4) and Mach number (4.7) and dividing through by  $T_1$ , equation (4.113) becomes:

$$\frac{T_2}{T_1} = 1 - \left( \frac{g-1}{2} \right) \frac{KM_1^2}{(1-q_1)^2} \quad (4.114)$$

Using the mixture Ideal “Gas” Law (4.1) and the definitions of speed of sound (4.4) and Mach number (4.7), and dividing through by  $P_1$ , equation (4.111) becomes:

$$\frac{P_2}{P_1} = 1 - \frac{KgM_1^2}{2(1-q_1)} \quad (4.115)$$

Squaring equation (4.89), and applying the definitions of speed of sound (4.4) and Mach number (4.7), and substituting in equation (4.114), with some re-arranging, the result becomes:

$$M_2^2 = \frac{\left(\frac{\mathbf{r}_1}{\mathbf{r}_2}\right)^2 \left(\frac{C_{d1}A_1}{C_{d2}A_2}\right)^2 \left(\frac{1-\mathbf{q}_2}{1-\mathbf{q}_1}\right)^2 M_1^2}{1 - \left(\left(\frac{\mathbf{g}-1}{2}\right) \frac{M_1^2}{(1-\mathbf{q}_1)^2} K\right)} \quad (4.116)$$

where the discharge coefficient  $C_{d1}$  is = 1.0.  $C_{d2}$  is some value less than 1.0 (empirically derived) if the node exits to the surrounding environment, and = 1.0 if the node is part of a piping network. The ratio of mixture densities across the discontinuity is derived using the mixture Ideal “Gas” Law (4.1). Taking the pressure ratio across the expansion, the result is:

$$\frac{P_2}{P_1} = \frac{\mathbf{r}_2 T_2}{\mathbf{r}_1 T_1} \left( \frac{1-\mathbf{q}_1}{1-\mathbf{q}_2} \right) \quad (4.117)$$

Equating equations (4.111) and (4.117):

$$\frac{\mathbf{r}_2 T_2}{\mathbf{r}_1 T_1} \left( \frac{1-\mathbf{q}_1}{1-\mathbf{q}_2} \right) = 1 - K \frac{\mathbf{r}_1 v_1^2}{2P_1} \quad (4.118)$$

Substituting the temperature ratio (4.114) and the pressure difference equation (4.115),

the result is:

$$\frac{\mathbf{r}_2}{\mathbf{r}_1} \left( \frac{1-\mathbf{q}_1}{1-\mathbf{q}_2} \right) \left( 1 - \left( \frac{\mathbf{g}-1}{2} \right) \frac{KM_1^2}{(1-\mathbf{q}_1)^2} \right) = 1 - \frac{KgM_1^2}{2(1-\mathbf{q}_1)} \quad (4.119)$$

After some manipulation:

$$\frac{\mathbf{r}_2}{\mathbf{r}_1} = \left( \frac{1-\mathbf{q}_2}{1-\mathbf{q}_1} \right) \frac{\left( 2(1-\mathbf{q}_1)^2 - K(1-\mathbf{q}_1)gM_1^2 \right)}{\left( 2(1-\mathbf{q}_1)^2 - (\mathbf{g}-1)KM_1^2 \right)} \quad (4.120)$$

Equation (4.120) is used to find the local mixture density at the downstream end of the sudden expansion.

The local solids volume fraction is calculated from equation (3.3). The local downstream velocity is calculated from the Conservation of Mass, equation (4.89). The local static temperature is calculated using the temperature ratio, equation (4.114). The local static pressure is calculated using the pressure ratio, equation (4.115). The local speed of sound is found using equation (4.4). The Mach number is determined using equation (4.7). The local stagnation temperature and pressure are determined using the isentropic relations for total-to-local temperature and pressure, equations (4.34) and (4.36) respectively. The local stagnation mixture density is calculated using equation (4.38). The local gas density is calculated using equation (3.4), and the local gas Reynolds number is calculated from equation (4.63), while the local mixture Reynolds number is calculated from equation (4.64). The friction factor is calculated from equation (4.65). The friction factor multiplier was calculated using either equation (3.39) or (3.45). The mass flow was calculated using equation (4.10), while the volumetric flow was calculated using equation (4.66).

#### **4.4.5.2 Incompressible Flow.**

If the Mach number at both ends of a sudden expansion are less than 0.2, and the current guess as to a new downstream Mach number is also less than 0.2, flow through the sudden expansion is treated as incompressible. Referring to Figure 4.4, the local mixture density, and stagnation temperature remain constant across the discontinuity. Because of the constant local mixture density, the local solids volume fraction remains constant across the contraction.

For incompressible flow, the local velocity  $v_2$  can be found by using equation (4.102). The local downstream Mach number is found using equation (4.106). Using equation (4.111) and the fact that density remains constant, equation (4.106) becomes:

$$M_2 = \frac{M_1 A_1 C_{d1}}{A_2 C_{d2} \sqrt{1 - K \frac{\rho_1 v_1^2}{2P_1}}} \quad (4.121)$$

The local pressure is found using equation (4.111). The local stagnation pressure is found using equation (4.108). The local stagnation density is found from equation (4.109). The local temperature is found from the mixture Ideal “Gas” Law (equation (4.1)). The local speed of sound is found from equation (4.4) and the local Mach number can be confirmed using equation (4.7). The local gas density is calculated using equation (3.4), and the local gas Reynolds number is calculated from equation (4.63), while the local mixture Reynolds number is calculated from equation (4.64). The friction factor is calculated from equation (4.65). The friction factor multiplier was calculated using either equation (3.39) or (3.45). The mass flow was calculated using equation (4.10) while the volumetric flow was calculated using equation (4.66).

#### 4.4.6 Nozzles.

There are several nozzles typically used in dry chemical suppression systems, depending on whether the system is used in a local application, total flooding application, tank-side application, or other applications. Typical nozzle designs are shown in Figure 4.5 and Figure 4.6. The local application nozzle (shown in Figure 4.5 as the “high” and “low” overhead nozzles), configured with a throat and simple discharge

downstream expansion of the cross-sectional area, is simplest to model, merely requiring an analysis based on an isentropic expansion based on the "composite" material properties. A discharge coefficient  $C_d$ , defined in texts such as **Sabersky et al (1971)** as

$$C_d = \frac{Q}{A_2 \sqrt{\frac{2}{r} \left[ \frac{P_1 - P_2}{1 - \frac{A_2^2}{A_1^2}} \right]}}$$

where  $Q$  is the volumetric flow, and areas and pressures are at the locations as shown in Figure 4.x.3, and accounts for irreversible losses in the flow as it passes through the nozzle to the outside environment. The total flooding nozzle requires additional modeling and testing to account for the discharge holes, designed to spread agent throughout the protected enclosure. Other alterations and changes to "traditional" nozzle designs require special analyses and testing to determine performance parameters of the non-traditional designs. An alternative to these design calculations, at least in terms of pressure losses, is to empirically test a nozzle design, to determine a loss coefficient that includes losses due to all design features of the nozzle. See Section 7.2.1.1 and Section 7.4.1.1 for discussion of nozzle testing and the results of the testing performed for this research project. Note that this loss coefficient will only account for losses in the nozzle; the impact of various design features, such as powder distribution once the agent leaves the nozzle, needs to be addressed by other design procedures.

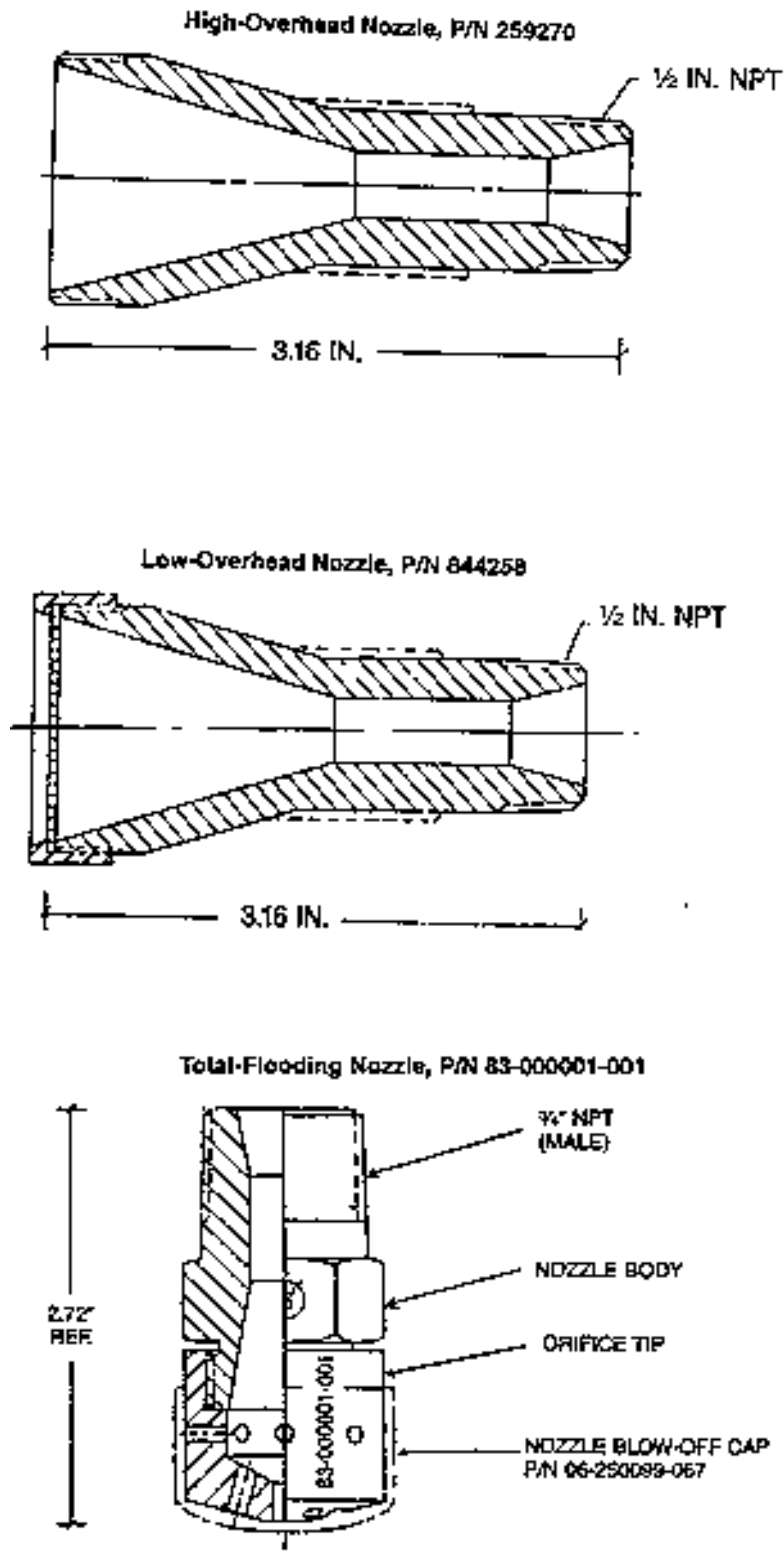


Figure 4.5 Typical Nozzles (Source: Kidde-Fenwal (1994)).



(a) Outlet view.



(b) Side View

**Figure 4.6 More Nozzles.**



The equations for fluid-only isentropic compression in a nozzle inlet are given in numerous fluid mechanics texts, such as **Sabersky *et al* (1971)**. Conditions downstream of the throat can be complex, the exact behavior – simple expansion, one or more shocks, etc, depend on conditions at the throat itself, and conditions at the downstream end of the component.

Since during choked flow conditions downstream of the throat have no effect on conditions upstream of the throat (which is choked), theoretical analyses have been restricted to this portion of the nozzle. Also, since most of the flows in the nozzle region occur either during choked flow, or flows well above 0.2 Mach, only compressible flow equations have been derived for nozzles. Furthermore, the equations derived include friction effects, accounting for fluid internal layer effects.

The analysis is covered, in part, in **Emanuel (1986)**. The Conservation of Mass is calculated using equation (4.89). A sketch of a section of variable area piping, representing the nozzle from inlet to throat, is shown in Figure 4.7. Note that location “1” denotes the nozzle inlet, while location “2” denotes the nozzle throat.

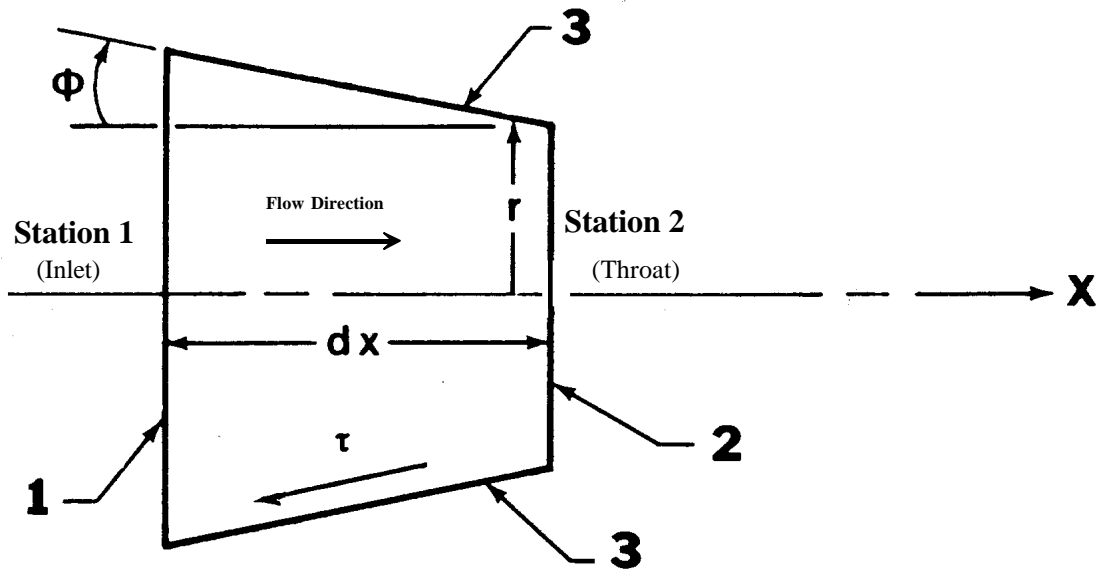


**Figure 4.7 Sketch of Differential Element of Variable Area Piping (Source: Emanuel (1986)).**

The sum of forces for one-dimensional flow on the differential region is:

$$\sum F = (PA)_1 + \left( \left( P + \frac{dP}{2} \right) dA \right)_3 - ((P + dP)(A + dA))_2 + dF_{s3} \quad (4.122)$$

where the subscripts refer to the numbered surfaces in the Figure,  $dF_{s3}$  represents the force opposing flow in the x-direction due to mixture friction  $\tau$  on the slanted surface “3”, and  $p + (dp/2)$  represents the average pressure on the wall surfaces of the differential region. Multiplying through, dropping second order terms, and simplifying results in:

$$\sum F = -Adp + dF_{s3} \quad (4.123)$$

The differential force due to friction is defined as:

$$dF_{s3} = -t \cos \phi dS_3 \quad (4.124)$$

where  $\phi$  is the angle of the slanted surface with the x-axis, as shown in the figure, and  $S_3$  is the surface area marked as “3”. As described in **Emanuel (1986)**, the differential area  $dS_3$  can be obtained by treating the surface as the frustrum of a right circular cone:

$$dS_3 = \mathbf{p} \left[ r + \left( r + \frac{\partial r}{\partial x} dx \right) \right] \left\{ (dx)^2 + \left[ r - \left( r + \frac{\partial r}{\partial x} dx \right) \right]^2 \right\}^{1/2} \quad (4.125)$$

This can be simplified to:

$$dS_3 = \frac{c dx}{\cos \mathbf{f}} \quad (4.126)$$

where

$$c = 2\mathbf{p} r \quad (4.127)$$

is the circumference, and

$$\cos \mathbf{f} = \left[ 1 + \left( \frac{\partial r}{\partial x} \right)^2 \right]^{1/2} \quad (4.128)$$

As a result,  $dF_{s_3}$  is

$$dF_{s_3} = -ct dx \quad (4.129)$$

Applying the derivative chain rule results in:

$$dF_{s_3} = -ct dx = -d(ctx) + xd(ct) \quad (4.130)$$

Since the area is changing over the range of the length of the portion of the nozzle upstream of the throat, the changed differential form shown in equation (4.130) allows integration of all terms except the distance x in the last term. Given the length of the nozzle being much shorter than most other lengths (pipe length, for instance) in a typical dry chemical system, taking an average value for x for the last term will have little effect on the overall magnitude of the last term.

Using this summing of the forces and the derived form of  $dF_{s3}$ , the linear momentum equation is:

$$C_{d1}A_1P_1 - C_{d1}A_1P_2 + \frac{\rho D_1 f_1 \mathbf{r}_1 v_1^2 x_1}{8} - \frac{\rho D_2 f_2 \mathbf{r}_2 v_2^2 x_2}{8} + \bar{x} \frac{\rho D_1 f_1 \mathbf{r}_1 v_1^2}{8} - \bar{x} \frac{\rho D_2 f_2 \mathbf{r}_2 v_2^2}{8} \quad (4.131)$$

$$= \frac{\mathbf{r}_2 v_2^2 C_{d2} A_2}{g_c} - \frac{\mathbf{r}_1 v_1^2 C_{d1} A_1}{g_c}$$

where the discharge coefficient  $C_{d1}$  is = 1.0.  $C_{d2}$  is some value less than 1.0 (empirically derived), and accounts for irreversible losses in the nozzle (the discharge coefficient for a nozzle is discussed earlier in this Section.) Since  $x_1$  is taken as =0, the third term of the left-hand side of the above equation is eliminated. Also,  $\bar{x}$  can be approximated as =  $L/2$ , and  $x_2 = L$ . Using equation (4.89), dividing through by  $C_{d1}A_1$ , with  $A = \pi D^2/4$  and simplifying yields:

$$P_2 = P_1 - \frac{D_2 \mathbf{r}_2 v_2^2}{C_{d1}} \frac{f_2 L}{2D_1^2} + \frac{\mathbf{r}_1 v_1^2}{C_{d1}} \frac{f_1 L}{4D_1} - \frac{D_2 \mathbf{r}_2 v_2^2}{C_{d1}} \frac{f_2 L}{4D_1^2} - \frac{\mathbf{r}_1 v_1}{g_c} (v_2 - v_1) \quad (4.132)$$

Using the continuity equation (equation (4.89)) in the form:

$$\mathbf{r}_2 v_2 = \mathbf{r}_1 v_1 \frac{C_{d1} A_1}{C_{d2} A_2} = \mathbf{r}_1 v_1 \frac{C_{d1} D_1^2}{C_{d2} D_2^2} \quad (4.133)$$

equation (4.132) becomes:

$$P_2 = P_1 - \frac{\mathbf{r}_1 v_1 v_2}{C_{d2}} \frac{f_2 L}{2D_2} + \frac{\mathbf{r}_1 v_1^2}{C_{d1}} \frac{f_1 L}{4D_1} - \frac{\mathbf{r}_1 v_1 v_2}{C_{d2}} \frac{f_2 L}{4D_2} - \frac{\mathbf{r}_1 v_1}{g_c} (v_2 - v_1) \quad (4.134)$$

Using the definition of speed of sound (equation (4.4)), and the definition of Mach number (equation (4.7)), dividing through by  $P_1$ , and simplifying, the result is:

$$\frac{P_2}{P_1} = 1 - \frac{3}{2} \frac{r_1}{P_1} \frac{M_1 M_2 g R \sqrt{T_1 T_2}}{(1-q_1)(1-q_2) C_{d2}} \frac{f_2 L}{2D_2} + \frac{r_1}{P_1} \frac{g M_1^2 R T_1}{(1-q_1)^2 C_{d1}} \frac{f_1 L}{4D_1} - \frac{r_1 M_1 g R \sqrt{T_1}}{P_1 (1-q_1)} \left( \frac{M_2 \sqrt{T_2}}{(1-q_2)} - \frac{M_1 \sqrt{T_1}}{(1-q_1)} \right) \quad (4.135)$$

Substituting in the relation  $\rho/P = (1-\theta)/RT$  and simplifying, the result is:

$$\frac{P_2}{P_1} = 1 - \frac{3}{2} \frac{g M_1 M_2}{C_{d2} (1-q_2)} \sqrt{\frac{T_2}{T_1}} \frac{f_2 L}{2D_2} + \frac{g M_1^2}{2 C_{d1} (1-q_1)^2} \frac{f_1 L}{2D_1} - g M_1 \left( \frac{M_2}{(1-q_2)} \sqrt{\frac{T_2}{T_1}} - \frac{M_1}{(1-q_1)} \right) \quad (4.136)$$

Using equation (4.89), and applying the definitions of speed of sound (4.4) and Mach number (4.7), with some re-arranging the result becomes:

$$M_2 = \frac{r_1}{r_2} \frac{C_{d1} A_1}{C_{d2} A_2} \left( \frac{1-q_2}{1-q_1} \right) \sqrt{\frac{T_1}{T_2}} M_1 \quad (4.137)$$

Substituting equation (4.137) into equation (4.136) and simplifying, the result is:

$$\frac{P_2}{P_1} = 1 - \frac{g M_1^2}{(1-q_1)} \left( 3 \frac{r_1}{r_2} \frac{C_{d1} A_1}{C_{d2} A_2} \frac{f_2 L}{4D_2} + \frac{r_1}{r_2} \frac{C_{d1} A_1}{C_{d2} A_2} - 1 \right) + \frac{g M_1^2}{C_{d1} (1-q_1)^2} \frac{f_1 L}{4D_1} \quad (4.138)$$

Equation (4.138), in turn, can be equated to the ratio of mixture Ideal “Gas” Laws (equation (4.117)):

$$\frac{r_2 T_2 (1-q_1)}{r_1 T_1 (1-q_2)} = 1 - \frac{g M_1^2}{(1-q_1)} \left( 3 \frac{r_1}{r_2} \frac{C_{d1} A_1}{C_{d2} A_2} \frac{f_2 L}{4D_2} + \frac{r_1}{r_2} \frac{C_{d1} A_1}{C_{d2} A_2} - 1 \right) + \frac{g M_1^2}{C_{d1} (1-q_1)^2} \frac{f_1 L}{4D_1} \quad (4.139)$$

The energy equation for two locations in a nozzle is:

$$c_p T_1 + \frac{v_1^2}{2g_c} = c_p T_2 + \frac{v_2^2}{2g_c} \quad (4.140)$$

Solving for  $T_2$ , and substituting for  $v_2$  using Conservation of Mass (equation (4.89)), the result is:

$$T_2 = T_1 + \frac{v_1^2}{2c_p g_c} - \frac{r_1}{r_2} \frac{C_{d1} A_1}{C_{d2} A_2} \frac{v_1^2}{2c_p g_c} \quad (4.141)$$

or

$$\frac{T_2}{T_1} = 1 + \frac{v_1^2}{2c_p T_1 g_c} \left( 1 - \frac{r_1}{r_2} \frac{C_{d1} A_1}{C_{d2} A_2} \right) \quad (4.142)$$

Using the relation  $c_p = \gamma R / (\gamma - 1)$ , the definition of speed of sound (equation (4.4)) and the definition of Mach number (equation (4.7)) and simplifying, the result is:

$$\frac{T_2}{T_1} = 1 + \frac{(\mathbf{g} - 1) M_1^2}{2(1 - \mathbf{q}_1)^2} \left( 1 - \frac{r_1}{r_2} \frac{C_{d1} A_1}{C_{d2} A_2} \right) \quad (4.143)$$

Substituting equation (4.143) into equation (4.139), the result is:

$$\begin{aligned} & \frac{r_2 (1 - \mathbf{q}_1)}{r_1 (1 - \mathbf{q}_2)} \left( 1 + \frac{(\mathbf{g} - 1) M_1^2}{2(1 - \mathbf{q}_1)^2} \left( 1 - \frac{r_1}{r_2} \frac{C_{d1} A_1}{C_{d2} A_2} \right) \right) \\ & = 1 - \frac{\mathbf{g} M_1^2}{(1 - \mathbf{q}_1)} \left( 3 \frac{r_1}{r_2} \frac{C_{d1} A_1}{C_{d2} A_2} \frac{f_2 L}{4D_2} + \frac{r_1}{r_2} \frac{C_{d1} A_1}{C_{d2} A_2} - 1 \right) + \frac{\mathbf{g} M_1^2}{C_{d1} (1 - \mathbf{q}_1)^2} \frac{f_1 L}{4D_1} \end{aligned} \quad (4.144)$$

With some manipulation, the mixture density was calculated by:

$$r_2 = r_1 \frac{(1 - \mathbf{q}_2)}{(1 - \mathbf{q}_1)} \frac{1 - \frac{\mathbf{g} M_1^2}{(1 - \mathbf{q}_1)} \left( 3 \frac{r_1}{r_2} \frac{C_{d1} A_1}{C_{d2} A_2} \frac{f_2 L}{4D_2} + \frac{r_1}{r_2} \frac{C_{d1} A_1}{C_{d2} A_2} - 1 \right) + \frac{\mathbf{g} M_1^2}{C_{d1} (1 - \mathbf{q}_1)^2} \frac{f_1 L}{4D_1}}{\left( 1 + \frac{(\mathbf{g} - 1) M_1^2}{2(1 - \mathbf{q}_1)^2} \left( 1 - \frac{r_1}{r_2} \frac{C_{d1} A_1}{C_{d2} A_2} \right) \right)} \quad (4.145)$$

Equation (4.145) was used to find the local mixture density at the downstream end of the nozzle component (nozzle throat). Note that the only unknown in equation (4.145) is  $\rho_2$ , which must be calculated iteratively.  $\theta_2$ , being defined as  $\theta_2 = \rho_2 \phi / \rho_D$ , varies in the current model only as a function of the mixture density  $\rho_2$ .  $C_{d1}$  is taken as = 1.0, and  $C_{d2}$  is empirically determined, usually from nozzle test data. The downstream friction term  $f_2$  is

initially guessed at to be identical to the upstream friction term  $f_1$ ; subsequently, friction terms from the previous time step are used. It is assumed that conditions in the nozzle change slowly enough over time that the friction terms at either end of the nozzle inlet interval do not change enough from time step to time step to significantly affect the calculations. Note also that the friction terms in the above equations are actually a combination of the gas-only friction factor, multiplied by the mixture friction factor multiplier appropriate to each location represented in the equation.

The current model implementation, as noted in subsequent sections, does very little error checking to verify the validity and order of user-entered data. One consequence is that, with this implementation of nozzle equations, it is possible for the user to enter “zero” for the length of the nozzle. Several options for handling this input are available:

- 1) Exit the program with an error message.
- 2) Allow the program to execute, but with the component type changed from “THROAT” to sudden “CONTRACTION” (which is, in effect, a nozzle with zero inlet length.)
- 3) Allow the program to execute, with a length of zero.

A comparison of outputs with a configuration ending in a sudden contraction, and a nozzle with throat diameter equal to the sudden contraction downstream diameter needs to be made before accepting any particular fix to this problem.

As with other components at the downstream end of a configuration, discharge coefficient data is needed to solve the derived equations.

The stagnation density and temperature are identical to those of the component immediately upstream. The local solids volume fraction was calculated using equation (3.3). The temperature ratio  $T_0/T$  was calculated using equation (4.34). The local pressure was calculated using the mixture ideal gas law, equation (4.1). The local speed of sound was calculated using equation (4.4), and the local mixture velocity from equation (4.7). The pressure ratio  $P_0/P$  was calculated from equation (4.36), and from this the local stagnation pressure is determined. The local stagnation density was calculated using equation (4.38). The local gas density was calculated using equation (3.4), and the local gas Reynolds number is found using equation (4.63). The mixture Reynolds number was calculated using equation (4.64). The friction factor was calculated from equation (4.65). The friction factor multiplier was determined from either equation (3.39) or (3.45). The mass flow was calculated using equation (4.10) while the volumetric flow was calculated using equation (4.66).

#### 4.4.7 Pipes.

Pipes can be generally handled using the equations developed in Section 4.3, assuming constant cross-sectional area throughout a given length. In the current model, pipe fittings such as elbows are handled similarly to pipe flow analyses for single fluids, treating fixtures as equivalent in flow resistance to an “equivalent” length of straight pipe of the same diameter and interior surface characteristics. Note that the same equivalent lengths for single fluids are utilized in the current model. Note also that while most investigators include gravitational forces when considering piping in the vertical direction, there is currently no distinction between horizontal and vertical pipe flows in



the model. A comparison of the effect of the multiphase flow on the solution to pipe flow momentum equations is shown in Appendix 10.2.

The density relation between upstream and downstream end of a pipe can be derived from the influence coefficients of the generalized one-dimensional flow equations as described in Section 4.3. Unlike the other general equations that can be applied to pipe flow, the relationship between Mach number and mixture density is integratable, since the differential is only in terms of density and Mach number. Other differential equations that can be generated from the influence coefficients contain integratable parameters that are not separable, resulting in differential equations that have to be integrated numerically.

Assuming a constant cross-sectional area for a given piece of piping, referring to Table 4.2, the differential equations of interest are:

$$\frac{dM^2}{M^2} = \frac{2d(b+c+1)}{2c-d+e} \quad (4.146)$$

and

$$\frac{dr}{r} = -\frac{d}{2c-d+e} \frac{fdx}{2D} \quad (4.147)$$

Dividing equation (4.146) by equation (4.147) results in:

$$\frac{dM^2}{dr} = -\frac{M^2}{r}(b+c+1) \quad (4.148)$$

Note that the friction factor cancels out of the equation. Substituting back in for the replacement variables from the identities in Table 4.2 and simplifying:

$$\frac{dM^2}{dr} = -\frac{M^2}{r} \left( \frac{2(1-q)^2 + 2q(1-q) + (g-1)M^2}{2(1-q)^2} \right) \quad (4.149)$$

With some manipulation, equation (4.149) can be converted to the form:

$$\frac{dM^2}{d\mathbf{r}} + M^2 \left( \frac{2}{\mathbf{r}} + \frac{2\mathbf{q}}{\mathbf{r}(1-\mathbf{q})} \right) = (M^2)^2 \left( \frac{(1-\mathbf{g})}{\mathbf{r}(1-\mathbf{q})^2} \right) \quad (4.150)$$

Equation (4.150) is of the form

$$\frac{dy}{dx} + P(x)y = Q(x)y^n \quad (4.151)$$

which is a Bernoulli differential equation. The solution to this equation can be found in most standard differential equation textbooks (example: **Ross (1964)**.) For Bernoulli differential equations in which  $n \neq 1$ , the transformation  $v = y^{1-n}$  reduces the equation to a linear differential equation in  $v$ . For equation (4.150),  $n = 2$ . Thus the transformation is  $v = y^{-1} = (M^2)^{-1}$ ; applied to equation (4.150), results in:

$$\frac{dv}{d\mathbf{r}} - \left( \frac{2}{\mathbf{r}} + \frac{2\mathbf{q}}{\mathbf{r}(1-\mathbf{q})} \right) v = - \left( \frac{(1-\mathbf{g})}{\mathbf{r}(1-\mathbf{q})^2} \right) \quad (4.152)$$

The integration factor for equation (4.152) is

$$e^{\int P(\mathbf{r})d\mathbf{r}} \quad (4.153)$$

where

$$P(\mathbf{r}) = - \left( \frac{2}{\mathbf{r}} + \frac{2\mathbf{f}}{\mathbf{r}_D \left( 1 - \frac{\mathbf{f}\mathbf{r}}{\mathbf{r}_D} \right)} \right) \quad (4.154)$$

(the first right-hand term of equation (4.152), re-arranged.) Carrying out the integration results in a multiplying factor of:

$$\left( \frac{\mathbf{r}_D - \mathbf{f}}{\mathbf{r}} \right)^2 \quad (4.155)$$

Multiplying equation (4.152) by factor (4.155) results in:

$$\left(\frac{\mathbf{r}_D - \mathbf{f}}{\mathbf{r}}\right)^2 \frac{dv}{d\mathbf{r}} - \left(\frac{2}{\mathbf{r}} + \frac{2\mathbf{q}}{\mathbf{r}(1-\mathbf{q})}\right) \left(\frac{\mathbf{r}_D - \mathbf{f}}{\mathbf{r}}\right)^2 v = - \left(\frac{(1-\mathbf{g})}{\mathbf{r}(1-\mathbf{q})^2}\right) \left(\frac{\mathbf{r}_D - \mathbf{f}}{\mathbf{r}}\right)^2 \quad (4.156)$$

After some further manipulation, this becomes:

$$\frac{d\left(v\left(\frac{\mathbf{r}_D - \mathbf{f}}{\mathbf{r}}\right)^2\right)}{d\mathbf{r}} = - \left(\frac{(1-\mathbf{g})}{\mathbf{r}(1-\mathbf{q})^2}\right) \left(\frac{\mathbf{r}_D - \mathbf{f}}{\mathbf{r}}\right)^2 \quad (4.157)$$

Integrating both sides, with some manipulation:

$$v\left(\frac{\mathbf{r}_D - \mathbf{f}}{\mathbf{r}}\right)^2 = (\mathbf{g}-1) \mathbf{r}_D^2 \int \frac{d\mathbf{r}}{\mathbf{r}^3} \quad (4.158)$$

Doing the integration results in:

$$v\left(\frac{\mathbf{r}_D - \mathbf{f}}{\mathbf{r}}\right)^2 = -\frac{(\mathbf{g}-1)}{2} \left(\frac{\mathbf{r}_D}{\mathbf{r}}\right)^2 + C \quad (4.159)$$

where C is a constant. If the integration is carried out between two endpoints of a pipe, calling these locations “1” and “2”, integration from “1” to “2” results in:

$$v_2 \left(\frac{\mathbf{r}_D - \mathbf{f}}{\mathbf{r}_2}\right)^2 - v_1 \left(\frac{\mathbf{r}_D - \mathbf{f}}{\mathbf{r}_1}\right)^2 = \frac{(\mathbf{g}-1)}{2} \left(\frac{\mathbf{r}_D}{\mathbf{r}_1}\right)^2 - \frac{(\mathbf{g}-1)}{2} \left(\frac{\mathbf{r}_D}{\mathbf{r}_2}\right)^2 \quad (4.160)$$

With some re-arrangement, equation (4.160) can be rewritten as a density ratio:

$$\left(\frac{\mathbf{r}_2}{\mathbf{r}_1}\right)^2 = \frac{v_2(1-\mathbf{q}_2)^2 + \frac{(\mathbf{g}-1)}{2}}{v_1(1-\mathbf{q}_1)^2 + \frac{(\mathbf{g}-1)}{2}} \quad (4.161)$$

Substituting back in for v, and re-arranging results in:

$$\frac{r_2}{r_1} = \frac{M_1}{M_2} \sqrt{\frac{(1-q_2)^2 + \frac{(g-1)}{2} M_2^2}{(1-q_1)^2 + \frac{(g-1)}{2} M_1^2}} \quad (4.162)$$

Note that if the values of  $\theta_1$  and  $\theta_2$  are set to zero, this equation reverts to equation (6.25) of **Shapiro (1953)**.

Another relation of importance in pipe flow calculations is the relationship between density and pipe length. Starting with equation (4.159), and substituting  $v = v_1$  and  $\rho = \rho_1$  (values at the upstream end of a pipe segment), the constant  $C$  takes on the value of

$$\begin{aligned} C &= \frac{1}{M_1^2} \left( \frac{r_D}{r_1} - f \right)^2 + \left( \frac{g-1}{2} \right) \left( \frac{r_D}{r_1} \right)^2 \\ &= \left( \frac{f}{q_1} \right)^2 \left( \frac{(1-q_1)^2}{M_1^2} + \frac{(g-1)}{2} \right) \end{aligned} \quad (4.163)$$

Substituting in for  $v$ , equation (4.159) can be rewritten as

$$M^2 = \frac{(r_D - fr)^2}{r^2 C - \left( \frac{g-1}{2} \right) r_D^2} \quad (4.164)$$

Using the Chain Rule, the density derivative can be written as

$$\frac{dr}{dx} = \frac{dr}{dM^2} \frac{dM^2}{dx} = \frac{1}{\left( \frac{dM^2}{dr} \right)} \frac{dM^2}{dx} \quad (4.165)$$

Differentiating equation (4.164) results in, with some re-arrangement,

$$\frac{dM^2}{dr} = \frac{2(r_D - fr) r_D \left( r_D f \left( \frac{g-1}{2} \right) - rC \right)}{\left( r^2 C - \left( \frac{g-1}{2} \right) r_D^2 \right)^2} \quad (4.166)$$

From Table 4.2, the relationship between Mach number and distance is:

$$\frac{dM^2}{dx} = 2gM^4 \frac{\left( 1 + \left( \frac{g-1}{2} \right) \frac{M^2}{(1-q)} \right) f}{(1-q) + M^2 (qg-1) 2D} \quad (4.167)$$

Substituting equations (4.166) and (4.167) into equation (4.165), the result is:

$$\frac{dr}{dx} = \frac{g(M^2)^2 \left( r^2 C - \left( \frac{g-1}{2} \right) r_D^2 \right)^2 \left( 1 + \left( \frac{g-1}{2} \right) \frac{M^2}{(1-q)} \right) f}{(r_D - fr) r_D \left( r_D f \left( \frac{g-1}{2} \right) - rC \right) (1-q) + M^2 (qg-1) 2D} \quad (4.168)$$

Substituting in equation (4.164) for  $M^2$  and simplifying, the result is:

$$\frac{dr}{dx} = \frac{(r_D - fr)^2 \left( 1 + \left( \frac{g-1}{2} \right) \frac{(r_D - fr)}{r^2 C - r_D^2 \left( \frac{g-1}{2} \right)} \right) r_D}{\left( r_D f \left( \frac{g-1}{2} \right) - rC \right) \left( 1 + (gfr - r_D) \frac{(r_D - fr)}{r^2 C - r_D^2 \left( \frac{g-1}{2} \right)} \right)} \frac{gf}{2D} \quad (4.169)$$

With some simplification, this results in:

$$\frac{dr}{dx} = \frac{(r_D - fr)^2 \left( r^2 C - \left( \frac{g-1}{2} \right) r_D fr \right)}{\left( r_D f \left( \frac{g-1}{2} \right) - rC \right) \left( r^2 C - (g-1) r_D \left( \frac{r_D - fr}{2} \right) - gf^2 r^2 \right)} \frac{gf}{2D} \quad (4.170)$$

With further simplification:

$$\frac{d\mathbf{r}}{dx} = -\frac{\mathbf{r}(\mathbf{r}_D - \mathbf{f}\mathbf{r})^2}{\left( (C - \mathbf{g}\mathbf{f}^2)\mathbf{r}^2 + (\mathbf{g} + 1)\mathbf{f}\mathbf{r}\mathbf{r}_D - \left(\frac{\mathbf{g} + 1}{2}\right)\mathbf{r}_D^2 \right)^{2D}} \frac{\mathbf{g}\mathbf{f}}{2D} \quad (4.171)$$

or:

$$\frac{dx}{d\mathbf{r}} = -\frac{\left( (C - \mathbf{g}\mathbf{f}^2)\mathbf{r}^2 + (\mathbf{g} + 1)\mathbf{f}\mathbf{r}\mathbf{r}_D - \left(\frac{\mathbf{g} + 1}{2}\right)\mathbf{r}_D^2 \right)}{\mathbf{r}(\mathbf{r}_D - \mathbf{f}\mathbf{r})^2 \frac{\mathbf{g}\mathbf{f}}{2D}} \quad (4.172)$$

The following substitutions can be used to simplify equation (4.172):  $a = \rho_D$ ,  $b = \phi$ ,  $e =$

$(\gamma + 1)\phi\rho_D$ ,  $F = ((\gamma + 1)/2)\rho_D^2$ ,  $g = C - \gamma\phi^2$ , and  $h = \gamma f/2D$ . The result:

$$\frac{dx}{d\mathbf{r}} = -\frac{(g\mathbf{r}^2 + e\mathbf{r} - F)}{rh(a - b\mathbf{r})^2} \quad (4.173)$$

The terms of equation (4.173) can now be separated, and integrated either by hand, or by use of some symbolic integrator, such as MatLab™. The result:

$$hx = -\frac{ga}{b^2} \frac{1}{(a - b\mathbf{r})} - \frac{g}{b^2} \ln\left(\frac{a - b\mathbf{r}}{a}\right) - \frac{e}{b(a - b\mathbf{r})} + \frac{F}{a^2} \ln\left(\frac{\mathbf{r}}{\mathbf{r}_D - \mathbf{f}\mathbf{r}}\right) + \frac{F}{a} \frac{1}{(a - b\mathbf{r})} + C_2 \quad (4.174)$$

where  $C_2$  is a constant. Substituting back in for the simplification variables (except for  $h$ ), and collecting terms:

$$hx = \left(\frac{\mathbf{g} + 1}{2}\right) \ln\left(\frac{\mathbf{r}}{\mathbf{r}_D - \mathbf{f}\mathbf{r}}\right) - \left(\frac{C - \mathbf{g}\mathbf{f}^2}{\mathbf{f}^2}\right) \ln\left(\frac{\mathbf{r}_D - \mathbf{f}\mathbf{r}}{\mathbf{r}_D}\right) - \frac{1}{(\mathbf{r}_D - \mathbf{f}\mathbf{r})} \left( \frac{(C - \mathbf{g}\mathbf{f}^2)\mathbf{r}_D}{\mathbf{f}^2} + \frac{2(\mathbf{g} + 1)\mathbf{r}_D}{2} - \frac{(\mathbf{g} + 1)\mathbf{r}_D}{2} \right) + C_2 \quad (4.175)$$

or:

$$h_x = \ln \left( \left( \frac{\mathbf{r}}{\mathbf{r}_D - \mathbf{f}\mathbf{r}} \right)^{\frac{g+1}{2}} \right) - \ln \left( \left( \frac{\mathbf{r}_D - \mathbf{f}\mathbf{r}}{\mathbf{r}_D} \right)^{\frac{C}{f^2} - g} \right) - \frac{\mathbf{r}_D}{(\mathbf{r}_D - \mathbf{f}\mathbf{r})} \left( \frac{C}{f^2} - \frac{(g-1)}{2} \right) + C_2 \quad (4.176)$$

At some arbitrary starting location “1” (like the location where the value of C was found),  $\rho = \rho_1$ , and  $x = 0$ . The value of  $C_2$  at this location is thus:

$$C_2 = -\ln \left( \left( \frac{\mathbf{r}_1}{\mathbf{r}_D - \mathbf{f}\mathbf{r}_1} \right)^{\frac{g+1}{2}} \right) + \ln \left( \left( \frac{\mathbf{r}_D - \mathbf{f}\mathbf{r}_1}{\mathbf{r}_D} \right)^{\frac{C}{f^2} - g} \right) + \frac{\mathbf{r}_D}{(\mathbf{r}_D - \mathbf{f}\mathbf{r}_1)} \left( \frac{C}{f^2} - \frac{(g-1)}{2} \right) \quad (4.177)$$

Equation (4.176) now becomes:

$$h_x = \ln \left( \left( \frac{\mathbf{r}}{\mathbf{r}_D - \mathbf{f}\mathbf{r}} \right)^{\frac{g+1}{2}} \right) - \ln \left( \left( \frac{\mathbf{r}_D - \mathbf{f}\mathbf{r}}{\mathbf{r}_D} \right)^{\frac{C}{f^2} - g} \right) - \frac{\mathbf{r}_D}{(\mathbf{r}_D - \mathbf{f}\mathbf{r})} \left( \frac{C}{f^2} - \frac{(g-1)}{2} \right) - \ln \left( \left( \frac{\mathbf{r}_1}{\mathbf{r}_D - \mathbf{f}\mathbf{r}_1} \right)^{\frac{g+1}{2}} \right) + \ln \left( \left( \frac{\mathbf{r}_D - \mathbf{f}\mathbf{r}_1}{\mathbf{r}_D} \right)^{\frac{C}{f^2} - g} \right) + \frac{\mathbf{r}_D}{(\mathbf{r}_D - \mathbf{f}\mathbf{r}_1)} \left( \frac{C}{f^2} - \frac{(g-1)}{2} \right) \quad (4.178)$$

Collecting terms and simplifying results in:

$$h_x = \ln \left( \left( \left( \frac{\mathbf{r}_D - \mathbf{f}\mathbf{r}_1}{\mathbf{r}_D - \mathbf{f}\mathbf{r}} \right) \left( \frac{\mathbf{r}}{\mathbf{r}_1} \right) \right)^{\frac{g+1}{2}} \right) - \ln \left( \left( \frac{\mathbf{r}_D - \mathbf{f}\mathbf{r}}{\mathbf{r}_D - \mathbf{f}\mathbf{r}_1} \right)^{\frac{C}{f^2} - g} \right) - \left( \frac{C}{f^2} - \frac{(g-1)}{2} \right) \left( \frac{\mathbf{r}_D}{(\mathbf{r}_D - \mathbf{f}\mathbf{r})} - \frac{\mathbf{r}_D}{(\mathbf{r}_D - \mathbf{f}\mathbf{r}_1)} \right) \quad (4.179)$$

Further simplification results in:

$$h_x = \ln \left( \left( \left( \frac{1 - \mathbf{q}_1}{1 - \mathbf{q}} \right)^{\frac{g+1}{2} - \frac{f^2}{C - g f^2}} \left( \frac{\mathbf{r}}{\mathbf{r}_1} \right) \right)^{\frac{g+1}{2}} \right) - \left( \frac{C}{f^2} - \frac{(g-1)}{2} \right) \left( \frac{\mathbf{q} - \mathbf{q}_1}{(1 - \mathbf{q})(1 - \mathbf{q}_1)} \right) \quad (4.180)$$

For a length L, from location “1” to location “2”, equation (4.180) becomes:

$$L = \frac{2D}{g f} \left[ \ln \left( \left( \left( \frac{1-q_1}{1-q_2} \right)^{\frac{g+1}{2}} \frac{f^2}{C-gf^2} \left( \frac{q_2}{q_1} \right) \right)^{\frac{g+1}{2}} \right) - \left( \frac{C}{f^2} - \frac{(g-1)}{2} \right) \left( \frac{q_2 - q_1}{(1-q_2)(1-q_1)} \right) \right] \quad (4.181)$$

where C is calculated using equation (4.163) at location “1”. Note that, as the friction  $ff \rightarrow 0$ ,  $L \rightarrow \infty$ . This is consistent with similar results for the gas-only integration relating optimum pipe length to pipe initial point Mach number (downstream end Mach number = 1.0):

$$L_{\max} = \frac{DC_d}{f} \left\{ \frac{1-M_1^2}{gM_1^2} + \frac{g-1}{2g} \ln \left[ \frac{(g+1)M_1^2}{2+(g-1)M_1^2} \right] \right\} \quad (4.182)$$

Giving a Mach number at the upstream end of a pipe, the pipe length can only be equal to the length at which Mach 1.0 occurs (increasing Mach number for subsonic flow, decreasing Mach number for supersonic flows. If an “optimum” pipe (with Mach 1.0 at the downstream end) is made longer, Mach 1.0 is held at the downstream end, and upstream end conditions are changed as required (reduced for subsonic conditions, increased for supersonic conditions.)) With no friction, subsonic flows never increase and supersonic flows never decrease; thus the maximum pipe length would become infinite.

The friction factor  $f$  is actually augmented with the multiplier (either equation (3.39) or (3.45)) accounting for the additional friction contributed by the solid phase.

#### 4.4.7.1 Compressible Flow.

Referring to Figure 4.1, from equation (4.10), the Conservation of Mass was calculated using equation (4.89). The local mixture density was calculated by equation



(4.162). Equation (4.181) was used to find the pipe length between two local mixture densities.

The local solids volume fraction was calculated using equation (3.3). The temperature ratio  $T_0/T$  was calculated using equation (4.34). The local pressure was calculated using the mixture ideal gas law, equation (4.1). The local mixture speed of sound was calculated using equation (4.4), and the local mixture velocity from equation (4.7). The pressure ratio  $P_0/P$  was calculated from equation (4.36), and from this the local stagnation pressure is determined. The local stagnation mixture density was calculated using equation (4.38). The local gas density was calculated using equation (3.4), and the local Reynolds number was found using equation (4.63). The mixture Reynolds number was calculated using equation (4.64). The friction factor was calculated from equation (4.65). The friction factor multiplier was determined from either equation (3.39) or (3.45). The mass flow is calculated using equation (4.10) while the volumetric flow is calculated using equation (4.66).

#### **4.4.7.2 Incompressible Flow.**

If the Mach number at both ends of a pipe are less than 0.2, and the current guess as to a new downstream Mach number is also less than 0.2, flow in the pipe is treated as incompressible. Referring to Figure 4.1, the local mixture density and stagnation temperature remain constant. Because of the constant local mixture density, the local solids volume fraction remains constant across the contraction.

For incompressible flow, the cross-sectional area remains constant for the length of the pipe. From the continuity equation, the local velocity  $v_2$  is thus equal to  $v_1$ . The local pressure was calculated from:

$$P_2 = P_1 - \rho v^2 \frac{ffL}{2D} \quad (4.183)$$

where  $f'$  is the friction multiplier accounting for the effect of solids in the mixture flow.

The local temperature was found using the mixture Ideal “Gas” Law, equation (4.1). The local downstream Mach number was found from the isentropic temperature relation for mixtures, equation (4.34). The local stagnation pressure was found using equation (4.36). The local stagnation density is found from equation (4.109). The local speed of sound is found from equation (4.4), and the local Mach number was confirmed using equation (4.7). The local gas density was calculated using equation (3.4), and the gas local Reynolds number was calculated from equation (4.63), while the local mixture Reynolds number was calculated from equation (4.64). The friction factor was calculated from equation (4.65). The friction factor multiplier was calculated using either equation (3.39) or (3.45). The mass flow was calculated using equation (4.10), while the volumetric flow was calculated using equation (4.66).

#### 4.4.8 Summary

A summary of the equations used to calculate parameters for each system component included in the model is shown below. Note that the Tables show only the references to the equations used in the calculation; no order of calculation of the parameters is implied by the ordering of parameters in the Tables.

**Table 4.3 Equations for Parameter Calculations for Cylinder.**

	Equation
Pressure (psia)	(4.61)
Mixture Density (lbm/ft <sup>3</sup> )	(3.2)
Temperature (°R)	(4.62)
Solid Volume Fraction	$((4.60) * \text{time step}) + \bar{q}_0 * \theta_{0,t=0}$
Solid Mass (lbm)	Integration of Mass Flow (Calculated in START node)
Mixture Speed of Sound (ft/sec)	(3.12)
Gas-Only Speed of Sound (ft/sec)	(3.13)
Gas-Only Density (lbm/ft <sup>3</sup> )	(3.4)

**Table 4.4 Equations for Parameter Calculations for START Node.**

Parameter	Equation
Mixture Density (lbm/ft <sup>3</sup> )	(4.38)
Solid Volume Fraction	(3.3)
Temperature Ratio T <sub>0</sub> /T	(4.34)
Temperature (°R)	From equation (4.34)
Pressure (psia)	(4.1)
Mixture Speed of Sound (ft/sec)	(4.4)
Gas-Only Speed of Sound (ft/sec)	(3.13)
Mixture velocity (ft/sec)	(4.7)
Pressure Ratio P <sub>0</sub> /P	(4.36)
Stagnation Pressure (psia)	From equation (4.36)
Gas-Only Density (lbm/ft <sup>3</sup> )	(3.4)
Gas Reynolds Number	(4.63)
Mixture Reynolds Number	(4.64)
Gas-Only friction factor	(4.65)
Friction Factor Multiplier	(3.39) or (3.45)
Mass Flow (lbm/sec)	(4.10)
Volumetric Flow (ft <sup>3</sup> /sec)	(4.66)

**Table 4.5 Equations for Parameter Calculations for Sudden Contraction.**

Parameter	Equation	
	Compressible	Incompressible
Mixture Density (lbm/ft <sup>3</sup> )	(4.101)	Constant
Solid Volume Fraction	(3.3)	Constant
Mixture Velocity (ft/sec)	(4.89)	(4.102)
Temperature (°R)	(4.94)	(4.1)
Pressure (psia)	(4.95)	(4.90)
Mixture Speed of Sound (ft/sec)	(4.4)	
Gas-Only Speed of Sound (ft/sec)	(3.13)	
Mach Number	(4.7)	(4.106)
Stagnation Temperature (°R)	(4.34)	Constant
Stagnation Pressure (psia)	(4.36)	(4.108)
Stagnation Density (lbm/ft <sup>3</sup> )	(4.38)	(4.109)
Gas-Only Density (lbm/ft <sup>3</sup> )	(3.4)	
Gas Reynolds Number	(4.63)	
Mixture Reynolds Number	(4.64)	
Gas-Only friction factor	(4.65)	
Friction Factor Multiplier	(3.39) or (3.45)	
Mass Flow (lbm/sec)	(4.10)	
Volumetric Flow (ft <sup>3</sup> /sec)	(4.66)	

**Table 4.6 Equations for Parameter Calculations for Sudden Expansion.**

Parameter	Equation	
	Compressible	Incompressible
Mixture Density (lbm/ft <sup>3</sup> )	(4.120)	Constant
Solid Volume Fraction	(3.3)	Constant
Mixture Velocity (ft/sec)	(4.89)	(4.102)
Temperature (°R)	(4.114)	(4.1)
Pressure (psia)	(4.115)	(4.111)
Mixture Speed of Sound (ft/sec)	(4.4)	
Gas-Only Speed of Sound (ft/sec)	(3.13)	
Mach Number	(4.7)	(4.121)
Stagnation Temperature (°R)	(4.34)	Constant
Stagnation Pressure (psia)	(4.36)	(4.108)
Stagnation Density (lbm/ft <sup>3</sup> )	(4.38)	(4.109)
Gas-Only Density (lbm/ft <sup>3</sup> )	(3.4)	
Gas Reynolds Number	(4.63)	
Mixture Reynolds Number	(4.64)	
Gas-Only friction factor	(4.65)	
Friction Factor Multiplier	(3.39) or (3.45)	
Mass Flow (lbm/sec)	(4.10)	
Volumetric Flow (ft <sup>3</sup> /sec)	(4.66)	

**Table 4.7 Equations for Parameter Calculations for Nozzle Throat.**

Parameter	Equation
Mixture Density (lbm/ft <sup>3</sup> )	(4.145)
Solid Volume Fraction	(3.3)
Temperature Ratio T <sub>0</sub> /T	(4.34)
Temperature (°R)	From equation (4.34)
Pressure (psia)	(4.1)
Mixture Speed of Sound (ft/sec)	(4.4)
Gas-Only Speed of Sound (ft/sec)	(3.13)
Mixture Velocity (ft/sec)	(4.7)
Pressure Ratio P <sub>0</sub> /P	(4.36)
Stagnation Pressure (psia)	From equation (4.36)
Stagnation Density (lbm/ft <sup>3</sup> )	(4.38)
Gas-Only Density (lbm/ft <sup>3</sup> )	(3.4)
Gas Reynolds Number	(4.63)
Mixture Reynolds Number	(4.64)
Gas-Only friction factor	(4.65)
Friction Factor Multiplier	(3.39) or (3.45)
Mass Flow (lbm/sec)	(4.10)
Volumetric Flow (ft <sup>3</sup> /sec)	(4.66)

**Table 4.8 Equations for Parameter Calculation for Pipe.**

Parameter	Equation	
	Compressible	Incompressible
Mixture Density (lbm/ft <sup>3</sup> )	(4.162)	Constant
Solid Volume Fraction	(3.3)	Constant
Pipe Length (ft)	(4.181)	N/A
Temperature (°R)	From equation (4.34)	(4.1)
Temperature Ratio T <sub>0</sub> /T	(4.34)	N/A
Stagnation Temperature (°R)	Constant	
Pressure (psia)	(4.1)	(4.183)
Mixture Speed of Sound (ft/sec)	(4.4)	
Gas-Only Speed of Sound (ft/sec)	(3.13)	
Mixture Velocity (ft/sec)	(4.7)	N/A
Mach Number	N/A	(4.34)
Pressure Ratio P <sub>0</sub> /P	(4.36)	
Stagnation Pressure (psia)	From equation (4.36)	
Stagnation Mixture Density (lbm/ft <sup>3</sup> )	(4.38)	(4.109)
Gas-Only Density (lbm/ft <sup>3</sup> )	(3.4)	
Gas Reynolds Number	(4.63)	
Mixture Reynolds Number	(4.64)	
Gas-Only friction factor	(4.65)	
Friction Factor Multiplier	(3.39) or (3.45)	
Mass Flow (lbm/sec)	(4.10)	
Volumetric Flow (ft <sup>3</sup> /sec)	(4.66)	



## **5.0 Computer Program – Implementation of the Theoretical Model.**

The choice of computer language to be used, and the approach to modeling a typical discharge system has a great impact on the type of program generated.

Programmability, code reliability and maintainability, the ability to adapt, change, and improve the code with time, and code understandability all will, in large part, drive and be driven by choices in programming environment and language, as well as the modeling approach to be used.

The modeling approach used for this program was Object-Oriented Design and Analysis. This technique treats the various components as a set of objects that interact with each other. Objects are grouped to take advantage of commonality amongst parts, such as different types of pipes and fittings. Data flow is analyzed to determine the best way of arranging data structures and objects to efficiently process the analysis.

Several aspects of this project mesh well with an object-oriented approach.

These include, but are not limited to:

- treating components as a hierarchy of parts (“inheritance”),
- requiring a function or operator to act differently depending on the number and object types of the arguments given to it (“polymorphism”), and
- dynamic programming, only using the amount of computer memory necessary to perform operations, obtaining memory space for computations and modeled configurations from available resources on the computer the program is running on only when needed, and releasing it when done.

These, and other features of object-oriented modeling approaches and languages, are discussed in detail in a number of standard texts, such as **Eckel (1989)** and **Swan (1992)**.

Given the various programming features available to the user, and the greater flexibility afforded by these and other features, clearly the “weapon of choice” for this project was an object-oriented language. In this instance, C++ was chosen as the language in which to implement the model

### **5.1 General Approach.**

A number of computational approaches were used to develop a working model of a dry chemical fire suppression delivery system. The development of the model was first and foremost driven by the demands of the physics of modeling gas/solids two-phase flow. Secondly, model development was driven by the assumptions made, and how closely the model matched test data as various assumptions were imposed or relaxed.

The model is capable of modeling in both the choked and unchoked conditions.  $P_{cyl}(t)/P(t)$ , the calculated value of equation (4.69) is used to verify choking. If there are piping network components downstream of the cylinder exit orifice, they need to be considered as to the number and location of the choke point(s). The logic for determining “static” choke points (i.e., either the smallest cross-sectional area in the piping network or the smallest cross-sectional area at the downstream end of a pipe component) and “dynamic” choke points (for example, a pipe with a sudden contraction at the downstream end of the pipe that, during discharge, results in choking occurring at the exit area of the sudden contraction) is built into the discharge modeling program.)

While simple to implement, applying the Runge-Kutta method to simultaneous differential equations resulted in computational stability problems, usually requiring

sufficiently small time steps to overcome instabilities. An alternative numerical method, the Bulirsch-Stoer numerical integration technique (See Section 5.6), was implemented to numerically integrate differential equations. This technique, requiring no iterative inputs, and able to integrate several differential equations simultaneously, does not have the stability problems generally occurring with Runge-Kutta numerical methods.

The spreadsheet model, re-implemented as a C++ program, retained many of the computational features already implemented in the spreadsheet version of the model. These features include multiple instances of pipe network components, iterative calculations of equations otherwise unsolvable for parameters of interest, and automatic recalculation of upstream component parameters when a given guessed parameter proves to give incorrect or inconsistent results.

## **5.2        *Data-structural Representation.***

### **5.2.1        Dry Chemical System Component Representation.**

Object-Oriented Design allows the programmer to create “data structures”, collections of data having features in common. C++ in particular allows for several types of user-defined data and computational structures. Taking advantage of these features, particularly the hierarchical nature of real system components, allows the user to 1) re-use already written code, rather than rewriting the same code for each component having commonality with some previously developed component, 2) more readily debug errors that occur, since the code appears only once in the program. Once this code is debugged, it should work correctly for all components using the code. 3), addition of new components is simplified, since a hierarchical structure already exists. The programmer

(either the original programmer, or someone following on in the work) need merely observe the work previously done to determine the correct format. Furthermore, if changes are needed or desired they can easily be built upon previous work, without having to redo the old work.

C++ allows for user-defined data types in a feature called “Classes.” A class is distinct from instances of the class; for example, the programmer defines a class called “integer\_array,” with various data variables of various types, and functional procedures that manipulate the variables. In use, the programmer then declares instances of integer\_arrays, much like declaring instances of integers, floating point numbers, etc.... Each instance will contain a set of its own parameters, and access to the procedures defined to handle the parameters. Note that, through Inheritance, a programmer may define a “child” class, which is derived from a “parent” class. The “child” inherits parameters and procedures defined for the parent, but can have additional parameters and procedures of its own. How classes work, and the complexities that can ensue with Inheritance, are well-documented in C++ texts, such as **Eckel (1989)**, and will not be discussed further here.

An ideal implementation modeling a dry chemical system would include a common parent class, “component”, with a few basic variables, such as component name, any particular user-labeling, and basic functions for accessing the variables. This would be a parent class, with child classes derived from it including “tank”, “pipe”, “nozzle”, and other components as required. Note that if additional components were desired, they could easily be implemented, derived also from the parent “component” class. Note that a programmer could further derive child classes as appropriate, such as for

“vertical\_pipe” and “horizontal\_pipe”. These component child classes would need to contain data storage for parameters at points of interest, including the ability to reference, or “point to” other components (example: the interface between two connected pipes is, in fact, a single location, and should be implemented so as to avoid redundancy). Functions peculiar to instances of each component child class would also be required; these components include the creation of (and destruction of) instances of the child component, parameter calculation functions (mixture local density, stagnation density, etc...), functions for application of the implemented solution technique to an instance of the child component, and other functions as appropriate and necessary. An example of this hierarchical implementation is shown in Figure 5.1.

The actual representation of a dry chemical fire suppression, as implemented in this research, followed a less rigorous approach than that discussed above. Since branching was not implemented in this model, there was no need to account for possible multiple interface locations in any implemented pipe system component.

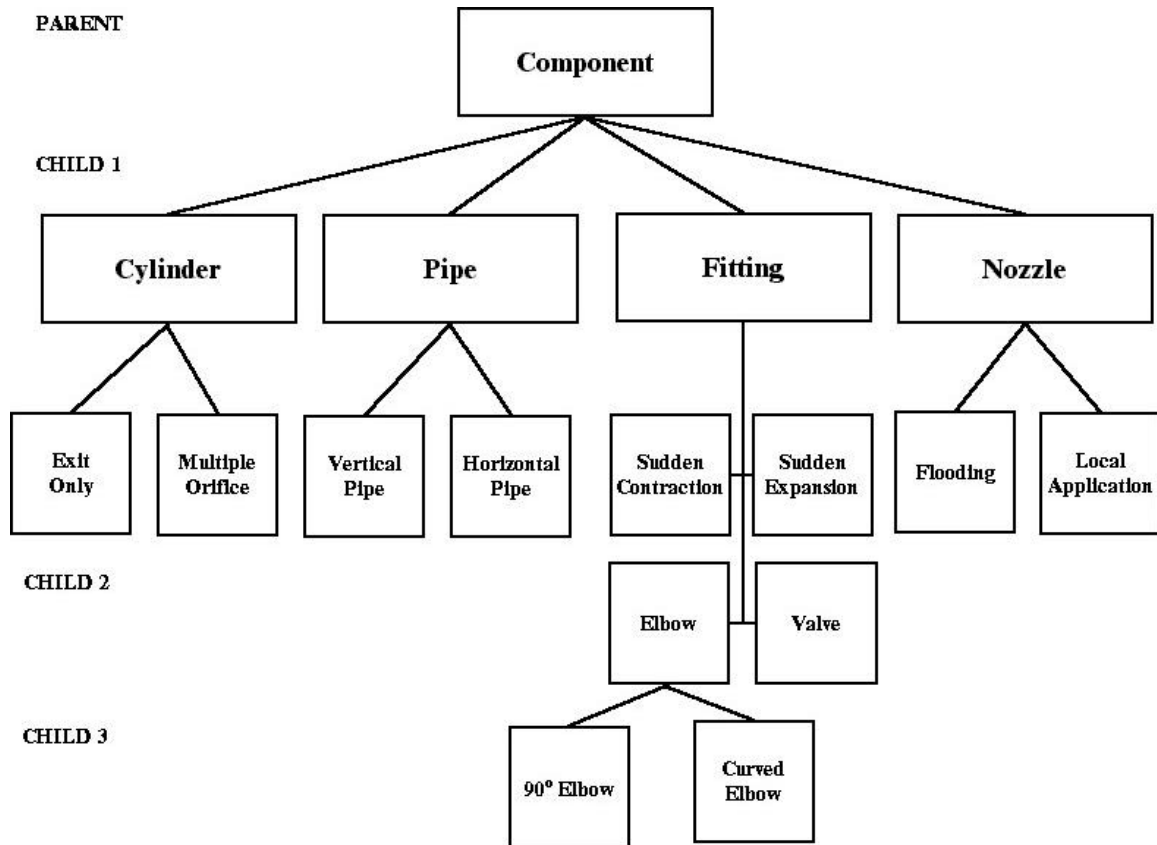


**Figure 5.1 Typical Object Oriented Design Hierarchical Relationship for Dry Chemical Fire Suppression System.**

Components either had one interface or “location of interest” (tanks with only an outlet, tank starting locations), or two interfaces (tanks with an inlet and outlet, pipes, sudden contractions and expansions, nozzles). In keeping with the general modeling of a single tank, single line piping, and single nozzle, the model was implemented as a double-linked list. A linked list representation organizes a sequence of items or objects as a “list,” much like the items on a grocery list. Each item or object is stored in the computer memory. Part of the information stored with each item or object is the means to find the next item or object in the list. To perform some action on each item in the list, a program need merely start at the first item of the list (the “head”), perform the function, and

progress to the next item in the list, using the location information for the next item, stored with the current item. When the last item (the “tail”) is reached and processed, the processing stops (the location of the “next” item or object from the tail should be a “Null”, indicating that it is the last item in the list.) In a “double-linked list,” information is stored with each item indicating both the immediately “next” AND immediately “previous” item in the list. As a result, a list can be processed starting with either end of the list. Also, each item in the list may access information about items coming “before” or “after” it in the list. The program must make sure that such accessing is not done inappropriately at the head and tail items in the list.

A schematic of a typical double-linked list is shown in Figure 5.2. The only components required for all discharges are the cylinder and START objects, representing a source cylinder and cylinder exit “orifice” (valve, and other components forming the exit assembly.) If a nozzle component is included in a configuration, it must be at the downstream end of the chain; however, the chain may end with any component other than a cylinder, or a START object not immediately preceded by a cylinder. Any combination of pipe, sudden contraction and / or sudden expansion objects may be used to represent a configuration. (Note: logic to enforce these configuration rules is not currently implemented in the program, but ultimately should be implemented to prevent nonsensical configurations.)

Two separate classes were implemented: `station_list`, and `station_list_node`. Instances of a “`station_list`” are instances of an entire chain of components, starting with a cylinder representation, and ending with at least a START (i.e., cylinder exit orifice) representation. Instances of a “`station_list_node`” are the downstream ends of

Station\_list object

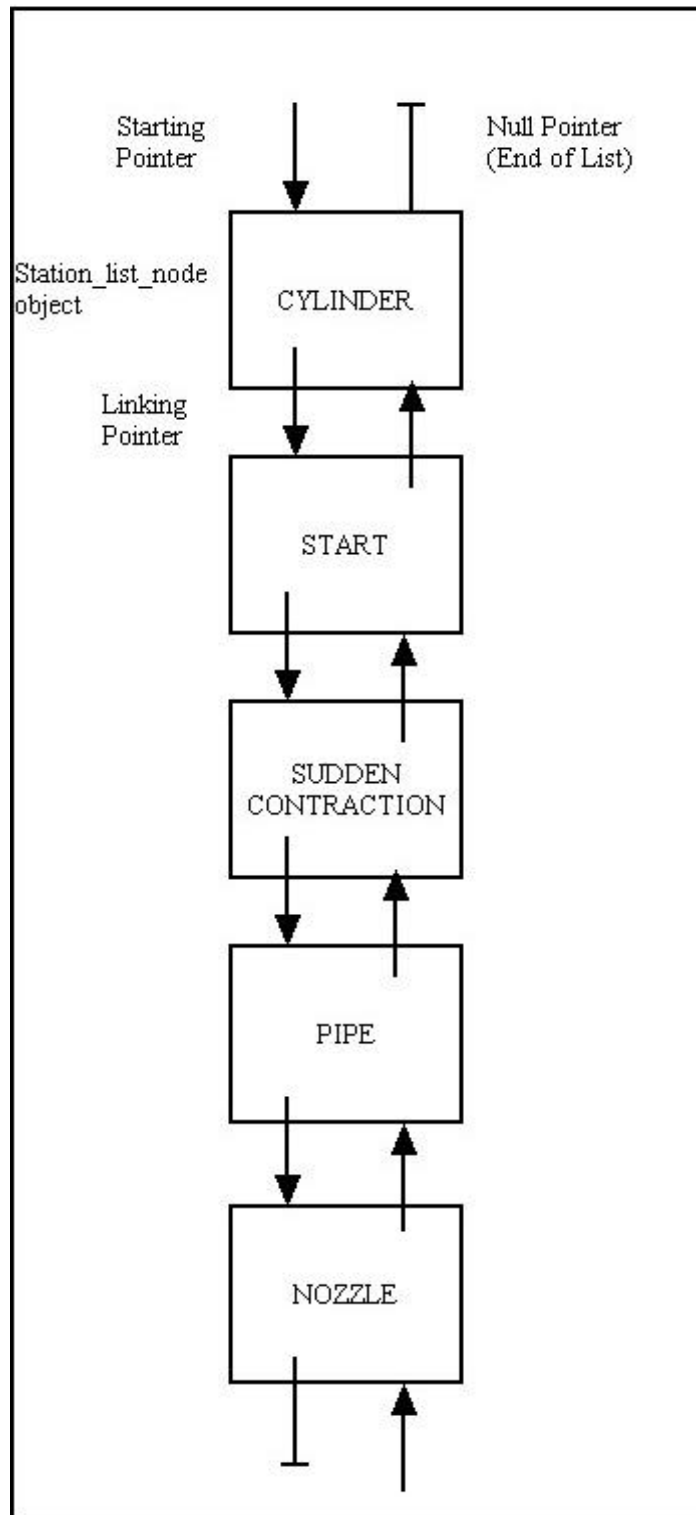


**Figure 5.2 Typical Double-Linked List.**



components, such as pipes, sudden contractions, etc.... (The upstream ends of components are simultaneously the downstream end of other components.) A simple dry chemical system is modeled in the program as a double-linked “station\_list”, with individual components represented as station\_list\_nodes. The approach taken was:

- A source tank contains parameters representing state variables and other parameters of interest. The tank, while at the head of a linked list, is computed separately from piping components. The mass flow calculated from the downstream piping system is used in reducing the agent/gas mixture in the cylinder at each time step.
- Immediately downstream of a cylinder is a “starting point.” This “starting point” contains a reference to the immediately upstream source cylinder, and obtains parameters for its calculations either from the upstream cylinder, local parameters already calculated, or the local flow velocity or Mach number received from downstream (See Section 5.3 for solution procedure details.) State parameters stored here are for the “starting point” only. If there is no further component connected downstream, this is then the point at which the system “sees” the surrounding environment. If there are downstream components (a pipe, for instance), this “starting point” not only represents the outlet of the cylinder, but also the upstream end of the next component in the system (and in the linked list.)
- Piping system components are connected to the “starting point,” in whatever order and as many as the user desires to use to model the system. The node immediately upstream of a component is considered to be the upstream end of the component, while the component node itself represents the downstream end of the real world

component. Calculations relevant to the component are controlled from the downstream end of the component. Note that a piping system component may be at the downstream-most end of a system (and a linked list.)

- Finally, the nozzle node, if there is a nozzle on the system being modeled, appears at the downstream-most end of the linked list.

Component nodes only reference (and thus are only “aware” of) the most immediate upstream node for state information. Each component node receives a velocity field guess from a source immediately downstream when the calculation procedure for the given node is called (called either by the main routine because the given component is at the downstream end of the chain, or by the component immediately downstream). The component node, however, has no particular awareness of whether there is another node downstream supplying velocity field information, or information is coming from the main routine of the program. As a result, each node performs its calculations as if it were the downstream-most node in the chain, making relevant assumptions regarding choking. These assumptions are challenged and changed as appropriate by nodes downstream of a given position in the chain.

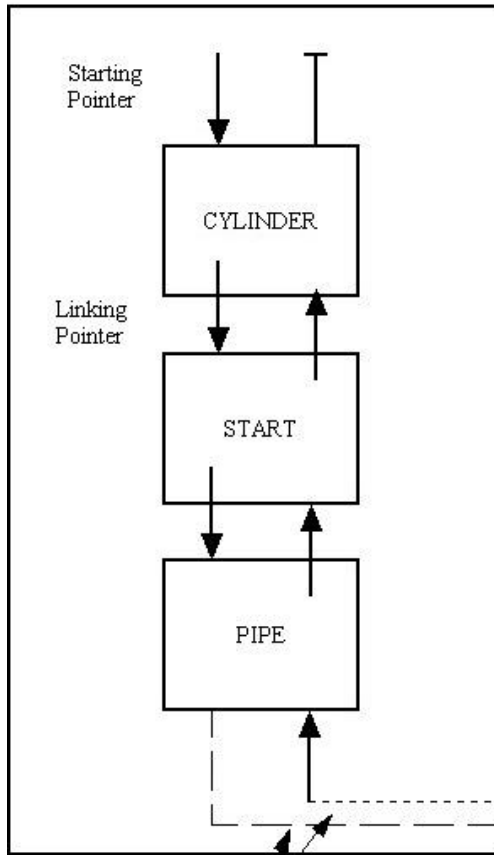
Also, since the “pointers” in the representation are actually variables carrying the memory location of the next node representation location in memory, they actually “point” in one direction only, thus requiring a “double link” in order to be able to traverse the chain in either an upstream or downstream direction.

The `station_list` class implements basic parameters and functionalities of a double-linked list. For most models, there will only be one linked list; however, capability is in the program to run multiple linked lists, with the downstream end of a linked list feeding

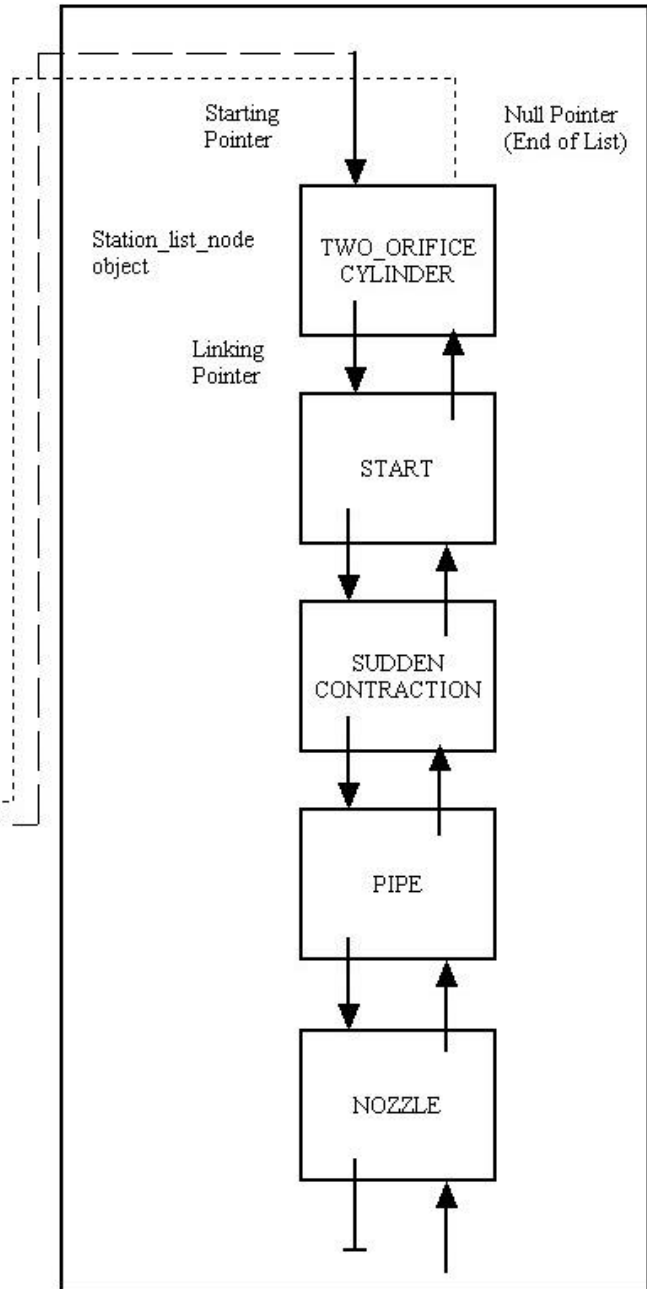
into a source cylinder for another chain. As an example configuration, a pressure transducer measuring source cylinder pressure would be implemented this way. An example of how this works is shown in Figure 5.3.

Appendix 10.5 shows the C++ implementation of both the `station_list`, and `station_list` node classes, including parameters stored, and functions implemented for each class. (Note: only class variables, and function declarations are shown (short functions are fully defined) – full listings of the class functions are in files on the enclosed CD.)

Station\_list object 1 - pressure transducer



Station\_list object 2 - main discharge system



Data transfer links between station\_list chains

**Figure 5.3 Double-Linked List for Pressure Transducer and Piping System.**

### 5.2.2 Other Data Structures.

Another user-defined data type was used in several locations in the program. This user-defined type, called a “structure”, allows the programmer to group data variables that are related to each other (state parameters, for instance) together. The variable data types may be different from each other, and may include other user-defined types.

Structures were used in two separate applications in the program. The first was a “catch-all” structure used to organize in one location a number of “universal” constants. Some of these included material properties, such as specific heats and densities of the agent and carrier gas, constants such as the gravitational constant  $g_c$ , and variables such as the specific heat ratios for the gas ( $\gamma_G$ ) and the mixture ( $\gamma$ ), which remain constant throughout a discharge. Collecting these variables into a structure allows for easier passing of the variables into called functions, as well as easier tracking of just what variables have been included in the model. Also, since variables are assigned names, constant variables are more intuitively obvious in the program code, making understanding of the code, and its long-term maintenance easier. A listing of the structure and its contents is shown in Appendix 10.6.

A simple structure was also implemented in the pipe flow calculations, to facilitate calculation and manipulation of several of the variables calculated there.

### 5.3 ***Computational Procedures.***

With a specified data structure generated to represent an arbitrary dry chemical suppression delivery system, the program then does the calculations necessary to predict system performance during discharge. A number of already-implemented software

packages were examined, to determine the kind of solution techniques implemented, and their feasibility for use in modeling dry chemical fire suppression system discharges.

The computational procedures implemented are described in the remaining sections of Section 5.3.

### 5.3.1 Solution Technique – General.

#### 5.3.1.1 Theoretical Model Solution Technique.

The basic solution to the theoretical model is based on a pipe flow problem solved in **Roberson & Crowe (1993)**. For each time step, the model initially assumes that flow in the discharge system is choked (i.e., Mach = 1.0), either at some minimum cross-sectional area, the downstream end of a sufficiently long pipe, or some combination of pipes and fittings resulting in a velocity of Mach 1.0 at the downstream end of the combination. Note that, as a consequence, when the flow is choked, it is possible to have more than one location at a velocity of Mach 1.0. Using recursive techniques described in Section 5.3.1.2, the procedure to calculate state parameters at each node is invoked, starting with the downstream-most (tail) node, and proceeding towards the upstream-most node (head). At each location, for a guessed Mach number, the local density, and other state and flow variables are calculated. The resulting conditions are checked against constraining equations and/or conditions. If the check fails, a new guess of the Mach number upstream of the failed location is attempted, a new set of parameters based on that guess are generated, and the process repeated until the constraining criteria are met. Once the criteria are met, the current calculation for that node is finished, and the function call for that node is ended. Note that if adjustment of the upstream conditions is

required, the upstream nodes will be recursively called again, as frequently as required, until conditions upstream of a given node result in acceptable conditions at the node itself. Once the main routine has established, for that time step, a flow field, and state and flow variables have been calculated for the entire piping network, a check is made to determine if the system is actually choked. The check is made by calculation of the critical cylinder/ambient pressure ratio using equation (4.69) for the given time step, and comparing that value to the ratio of the calculated cylinder pressure to ambient pressure. If the actual ratio  $P_{cy}/P_{amb}$  is greater than critical, the flow is choked; otherwise, the flow is unchoked. If the configuration is choked, the changes in the source cylinder are calculated, results are output to output data files, and the time step advanced. If the flow proves to be unchoked, calculation procedures for unchoked flow are invoked. These involve the same network calculations described above, but with the constraint that flow at the exit must be at ambient pressure. Mach number guesses in the unchoked state are generated for each call of a node, including the initial call from the main routine. Assumptions regarding choking conditions (as discussed in Section 5.3.1.2) are not applied; however, other constraints and equations are still applied. These calculations are carried forward in time until the source cylinder reaches ambient pressure, at which time the calculation procedure stops.

### **5.3.1.2 Computational Model Solution Technique.**

A computational procedure was implemented, the basis for which was a recursion procedure call to initiate solving of the model at each time step. The general philosophy of the solution is to maximize the flow of mixture from the cylinder to the piping network exit, consistent with conditions in the cylinder, the system and the surrounding

environment, and with the physical geometry of the system. At each node, an attempt is made to maximize the mixture velocity, with adjustments made to the upstream node(s) using constraint equations. Note that, as a result, some nodes will end up with less than maximum capacity flow; but this is a result of constraints imposed by other components in the system. For example, the downstream end of a pipe is initially assumed to be choked, which may be true if the pipe is the downstream end of a network, and is of “optimum” length. If there were a sudden contraction on the downstream end of the pipe, then the downstream end of the pipe (which is also the upstream end of the sudden contraction) CANNOT be at sonic velocity. The program must adjust the pipe flow so that the velocity at the downstream end of the pipe is consistent with flow into the sudden contraction, and the velocity at the exit of the contraction.

Whether a node, at a smallest cross-sectional diameter in a network or not, is choked or unchoked during the choked portion of discharge is highly dependant on the location of the node in the network, and flow conditions in the network. Nodes at the smallest cross-sectional areas can be found prior to modeling discharge; however, only during discharge can actual choke points be determined. The program is designed to determine choke points during the choked portion of the program, and generally initially assumes maximum flow through a node until constraints require flow adjustments (initially downwards).

The general flow of the solution is:

1. Before the first time step, the natural choke points in the modeled configuration are determined (See Section 5.3.7 for discussion of how “natural” choke points are determined, and how choking is handled in the calculations.) Note that, as a result of



this search, two flags are set; the first is a permanent indicator that the node is naturally either the smallest cross sectional area as a component (sudden contraction, nozzle throat, etc...), or the downstream end of a pipe with the smallest cross-sectional area. The second flag is initially set to indicate that initial calculations for this location should assume a Mach number of 1.0. After the first recursive call to this node is finished, this flag is unset for the rest of the time step calculation, to allow the Mach number to change if there are downstream nodes affecting the upstream flow conditions. At the end of a time step, this second flag is reset, to again allow for an initial Mach 1.0 calculation during the first recursive call to this node in the next time step.

2. An initial call to the solution routine is made using a Mach number guess. This initial call is made at the downstream-most node in the double-linked list representing the physical system. For each time step, the initial call is made with a negative value for the Mach number guess, indicating to the called procedure that this call is the first for that time step; appropriate actions at each node are taken to generate initially guessed Mach number. Subsequent recalls of a node, including calls from the main routine when dealing with unchoked conditions, will be made with "improved" guesses made by the "zero" routine programming controlling the given calling of the upstream node.
3. The called node immediately recursively calls the subroutine routine with its initial guess of Mach number, calling for the node immediately upstream of itself. This recursive calling up the chain continues until a TANK or TWO-TANK node is reached, where the recursive calling stops. For a TANK or TWO-TANK node, the

- only action is to return from it's recursive call (tank calculations will be done after the network flow field and state variables are calculated.)
4. The node immediately downstream of a TANK or TWO-TANK node should be a START node (indicating the source cylinder outlet or outlet assembly). An isentropic expansion from the cylinder interior to the exit of the START node is assumed; thus stagnation conditions in the cylinder at each time step are also the stagnation conditions for the START node. Using these stagnation conditions, and the guessed Mach number, local parameters for the START node are calculated. The local density is calculated first, since, through the local volume fraction, it appears in many of the subsequent calculations for that location. The rest of the parameters are then calculated, and the node then returns from its recursive call. The mass flow is one of the local parameters calculated. (One result of the calculations is that mass flow SHOULD be constant (or almost constant) for all non-cylinder nodes (for this single-pipe "network" model.) Some components may differ in the third or fourth decimal places, due to relaxation of convergence criteria for the nozzle and pipe equations – but these differences are very minor.)
  5. For as many nodes as are downstream, each node calculates the local density, and then the rest of the local parameters. The node then returns from its recursive call. Once the initial call is returned from (from the downstream-most node in the chain), the network calculation is completed.
  6. If, with the current parameters just calculated, the configuration is choked, the time step is finished. Otherwise, the procedure is repeated until the criteria for an unchoked flow are met. For unchoked flow, the time step is then completed.

7. New tank conditions for the next time step are calculated, using the mass flow calculated for the START node to determine the mass discharged during that time step, and calculating a new volume fraction for the cylinder, and other cylinder stagnation conditions using the Chenowith & Paolucci isentropic relations for gas/solids mixtures. If the cylinder has reached ambient, the discharge is over. Otherwise, time is advanced, and the process is repeated.

This solution technique is not only fairly simple to implement, it also allows for varying numbers of nodes in different configurations. Also, any Mach number guess that yields impossible or unusable state variables is not retained. Mach number guesses are made until conditions at each node are determined by constraining equations to be consistent with upstream and downstream conditions, or until an “unacceptable” number of guesses have been attempted. If the latter occurs, the program stops, with an error message attempting to give some indication as to the source of the problem – oftentimes a mathematical difficulty with convergence in an iterative procedure.

### 5.3.2 Solution Technique – Components.

Numerical solutions as applied to the various system components included in the model are discussed below. The initial Mach number guess is utilized by an iterative routine called “zero” (See Section 5.4), which makes the Mach number guesses, and evaluates the results of each guess. The routine then either generates a new Mach number guess for the upstream nodes, or ends the iterative portion of the calculation routine for that node. Except for the START and TANK and TWO\_TANK nodes, each recursive call to a node includes “zero” routine parameters and functions. Also, as currently implemented, iterations only look at the current state variables to determine

iterative steps, and are not “contaminated” either by prior recursive calls, or iterative processes at any other node.

#### **5.3.2.1 START – Cylinder Exit.**

The equations used to solve for conditions at the cylinder exit are discussed in Section 4.4.3, and summarized in Table 4.4. If a configuration ends with a START node (example: a hand-held extinguisher only requiring cylinder and START nodes, venting directly to the surroundings), the user can adjust for irreversible losses and other component characteristics not otherwise included in the analytical modeling through a discharge coefficient. If the START node is part of a piping network, the START node discharge coefficient should be set to = 1.0.

A flowchart of the solution is shown in Figure 5.4. A Mach number guess is received from the caller of the routine. Using cylinder state parameters and the guessed Mach number, the density equation is solved iteratively in a separately implemented function. Density solutions may be iterated using either a Newtonian or Richmond iterative technique (See Section 5.5). Once the Mach number and density are found, the other local state parameters are calculated using equations in Section 4.4.3.

If the calculation procedure is assuming the flow to be choked, the initial call in a given time step to the START node passes a negative value for the Mach number guess. When this happens, the START node calculates values assuming Mach 1.0 (i.e., choked throat flow). All subsequent calls during the given time step are made using positive Mach number values between 0.0 and 1.0.

The initial call in a given time step forces the velocity at the START node to be Mach 1.0 (or the value passed by the calling routine if it is between zero and one. If there are subsequent calls in a given time step, the value of the Mach number used is the value passed by the calling routine, with the value adjusted to meet velocity requirements of downstream components.

If there are nodes downstream, the calculation routine for START may be called multiple times. If START is the downstream-most node, then it will be called only once per time step if the flow is choked, and twice if the flow is unchoked.

Starting Node  
1/1/01

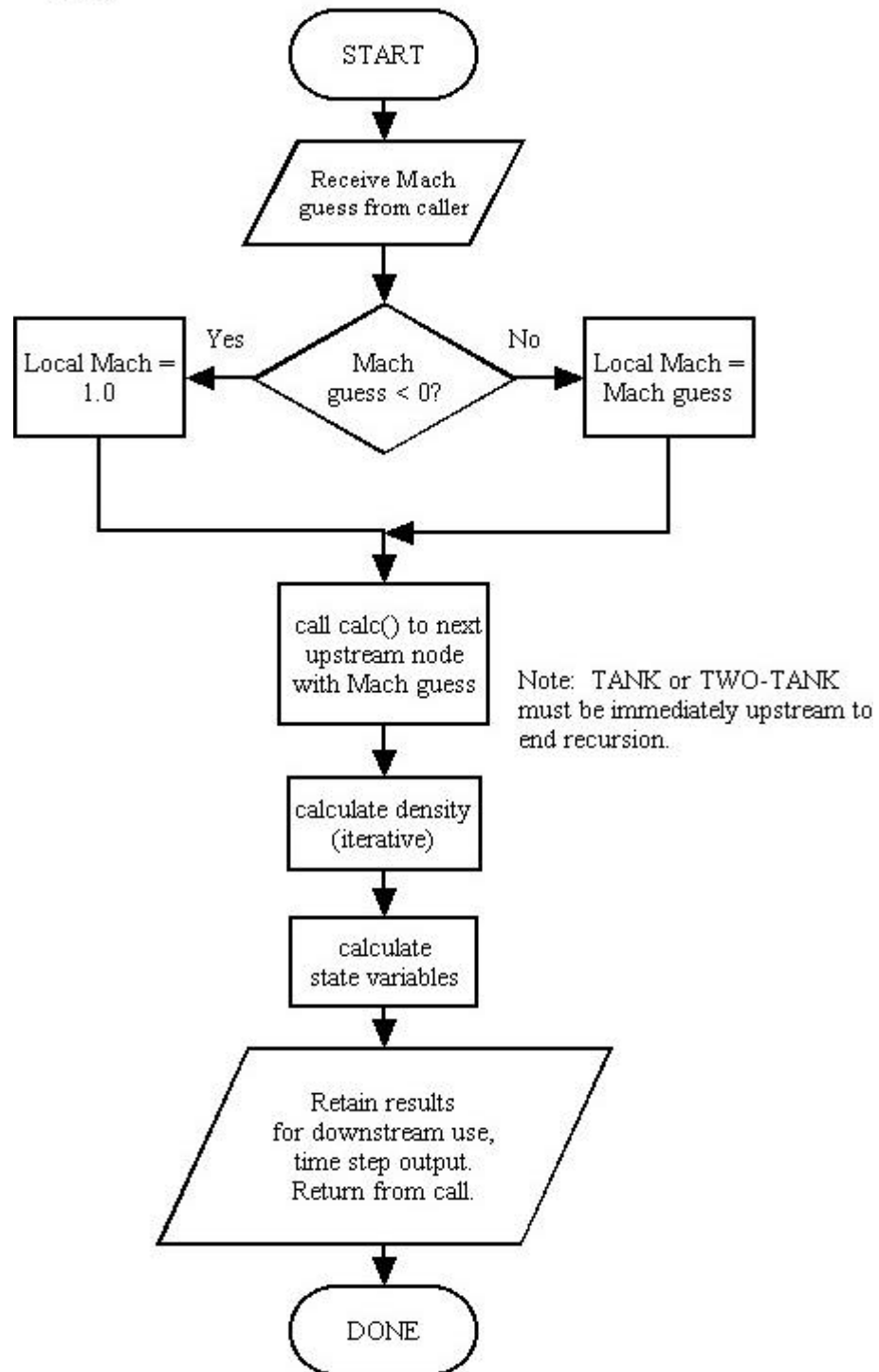


Figure 5.4 START Node - Flow Chart.

### 5.3.2.2 Sudden Contractions.

The equations used to solve for conditions at the downstream end of a sudden contraction are discussed in Section 4.4.4, and summarized in Table 4.5. A flowchart of the computational procedure is shown in Figure 5.5 (located on CD-ROM). Initially, a recursive call is made to the upstream node(s), after which the local density is calculated, and a match made to the target Mach number for the sudden contraction node. Using upstream state parameters, and the guessed Mach number for the sudden contraction node, the density equation for sudden contractions is solved in a separately implemented function.

If a configuration ends with a CONTRACTION node, the user can adjust for irreversible losses and other component characteristics not otherwise included in the analytical modeling through a discharge coefficient. If the CONTRACTION node is part of a piping network, the CONTRACTION node discharge coefficient should be set to = 1.0.

The program user can adjust for component characteristics not otherwise included in the analytical modeling through a discharge coefficient, as noted in Section 6.0.

If the calculation procedure is assuming the flow to be choked, the initial call in a given time step to the CONTRACTION node passes a negative value for the Mach number guess. When this happens, the CONTRACTION node calculates values assuming Mach 1.0 (i.e., choked throat flow). All subsequent calls during the given time step are made using positive Mach number values between 0.0 and 1.0.

The initial call in a given time step forces the velocity at the CONTRACTION node to be Mach 1.0 (or the value passed by the calling routine if it is between zero and

one. If there are subsequent calls in a given time step, the value of the Mach number used is the value passed by the calling routine, with the value adjusted to meet velocity requirements of downstream components.

If there are nodes downstream, the calculation routine for CONTRACTION may be called multiple times. If CONTRACTION is the downstream-most node, then it will be called only once per time step if the flow is choked, and twice if the flow is unchoked.

Both incompressible and compressible flow procedures are implemented and operational. The criteria for deciding upon which to use depend on the incoming Mach number guess from the caller, and the results of the previous time step. If the guessed Mach number, the node upstream (the upstream end of the contraction), and the current node (the downstream end of the contraction) are all at Mach 0.2 or less, incompressible flow is assumed; otherwise, the compressible flow equations are utilized. A “zero” routine iteration is initiated to adjust the upstream node flow conditions until they are such that using these upstream conditions to calculate the downstream Mach number results in a Mach number matching the guess from the caller. Once this match is achieved, the local state parameters are calculated using the equations in Section 4.4.4.

For compressible flow, if the call is the first one for the time step, and the choked flow flag was set, the downstream Mach number is assumed 1.0; otherwise, the guess made by the calling routine is used as the target downstream Mach number. The “zero” routine iterates the upstream flows to match the target flow. Once a match is achieved, the other local parameters are calculated. If too many steps are taken in the iteration, or an iteration error is reported, the program is exited, with appropriate error messages.



For incompressible flow, again the “zero” routine controls the iterations of the Mach number determination. If the results are close enough to the target Mach number, or if the change of guesses from one iteration to the next is less than the maximum allowable change between iterations, the results are considered “close enough”, and local variables are calculated. As a means of preventing Mach number guesses producing impossible results, such as negative densities, etc, if the upstream Mach number guess produces results close to the target, further refinement of the guesses is performed by code looking at the current and previous guesses, and doing a linear interpolation to find the optimum Mach number guess. If no errors are produced (and reported, causing the program to exit), once this portion of the routine successfully adjusts the upstream properties, local parameters are calculated, and the recursively called routine ends for that node.

### **5.3.2.3 Sudden Expansions.**

The equations used to solve for conditions at the downstream end of a sudden expansion are discussed in Section 4.4.5, and summarized in Table 4.6. A flowchart of the computational procedure is shown in Figure 5.6 (located on CD-ROM).

Computations are similar to those for a sudden contraction, with the exception that the downstream node Mach number is NEVER 1.0, but (since only sub-sonic flows are modeled in this program) always less than sonic.

If a configuration ends with a EXPANSION node, the user can adjust for irreversible losses and other component characteristics not otherwise included in the

analytical modeling through a discharge coefficient. If the EXPANSION node is part of a piping network, the EXPANSION node discharge coefficient should be set to = 1.0.

Initially, a recursive call is made to the upstream node(s), after which the local density is calculated, and a match made to the target Mach number for the sudden expansion node. Using upstream state parameters, and the guessed Mach number for the sudden expansion node, the density equation for sudden expansions is solved in a separately implemented function. Solutions may be iterated using either a Newtonian or Richmond iterative technique (See Section 5.5).

The initial call to a sudden expansion node for a given time step results in a straight calculation of downstream Mach number and state parameters. Subsequent calls in a given time step force iteration of the upstream nodes until the target downstream Mach number can be calculated from the upstream conditions.

If there are nodes downstream, the calculation routine for EXPANSION may be called multiple times. If EXPANSION is the downstream-most node, then it will be called only once per time step if the flow is choked, and twice if the flow is unchoked.

Both incompressible and compressible flow procedures are implemented and operational. The decision as to which to use is based on the incoming Mach number guess from the caller, and the results of the previous time step. If the guessed Mach number, the node upstream (the upstream end of the expansion), and the current node (the downstream end of the expansion) are all at Mach 0.2 or less, incompressible flow is assumed; otherwise, the compressible flow equations are utilized. A “zero” routine iteration is initiated to adjust the upstream node flow conditions until they are such that using these upstream conditions to calculate the downstream Mach number results in a

Mach number matching the guess from the caller. Once this match is achieved, the local state parameters are calculated using the equations in Section 4.4.5.

For compressible flow, the guess made by the calling routine is used as the target downstream Mach number. The zero routine iterates the upstream flows to match the target flow. Once a match is achieved, the other local parameters are calculated. If too many steps are taken in the iteration, or an iteration error is reported, the program is exited, with appropriate error messages.

For incompressible flow, again the zero routine controls the iterations of the Mach number determination. If the results are close enough to the target Mach number, the results are considered “close enough”, and local variables are calculated. As a means of preventing Mach number guesses producing impossible results, such as negative densities, etc..., if the upstream Mach number guess produces results close to the target, further refinement of the guesses is performed by code looking at the current and previous guesses, and doing a linear interpolation to find the optimum Mach number guess. If no errors are produced (and reported, causing the program to exit), once this portion of the routine successfully adjusts the upstream properties, local parameters are calculated, and the recursively called routine ends for that node.

#### **5.3.2.4 Pipes.**

The equations used to solve for conditions at the downstream end of a pipe are discussed in Section 4.4.7, and summarized in Table 4.8. A flowchart of the computational procedure is shown in Figure 5.7 (located on CD-ROM). Constant cross sectional areas in the pipe length are assumed, as well as constant material and wall

properties in the section modeled. If a configuration ends with a PIPE node, the user can adjust for irreversible losses and other component characteristics not otherwise included in the analytical modeling through a discharge coefficient. If the PIPE node is part of a piping network, the PIPE node discharge coefficient should be set to = 1.0.

There are additional constraints on pipe flow that can be exploited for computational purposes. The downstream end of a pipe can be subsonic, but only if the upstream velocity is below the velocity of the downstream end of the pipe – subsonic compressible flow accelerates in a pipe. No transition from sub- to super-sonic or vice versa is allowed. Also, a pipe with an upstream end flow sufficient to result in Mach 1.0 at the downstream is considered “optimum” in length. If a flow is already (or assumed to be) Mach 1.0 at the downstream end, the flow at the upstream end must be adjusted to achieve “optimum” conditions. Note that, for computational purposes, “optimum conditions” are assumed if the pipe length and upstream conditions and Mach number guess result in the target downstream Mach number, whether it is 1.0 or some lower value. In the implemented model, velocities at the upstream end of a pipe are adjusted so that subsonic compressible acceleration results in the called-for velocity at the downstream end. The adjustments, using the pipe flow equations described in Section 4.4.7, depend upon the velocity called for by the calling routine for the downstream velocity, and the already-calculated upstream state parameters.

As with the START node, a PIPE node may be either the downstream-most node in a configuration, or part of a larger configuration of components.

When the calculation routine is called for a PIPE node, a recursive call is initially made to upstream node(s). Once the program returns from these calls, the local density is

calculated, and a match made to the target Mach number for the pipe node. Using upstream state parameters, and the guessed Mach number for the pipe node, the density equation for pipes is solved in a separately implemented function.

If the calculation procedure is assuming the flow to be choked, the initial call in a given time step to the PIPE node passes a negative value for the Mach number guess. When this happens, the PIPE node calculates values assuming Mach 1.0 (i.e., choked throat flow). All subsequent calls during the given time step are made using positive Mach number values between 0.0 and 1.0.

The initial call in a given time step forces the velocity at the PIPE node to be Mach 1.0 (or the value passed by the calling routine if it is between zero and one. If there are subsequent calls in a given time step, the value of the Mach number used is the value passed by the calling routine, with the value adjusted to meet velocity requirements of downstream components.

If there are nodes downstream, the calculation routine for PIPE may be called multiple times. If PIPE is the downstream-most node, then it will be called only once per time step if the flow is choked, and twice if the flow is unchoked.

Both incompressible and compressible flow procedures are implemented and operational. The decision as to which to use is based on the incoming Mach number guess from the caller, and the results of the previous time step. If the guessed Mach number, the node upstream (the upstream end of the pipe), and the current node (the downstream end of the pipe) are all at Mach 0.2 or less, incompressible flow is assumed; otherwise, the compressible flow equations are utilized. A zero routine iteration is initiated to adjust the upstream node flow conditions until they are such that using these

upstream conditions to calculate the downstream Mach number results in a Mach number matching the guess from the caller. Once this match is achieved, the local state parameters are calculated using the equations in Section 4.4.7.

For compressible flow, the guess made by the calling routine is used as the target downstream Mach number. The local density of the downstream location, and the pipe length for an “optimum” pipe length using the upstream conditions is calculated. If the calculated length is greater than the physical pipe length, flow is assumed “sub-optimum”, and local density, Mach number, and other state parameters are calculated. If the pipe length is found to be “optimum”, no further action, other than calculation of local state variables at the downstream end of the pipe, is required. If the pipe is found to be neither “sub-optimum” or “optimum” given the upstream conditions, the zero routine is invoked to adjust upstream flow conditions until the target downstream Mach number is achieved. As before, if the number of iterations becomes excessive, the program quits, with an error message.

For incompressible flow, the zero routine controls the iterations of the Mach number determination. If the results are close enough to the target Mach number, the results are considered “close enough”, and local variables are calculated. If no errors are produced (and reported, causing the program to exit), once this portion of the routine successfully adjusts the upstream properties, local parameters are calculated, and the recursively called routine ends for that node.

### **5.3.2.5 Nozzle Throats.**

The equations used to solve for conditions at a nozzle throat are discussed in Section 4.4.6, and summarized in Table 4.7. A flowchart of the computational procedure

is shown in Figure 5.8 (located on CD-ROM). The effects of friction in the inlet are included in the calculations. If a configuration ends with a THROAT node, the user can adjust for irreversible losses and other component characteristics not otherwise included in the analytical modeling through a discharge coefficient. If the THROAT node is part of a piping network, the THROAT node discharge coefficient should be set to = 1.0.

While the main passage of a nozzle is identical to those of nozzles of other systems, such as rocket motors, dry chemical fire suppression system nozzles are designed to deliver agent to control or extinguish fires. As a result, some designs will differ from “conventional” designs; for example, extra outlet holes to facilitate widespread distribution of agent. These openings must be accounted for when determining nozzle parameters. Currently, adjustments can be made by either use of the nozzle discharge coefficient, or through adjustment of one of the other user configuration inputs.

Initially, a recursive call is made to the upstream node(s). Then, using upstream state parameters, and the guessed Mach number, the density equation for nozzle throats (equation (4.145)) is solved for the throat density ( $\rho_2$  in the equation) in a separately implemented function. The methodology of establishing the velocities in the nozzle inlet and throat are described below.

Only a compressible flow solution was implemented for this component. A zero routine iteration is used to adjust the upstream node flow conditions until the nozzle inlet Mach number based on upstream velocity conditions is matched to the nozzle inlet Mach number calculated from nozzle throat conditions, using equation (4.137). Once this

match is achieved, the local state parameters are calculated using the equations in Section 4.4.6.

A number of the state variable equations have computational difficulties with Mach numbers on opposite sides of sonic, problems ranging from inability to distinguish, in the calculated parameter from subsonic to supersonic conditions, to negative values, etc.... The problems stem not from the physical nature of the nozzle (since only a converging – diverging nozzle could go supersonic), but from 1) difficulties in confining the iterative solver “zero” to solution guesses between Mach 0 and 1.0 inclusive, and 2) the sensitivity of calculations close to Mach 1.0. As can be seen in Section 4.3, general solutions to the one-dimensional differential equations are sensitive to Mach number changes close to Mach 1.0, even with the solid phase included in the model. As a result, many of the iterative computations are easier to handle and bring to convergence at a location with Mach number somewhat less than 1.0. Instead of iterating to match the called input Mach number at the throat, the point of iteration was taken as the node just upstream of the nozzle throat node. This upstream node represents the nozzle inlet, and is lower in velocity than the throat. If the throat is choked (Mach = 1.0), the upstream node (for subsonic flows) is less than 1.0; iterating at this location causes fewer difficulties in the state variable calculations.

The model allows for an almost infinite variety of piping combinations to be modeled, and allowance was made for not only having choking take place at the so-called “natural” choke points, but also at locations not intuitively identifiable prior to program runtime without experimental data. Thus, the general approach was taken that, even though for a given configuration the choke points, “natural” or otherwise, do not change



appreciably either in velocity or location during the choked portion of the run, it was better to allow the program to re-establish the velocities in a configuration at each time step. This approach becomes more important if transient events, such as a valve opening and/or closing during discharge, are modeled. As the cross-sectional area of the component changes with time, the choke points would be expected to change, and the program must be flexible enough to re-adjust the flow field as these “events” occur.

If no initial guess at the throat Mach number is made (a dummy value of  $-1$  is used in the initial call at each time step), and the throat is a “natural” choke point (i.e., the smallest cross-sectional area in the system – See Section 5.3.3), or if the guessed Mach number = 1.0, the Mach number at the throat is assumed to be 1.0, and an approximate initial guess as to the Mach number at the nozzle inlet (the node immediately upstream of the nozzle node) using a look-up table of upstream area ratio versus subsonic Mach number for a single fluid (air) as an approximate initial guess. (Note: the mixture critical pressure equation is of no use in this calculation, since it only looks at the overall pressure difference between the cylinder and surrounding environment, whereas this approach attempts to establish the local Mach number at the nozzle inlet. Depending on the piping configuration, the pressure at the nozzle inlet may or may NOT be close to that in the cylinder. The program cannot depend on the nozzle pressure ALWAYS being close to, if not identical to, the cylinder pressure.) The upstream flow field is re-adjusted with guesses generated by the “zero” routine until the Mach number at the nozzle inlet, as determined by upstream conditions, matches the nozzle inlet Mach number calculated using upstream conditions and the throat sonic Mach (equation (4.137)). As “zero” routine guesses bring the two Mach numbers for the nozzle inlet closer to convergence,

there are sometimes problems with the calculations if the guess coming from upstream is larger than the guess coming from downstream. In these instances, as convergence is approached, several additional approaches are utilized to force convergence on a single value of nozzle inlet Mach number. A linear interpolation routine is first invoked to simplify the convergence process on the upstream flow field. If the linear interpolation fails to converge, a routine implementing the bisection interpolation algorithm (**Shammas (1995)**) makes further refinements to the guesses. If the nozzle inlet Mach number converged on results in the calculation of negative densities, a second linear interpolation routine recalculates a Mach number to keep the local density a positive value.

If no initial guess at the throat Mach number is made, and the throat is NOT a “natural” choke point (i.e., the smallest cross-sectional area in the system – See Section 5.3.4), an initial guess for the nozzle throat Mach number of 1.0 is made, and a calculation is made of the nozzle inlet node Mach number, based on a throat Mach of 1.0 (equation (4.137)). One of three conditions will result:

- 1) the nozzle inlet Mach number calculated from the upstream conditions matches that calculated from the nozzle throat, or
- 2) the nozzle inlet Mach number calculated from the throat is less than that calculated from upstream conditions (the upstream conditions are giving more flow than the nozzle throat can handle, and thus must be reduced), or
- 3) the nozzle inlet Mach number calculated from the throat is larger than that calculated from upstream conditions (flow upstream of the nozzle is already

maximized, and cannot be increased; thus nozzle velocities must be reduced to match the already maximized flow).

If the first condition results, Mach 1.0 at the throat is assumed to be correct. If the second condition results, the throat flow for that portion of the calculations is fixed at Mach 1.0, and the upstream flow field adjusted downwards until the Mach number calculated from upstream conditions matches the nozzle inlet Mach number calculated from the throat. Finally, if the third condition results, the already-maximized upstream conditions are fixed for that portion of the calculations, and the throat flow adjusted downwards until the calculated Mach number at the immediate upstream node matches that calculated from upstream conditions. Once the flow field is established, state variables at the throat are calculated

If the calling routine guesses a definite subsonic value for the Mach number for the throat, as with the choked flow calculation, the Mach number of the nozzle inlet is matched between that calculated from the area ratio equation for mixtures, and matched against the upstream inlet Mach number calculated from upstream recursive calls. As before, adjustments are made using linear interpolations to converge on a solution, and further adjustments made if negative densities are encountered.

Once the flow field is established, the state variables at the throat are calculated, and the recursively called routine ends for that node.

#### **5.3.2.6 Source Cylinder (TANK, TWO\_TANK).**

The equations used to solve for conditions in the source cylinder are discussed in Section 4.4.2, and summarized in Table 4.3. Changes in conditions in the tank over the current time step are calculated once the piping network flow field and state variables are

calculated. Out of these network calculations, the net mass flow into the piping network is determined using equation (4.10) to calculate mass flow in the START node.

Stagnation conditions in the cylinder are used as stagnation conditions for the START node, assuming an isentropic expansion from the cylinder into the START “assembly.” The START node Mach number is determined iteratively using equations and constraints describing the flow field in the discharge piping assembly. Using the cylinder stagnation conditions, there is generally only one possible flow field configuration meeting the cylinder, environmental, and piping network constraints; this flow field is found iteratively using applications of the “zero” routine, and is dependent on both Mach number and mixture density at each of the locations represented in a given configuration. Once the flow field is fixed, state variables, including mass flow, can be calculated. The mass flow calculated for the START node is applied to the cylinder to determine changes in the cylinder conditions.

The basic calculation procedure assumes the maximum flow rates allowable by state conditions and piping network geometry. If there were only a TANK and START nodes in the list, the START node would be at Mach 1.0 as long as the system were choked. The addition of piping network components results in a lowering of the mass flow out of the cylinder. Since only one flow field solution can result from the piping network, and the cylinder is attached to the piping network, it can only have one mass flow flowing out of the cylinder itself. And this flow is controlled by the piping network. This will be the maximum flow the piping network can handle, even though the cylinder might conceivably handle more flow. As a result, once the piping network determines the maximum mass flow it can transport, the mass removed from the cylinder is based on

this piping network mass flow, rather than the maximum mass flow the cylinder alone could deliver.

The only difference between TANK and TWO\_TANK is that TANK allows only one orifice, an exit from the cylinder. TWO\_TANK allows for both exit and inlet orifices. The outlet orifice connects to the piping network, and the inlet allows for simple modeling of pressure transducers. Flow fields and state variables for chains representing both the transducer and its piping, and the discharge system piping are determined, and the mass flows for both applied to the change in mass for TWO\_TANK.

The mass of agent in the tank is calculated cumulatively, using a trapezoidal rule numerical integration. A description of this numerical integration technique is readily available in most calculus texts and mathematical handbooks.

### 5.3.3 Modeling of Flow Conditions – Choking.

Since the bulk of discharges take place under choked flow conditions, determining where choked flow (i.e., Mach = 1.0) occurs is of importance in the calculations. For relevant locations, choked flow (at least for the initial recursive call in a given time step) can and should be forced. This forcing simplifies the iterative process, and can be useful in determining if an acceptable flow field down to that node has been found.

However, there are some complications. First, depending on the physical network configuration, it is potentially possible, given the calculation technique described above (Section 5.3.2), for a location to become unchoked - if somewhere downstream, it is necessary to reduce flows upstream in order to achieve a flowfield, then what seemed like a choke point initially in a time step may become unchoked. Second, while some

locations would intuitively seem to be choke points, they may not be; and some non-intuitively obvious places may turn out to be choke points. As an example, consider a pipe ending in a sudden contraction venting to the environment. Assuming the pipe is sub-optimum, it may still be sufficiently long to accelerate the flow such that when the flow enters the sudden contraction, it reaches Mach 1.0 at the smallest cross-sectional area. If it is long enough, and the area change sufficiently large, choking can occur. Furthermore, even if there is a minimum cross-sectional area location upstream of this pipe/contraction, if the pipe length and contraction area ratio are both sufficiently large, flow at what might have intuitively seemed a choke point may not be choked there at all. Furthermore, it may not be certain that the pipe/contraction combo is a choke point until the flow fields and state variables are calculated for a given time step.

As a result, certain strategies have been included in the model to deal with these situations. First, before the discharge simulation begins, a scan is made of the nodes to determine the “natural” choke point(s). These points include both minimum cross-sectional areas such as nozzle throats, START orifices, and sudden contractions, and the downstream end of minimum cross-section area pipes. A bubble sort (**Tenenbaum & Augenstein (1986)**) is applied to the nodes, to sort nodes by area. (Bubble sorts are notorious for being slow; however, for small amounts of sorting, such as the nodes representing typical dry chemical fire suppression delivery systems, bubble sorts are just as fast as more efficient and complex sorts such as QuickSort, Shell Sort, and HeapSort – and simpler to implement. See **Tenenbaum & Augenstein (1986)**, or other books on computer algorithms, for discussion regarding these and other sorting routines.) If non-sequential minimum areas are found, they are flagged as choke points. If sequential

minimum areas are found, the downstream-most area in a sequence is flagged, as it is assumed to be the downstream end of a pipe. Note that more than one location may be a “natural” choke point, if more than one location qualifies by the above criteria.

In actuality, two flags are set at these natural choke points. The first one is permanent, and marks these “natural” locations. The second flag is unset after the first recursive call to that node in a given time step, and reset once the time step is completed. This is to indicate that initially, these points should be forced to Mach 1.0. Once the first recursive call is resolved, this second flag is unset, allowing subsequent guesses at these locations to stray downwards from Mach 1.0 as appropriate, for the remainder of that time step.

Note that, as described in Section 5.3.3, the calculation procedures for some components may initially assume Mach 1.0, and adjust that assumption as adjustments to the flow field require. In such locations, such as the pipe/contraction scenario described above, choking may be determined by calculation. The exact location of these calculated choke points is not tracked in the program, but may be found by inspection of the output files for a given location.

#### **5.4 “Zero” Routine.**

The “zero” routine is described in detail in **Van Zandt (1994)**. The routine is designed to find the roots of equations; an equation that may be arranged so as to result in zero when calculated can use this routine to find values of the variable giving a zero result. While a number of algorithms exist for finding roots (with varying levels of success, speed and efficiency), these algorithms generally are concerned only with the

calculation to find the root, and not with the iterative process such an algorithm should be a part of.

The “zero” routine proceeds to find a root by looking for values of the independent variable straddling a zero result for the dependent variable. From a starting location, a direction on the independent-dependent variable curve with decreasing dependent values is sought. A "valley" in the curve is sought, and a determination made if there is a root in that valley. If there is one (or more), one of several root-finding algorithms is applied (Newton, false position, etc...) to find the actual value of the independent variable (i.e., the root). Step sizes in the guesses made are controlled by the routine, looking at previous success or failure in the process, and tracking of previous guesses is done through a user-defined structure called “zero\_t”. Note that the criteria for ending the root search; i.e., the test for how close a dependent variable has to be to zero for the root value to be acceptable, is kept separate from the routine making the guesses. Thus the user can specify when the process can end, independent of the guessing routine.

Three routines are included in the software package. `Init_zero()` initializes the storage structure with the initial guess the program is to use. `Advise_zero()` allows for user specification of additional guesses, which the program may or may not use, depending on how the root finding progresses. `Seek_zero()` does the actual work in suggesting guesses, based on the results of past guesses. The software can report back to the user on the status of the results; either success in closing in on a root, or possible other results, such as finding a DISCONTINUITY or DIVERGENCE in the evolving curve, SLOW\_CONVERGENCE, LOCAL\_EXTREMUM if a local valley is found without a root, OK for a single successful calculation step, and FINISHED when the



routine finds a root. If an error condition is reported, a number of diagnostics are printed out, along with the original error message, as a means of helping to identify the source of the problem causing iteration failure. Extreme slopes in curves are controlled by variables in the routine's data structure, as well as the number of steps allowed for the iteration. For some iterations, a solution may be found quickly, within a few calculation steps. Also, in some instances in the model, the level of convergence required for the routine to finish may vary. Instances have occurred where the "zero" routine has reported failure to find a root, but the convergence has failed only by a tiny amount; a slight relaxation of the convergence criteria allows for successful completion of the iteration without any significant sacrifice of accuracy.

One difficulty in using this routine is that the algorithm requires a continuous function to iterate on. For the current application, the "zero" routine has been applied to find Mach numbers. There is a fixed range for subsonic Mach numbers, between 0 and 1.0 inclusive. Attempting to use some of the equations in Section 4.0 for Mach numbers outside the range can have results ranging from mild to fatal. In order to force the routine to remain within the target boundaries, mapping functions have been included in the routine; once a new guess is generated, before it is used, it is checked to see if it is in the range. If it is, calculations proceed. If it is not, the proper mapping function is applied to map the guess into a range of values between either 0.0 and 0.1 or 0.9 and 1.0, depending on the guess's value. Based on recommendations for mapping functions in **Van Zandt (1994)**, for the low end of the range, the following mapping is used:

$$x_{new} \leftarrow \frac{0.1}{1.0 - x_{old}} \quad (5.1)$$

For the high end mapping, the inverse of equation (5.1) is used:

$$x_{new} \leftarrow 1.0 - \frac{0.1}{x_{old}} \quad (5.2)$$

These mappings have been included in the model, but have not yet been extensively tested to verify that they do indeed prevent Mach number guesses outside the 0 to 1 range. Several of the implemented computational procedures may be shortened if these mappings prove to be successful.

For a full discussion of “zero”, and an annotated listing of the source code, see **Van Zandt (1994)**, and Appendix 10.1.

### **5.5 Newton-Raphson and Richmond Iteration Algorithms.**

As a simpler (though less robust) alternative to the zero routine for finding roots, two standard algorithms were also implemented in the model. One, the Newton-Raphson algorithm, is a well-known routine described in numerous mathematical and computer algorithm texts. The other, the Richmond algorithm, is less well known. Both are described, and implementations illustrated in **Shammas (1995)**.

The Newton-Raphson algorithm starts with an initial guess, and refines it through the equation:

$$D = \frac{f'(x)}{f(x)} \quad (5.3)$$

An alternative form avoids having to directly find the derivative of a function:

$$D = \frac{(f(x+h) - f(x-h))}{2hf(x)} \quad (5.4)$$

where h specifies the interval over which the derivative is to be calculated.

As an alternative, the Richmond algorithm has a higher order of convergence than the Newton algorithm, at a price of having to calculate the second derivative of the function being evaluated. It, too, starts with an initial guess, and calculates the guess refinement as:

$$D = \frac{f(x)f'(x)}{(f'(x)^2 - 0.5f(x)f''(x))} \quad (5.5)$$

The alternative form for equation (5.5), without directly deriving derivatives, is:

$$D = \frac{f(x)fd1}{(fd1^2 - 0.5f(x)fd2)} \quad (5.6)$$

with

$$fd1 = \frac{(f(x+h) - f(x-h))}{2h} \quad (5.7)$$

and

$$fd2 = \frac{(f(x+h) - 2f(x) + f(x-h))}{h^2} \quad (5.8)$$

These iteration algorithms are used for some of the iteration routines calculating mixture densities for individual components, and anywhere else deemed appropriate. The executing function can choose between the two algorithms depending on immediate values of the calculated guess refinement, relative to the variables being iterated.

## **5.6 Bulirsch-Stoerr Numerical Integration Algorithm.**

While no numerical integrations were required in the digital model (pipe equations have been successfully integrated), the Chenowith & Paolucci mass balance equation (equation (4.60)) was numerically integrated in the spreadsheet model (the

current model calculates the maximum mass flow permitted by the piping network (or START node if it is the downstream-most node in the network), and uses this mass flow to determine mass removal from the cylinder.) A fourth order Runge-Kutta algorithm was originally used, but later changed to a simple form of the Bulirsch-Stoerr algorithm **Acton (1970)**. The Runge-Kutta algorithm requires iterative guesses to converge on a solution, and may have convergence problems. The Bulirsch-Stoerr method, however, requires no iterations - calculations are straight-forward in comparison to Runge-Kutta. Also, while the Runge-Kutta method works well with a single differential equation, it has significant stability problems when trying to numerically integrate simultaneous differential equations. Oftentimes, very small steps are required, thus significantly increasing run time without generating any more useful information. The Bulirsch-Stoerr algorithm seems to have no problem with calculation of simultaneous differential equations.

The basic algorithm calculation step is described in **Acton (1970)**, and in **Press *et al* (1999)**. The technique consists of dividing an interval of interest into sub intervals, and using the differential equation to calculate intermediate values of the dependent variable and derivative values at each of the sub-intervals. The intermediate points calculate two curves surrounding what should be the actual trace of dependent versus independent variable, with a final averaging step to find the integrated value of the dependent variable at the end of the calculation interval. In the course of applying this algorithm, only a single interval size was selected. Properly implemented, the integration step should be repeated for a series of successively smaller interval steps, until changes from one interval size to the next in the integrated values is sufficiently small. However,

while the result of only carrying out the integration for only one step is some inaccuracy in the results, for the purpose of establishing the overall solution technique for the model, some error in reaching the target integrated values was acceptable. Furthermore, as noted earlier, there are no numerical integrations in the current model.

### **5.7 *Run-Time Characteristics***

While the program that has been written to model the discharge of dry chemical fire suppression systems is incomplete from the standpoint of being able to model all possible piping network configurations, and does not include a number of desirable features such as a user-friendly graphical interface, post-processing capabilities, and more rigorous error checking of piping network designs and other user inputs, it is easily capable of being used to model single-pipe networks, with several practical piping components included in the model. The compiled code is approximately 134 kilobytes in size, and has been run on PC workstations with Pentium chips, as well as Pentium-based laptop computers.

Compatibility with other systems has currently not been investigated. Run time is highly dependent on the piping network. However, networks with up to five components (including cylinder, START, sudden contraction, pipe, and a nozzle) have been run with total run times of approximately 30-40 seconds. The success of runs is highly dependent on the capabilities of the iterative solvers to converge successfully on solutions without generating erroneous results (such as negative parameter values, etc...). Run time memory requirements are dynamic, depending on the piping network being modeled. As long as sufficient time is available to model a discharge, the maximum piping network

configuration that could be run is limited only by the amount of free memory in the given computer available for allocation by the program. Note that, once a discharge run is completed, the program returns memory allocated to the configuration to the computer operating system; thus free memory levels should not diminish with repeated runs of the program.

User inputs to the program are defined in Section 6.0, and in the User Guide.

## 6.0 Illustration of Procedure.

To show how the dry chemical fire suppression delivery system model described in the previous chapters operates, a sample implementation is presented. While not all the features and constructs of the model are exercised, an understanding of the essential features and operations of the model, as implemented should result from following the example. Note that only a few time steps will be presented here, since time step outputs are identical for each component.

An example configuration is shown in Figure 6.1. This configuration is based on the cylinder/sudden contraction/pipe/nozzle configuration tested in the Worcester Polytechnic Institute (WPI) Center for Firesafety Studies (CFS) Wet Laboratory, and designated PNS-1 (See Section 7.0). The system is charged with 25 lbm sodium bicarbonate agent, and pressurized with nitrogen to 314.7 PSIA.

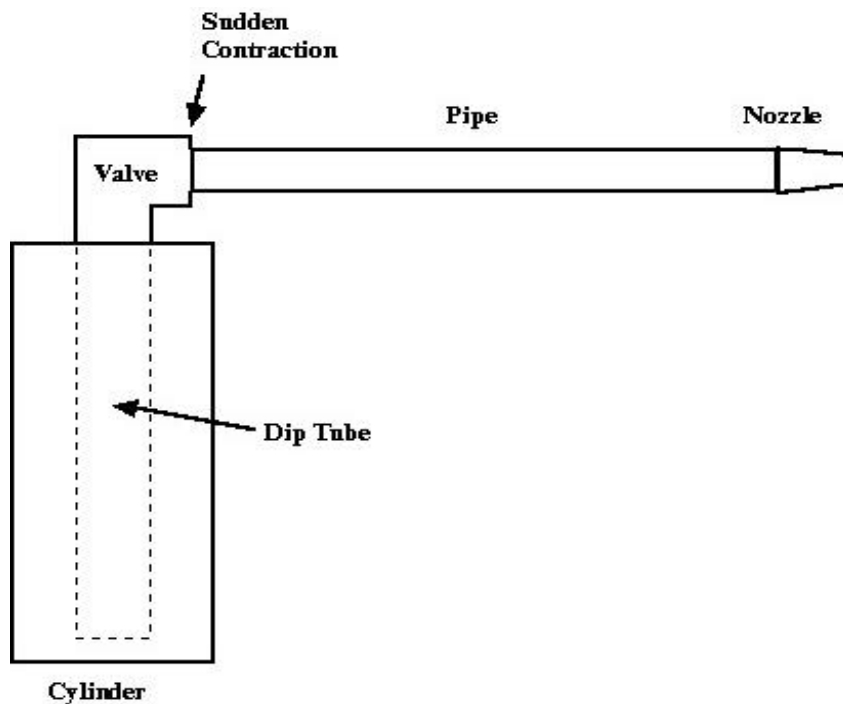


**Figure 6.1 Experimental Test PNS-1 - Model Representation of Configuration.**

The case being modeled starts the discharge 0.87 seconds after initiating the opening of the cylinder valve, so as to avoid problems modeling the START node with incorrect (and changing) valve cross-sectional areas, until valve opening is complete (See Section 7.4.1.2 for discussion.) (Note: this requires, for the first 0.87 seconds, a changing area in the START node, with corresponding change in the discharge coefficient. This initially variable START node area may be included in future releases of the program.) Input parameters are as follows:

General Conditions:

Time step	=	0.001 Second	
$R_G$	=	55.15 ft-lbf/lbm-°R	(Gas Ideal Gas Constant)
$c_{pg}$	=	0.248 BTU/lbm-°R	(Gas Specific Heat Constant Press.)
$c_{vg}$	=	0.177 BTU/lbm-°R	(Gas Specific Heat Constant Temp.)
$\rho_D$	=	137.38 lbf/ft <sup>3</sup>	(Solids Density)
$c$	=	0.249 BTU/lbm-°R	(Solids Specific Heat)
$m_p$	=	22.618 lbf	(Solids Mass)
$d_p$	=	53.0 microns	(Solids Particle Diameter)
fprime_flag	=	0	(Friction Multiplier Method Flag - 0 = Pfeiffer Model, 1 = Fan & Zhu Model)
$P_a$	=	14.7 PSIA	(Ambient Pressure)
$n_{lists}$	=	1	(Number of Lists – 1 for piping network, >1 for including list for pressure transducer, for instance.)



$n_{\text{nodes}}$  = 5                      Number of components in first (and here, only) list.

Cylinder:

Type = 1 (= "TANK")                      (Component type)  
# = 0                                      (Component "Number" in List)  
V = 0.43 ft<sup>3</sup>                              (Volume)  
 $P_c$  = 265.93 PSIA                      (Initial Pressure)  
 $T_c$  = 529.62 °R                      (Initial Temperature)

Start:

Type = 0 (= "START")                      (Component Type)  
# = 1                                      (Component "Number" in List)  
D = 0.750 inch                              (Inside Diameter)  
 $C_D$  = 1.00                              (Discharge Coefficient)

Contraction:

TYPE = 3 (= "CONTRACTION")                      (Component Type)  
# = 2                                      (Component "Number" in List)  
 $D_{ds}$  = 0.525 inch                      (Downstream End Inside Diameter)  
 $C_D$  = 1.00                              (Discharge Coefficient)

Pipe:

TYPE = 2 (= "PIPE")                      (Component Type)  
# = 3                                      (Component "Number" in List)  
L = 8.0 ft                              (Length)

D	=	0.5625 inch	(Inside Diameter)
$k_s/d$	=	0.00006	(Roughness Factor)
$C_D$	=	1.00	(Discharge Coefficient)

Throat:

TYPE	=	5 (= "THROAT")	(Component Type)
#	=	4	(Component "Number" in List)
D	=	0.1730 inch	(Inside Throat Diameter)
L	=	1.50 inch	(Inlet to Throat Distance)
$C_D$	=	0.470	(Discharge Coefficient)

The program user approximates the schematic in Figure 6.1 as a double-linked list of nodes representing each of the components. Two notes: first, the current implementation does NOT check for correctness of the component chain implemented. As an example, a nozzle throat could appear anywhere in the chain, but what effect this would have on the satisfactory running of the model, much less how sensible it is to allow this configuration is another question. The ability of a given model configuration of piping to accurately model all behaviors that might occur in a network during discharge depends greatly on the amount of detail modeled in the simulation configuration. For this example, the dip tube/valve/90° elbow have been combined into one comprehensive unit, with a discharge coefficient determined from test data described in Sections 4.0 and 7.0, covering losses in all three components combined.

Furthermore, the combination of components included in the model will be influenced by the amount of detail desired to represent a given configuration. As an

example, if the START node represents the entire cylinder exit assembly (dip tube, valve, elbow, etc...), a SUDDEN CONTRACTION just downstream of this START node representation is a reasonable representation. If the START node only represented an exit orifice, the configuration would be computationally simpler by not putting a SUDDEN contraction just downstream of the START node – the user should just make the orifice represented by the START node smaller in inside diameter. If empirical performance data is available for the assembly, the user can determine a discharge coefficient covering overall assembly performance; thus adjusting the START node discharge response to reflect the assembly sub-components not actually included in the configuration as modeled. If empirical data is not readily available, the user could either come up with an approximate value based on one or more of the most important components being combined in the START node, or derive an approximate discharge coefficient from a hand calculation of flow through the component parts. Note that, if the START node is only one part of a more complex piping network, the discharge coefficient variable should be set to 1.0.

Second, at least one source cylinder must appear in the chain, partially because the cylinder sets the conditions for discharge and choking/unchoking, and partially because the tank (or TWO\_TANK for the two-orifice tank) is the stopping point in the recursive calculation process.

The double-linked list representation of the configuration of Figure 6.1 is shown in Figure 5.2.

With the configuration and list representations shown in Figure 6.1 and Figure 5.2, and the configuration data given above, an input text file is established. The text file for this configuration is shown in Figure 6.2.

Line Number	Data	Information
1	0.100	// timestep s
2	55.15,0.248,0.177	// gas constant R, cpg, cvg - Nitrogen
3	137.38,0.249,22.618	// solid density, c, mass lbm - Sod. Bicarb.
4	53.0	// solid particle average dia microns
5	0	// friction multiplier flag
6	14.7	// ambient pressure (psia)
7	1	// number of chains
8	5	// number of nodes in first chain
9	1	// TANK - first node
10	0,0.430,265.924,529.62	// node number, volume cu ft, press. PSIA, temp R
11	0	// START - second node
12	1,0.750,1.00	// node number, dia in, inlet Cd
13	3	// CONTRACTION - third node
14	2,0.5625,1.00	// node number, ds dia in, ds cd
15	2	// PIPE - fourth node
16	3,8.00,0.5625,0.00006	// node number, length ft, dia in, ks/d
17	1.00	// pipe ds cd
18	5	// THROAT - fifth node
19	4,0.1730,1.50,0.900	// node number, dia inch, length in, ds cd

Notes:

ds = "downstream".

Omit the title line and line numbers in actual user input file. See example on CD-ROM for format.

### **Figure 6.2 Input File for Configuration of Figure 6.1 and Figure 5.2.**

The input text file contains all required information regarding the physical geometry of the configuration, and the relevant starting conditions in the source cylinder and ambient. For the current implementation, this file must be located in the same directory (either disk or hard drive) as the executable, and must be named "infile.txt" in the directory. A complete description of the input file and its allowable contents appears in Section 6.1.

To execute the program, the user either clicks on the program icon in a Windows environment, or clicks on the program name in a directory environment. The program

name in the directory is “DryRun.exe”. The current implementation produces an MS-DOS window showing a number of messages as execution progresses. Output files are generated for each component in the linked list, containing state variable values at each time step in the discharge, both in list form, and at the end of each time step, a one-line output of the most important parameters. Output text files are labeled “e\_nodexx.txt”, where xx is the identification number of the node. Numbering starts at 00 for the main system chain, and 10 a secondary chain (example: pressure transducer sub-system), which corresponds to the first node in a chain (either a TANK or TWO\_TANK node). Identification numbers are keyed to the nodes in the linked list, and must be numbered in ascending order, from the TANK (or TWO\_TANK) node, in the downstream direction. ID numbers are used by the program in labeling output files, and in the sorting process by which “natural” choke points are identified prior to the start of the discharge simulation (see Section 5.3.3.)

Output files may be edited using any text editor, loaded directly into a spreadsheet program, or brought into any program accepting text file inputs in tabular form. Figure 6.3 through Figure 6.7 show output for each component in the example configuration.

Figure 6.3 shows the program output for the source TANK for the configuration in Figure 6.1, using the input file of Figure 6.2. After a header indicating the node type, and information about the configuration being modeled and the node, a line of output is generated for each time step reported.

For TANK and TWO\_TANK, the following parameters are reported: time step (seconds), pressure (psia), mixture density (lbm/ft<sup>3</sup>), temperature (°R), solids volume fraction, solids mass remaining in the tank (lbm), an indication as to whether the

configuration is choked (“c”) or unchoked (“u”), and the mass flow from the cylinder (calculated by the START node, and reported both here and with the START node) (lbm/sec). At the end of the output, the approximate elapsed time for the discharge calculation execute is shown.

Output for TANK node (node # 0).  
 gamma\_mix = 1.004338  
 ambient pressure = 14.70 psia  
 gas cp = 0.248 btu/lbm-R cv = 0.177 btu/lbm-R  
 gas gamma = 1.401130 gas constant R = 55.150 ft-lbf/lbm-R  
 mass fraction = 0.98485  
 initial solids mass = 22.62 lbm  
 particle diameter = 53.00 microns specific heat = 0.249 btu/lbm-R  
 solid density = 137.380 lbm/cu ft  
 cylinder volume = 0.430 cu ft initial gas volume = 0.265 cu ft  
 initial pressure = 265.924 psia initial temperature = 529.62 R  
 initial theta = 0.38288  
 Pfeiffer friction multiplier used.

time(s)	p(psia)	rho (lbf/ft3)	t(R)	theta	magent (lbm)	c/u	mdot (lbm/s)
0.00000	265.924	53.409	529.62	0.38288	22.618	c	0.70133
0.10000	264.605	53.246	529.61	0.38171	22.583	c	0.69095
1.00000	253.339	51.827	529.51	0.37154	21.982	c	0.66183
2.00000	241.764	50.320	529.40	0.36073	21.343	c	0.63186
3.00000	231.068	48.880	529.30	0.35041	20.732	c	0.60414
4.00000	221.151	47.502	529.20	0.34053	20.148	c	0.57841
5.00000	211.926	46.182	529.10	0.33107	19.589	c	0.55446
6.00000	203.323	44.917	529.01	0.32200	19.052	c	0.53209
7.00000	195.278	43.701	528.91	0.31329	18.537	c	0.51116
8.00000	187.738	42.534	528.82	0.30491	18.042	c	0.49152
9.00000	180.655	41.410	528.74	0.29686	17.566	c	0.47307
10.00000	173.988	40.328	528.65	0.28911	17.107	c	0.45568
11.00000	167.702	39.286	528.57	0.28163	16.665	c	0.43927
12.00000	161.763	38.281	528.48	0.27443	16.239	c	0.42376
13.00000	156.143	37.311	528.40	0.26747	15.828	c	0.40908
14.00000	150.818	36.374	528.32	0.26076	15.431	c	0.39516
15.00000	145.765	35.469	528.25	0.25427	15.047	c	0.38194
16.00000	140.963	34.594	528.17	0.24800	14.677	c	0.36937
17.00000	136.394	33.748	528.09	0.24193	14.318	c	0.35741
18.00000	132.042	32.929	528.02	0.23606	13.971	c	0.34601
19.00000	127.892	32.135	527.95	0.23037	13.634	c	0.33513
20.00000	123.930	31.367	527.88	0.22486	13.309	c	0.32474
21.00000	120.143	30.622	527.81	0.21953	12.993	c	0.31481
22.00000	116.522	29.900	527.74	0.21435	12.687	c	0.30531
23.00000	113.055	29.200	527.67	0.20933	12.390	c	0.29621
24.00000	109.733	28.520	527.60	0.20446	12.102	c	0.28749
25.00000	106.548	27.860	527.53	0.19973	11.823	c	0.27912
26.00000	103.491	27.220	527.47	0.19513	11.551	c	0.27109
27.00000	100.555	26.597	527.40	0.19067	11.287	c	0.26337
28.00000	97.733	25.993	527.33	0.18634	11.031	c	0.25595
29.00000	95.020	25.405	527.27	0.18212	10.782	c	0.24882
30.00000	92.408	24.834	527.21	0.17803	10.540	c	0.24195

**Figure 6.3 Output File enode\_00.txt - Source Tank Predicted Behavior.**

31.00000	89.894	24.278	527.14	0.17404	10.304	c	0.23534
32.00000	87.472	23.737	527.08	0.17017	10.075	c	0.22896
33.00000	85.136	23.211	527.02	0.16640	9.852	c	0.22282
34.00000	82.884	22.699	526.96	0.16273	9.635	c	0.21689
35.00000	80.711	22.201	526.90	0.15915	9.424	c	0.21117
36.00000	78.612	21.716	526.84	0.15568	9.219	c	0.20564
37.00000	76.585	21.243	526.78	0.15229	9.018	c	0.20031
38.00000	74.627	20.783	526.72	0.14899	8.823	c	0.19515
39.00000	72.733	20.334	526.66	0.14577	8.633	c	0.19016
40.00000	70.901	19.897	526.60	0.14264	8.448	c	0.18533
41.00000	69.129	19.471	526.55	0.13958	8.267	c	0.18066
42.00000	67.414	19.055	526.49	0.13661	8.091	c	0.17614
43.00000	65.753	18.650	526.43	0.13370	7.920	c	0.17177
44.00000	64.143	18.255	526.38	0.13087	7.752	c	0.16752
45.00000	62.584	17.870	526.32	0.12811	7.589	c	0.16341
46.00000	61.073	17.494	526.27	0.12541	7.430	c	0.15943
47.00000	59.607	17.128	526.21	0.12278	7.274	c	0.15557
48.00000	58.186	16.770	526.15	0.12022	7.123	c	0.15182
49.00000	56.806	16.421	526.10	0.11772	6.975	c	0.14818
50.00000	55.468	16.080	526.05	0.11527	6.830	c	0.14465
51.00000	54.168	15.747	525.99	0.11289	6.689	c	0.14122
52.00000	52.906	15.422	525.94	0.11056	6.552	c	0.13790
53.00000	51.680	15.105	525.89	0.10828	6.417	c	0.13466
54.00000	50.489	14.795	525.83	0.10606	6.286	c	0.13152
55.00000	49.331	14.492	525.78	0.10389	6.158	c	0.12847
56.00000	48.206	14.196	525.73	0.10177	6.032	c	0.12550
57.00000	47.112	13.908	525.68	0.09970	5.910	c	0.12262
58.00000	46.048	13.625	525.62	0.09768	5.790	c	0.11981
59.00000	45.013	13.350	525.57	0.09570	5.674	c	0.11708
60.00000	44.006	13.080	525.52	0.09377	5.559	c	0.11443
61.00000	43.026	12.817	525.47	0.09188	5.448	c	0.11184
62.00000	42.072	12.559	525.42	0.09004	5.339	c	0.10933
63.00000	41.144	12.308	525.37	0.08823	5.232	c	0.10688
64.00000	40.239	12.062	525.32	0.08647	5.128	c	0.10449
65.00000	39.359	11.821	525.27	0.08474	5.026	c	0.10217
66.00000	38.501	11.586	525.22	0.08306	4.926	c	0.09991
67.00000	37.665	11.356	525.17	0.08141	4.829	c	0.09771
68.00000	36.851	11.131	525.12	0.07979	4.733	c	0.09556
69.00000	36.057	10.911	525.07	0.07822	4.640	c	0.09347
70.00000	35.284	10.696	525.02	0.07667	4.549	c	0.09143
71.00000	34.529	10.485	524.97	0.07517	4.460	c	0.08944
72.00000	33.794	10.279	524.92	0.07369	4.372	c	0.08750
73.00000	33.077	10.078	524.87	0.07224	4.287	c	0.08561
74.00000	32.377	9.880	524.82	0.07083	4.204	c	0.08377
75.00000	31.695	9.687	524.78	0.06945	4.122	c	0.08197
76.00000	31.030	9.499	524.73	0.06809	4.042	c	0.08022
77.00000	30.380	9.314	524.68	0.06677	3.964	c	0.07851
78.00000	29.746	9.133	524.63	0.06547	3.887	c	0.07684
79.00000	29.128	8.956	524.58	0.06421	3.812	c	0.07521

**Figure 6.3 Output File enode\_00.txt – Source Tank Predicted Behavior (Continued).**



80.00000	28.524	8.783	524.54	0.06296	3.739	c	0.07362
81.00000	27.934	8.613	524.49	0.06175	3.667	c	0.07206
82.00000	27.359	8.447	524.44	0.06056	3.596	c	0.07055
83.00000	26.797	8.285	524.40	0.05939	3.527	c	0.06907
84.00000	26.248	8.126	524.35	0.05825	3.460	c	0.06762
85.00000	25.712	7.970	524.30	0.05714	3.394	c	0.06621
85.60000	25.392	7.877	524.27	0.05647	3.353	u	0.06690
86.60000	24.873	7.725	524.23	0.05538	3.289	u	0.06354
87.60000	24.382	7.582	524.18	0.05435	3.228	u	0.06091
88.60000	23.904	7.442	524.14	0.05335	3.169	u	0.05972
89.60000	23.437	7.304	524.09	0.05236	3.110	u	0.05717
90.60000	22.993	7.174	524.05	0.05143	3.055	u	0.05518
91.60000	22.565	7.047	524.01	0.05052	3.002	u	0.05326
92.60000	22.155	6.926	523.96	0.04965	2.950	u	0.05051
93.60000	21.762	6.810	523.92	0.04882	2.901	u	0.04961
94.60000	21.376	6.696	523.88	0.04800	2.853	u	0.04873
95.60000	21.006	6.586	523.84	0.04721	2.806	u	0.04610
96.60000	20.652	6.480	523.81	0.04646	2.761	u	0.04444
97.60000	20.313	6.379	523.77	0.04573	2.718	u	0.04187
98.60000	19.989	6.282	523.73	0.04504	2.677	u	0.04120
99.60000	19.671	6.187	523.70	0.04436	2.637	u	0.04055
100.60000	19.366	6.096	523.66	0.04370	2.598	u	0.03823
101.60000	19.083	6.011	523.63	0.04309	2.562	u	0.03548
102.60000	18.810	5.929	523.59	0.04250	2.528	u	0.03497
103.60000	18.541	5.848	523.56	0.04192	2.494	u	0.03447
104.60000	18.282	5.770	523.53	0.04137	2.460	u	0.03271
105.60000	18.039	5.697	523.50	0.04084	2.429	u	0.03086
106.60000	17.802	5.625	523.47	0.04033	2.399	u	0.03046
107.60000	17.571	5.556	523.44	0.03983	2.369	u	0.02884
108.60000	17.354	5.490	523.41	0.03936	2.342	u	0.02760
109.60000	17.146	5.427	523.39	0.03891	2.315	u	0.02639
110.60000	16.948	5.367	523.36	0.03847	2.290	u	0.02520
111.60000	16.759	5.310	523.33	0.03806	2.265	u	0.02403
112.60000	16.583	5.256	523.31	0.03768	2.243	u	0.02256
113.60000	16.411	5.204	523.29	0.03731	2.221	u	0.02233
114.60000	16.246	5.154	523.26	0.03695	2.199	u	0.02064
115.60000	16.092	5.107	523.24	0.03661	2.179	u	0.01794
116.60000	15.956	5.065	523.22	0.03631	2.162	u	0.01778
117.60000	15.821	5.024	523.20	0.03602	2.144	u	0.01763
118.60000	15.690	4.984	523.18	0.03573	2.127	u	0.01642
119.60000	15.569	4.947	523.17	0.03547	2.112	u	0.01537
120.60000	15.455	4.913	523.15	0.03522	2.097	u	0.01433
121.60000	15.350	4.881	523.14	0.03499	2.083	u	0.01331
122.60000	15.256	4.852	523.12	0.03478	2.071	u	0.01219
123.60000	15.164	4.824	523.11	0.03458	2.059	u	0.01212
124.60000	15.080	4.798	523.10	0.03440	2.049	u	0.01025
125.60000	15.006	4.776	523.08	0.03423	2.039	u	0.00924
126.60000	14.940	4.755	523.07	0.03409	2.030	u	0.00822
127.30000	14.898	4.742	523.07	0.03400	2.025	u	0.00751
127.35000	14.895	4.741	523.07	0.03399	2.024	u	0.00746
127.40000	14.892	4.741	523.07	0.03398	2.024	u	0.00741
127.45000	14.889	4.740	523.07	0.03398	2.024	u	0.00736
127.50000	14.886	4.739	523.07	0.03397	2.023	u	0.00731

**Figure 6.3 Output File enode\_00.txt – Source TANK Predicted Behavior (Continued).**

127.55000	14.884	4.738	523.07	0.03397	2.023	u	0.00726
127.60000	14.881	4.737	523.06	0.03396	2.023	u	0.00720
127.65000	14.878	4.736	523.06	0.03395	2.022	u	0.00715
127.70000	14.875	4.735	523.06	0.03395	2.022	u	0.00710
127.75000	14.873	4.735	523.06	0.03394	2.022	u	0.00705
127.80000	14.870	4.734	523.06	0.03394	2.021	u	0.00700
127.85000	14.867	4.733	523.06	0.03393	2.021	u	0.00549
127.90000	14.865	4.732	523.06	0.03393	2.021	u	0.00549
127.95000	14.863	4.732	523.06	0.03392	2.020	u	0.00549
128.00000	14.861	4.731	523.06	0.03392	2.020	u	0.00549
128.05000	14.859	4.730	523.06	0.03391	2.020	u	0.00549
128.10000	14.857	4.730	523.06	0.03391	2.020	u	0.00549
128.15000	14.855	4.729	523.06	0.03390	2.019	u	0.00549
128.20000	14.853	4.729	523.06	0.03390	2.019	u	0.00548
128.25000	14.851	4.728	523.06	0.03389	2.019	u	0.00548
128.30000	14.849	4.727	523.06	0.03389	2.018	u	0.00548
128.35000	14.846	4.727	523.06	0.03388	2.018	u	0.00548
128.40000	14.844	4.726	523.06	0.03388	2.018	u	0.00548
128.45000	14.842	4.725	523.06	0.03388	2.018	u	0.00548
128.50000	14.840	4.725	523.06	0.03387	2.017	u	0.00548
128.55000	14.838	4.724	523.06	0.03387	2.017	u	0.00548
128.60000	14.836	4.723	523.06	0.03386	2.017	u	0.00548
128.65000	14.834	4.723	523.06	0.03386	2.017	u	0.00548
128.70000	14.832	4.722	523.06	0.03385	2.016	u	0.00548
128.75000	14.830	4.722	523.06	0.03385	2.016	u	0.00548
128.80000	14.828	4.721	523.06	0.03384	2.016	u	0.00548
128.85000	14.826	4.720	523.06	0.03384	2.015	u	0.00547
128.90000	14.824	4.720	523.06	0.03383	2.015	u	0.00547
128.95000	14.822	4.719	523.06	0.03383	2.015	u	0.00547
129.00000	14.819	4.718	523.06	0.03383	2.015	u	0.00547
129.05000	14.817	4.718	523.06	0.03382	2.014	u	0.00547
129.10000	14.815	4.717	523.05	0.03382	2.014	u	0.00547
129.15000	14.813	4.716	523.05	0.03381	2.014	u	0.00547
129.20000	14.811	4.716	523.05	0.03381	2.014	u	0.00547
129.25000	14.809	4.715	523.05	0.03380	2.013	u	0.00547
129.30000	14.807	4.715	523.05	0.03380	2.013	u	0.00547
129.35000	14.805	4.714	523.05	0.03379	2.013	u	0.00547
129.40000	14.803	4.713	523.05	0.03379	2.013	u	0.00547
129.45000	14.801	4.713	523.05	0.03378	2.012	u	0.00547
129.50000	14.799	4.712	523.05	0.03378	2.012	u	0.00547

Elapsed time: 29.4600 seconds.

**Figure 6.3 Output File enode\_00.txt – Source TANK Predicted Behavior (Continued).**

Figure 6.4 through Figure 6.7 show printed output for the START, SUDDEN CONTRACTION, PIPE, and nozzle THROAT nodes, respectively. Outputs are reported for the downstream end of the component. Depending on the configuration, this node will also be the upstream end of a component immediately downstream (except for the THROAT node, which has nothing downstream of it.) After a header giving relevant

configuration information about the component, the following parameters are reported: time step (seconds), pressure (psia), mixture density (lbm/ft<sup>3</sup>), temperature (°R), solids volume fraction, mixture velocity (ft/s), mixture Mach number, and the mass flow through the component (lbm/sec).

Note that the small inaccuracies in matching mass flows at each location are due to differing convergence criteria used in the iterative calculations for each component; this in turn resulted from difficulties encountered when trying to get the calculations to converge on a solution. Relatively “tight” convergence criteria were required in the computer model, in order to assure accurate results. As an example, the mass flow calculated for each non-cylinder component was found to differ significantly from component to component if convergence criteria for the guessed Mach numbers at each component were allowed to become too large (on the order of 0.01 or greater) (There should be only ONE mass flow for a configuration, identical for all components, controlled in choked flow by the upstream-most choke point.) On the other hand, relatively tight convergence criteria occasionally cause convergence problems for one or more of the iterative routines. As a result, a balance has been sought between tight convergences (and better accuracy), and loose convergence criteria (with easier convergences and less accuracy.)

Note that, for the configuration in this example, sudden expansions were not used. The output for sudden expansions is identical to that for sudden contractions.

Output for START node (node # 1).  
 discharge coefficient = 1.000  
 local diameter = 0.7500 inches

time(s)	p(psia)	rho (lbf/ft <sup>3</sup> )	t(R)	theta	velocity (ft/s)	Mach	mdot (lbm/s)
0.00000	265.753	53.388	529.62	0.38273	4.28	0.0221	0.70133
0.10000	264.439	53.225	529.61	0.38156	4.23	0.0219	0.69095
1.00000	253.185	51.807	529.51	0.37140	4.16	0.0219	0.66183
2.00000	241.622	50.301	529.40	0.36060	4.09	0.0219	0.63186
3.00000	230.936	48.862	529.30	0.35028	4.03	0.0219	0.60414
4.00000	221.028	47.485	529.20	0.34041	3.97	0.0219	0.57841
5.00000	211.812	46.166	529.10	0.33095	3.91	0.0219	0.55446
6.00000	203.217	44.901	529.01	0.32189	3.86	0.0219	0.53209
7.00000	195.179	43.686	528.91	0.31318	3.81	0.0219	0.51116
8.00000	187.644	42.519	528.82	0.30481	3.77	0.0219	0.49152
9.00000	180.567	41.396	528.74	0.29676	3.72	0.0219	0.47307
10.00000	173.905	40.315	528.65	0.28901	3.68	0.0219	0.45568
11.00000	167.623	39.273	528.57	0.28154	3.65	0.0219	0.43927
12.00000	161.688	38.268	528.48	0.27434	3.61	0.0219	0.42376
13.00000	156.073	37.298	528.40	0.26739	3.57	0.0219	0.40908
14.00000	150.752	36.362	528.32	0.26067	3.54	0.0219	0.39516
15.00000	145.702	35.458	528.25	0.25419	3.51	0.0219	0.38194
16.00000	140.903	34.583	528.17	0.24792	3.48	0.0219	0.36937
17.00000	136.337	33.737	528.09	0.24185	3.45	0.0219	0.35741
18.00000	131.987	32.918	528.02	0.23598	3.43	0.0219	0.34601
19.00000	127.840	32.125	527.95	0.23030	3.40	0.0219	0.33513
20.00000	123.880	31.357	527.88	0.22479	3.38	0.0219	0.32474
21.00000	120.096	30.613	527.80	0.21946	3.35	0.0219	0.31481
22.00000	116.477	29.891	527.73	0.21428	3.33	0.0219	0.30531
23.00000	113.011	29.191	527.67	0.20926	3.31	0.0219	0.29621
24.00000	109.691	28.511	527.60	0.20439	3.29	0.0219	0.28749
25.00000	106.508	27.852	527.53	0.19967	3.27	0.0219	0.27912
26.00000	103.452	27.212	527.46	0.19507	3.25	0.0219	0.27109
27.00000	100.518	26.589	527.40	0.19062	3.23	0.0219	0.26337
28.00000	97.698	25.985	527.33	0.18628	3.21	0.0219	0.25595
29.00000	94.985	25.398	527.27	0.18207	3.19	0.0219	0.24882
30.00000	92.375	24.826	527.21	0.17798	3.18	0.0219	0.24195

**Figure 6.4 Output File enode\_01.txt - START Predicted Behavior.**

31.00000	89.862	24.271	527.14	0.17399	3.16	0.0219	0.23534
32.00000	87.441	23.730	527.08	0.17012	3.14	0.0219	0.22896
33.00000	85.107	23.205	527.02	0.16635	3.13	0.0219	0.22282
34.00000	82.856	22.693	526.96	0.16268	3.12	0.0219	0.21689
35.00000	80.683	22.195	526.90	0.15911	3.10	0.0219	0.21117
36.00000	78.586	21.710	526.84	0.15563	3.09	0.0219	0.20564
37.00000	76.560	21.237	526.78	0.15224	3.07	0.0219	0.20031
38.00000	74.602	20.777	526.72	0.14895	3.06	0.0219	0.19515
39.00000	72.709	20.328	526.66	0.14573	3.05	0.0218	0.19016
40.00000	70.878	19.891	526.60	0.14260	3.04	0.0218	0.18533
41.00000	69.107	19.465	526.55	0.13954	3.03	0.0218	0.18066
42.00000	67.392	19.050	526.49	0.13657	3.01	0.0218	0.17614
43.00000	65.732	18.645	526.43	0.13366	3.00	0.0218	0.17177
44.00000	64.123	18.250	526.38	0.13083	2.99	0.0218	0.16752
45.00000	62.565	17.865	526.32	0.12807	2.98	0.0218	0.16341
46.00000	61.054	17.490	526.26	0.12538	2.97	0.0218	0.15943
47.00000	59.589	17.123	526.21	0.12275	2.96	0.0218	0.15557
48.00000	58.168	16.765	526.15	0.12019	2.95	0.0218	0.15182
49.00000	56.789	16.416	526.10	0.11768	2.94	0.0218	0.14818
50.00000	55.451	16.075	526.05	0.11524	2.93	0.0218	0.14465
51.00000	54.152	15.743	525.99	0.11286	2.92	0.0218	0.14122
52.00000	52.890	15.418	525.94	0.11053	2.92	0.0218	0.13790
53.00000	51.665	15.101	525.88	0.10825	2.91	0.0218	0.13466
54.00000	50.474	14.791	525.83	0.10603	2.90	0.0217	0.13152
55.00000	49.317	14.488	525.78	0.10386	2.89	0.0217	0.12847
56.00000	48.192	14.193	525.73	0.10175	2.88	0.0217	0.12550
57.00000	47.098	13.904	525.67	0.09968	2.87	0.0217	0.12262
58.00000	46.035	13.622	525.62	0.09765	2.87	0.0217	0.11981
59.00000	45.000	13.346	525.57	0.09568	2.86	0.0217	0.11708
60.00000	43.993	13.077	525.52	0.09375	2.85	0.0217	0.11443
61.00000	43.014	12.813	525.47	0.09186	2.85	0.0217	0.11184
62.00000	42.060	12.556	525.42	0.09001	2.84	0.0217	0.10933
63.00000	41.132	12.305	525.37	0.08821	2.83	0.0217	0.10688
64.00000	40.228	12.059	525.32	0.08645	2.82	0.0217	0.10449
65.00000	39.348	11.818	525.27	0.08472	2.82	0.0217	0.10217
66.00000	38.490	11.583	525.22	0.08304	2.81	0.0217	0.09991
67.00000	37.655	11.353	525.17	0.08139	2.81	0.0216	0.09771
68.00000	36.841	11.128	525.12	0.07977	2.80	0.0216	0.09556
69.00000	36.047	10.908	525.07	0.07820	2.79	0.0216	0.09347
70.00000	35.274	10.693	525.02	0.07666	2.79	0.0216	0.09143
71.00000	34.520	10.482	524.97	0.07515	2.78	0.0216	0.08944
72.00000	33.785	10.276	524.92	0.07367	2.78	0.0216	0.08750
73.00000	33.068	10.075	524.87	0.07223	2.77	0.0216	0.08561
74.00000	32.369	9.878	524.82	0.07081	2.76	0.0216	0.08377
75.00000	31.687	9.685	524.78	0.06943	2.76	0.0216	0.08197
76.00000	31.021	9.496	524.73	0.06808	2.75	0.0216	0.08022
77.00000	30.372	9.312	524.68	0.06675	2.75	0.0215	0.07851
78.00000	29.738	9.131	524.63	0.06546	2.74	0.0215	0.07684
79.00000	29.120	8.954	524.58	0.06419	2.74	0.0215	0.07521

**Figure 6.4 Output File enode\_01.txt – START Predicted Behavior (Continued).**

80.00000	28.516	8.781	524.54	0.06295	2.73	0.0215	0.07362
81.00000	27.927	8.611	524.49	0.06173	2.73	0.0215	0.07206
82.00000	27.352	8.445	524.44	0.06054	2.72	0.0215	0.07055
83.00000	26.790	8.283	524.40	0.05938	2.72	0.0215	0.06907
84.00000	26.241	8.124	524.35	0.05824	2.71	0.0215	0.06762
85.00000	25.705	7.968	524.30	0.05712	2.71	0.0215	0.06621
85.60000	25.385	7.875	524.27	0.05645	2.77	0.0220	0.06690
86.60000	24.867	7.724	524.23	0.05537	2.68	0.0213	0.06354
87.60000	24.376	7.580	524.18	0.05434	2.62	0.0208	0.06091
88.60000	23.898	7.440	524.14	0.05333	2.62	0.0208	0.05972
89.60000	23.431	7.303	524.09	0.05235	2.55	0.0203	0.05717
90.60000	22.988	7.172	524.05	0.05142	2.51	0.0200	0.05518
91.60000	22.560	7.046	524.01	0.05051	2.46	0.0197	0.05326
92.60000	22.151	6.925	523.96	0.04964	2.38	0.0190	0.05051
93.60000	21.758	6.809	523.92	0.04881	2.38	0.0190	0.04961
94.60000	21.372	6.694	523.88	0.04799	2.37	0.0190	0.04873
95.60000	21.002	6.584	523.84	0.04720	2.28	0.0183	0.04610
96.60000	20.648	6.479	523.81	0.04645	2.24	0.0179	0.04444
97.60000	20.309	6.378	523.77	0.04572	2.14	0.0172	0.04187
98.60000	19.986	6.281	523.73	0.04503	2.14	0.0172	0.04120
99.60000	19.668	6.186	523.70	0.04435	2.14	0.0172	0.04055
100.60000	19.363	6.095	523.66	0.04369	2.04	0.0164	0.03823
101.60000	19.080	6.010	523.63	0.04309	1.92	0.0155	0.03548
102.60000	18.807	5.928	523.59	0.04250	1.92	0.0155	0.03497
103.60000	18.539	5.847	523.56	0.04192	1.92	0.0155	0.03447
104.60000	18.280	5.770	523.53	0.04136	1.85	0.0149	0.03271
105.60000	18.037	5.696	523.50	0.04083	1.77	0.0142	0.03086
106.60000	17.800	5.625	523.47	0.04032	1.77	0.0142	0.03046
107.60000	17.569	5.555	523.44	0.03982	1.69	0.0137	0.02884
108.60000	17.352	5.489	523.41	0.03935	1.64	0.0132	0.02760
109.60000	17.145	5.427	523.38	0.03890	1.59	0.0128	0.02639
110.60000	16.947	5.367	523.36	0.03847	1.53	0.0124	0.02520
111.60000	16.758	5.309	523.33	0.03806	1.48	0.0119	0.02403
112.60000	16.582	5.256	523.31	0.03768	1.40	0.0113	0.02256
113.60000	16.410	5.204	523.29	0.03730	1.40	0.0113	0.02233
114.60000	16.245	5.153	523.26	0.03694	1.31	0.0106	0.02064
115.60000	16.091	5.107	523.24	0.03661	1.14	0.0093	0.01794
116.60000	15.955	5.065	523.22	0.03631	1.14	0.0093	0.01778
117.60000	15.820	5.024	523.20	0.03602	1.14	0.0093	0.01763
118.60000	15.689	4.984	523.18	0.03573	1.07	0.0087	0.01642
119.60000	15.568	4.947	523.17	0.03547	1.01	0.0082	0.01537
120.60000	15.455	4.913	523.15	0.03522	0.95	0.0077	0.01433
121.60000	15.349	4.880	523.13	0.03499	0.89	0.0072	0.01331
122.60000	15.256	4.852	523.12	0.03478	0.82	0.0067	0.01219
123.60000	15.163	4.824	523.11	0.03458	0.82	0.0067	0.01212
124.60000	15.080	4.798	523.09	0.03440	0.70	0.0057	0.01025
125.60000	15.006	4.775	523.08	0.03423	0.63	0.0051	0.00924
126.60000	14.939	4.755	523.07	0.03409	0.56	0.0046	0.00822
127.30000	14.897	4.742	523.07	0.03400	0.52	0.0042	0.00751
127.35000	14.895	4.741	523.07	0.03399	0.51	0.0042	0.00746
127.40000	14.892	4.741	523.07	0.03398	0.51	0.0041	0.00741
127.45000	14.889	4.740	523.07	0.03398	0.51	0.0041	0.00736
127.50000	14.886	4.739	523.07	0.03397	0.50	0.0041	0.00731

**Figure 6.4 Output File enode\_01.txt – START Predicted Behavior (Continued).**

127.55000	14.883	4.738	523.07	0.03397	0.50	0.0041	0.00726
127.60000	14.881	4.737	523.06	0.03396	0.50	0.0040	0.00720
127.65000	14.878	4.736	523.06	0.03395	0.49	0.0040	0.00715
127.70000	14.875	4.735	523.06	0.03395	0.49	0.0040	0.00710
127.75000	14.873	4.735	523.06	0.03394	0.49	0.0039	0.00705
127.80000	14.870	4.734	523.06	0.03394	0.48	0.0039	0.00700
127.85000	14.867	4.733	523.06	0.03393	0.38	0.0031	0.00549
127.90000	14.865	4.732	523.06	0.03393	0.38	0.0031	0.00549
127.95000	14.863	4.732	523.06	0.03392	0.38	0.0031	0.00549
128.00000	14.861	4.731	523.06	0.03392	0.38	0.0031	0.00549
128.05000	14.859	4.730	523.06	0.03391	0.38	0.0031	0.00549
128.10000	14.857	4.730	523.06	0.03391	0.38	0.0031	0.00549
128.15000	14.855	4.729	523.06	0.03390	0.38	0.0031	0.00549
128.20000	14.853	4.729	523.06	0.03390	0.38	0.0031	0.00548
128.25000	14.851	4.728	523.06	0.03389	0.38	0.0031	0.00548
128.30000	14.849	4.727	523.06	0.03389	0.38	0.0031	0.00548
128.35000	14.846	4.727	523.06	0.03388	0.38	0.0031	0.00548
128.40000	14.844	4.726	523.06	0.03388	0.38	0.0031	0.00548
128.45000	14.842	4.725	523.06	0.03388	0.38	0.0031	0.00548
128.50000	14.840	4.725	523.06	0.03387	0.38	0.0031	0.00548
128.55000	14.838	4.724	523.06	0.03387	0.38	0.0031	0.00548
128.60000	14.836	4.723	523.06	0.03386	0.38	0.0031	0.00548
128.65000	14.834	4.723	523.06	0.03386	0.38	0.0031	0.00548
128.70000	14.832	4.722	523.06	0.03385	0.38	0.0031	0.00548
128.75000	14.830	4.722	523.06	0.03385	0.38	0.0031	0.00548
128.80000	14.828	4.721	523.06	0.03384	0.38	0.0031	0.00548
128.85000	14.826	4.720	523.06	0.03384	0.38	0.0031	0.00547
128.90000	14.824	4.720	523.06	0.03383	0.38	0.0031	0.00547
128.95000	14.821	4.719	523.06	0.03383	0.38	0.0031	0.00547
129.00000	14.819	4.718	523.06	0.03382	0.38	0.0031	0.00547
129.05000	14.817	4.718	523.06	0.03382	0.38	0.0031	0.00547
129.10000	14.815	4.717	523.05	0.03382	0.38	0.0031	0.00547
129.15000	14.813	4.716	523.05	0.03381	0.38	0.0031	0.00547
129.20000	14.811	4.716	523.05	0.03381	0.38	0.0031	0.00547
129.25000	14.809	4.715	523.05	0.03380	0.38	0.0031	0.00547
129.30000	14.807	4.715	523.05	0.03380	0.38	0.0031	0.00547
129.35000	14.805	4.714	523.05	0.03379	0.38	0.0031	0.00547
129.40000	14.803	4.713	523.05	0.03379	0.38	0.0031	0.00547
129.45000	14.801	4.713	523.05	0.03378	0.38	0.0031	0.00547

**Figure 6.4 Output File enode\_01.txt – START Predicted Behavior (Continued).**

Output for Sudden CONTRACTION node (node # 2).  
 discharge coefficient = 1.000  
 upstream diameter = 0.7500 inches  
 downstream diameter = 0.5625 inches  
 K factor = 0.218750

time(s)	p(psia)	rho (lbf/ft <sup>3</sup> )	t(R)	theta	velocity (ft/s)	Mach	mdot (lbm/s)
0.00000	265.680	53.379	529.62	0.38266	7.61	0.0393	0.70133
0.10000	264.367	53.225	529.46	0.38156	7.52	0.0389	0.69095
1.00000	253.118	51.807	529.37	0.37140	7.40	0.0389	0.66183
2.00000	241.559	50.301	529.26	0.36060	7.28	0.0389	0.63186
3.00000	230.877	48.862	529.16	0.35028	7.16	0.0389	0.60414
4.00000	220.972	47.485	529.06	0.34041	7.06	0.0390	0.57841
5.00000	211.760	46.166	528.97	0.33095	6.96	0.0390	0.55446
6.00000	203.167	44.901	528.87	0.32189	6.87	0.0390	0.53209
7.00000	195.131	43.686	528.78	0.31318	6.78	0.0390	0.51116
8.00000	187.599	42.519	528.70	0.30481	6.70	0.0390	0.49152
9.00000	180.524	41.396	528.61	0.29676	6.62	0.0390	0.47307
10.00000	173.864	40.315	528.53	0.28901	6.55	0.0390	0.45568
11.00000	167.584	39.273	528.44	0.28154	6.48	0.0390	0.43927
12.00000	161.651	38.268	528.36	0.27434	6.42	0.0390	0.42376
13.00000	156.038	37.298	528.28	0.26739	6.36	0.0390	0.40908
14.00000	150.718	36.362	528.20	0.26067	6.30	0.0390	0.39516
15.00000	145.669	35.458	528.13	0.25419	6.24	0.0390	0.38194
16.00000	140.871	34.583	528.05	0.24792	6.19	0.0390	0.36937
17.00000	136.307	33.737	527.98	0.24185	6.14	0.0390	0.35741
18.00000	131.959	32.918	527.90	0.23598	6.09	0.0390	0.34601
19.00000	127.812	32.125	527.83	0.23030	6.04	0.0390	0.33513
20.00000	123.853	31.357	527.76	0.22479	6.00	0.0390	0.32474
21.00000	120.070	30.613	527.69	0.21946	5.96	0.0390	0.31481
22.00000	116.452	29.891	527.62	0.21428	5.92	0.0390	0.30531
23.00000	112.988	29.191	527.55	0.20926	5.88	0.0390	0.29621
24.00000	109.668	28.511	527.49	0.20439	5.84	0.0390	0.28749
25.00000	106.485	27.852	527.42	0.19967	5.81	0.0389	0.27912
26.00000	103.431	27.212	527.36	0.19507	5.77	0.0389	0.27109
27.00000	100.497	26.589	527.29	0.19062	5.74	0.0389	0.26337
28.00000	97.678	25.985	527.23	0.18628	5.71	0.0389	0.25595
29.00000	94.966	25.398	527.16	0.18207	5.68	0.0389	0.24882
30.00000	92.357	24.826	527.10	0.17798	5.65	0.0389	0.24195

**Figure 6.5 Output File enode\_02.txt - SUDDEN CONTRACTION Predicted Behavior.**



31.00000	89.844	24.271	527.04	0.17399	5.62	0.0389	0.23534
32.00000	87.424	23.730	526.98	0.17012	5.59	0.0389	0.22896
33.00000	85.090	23.205	526.91	0.16635	5.56	0.0389	0.22282
34.00000	82.839	22.693	526.85	0.16268	5.54	0.0389	0.21689
35.00000	80.667	22.195	526.79	0.15911	5.51	0.0389	0.21117
36.00000	78.570	21.710	526.73	0.15563	5.49	0.0389	0.20564
37.00000	76.545	21.237	526.68	0.15224	5.47	0.0389	0.20031
38.00000	74.587	20.777	526.62	0.14895	5.44	0.0388	0.19515
39.00000	72.695	20.328	526.56	0.14573	5.42	0.0388	0.19016
40.00000	70.865	19.891	526.50	0.14260	5.40	0.0388	0.18533
41.00000	69.093	19.465	526.44	0.13954	5.38	0.0388	0.18066
42.00000	67.379	19.050	526.39	0.13657	5.36	0.0388	0.17614
43.00000	65.719	18.645	526.33	0.13366	5.34	0.0388	0.17177
44.00000	64.111	18.250	526.28	0.13083	5.32	0.0388	0.16752
45.00000	62.553	17.865	526.22	0.12807	5.30	0.0388	0.16341
46.00000	61.042	17.490	526.17	0.12538	5.28	0.0388	0.15943
47.00000	59.577	17.123	526.11	0.12275	5.26	0.0388	0.15557
48.00000	58.157	16.765	526.06	0.12019	5.25	0.0387	0.15182
49.00000	56.778	16.416	526.00	0.11768	5.23	0.0387	0.14818
50.00000	55.440	16.075	525.95	0.11524	5.21	0.0387	0.14465
51.00000	54.142	15.743	525.89	0.11286	5.20	0.0387	0.14122
52.00000	52.880	15.418	525.84	0.11053	5.18	0.0387	0.13790
53.00000	51.655	15.101	525.79	0.10825	5.17	0.0387	0.13466
54.00000	50.465	14.791	525.74	0.10603	5.15	0.0387	0.13152
55.00000	49.308	14.488	525.68	0.10386	5.14	0.0387	0.12847
56.00000	48.183	14.193	525.63	0.10175	5.12	0.0386	0.12550
57.00000	47.090	13.904	525.58	0.09968	5.11	0.0386	0.12262
58.00000	46.026	13.622	525.53	0.09765	5.10	0.0386	0.11981
59.00000	44.992	13.346	525.48	0.09568	5.08	0.0386	0.11708
60.00000	43.986	13.077	525.43	0.09375	5.07	0.0386	0.11443
61.00000	43.006	12.813	525.37	0.09186	5.06	0.0386	0.11184
62.00000	42.053	12.556	525.32	0.09001	5.05	0.0386	0.10933
63.00000	41.125	12.305	525.27	0.08821	5.03	0.0385	0.10688
64.00000	40.221	12.059	525.22	0.08645	5.02	0.0385	0.10449
65.00000	39.341	11.818	525.17	0.08472	5.01	0.0385	0.10217
66.00000	38.483	11.583	525.12	0.08304	5.00	0.0385	0.09991
67.00000	37.648	11.353	525.07	0.08139	4.99	0.0385	0.09771
68.00000	36.834	11.128	525.02	0.07977	4.98	0.0385	0.09556
69.00000	36.041	10.908	524.98	0.07820	4.97	0.0384	0.09347
70.00000	35.268	10.693	524.93	0.07666	4.95	0.0384	0.09143
71.00000	34.514	10.482	524.88	0.07515	4.94	0.0384	0.08944
72.00000	33.779	10.276	524.83	0.07367	4.93	0.0384	0.08750
73.00000	33.062	10.075	524.78	0.07223	4.92	0.0384	0.08561
74.00000	32.363	9.878	524.73	0.07081	4.91	0.0384	0.08377
75.00000	31.681	9.685	524.68	0.06943	4.90	0.0383	0.08197
76.00000	31.016	9.496	524.64	0.06808	4.89	0.0383	0.08022
77.00000	30.367	9.312	524.59	0.06675	4.89	0.0383	0.07851
78.00000	29.733	9.131	524.54	0.06546	4.88	0.0383	0.07684
79.00000	29.115	8.954	524.49	0.06419	4.87	0.0383	0.07521

**Figure 6.5 Output File enode\_02.txt – SUDDEN CONTRACTION Predicted Behavior (Continued).**

80.00000	28.511	8.781	524.45	0.06295	4.86	0.0383	0.07362
81.00000	27.922	8.611	524.40	0.06173	4.85	0.0382	0.07206
82.00000	27.347	8.445	524.35	0.06054	4.84	0.0382	0.07055
83.00000	26.785	8.283	524.31	0.05938	4.83	0.0382	0.06907
84.00000	26.237	8.124	524.26	0.05824	4.82	0.0382	0.06762
85.00000	25.701	7.968	524.21	0.05712	4.82	0.0382	0.06621
85.60000	25.380	7.875	524.18	0.05645	4.92	0.0390	0.06690
86.60000	24.863	7.724	524.14	0.05537	4.77	0.0379	0.06354
87.60000	24.373	7.580	524.10	0.05434	4.66	0.0370	0.06091
88.60000	23.894	7.440	524.05	0.05333	4.65	0.0370	0.05972
89.60000	23.428	7.303	524.01	0.05235	4.54	0.0361	0.05717
90.60000	22.984	7.172	523.97	0.05142	4.46	0.0356	0.05518
91.60000	22.557	7.046	523.93	0.05051	4.38	0.0350	0.05326
92.60000	22.148	6.925	523.90	0.04964	4.23	0.0338	0.05051
93.60000	21.755	6.809	523.85	0.04881	4.22	0.0338	0.04961
94.60000	21.369	6.694	523.81	0.04799	4.22	0.0338	0.04873
95.60000	21.000	6.584	523.78	0.04720	4.06	0.0325	0.04610
96.60000	20.646	6.479	523.74	0.04645	3.97	0.0319	0.04444
97.60000	20.307	6.378	523.71	0.04572	3.80	0.0305	0.04187
98.60000	19.984	6.281	523.68	0.04503	3.80	0.0305	0.04120
99.60000	19.666	6.186	523.64	0.04435	3.80	0.0305	0.04055
100.60000	19.361	6.095	523.61	0.04369	3.63	0.0292	0.03823
101.60000	19.079	6.010	523.58	0.04309	3.42	0.0275	0.03548
102.60000	18.806	5.928	523.55	0.04250	3.42	0.0275	0.03497
103.60000	18.537	5.847	523.52	0.04192	3.42	0.0275	0.03447
104.60000	18.279	5.770	523.49	0.04136	3.28	0.0265	0.03271
105.60000	18.035	5.696	523.46	0.04083	3.14	0.0253	0.03086
106.60000	17.799	5.625	523.43	0.04032	3.14	0.0253	0.03046
107.60000	17.568	5.555	523.40	0.03982	3.01	0.0243	0.02884
108.60000	17.351	5.489	523.38	0.03935	2.91	0.0235	0.02760
109.60000	17.144	5.427	523.35	0.03890	2.82	0.0228	0.02639
110.60000	16.946	5.367	523.33	0.03847	2.72	0.0220	0.02520
111.60000	16.757	5.309	523.31	0.03806	2.62	0.0212	0.02403
112.60000	16.581	5.256	523.29	0.03768	2.49	0.0201	0.02256
113.60000	16.409	5.204	523.26	0.03730	2.49	0.0201	0.02233
114.60000	16.244	5.153	523.24	0.03694	2.32	0.0188	0.02064
115.60000	16.091	5.107	523.23	0.03661	2.04	0.0165	0.01794
116.60000	15.954	5.065	523.21	0.03631	2.03	0.0165	0.01778
117.60000	15.819	5.024	523.19	0.03602	2.03	0.0165	0.01763
118.60000	15.689	4.984	523.17	0.03573	1.91	0.0155	0.01642
119.60000	15.568	4.947	523.15	0.03547	1.80	0.0146	0.01537
120.60000	15.454	4.913	523.14	0.03522	1.69	0.0137	0.01433
121.60000	15.349	4.880	523.13	0.03499	1.58	0.0128	0.01331
122.60000	15.256	4.852	523.11	0.03478	1.46	0.0118	0.01219
123.60000	15.163	4.824	523.10	0.03458	1.46	0.0118	0.01212
124.60000	15.080	4.798	523.09	0.03440	1.24	0.0101	0.01025
125.60000	15.006	4.775	523.08	0.03423	1.12	0.0091	0.00924
126.60000	14.939	4.755	523.07	0.03409	1.00	0.0081	0.00822
127.30000	14.897	4.742	523.06	0.03400	0.92	0.0075	0.00751
127.35000	14.895	4.741	523.06	0.03399	0.91	0.0074	0.00746
127.40000	14.892	4.741	523.06	0.03398	0.91	0.0074	0.00741
127.45000	14.889	4.740	523.06	0.03398	0.90	0.0073	0.00736
127.50000	14.886	4.739	523.06	0.03397	0.89	0.0073	0.00731

**Figure 6.5 Output File enode\_02.txt – SUDDEN CONTRACTION Predicted Behavior (Continued).**

127.55000	14.883	4.738	523.06	0.03397	0.89	0.0072	0.00726
127.60000	14.881	4.737	523.06	0.03396	0.88	0.0072	0.00720
127.65000	14.878	4.736	523.06	0.03395	0.88	0.0071	0.00715
127.70000	14.875	4.735	523.06	0.03395	0.87	0.0071	0.00710
127.75000	14.872	4.735	523.06	0.03394	0.86	0.0070	0.00705
127.80000	14.870	4.734	523.06	0.03394	0.86	0.0070	0.00700
127.85000	14.867	4.733	523.06	0.03393	0.67	0.0055	0.00549
127.90000	14.865	4.732	523.06	0.03393	0.67	0.0055	0.00549
127.95000	14.863	4.732	523.06	0.03392	0.67	0.0055	0.00549
128.00000	14.861	4.731	523.06	0.03392	0.67	0.0055	0.00549
128.05000	14.859	4.730	523.06	0.03391	0.67	0.0055	0.00549
128.10000	14.857	4.730	523.06	0.03391	0.67	0.0055	0.00549
128.15000	14.855	4.729	523.06	0.03390	0.67	0.0055	0.00549
128.20000	14.853	4.729	523.06	0.03390	0.67	0.0055	0.00548
128.25000	14.851	4.728	523.06	0.03389	0.67	0.0055	0.00548
128.30000	14.848	4.727	523.06	0.03389	0.67	0.0055	0.00548
128.35000	14.846	4.727	523.06	0.03388	0.67	0.0055	0.00548
128.40000	14.844	4.726	523.06	0.03388	0.67	0.0055	0.00548
128.45000	14.842	4.725	523.06	0.03388	0.67	0.0055	0.00548
128.50000	14.840	4.725	523.06	0.03387	0.67	0.0055	0.00548
128.55000	14.838	4.724	523.06	0.03387	0.67	0.0055	0.00548
128.60000	14.836	4.723	523.06	0.03386	0.67	0.0055	0.00548
128.65000	14.834	4.723	523.06	0.03386	0.67	0.0055	0.00548
128.70000	14.832	4.722	523.06	0.03385	0.67	0.0055	0.00548
128.75000	14.830	4.722	523.06	0.03385	0.67	0.0055	0.00548
128.80000	14.828	4.721	523.06	0.03384	0.67	0.0055	0.00548
128.85000	14.826	4.720	523.05	0.03384	0.67	0.0055	0.00547
128.90000	14.823	4.720	523.05	0.03383	0.67	0.0055	0.00547
128.95000	14.821	4.719	523.05	0.03383	0.67	0.0055	0.00547
129.00000	14.819	4.718	523.05	0.03382	0.67	0.0055	0.00547
129.05000	14.817	4.718	523.05	0.03382	0.67	0.0055	0.00547
129.10000	14.815	4.717	523.05	0.03382	0.67	0.0055	0.00547
129.15000	14.813	4.716	523.05	0.03381	0.67	0.0055	0.00547
129.20000	14.811	4.716	523.05	0.03381	0.67	0.0055	0.00547
129.25000	14.809	4.715	523.05	0.03380	0.67	0.0055	0.00547
129.30000	14.807	4.715	523.05	0.03380	0.67	0.0055	0.00547
129.35000	14.805	4.714	523.05	0.03379	0.67	0.0055	0.00547
129.40000	14.803	4.713	523.05	0.03379	0.67	0.0055	0.00547
129.45000	14.801	4.713	523.05	0.03378	0.67	0.0055	0.00547

**Figure 6.5 Output File enode\_02.txt – SUDDEN CONTRACTION Predicted Behavior (Continued).**

Output for PIPE node (node # 3).  
 discharge coefficient = 1.000  
 length = 8.000 ft diameter = 0.5625 inches

time(s)	p(psia)	rho (lbf/ft <sup>3</sup> )	t(R)	theta	velocity (ft/s)	Mach	mdot (lbm/s)
0.00000	263.050	53.052	529.62	0.38032	7.66	0.0397	0.70119
0.10000	264.027	53.225	528.78	0.38156	7.52	0.0389	0.69095
1.00000	252.796	51.807	528.69	0.37140	7.40	0.0389	0.66183
2.00000	241.255	50.301	528.60	0.36060	7.28	0.0390	0.63186
3.00000	230.590	48.862	528.50	0.35028	7.16	0.0390	0.60414
4.00000	220.701	47.485	528.41	0.34041	7.06	0.0390	0.57841
5.00000	211.502	46.166	528.32	0.33095	6.96	0.0390	0.55446
6.00000	202.921	44.901	528.24	0.32189	6.87	0.0390	0.53209
7.00000	194.898	43.686	528.15	0.31318	6.78	0.0390	0.51116
8.00000	187.377	42.519	528.07	0.30481	6.70	0.0390	0.49152
9.00000	180.311	41.396	527.99	0.29676	6.62	0.0390	0.47307
10.00000	173.661	40.315	527.91	0.28901	6.55	0.0390	0.45568
11.00000	167.389	39.273	527.83	0.28154	6.48	0.0390	0.43927
12.00000	161.464	38.268	527.75	0.27434	6.42	0.0390	0.42376
13.00000	155.858	37.298	527.67	0.26739	6.36	0.0390	0.40908
14.00000	150.545	36.362	527.60	0.26067	6.30	0.0390	0.39516
15.00000	145.503	35.458	527.53	0.25419	6.24	0.0390	0.38194
16.00000	140.712	34.583	527.45	0.24792	6.19	0.0390	0.36937
17.00000	136.153	33.737	527.38	0.24185	6.14	0.0390	0.35741
18.00000	131.810	32.918	527.31	0.23598	6.09	0.0390	0.34601
19.00000	127.669	32.125	527.24	0.23030	6.04	0.0390	0.33513
20.00000	123.715	31.357	527.17	0.22479	6.00	0.0390	0.32474
21.00000	119.937	30.613	527.11	0.21946	5.96	0.0390	0.31481
22.00000	116.323	29.891	527.04	0.21428	5.92	0.0390	0.30531
23.00000	112.863	29.191	526.97	0.20926	5.88	0.0390	0.29621
24.00000	109.548	28.511	526.91	0.20439	5.84	0.0390	0.28749
25.00000	106.368	27.852	526.84	0.19967	5.81	0.0390	0.27912
26.00000	103.317	27.212	526.78	0.19507	5.77	0.0390	0.27109
27.00000	100.387	26.589	526.71	0.19062	5.74	0.0390	0.26337
28.00000	97.571	25.985	526.65	0.18628	5.71	0.0390	0.25595
29.00000	94.862	25.398	526.59	0.18207	5.68	0.0389	0.24882
30.00000	92.256	24.826	526.53	0.17798	5.65	0.0389	0.24195

**Figure 6.6 Output File enode\_03.txt - PIPE Predicted Behavior.**

31.00000	89.747	24.271	526.46	0.17399	5.62	0.0389	0.23534
32.00000	87.329	23.730	526.40	0.17012	5.59	0.0389	0.22896
33.00000	84.998	23.205	526.34	0.16635	5.56	0.0389	0.22282
34.00000	82.750	22.693	526.28	0.16268	5.54	0.0389	0.21689
35.00000	80.580	22.195	526.22	0.15911	5.51	0.0389	0.21117
36.00000	78.485	21.710	526.17	0.15563	5.49	0.0389	0.20564
37.00000	76.462	21.237	526.11	0.15224	5.47	0.0389	0.20031
38.00000	74.507	20.777	526.05	0.14895	5.44	0.0389	0.19515
39.00000	72.616	20.328	525.99	0.14573	5.42	0.0389	0.19016
40.00000	70.788	19.891	525.93	0.14260	5.40	0.0388	0.18533
41.00000	69.019	19.465	525.88	0.13954	5.38	0.0388	0.18066
42.00000	67.306	19.050	525.82	0.13657	5.36	0.0388	0.17614
43.00000	65.648	18.645	525.76	0.13366	5.34	0.0388	0.17177
44.00000	64.042	18.250	525.71	0.13083	5.32	0.0388	0.16752
45.00000	62.485	17.865	525.65	0.12807	5.30	0.0388	0.16341
46.00000	60.976	17.490	525.60	0.12538	5.28	0.0388	0.15943
47.00000	59.513	17.123	525.54	0.12275	5.26	0.0388	0.15557
48.00000	58.094	16.765	525.49	0.12019	5.25	0.0388	0.15182
49.00000	56.717	16.416	525.43	0.11768	5.23	0.0387	0.14818
50.00000	55.381	16.075	525.38	0.11524	5.21	0.0387	0.14465
51.00000	54.083	15.743	525.33	0.11286	5.20	0.0387	0.14122
52.00000	52.823	15.418	525.27	0.11053	5.18	0.0387	0.13790
53.00000	51.599	15.101	525.22	0.10825	5.17	0.0387	0.13466
54.00000	50.410	14.791	525.17	0.10603	5.15	0.0387	0.13152
55.00000	49.254	14.488	525.11	0.10386	5.14	0.0387	0.12847
56.00000	48.131	14.193	525.06	0.10175	5.12	0.0387	0.12550
57.00000	47.039	13.904	525.01	0.09968	5.11	0.0386	0.12262
58.00000	45.977	13.622	524.96	0.09765	5.10	0.0386	0.11981
59.00000	44.943	13.346	524.91	0.09568	5.08	0.0386	0.11708
60.00000	43.938	13.077	524.85	0.09375	5.07	0.0386	0.11443
61.00000	42.959	12.813	524.80	0.09186	5.06	0.0386	0.11184
62.00000	42.007	12.556	524.75	0.09001	5.05	0.0386	0.10933
63.00000	41.080	12.305	524.70	0.08821	5.03	0.0386	0.10688
64.00000	40.177	12.059	524.65	0.08645	5.02	0.0385	0.10449
65.00000	39.298	11.818	524.60	0.08472	5.01	0.0385	0.10217
66.00000	38.441	11.583	524.55	0.08304	5.00	0.0385	0.09991
67.00000	37.607	11.353	524.50	0.08139	4.99	0.0385	0.09771
68.00000	36.794	11.128	524.45	0.07977	4.98	0.0385	0.09556
69.00000	36.001	10.908	524.40	0.07820	4.97	0.0385	0.09347
70.00000	35.229	10.693	524.35	0.07666	4.95	0.0385	0.09143
71.00000	34.476	10.482	524.30	0.07515	4.94	0.0384	0.08944
72.00000	33.742	10.276	524.25	0.07367	4.93	0.0384	0.08750
73.00000	33.026	10.075	524.20	0.07223	4.92	0.0384	0.08561
74.00000	32.327	9.878	524.15	0.07081	4.91	0.0384	0.08377
75.00000	31.646	9.685	524.10	0.06943	4.90	0.0384	0.08197
76.00000	30.981	9.496	524.06	0.06808	4.89	0.0384	0.08022
77.00000	30.333	9.312	524.01	0.06675	4.89	0.0383	0.07851
78.00000	29.700	9.131	523.96	0.06546	4.88	0.0383	0.07684
79.00000	29.083	8.954	523.91	0.06419	4.87	0.0383	0.07521

**Figure 6.6 Output File enode\_03.txt – PIPE Predicted Behavior (Continued).**

80.00000	28.480	8.781	523.86	0.06295	4.86	0.0383	0.07362
81.00000	27.891	8.611	523.81	0.06173	4.85	0.0383	0.07206
82.00000	27.316	8.445	523.77	0.06054	4.84	0.0382	0.07055
83.00000	26.755	8.283	523.72	0.05938	4.83	0.0382	0.06907
84.00000	26.207	8.124	523.67	0.05824	4.82	0.0382	0.06762
85.00000	25.672	7.968	523.62	0.05712	4.82	0.0382	0.06621
85.60000	25.351	7.875	523.57	0.05645	4.92	0.0391	0.06690
86.60000	24.835	7.724	523.56	0.05537	4.77	0.0379	0.06354
87.60000	24.347	7.580	523.54	0.05434	4.66	0.0370	0.06091
88.60000	23.868	7.440	523.49	0.05333	4.65	0.0370	0.05972
89.60000	23.404	7.303	523.47	0.05235	4.54	0.0362	0.05717
90.60000	22.961	7.172	523.45	0.05142	4.46	0.0356	0.05518
91.60000	22.535	7.046	523.42	0.05051	4.38	0.0350	0.05326
92.60000	22.128	6.925	523.41	0.04964	4.23	0.0338	0.05051
93.60000	21.735	6.809	523.37	0.04881	4.22	0.0338	0.04961
94.60000	21.349	6.694	523.33	0.04799	4.22	0.0338	0.04873
95.60000	20.982	6.584	523.33	0.04720	4.06	0.0325	0.04610
96.60000	20.629	6.479	523.31	0.04645	3.97	0.0319	0.04444
97.60000	20.292	6.378	523.31	0.04572	3.80	0.0305	0.04187
98.60000	19.968	6.281	523.27	0.04503	3.80	0.0305	0.04120
99.60000	19.651	6.186	523.23	0.04435	3.80	0.0305	0.04055
100.60000	19.347	6.095	523.23	0.04369	3.63	0.0292	0.03823
101.60000	19.066	6.010	523.24	0.04309	3.42	0.0275	0.03548
102.60000	18.794	5.928	523.21	0.04250	3.42	0.0275	0.03497
103.60000	18.525	5.847	523.17	0.04192	3.42	0.0275	0.03447
104.60000	18.267	5.770	523.17	0.04136	3.28	0.0265	0.03271
105.60000	18.025	5.696	523.17	0.04083	3.14	0.0253	0.03086
106.60000	17.789	5.625	523.14	0.04032	3.14	0.0253	0.03046
107.60000	17.559	5.555	523.13	0.03982	3.01	0.0243	0.02884
108.60000	17.342	5.489	523.12	0.03935	2.91	0.0236	0.02760
109.60000	17.136	5.427	523.11	0.03890	2.82	0.0228	0.02639
110.60000	16.938	5.367	523.10	0.03847	2.72	0.0220	0.02520
111.60000	16.750	5.309	523.09	0.03806	2.62	0.0212	0.02403
112.60000	16.575	5.256	523.09	0.03768	2.49	0.0201	0.02256
113.60000	16.403	5.204	523.06	0.03730	2.49	0.0201	0.02233
114.60000	16.239	5.153	523.07	0.03694	2.32	0.0188	0.02064
115.60000	16.087	5.107	523.09	0.03661	2.04	0.0165	0.01794
116.60000	15.950	5.065	523.07	0.03631	2.03	0.0165	0.01778
117.60000	15.815	5.024	523.05	0.03602	2.03	0.0165	0.01763
118.60000	15.685	4.984	523.04	0.03573	1.91	0.0155	0.01642
119.60000	15.564	4.947	523.04	0.03547	1.80	0.0146	0.01537
120.60000	15.451	4.913	523.04	0.03522	1.69	0.0137	0.01433
121.60000	15.346	4.880	523.03	0.03499	1.58	0.0128	0.01331
122.60000	15.253	4.852	523.03	0.03478	1.46	0.0118	0.01219
123.60000	15.161	4.824	523.02	0.03458	1.46	0.0118	0.01212
124.60000	15.078	4.798	523.03	0.03440	1.24	0.0101	0.01025
125.60000	15.004	4.775	523.03	0.03423	1.12	0.0091	0.00924
126.60000	14.938	4.755	523.03	0.03409	1.00	0.0081	0.00822
127.30000	14.896	4.742	523.03	0.03400	0.92	0.0075	0.00751
127.35000	14.894	4.741	523.03	0.03399	0.91	0.0074	0.00746
127.40000	14.891	4.741	523.03	0.03398	0.91	0.0074	0.00741
127.45000	14.888	4.740	523.03	0.03398	0.90	0.0073	0.00736
127.50000	14.885	4.739	523.03	0.03397	0.89	0.0073	0.00731

**Figure 6.6 Output File enode\_03.txt – PIPE Predicted Behavior (Continued).**

127.55000	14.882	4.738	523.03	0.03397	0.89	0.0072	0.00726
127.60000	14.880	4.737	523.03	0.03396	0.88	0.0072	0.00720
127.65000	14.877	4.736	523.03	0.03395	0.88	0.0071	0.00715
127.70000	14.874	4.735	523.03	0.03395	0.87	0.0071	0.00710
127.75000	14.872	4.735	523.03	0.03394	0.86	0.0070	0.00705
127.80000	14.869	4.734	523.03	0.03394	0.86	0.0070	0.00700
127.85000	14.867	4.733	523.04	0.03393	0.67	0.0055	0.00549
127.90000	14.865	4.732	523.04	0.03393	0.67	0.0055	0.00549
127.95000	14.862	4.732	523.04	0.03392	0.67	0.0055	0.00549
128.00000	14.860	4.731	523.04	0.03392	0.67	0.0055	0.00549
128.05000	14.858	4.730	523.04	0.03391	0.67	0.0055	0.00549
128.10000	14.856	4.730	523.04	0.03391	0.67	0.0055	0.00549
128.15000	14.854	4.729	523.04	0.03390	0.67	0.0055	0.00549
128.20000	14.852	4.729	523.04	0.03390	0.67	0.0055	0.00548
128.25000	14.850	4.728	523.04	0.03389	0.67	0.0055	0.00548
128.30000	14.848	4.727	523.04	0.03389	0.67	0.0055	0.00548
128.35000	14.846	4.727	523.04	0.03388	0.67	0.0055	0.00548
128.40000	14.844	4.726	523.04	0.03388	0.67	0.0055	0.00548
128.45000	14.842	4.725	523.04	0.03388	0.67	0.0055	0.00548
128.50000	14.840	4.725	523.04	0.03387	0.67	0.0055	0.00548
128.55000	14.837	4.724	523.04	0.03387	0.67	0.0055	0.00548
128.60000	14.835	4.723	523.04	0.03386	0.67	0.0055	0.00548
128.65000	14.833	4.723	523.04	0.03386	0.67	0.0055	0.00548
128.70000	14.831	4.722	523.04	0.03385	0.67	0.0055	0.00548
128.75000	14.829	4.722	523.04	0.03385	0.67	0.0055	0.00548
128.80000	14.827	4.721	523.03	0.03384	0.67	0.0055	0.00548
128.85000	14.825	4.720	523.03	0.03384	0.67	0.0055	0.00547
128.90000	14.823	4.720	523.03	0.03383	0.67	0.0055	0.00547
128.95000	14.821	4.719	523.03	0.03383	0.67	0.0055	0.00547
129.00000	14.819	4.718	523.03	0.03382	0.67	0.0055	0.00547
129.05000	14.817	4.718	523.03	0.03382	0.67	0.0055	0.00547
129.10000	14.815	4.717	523.03	0.03382	0.67	0.0055	0.00547
129.15000	14.813	4.716	523.03	0.03381	0.67	0.0055	0.00547
129.20000	14.810	4.716	523.03	0.03381	0.67	0.0055	0.00547
129.25000	14.808	4.715	523.03	0.03380	0.67	0.0055	0.00547
129.30000	14.806	4.715	523.03	0.03380	0.67	0.0055	0.00547
129.35000	14.804	4.714	523.03	0.03379	0.67	0.0055	0.00547
129.40000	14.802	4.713	523.03	0.03379	0.67	0.0055	0.00547
129.45000	14.800	4.713	523.03	0.03378	0.67	0.0055	0.00547

**Figure 6.6 Output File enode\_03.txt – PIPE Predicted Behavior (Continued).**

Output for Nozzle THROAT node (node # 4).  
 discharge coefficient = 0.470  
 length = 1.50000 inches  
 inlet diameter = 0.5625 inches  
 throat diameter = 0.1730 inches

time(s)	p(psia)	rho (lbf/ft <sup>3</sup> )	t(R)	theta	velocity (ft/s)	Mach	mdot (lbm/s)
0.00000	233.678	49.383	526.88	0.35402	184.62	1.0000	0.69948
0.10000	235.931	49.691	526.85	0.35623	185.25	1.0000	0.70625
1.00000	226.066	48.335	526.83	0.34650	182.49	1.0000	0.67673
2.00000	215.905	46.894	526.81	0.33617	179.65	1.0000	0.64633
3.00000	206.493	45.518	526.78	0.32631	177.01	1.0000	0.61817
4.00000	197.747	44.203	526.75	0.31688	174.56	1.0000	0.59200
5.00000	189.595	42.944	526.72	0.30786	172.28	1.0000	0.56762
6.00000	181.978	41.737	526.68	0.29920	170.15	1.0000	0.54483
7.00000	174.843	40.578	526.64	0.29090	168.15	1.0000	0.52349
8.00000	168.144	39.466	526.60	0.28292	166.27	1.0000	0.50345
9.00000	161.842	38.396	526.56	0.27525	164.51	1.0000	0.48460
10.00000	155.902	37.366	526.52	0.26787	162.84	1.0000	0.46683
11.00000	150.294	36.375	526.48	0.26076	161.27	1.0000	0.45006
12.00000	144.989	35.419	526.43	0.25391	159.78	1.0000	0.43419
13.00000	139.964	34.497	526.39	0.24730	158.37	1.0000	0.41916
14.00000	135.196	33.607	526.34	0.24092	157.04	1.0000	0.40490
15.00000	130.668	32.748	526.30	0.23476	155.76	1.0000	0.39135
16.00000	126.360	31.918	526.25	0.22881	154.56	1.0000	0.37847
17.00000	122.258	31.115	526.20	0.22306	153.40	1.0000	0.36620
18.00000	118.348	30.338	526.16	0.21749	152.31	1.0000	0.35450
19.00000	114.616	29.586	526.11	0.21210	151.26	1.0000	0.34334
20.00000	111.050	28.858	526.06	0.20688	150.25	1.0000	0.33267
21.00000	107.640	28.153	526.01	0.20183	149.30	1.0000	0.32247
22.00000	104.377	27.470	525.97	0.19693	148.38	1.0000	0.31271
23.00000	101.251	26.807	525.92	0.19217	147.50	1.0000	0.30336
24.00000	98.254	26.164	525.87	0.18757	146.66	1.0000	0.29439
25.00000	95.378	25.541	525.82	0.18310	145.85	1.0000	0.28579
26.00000	92.617	24.935	525.77	0.17876	145.07	1.0000	0.27753
27.00000	89.964	24.348	525.73	0.17454	144.32	1.0000	0.26959
28.00000	87.413	23.777	525.68	0.17045	143.60	1.0000	0.26196
29.00000	84.959	23.222	525.63	0.16647	142.91	1.0000	0.25462
30.00000	82.597	22.683	525.58	0.16261	142.25	1.0000	0.24755

**Figure 6.7 Output File enode\_04.txt - Nozzle THROAT Predicted Behavior.**



31.00000	80.321	22.159	525.53	0.15885	141.60	1.0000	0.24074
32.00000	78.128	21.650	525.49	0.15520	140.99	1.0000	0.23418
33.00000	76.013	21.154	525.44	0.15165	140.39	1.0000	0.22785
34.00000	73.972	20.672	525.39	0.14819	139.81	1.0000	0.22174
35.00000	72.003	20.203	525.34	0.14483	139.26	1.0000	0.21585
36.00000	70.101	19.746	525.29	0.14156	138.72	1.0000	0.21015
37.00000	68.263	19.302	525.25	0.13837	138.20	1.0000	0.20465
38.00000	66.486	18.869	525.20	0.13527	137.70	1.0000	0.19934
39.00000	64.769	18.447	525.15	0.13224	137.21	1.0000	0.19420
40.00000	63.107	18.037	525.10	0.12930	136.74	1.0000	0.18922
41.00000	61.499	17.636	525.05	0.12643	136.29	1.0000	0.18441
42.00000	59.942	17.247	525.01	0.12364	135.85	1.0000	0.17975
43.00000	58.434	16.867	524.96	0.12091	135.42	1.0000	0.17524
44.00000	56.974	16.496	524.91	0.11826	135.00	1.0000	0.17086
45.00000	55.558	16.135	524.86	0.11567	134.60	1.0000	0.16663
46.00000	54.186	15.783	524.82	0.11314	134.21	1.0000	0.16252
47.00000	52.855	15.439	524.77	0.11068	133.84	1.0000	0.15853
48.00000	51.564	15.104	524.72	0.10828	133.47	1.0000	0.15467
49.00000	50.312	14.777	524.68	0.10594	133.11	1.0000	0.15092
50.00000	49.096	14.458	524.63	0.10365	132.77	1.0000	0.14728
51.00000	47.916	14.147	524.58	0.10142	132.43	1.0000	0.14374
52.00000	46.769	13.843	524.54	0.09924	132.11	1.0000	0.14031
53.00000	45.656	13.547	524.49	0.09712	131.79	1.0000	0.13698
54.00000	44.574	13.258	524.44	0.09504	131.48	1.0000	0.13374
55.00000	43.523	12.975	524.40	0.09302	131.18	1.0000	0.13059
56.00000	42.501	12.699	524.35	0.09104	130.89	1.0000	0.12753
57.00000	41.507	12.430	524.30	0.08911	130.61	1.0000	0.12455
58.00000	40.541	12.167	524.26	0.08722	130.33	1.0000	0.12166
59.00000	39.601	11.910	524.21	0.08538	130.06	1.0000	0.11884
60.00000	38.687	11.658	524.17	0.08358	129.80	1.0000	0.11610
61.00000	37.797	11.413	524.12	0.08182	129.55	1.0000	0.11344
62.00000	36.931	11.174	524.08	0.08010	129.30	1.0000	0.11084
63.00000	36.088	10.939	524.03	0.07842	129.06	1.0000	0.10832
64.00000	35.267	10.711	523.98	0.07678	128.83	1.0000	0.10586
65.00000	34.468	10.487	523.94	0.07518	128.60	1.0000	0.10347
66.00000	33.690	10.268	523.89	0.07361	128.37	1.0000	0.10113
67.00000	32.931	10.055	523.85	0.07208	128.16	1.0000	0.09886
68.00000	32.192	9.846	523.80	0.07058	127.94	1.0000	0.09665
69.00000	31.473	9.642	523.76	0.06912	127.74	1.0000	0.09449
70.00000	30.771	9.442	523.71	0.06769	127.54	1.0000	0.09239
71.00000	30.087	9.247	523.67	0.06629	127.34	1.0000	0.09034
72.00000	29.420	9.056	523.62	0.06492	127.15	1.0000	0.08834
73.00000	28.770	8.869	523.58	0.06358	126.96	1.0000	0.08639
74.00000	28.136	8.687	523.53	0.06227	126.78	1.0000	0.08449
75.00000	27.518	8.508	523.49	0.06099	126.60	1.0000	0.08264
76.00000	26.915	8.333	523.44	0.05974	126.43	1.0000	0.08083
77.00000	26.326	8.162	523.40	0.05852	126.26	1.0000	0.07907
78.00000	25.752	7.995	523.35	0.05732	126.09	1.0000	0.07735
79.00000	25.192	7.832	523.31	0.05614	125.93	1.0000	0.07567

**Figure 6.7 Output File enode\_04.txt – Nozzle THROAT Predicted Behavior (Continued).**

80.00000	24.646	7.672	523.27	0.05500	125.77	1.0000	0.07403
81.00000	24.112	7.515	523.22	0.05388	125.62	1.0000	0.07243
82.00000	23.591	7.362	523.18	0.05278	125.46	1.0000	0.07087
83.00000	23.083	7.212	523.13	0.05170	125.32	1.0000	0.06934
84.00000	22.587	7.066	523.09	0.05065	125.17	1.0000	0.06785
85.00000	22.102	6.922	523.05	0.04962	125.03	1.0000	0.06640
85.60000	21.649	6.787	523.04	0.04866	124.00	0.9927	0.06457
86.60000	21.395	6.712	523.04	0.04811	121.69	0.9748	0.06266
87.60000	21.093	6.621	523.04	0.04747	119.40	0.9571	0.06065
88.60000	20.657	6.491	523.04	0.04653	117.03	0.9391	0.05828
89.60000	20.373	6.405	523.04	0.04592	114.66	0.9207	0.05635
90.60000	20.058	6.311	523.04	0.04524	112.31	0.9024	0.05438
91.60000	19.755	6.220	523.04	0.04459	109.94	0.8840	0.05247
92.60000	19.552	6.159	523.03	0.04415	107.61	0.8656	0.05084
93.60000	19.189	6.049	523.03	0.04337	105.23	0.8471	0.04884
94.60000	18.832	5.942	523.03	0.04260	102.80	0.8282	0.04686
95.60000	18.661	5.890	523.03	0.04222	100.40	0.8093	0.04537
96.60000	18.414	5.815	523.03	0.04169	98.00	0.7903	0.04372
97.60000	18.263	5.770	523.03	0.04136	95.61	0.7714	0.04232
98.60000	17.961	5.678	523.03	0.04070	93.20	0.7524	0.04060
99.60000	17.663	5.588	523.03	0.04006	90.74	0.7330	0.03890
100.60000	17.525	5.546	523.03	0.03976	88.29	0.7135	0.03757
101.60000	17.442	5.521	523.03	0.03958	85.93	0.6946	0.03640
102.60000	17.184	5.442	523.03	0.03901	83.53	0.6755	0.03487
103.60000	16.931	5.365	523.03	0.03846	81.05	0.6558	0.03336
104.60000	16.789	5.322	523.03	0.03815	78.57	0.6360	0.03208
105.60000	16.668	5.285	523.03	0.03789	76.13	0.6164	0.03087
106.60000	16.443	5.216	523.03	0.03739	73.63	0.5965	0.02947
107.60000	16.316	5.177	523.03	0.03711	71.09	0.5760	0.02824
108.60000	16.173	5.134	523.03	0.03680	68.57	0.5558	0.02701
109.60000	16.038	5.092	523.03	0.03651	66.04	0.5355	0.02580
110.60000	15.910	5.053	523.03	0.03622	63.51	0.5151	0.02462
111.60000	15.788	5.016	523.03	0.03596	60.96	0.4946	0.02346
112.60000	15.699	4.989	523.04	0.03576	58.46	0.4744	0.02238
113.60000	15.533	4.938	523.04	0.03540	55.87	0.4535	0.02116
114.60000	15.467	4.917	523.04	0.03525	53.25	0.4323	0.02009
115.60000	15.466	4.917	523.04	0.03525	50.67	0.4114	0.01911
116.60000	15.333	4.876	523.04	0.03496	48.22	0.3916	0.01804
117.60000	15.201	4.836	523.04	0.03467	45.65	0.3709	0.01694
118.60000	15.133	4.815	523.04	0.03452	43.00	0.3494	0.01589
119.60000	15.064	4.794	523.04	0.03437	40.36	0.3280	0.01484
120.60000	15.000	4.774	523.04	0.03423	37.71	0.3065	0.01381
121.60000	14.943	4.756	523.04	0.03410	35.04	0.2848	0.01279
122.60000	14.899	4.743	523.04	0.03400	32.48	0.2640	0.01182
123.60000	14.808	4.715	523.04	0.03380	29.70	0.2415	0.01074
124.60000	14.805	4.714	523.04	0.03379	26.94	0.2190	0.00974
125.60000	14.771	4.703	523.04	0.03372	24.20	0.1968	0.00873
126.60000	14.742	4.695	523.04	0.03365	21.43	0.1743	0.00772
127.30000	14.725	4.689	523.04	0.03362	19.48	0.1584	0.00701
127.35000	14.724	4.689	523.04	0.03362	19.34	0.1573	0.00696
127.40000	14.723	4.689	523.04	0.03361	19.20	0.1561	0.00691
127.45000	14.722	4.688	523.04	0.03361	19.06	0.1550	0.00686
127.50000	14.721	4.688	523.04	0.03361	18.92	0.1539	0.00680

**Figure 6.7 Output File enode\_04.txt – Nozzle THROAT Predicted Behavior (Continued).**

127.55000	14.719	4.688	523.04	0.03361	18.78	0.1527	0.00675
127.60000	14.718	4.687	523.04	0.03360	18.64	0.1516	0.00670
127.65000	14.717	4.687	523.04	0.03360	18.50	0.1504	0.00665
127.70000	14.716	4.687	523.04	0.03360	18.36	0.1493	0.00660
127.75000	14.715	4.687	523.04	0.03360	18.22	0.1481	0.00655
127.80000	14.714	4.686	523.04	0.03359	18.07	0.1470	0.00650
127.85000	14.759	4.700	523.04	0.03369	17.94	0.1459	0.00647
127.90000	14.757	4.699	523.04	0.03369	17.82	0.1449	0.00643
127.95000	14.755	4.699	523.04	0.03368	17.71	0.1440	0.00638
128.00000	14.753	4.698	523.04	0.03368	17.60	0.1431	0.00634
128.05000	14.751	4.697	523.04	0.03368	17.49	0.1422	0.00630
128.10000	14.749	4.697	523.04	0.03367	17.37	0.1413	0.00626
128.15000	14.747	4.696	523.04	0.03367	17.26	0.1403	0.00622
128.20000	14.745	4.696	523.04	0.03366	17.14	0.1394	0.00617
128.25000	14.743	4.695	523.04	0.03366	17.02	0.1384	0.00613
128.30000	14.741	4.694	523.04	0.03365	16.91	0.1375	0.00609
128.35000	14.739	4.694	523.04	0.03365	16.79	0.1365	0.00605
128.40000	14.736	4.693	523.04	0.03364	16.67	0.1356	0.00600
128.45000	14.734	4.692	523.04	0.03364	16.55	0.1346	0.00596
128.50000	14.732	4.692	523.04	0.03363	16.43	0.1336	0.00591
128.55000	14.730	4.691	523.04	0.03363	16.31	0.1326	0.00587
128.60000	14.728	4.690	523.04	0.03362	16.18	0.1316	0.00582
128.65000	14.726	4.690	523.04	0.03362	16.06	0.1306	0.00578
128.70000	14.724	4.689	523.04	0.03362	15.94	0.1296	0.00573
128.75000	14.722	4.689	523.04	0.03361	15.81	0.1286	0.00569
128.80000	14.720	4.688	523.04	0.03361	15.68	0.1275	0.00564
128.85000	14.718	4.687	523.04	0.03360	15.56	0.1265	0.00559
128.90000	14.716	4.687	523.04	0.03360	15.43	0.1255	0.00555
128.95000	14.714	4.686	523.04	0.03359	15.30	0.1244	0.00550
129.00000	14.712	4.685	523.04	0.03359	15.17	0.1233	0.00545
129.05000	14.710	4.685	523.04	0.03358	15.03	0.1223	0.00540
129.10000	14.708	4.684	523.04	0.03358	14.90	0.1212	0.00536
129.15000	14.706	4.683	523.04	0.03357	14.77	0.1201	0.00531
129.20000	14.703	4.683	523.04	0.03357	14.63	0.1190	0.00526
129.25000	14.701	4.682	523.04	0.03357	14.49	0.1179	0.00521
129.30000	14.699	4.682	523.04	0.03356	14.36	0.1168	0.00516
129.35000	14.697	4.681	523.04	0.03356	14.22	0.1156	0.00511
129.40000	14.695	4.680	523.04	0.03355	14.08	0.1145	0.00505
129.45000	14.693	4.680	523.04	0.03355	13.93	0.1133	0.00500

**Figure 6.7 Output File enode\_04.txt – Nozzle THROAT Predicted Behavior (Continued).**

Plots of pressure, mass flow, and Mach number for the various components in the sample configuration are shown in Figure 6.8 through Figure 6.10 (except for Cylinder, which has no Mach number plot.)

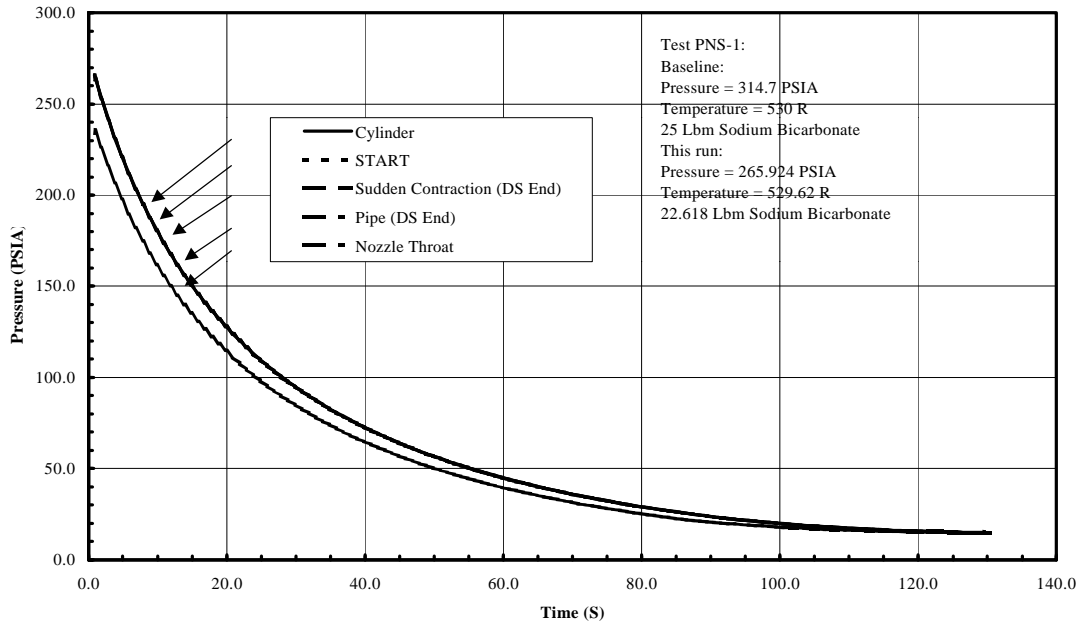


**Figure 6.8 Test PNS-1 - Predicted Pressure Response of Components.**

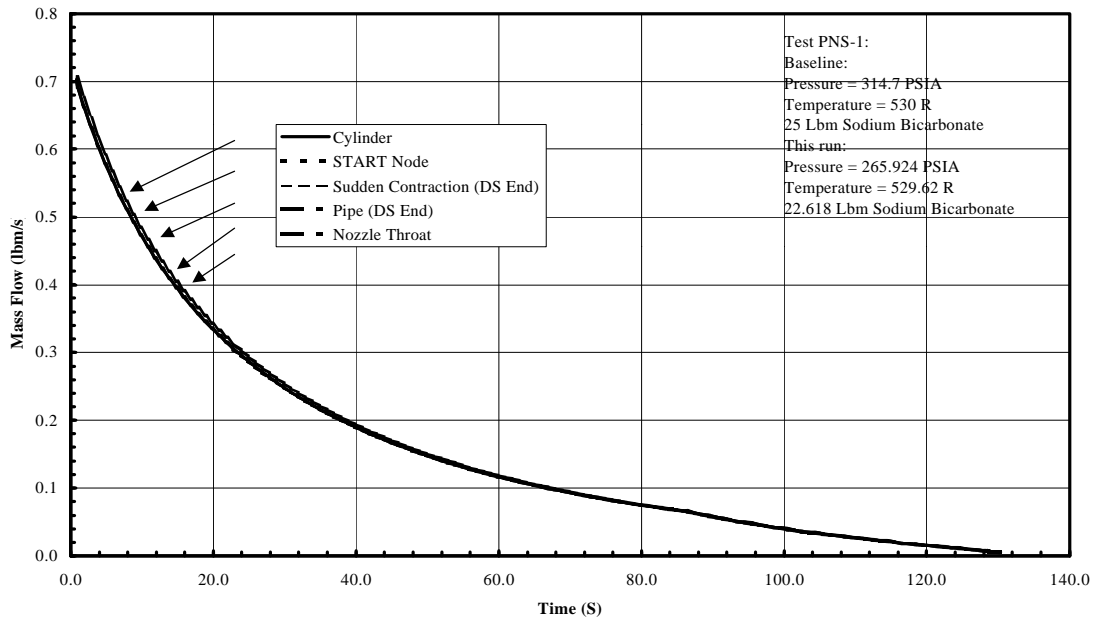


**Figure 6.9 Test PNS-1 - Predicted Mass Flow Response of Components.**

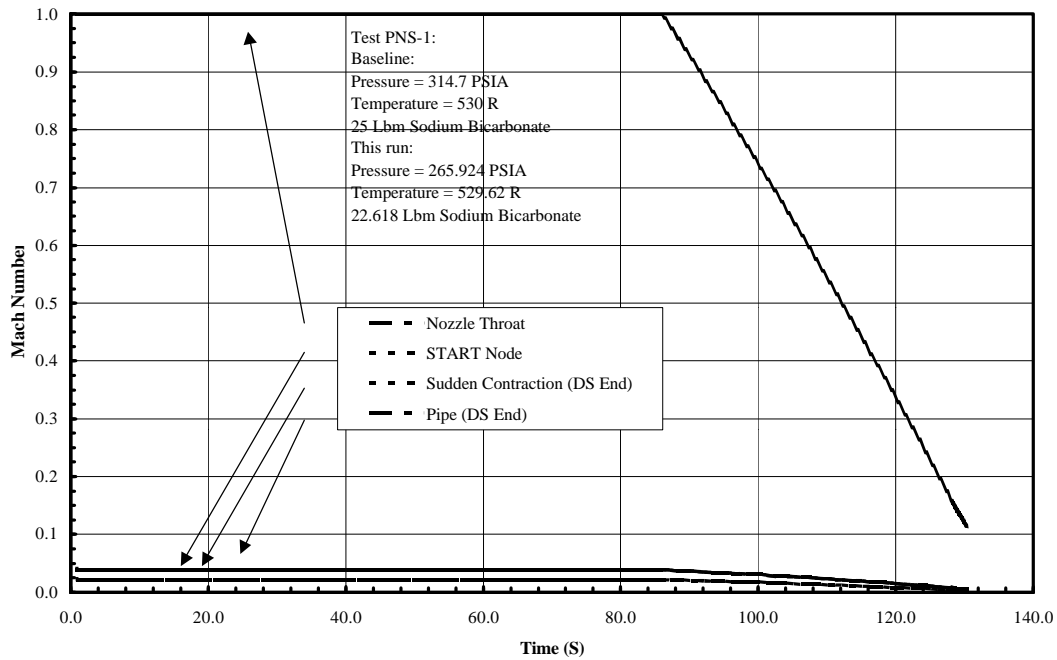


**Figure 6.10 Test PNS-1 - Mach Number Response of Piping Network Components.**

These plots were generated using Excel™; the output file for each component was imported into an Excel™ file, each file on a separate spreadsheet, and data from each sheet was extracted and overplotted to create the results seen above. Additional formatting and labels were applied in the spreadsheet program. As noted earlier, any program capable of plotting data and importing text files can be used to manipulate and plot output data. The behaviors shown in the plots are as expected. Figure 6.8 shows the predicted pressure response, starting at 1.355 seconds into the test discharge run. The curves show expected results, with pressure decreasing as the sample system is traversed from cylinder downstream to nozzle inlet. The large drop in pressure from the nozzle inlet to throat is also as expected, based on the theoretical predictions of the influence

coefficients. The mass flow plot (Figure 6.9) is also as expected, with the mass flows calculated throughout the network approximately the same. While the mass flow may vary a little between components (and over time), overall, the mass flow response is also as would be expected in the real system. The Mach number plot (Figure 6.10) is also as expected, with low flows everywhere except at the nozzle throat, which, given the configuration, would be expected to run at Mach 1.0 while choked.

### **6.1 *Input File Description.***

A typical input file for a single chain of nodes (for a tank/piping/nozzle configuration) is shown in Figure 6.2 (Note: the title line and line numbers **MUST NOT BE INCLUDED** in the actual user input file. They appear here only to aid in describing the inputs.) Any number of pipes, sudden contractions and/or sudden extractions may be used in any order desired by the user (although some configurations will a) work better than others, b) compute better (and faster), and c) make sense in a real world application than others.) A nozzle is not required as part of the configuration.

Lines 1 through 6 give running information, agent/gas properties, and linked list representation information. The rest of the lines describe each of the components in the configuration. Data entry for all input files starts at column 1 of each line (do not include the line numbers shown in – they are for reference purposes only.) Entries are either integers or floating point numbers, as indicated in the description below. Each entry is separated by a comma, and there should be at least one blank space at the end of the data. The text entries on each line, starting at the double slashes, is for user reference, and has no impact on program performance; but there should be at least one blank space between these comments and the data on each line. There must be no blank lines within the

entries; however, any number of blank lines or text may appear after entries for the last node in the last chain. Characters appearing on lines after the last entry will be ignored by the program. Note that “Required” parameters are necessary for the program to successfully run; there is currently no error checking to verify that parameters have been entered, that they are in a “reasonable” range for the inputs given, or even that they are formatted properly. Also, if a program feature is not being used for a particular case, a dummy value may be used to provide input that is not actually used in the particular case (example, for a gas-only run, a particle diameter of 1.0 will satisfy the input requirements without any effect on program results.)

The layout of the file is as follows:

Line 1: time\_step (float, seconds) – time interval used in choked portion; unchoked portion uses 2 x time\_step as an interval. (Required)

Note: time step selection is very important! Too small a time step will result in unnecessarily long run times, and unnecessary data generated. Too large a time step will result in an inadequate number of output steps to model discharge, and inaccuracies in interpolating steps to pinpoint events.

Line 2: Gas Ideal Gas Law Constant  $R_G (= \bar{R} / M_{w-gas}$ , the universal Ideal Gas constant divided by the gas molecular weight)(float, ft-lbf/lbm-°R) (Required)

Gas specific heat at constant pressure  $c_{pg}$  (float, BTU/lbm-°R) (Required)

Gas specific heat at constant volume  $c_{pv}$  (float, BTU/lbm-°R) (Required)

Line 3: Solid particle density  $\rho_D$  (float, lbf/ft<sup>3</sup>) (Required)

Solid particle specific heat  $c$  (float, BTU/lbm-°R) (Required)

Solid mass (float, lbf) (Required)

Line 4: Solid particle average diameter (microns) (Required)

Line 5: Friction multiplier method flag (0 = Pfeffer method, 1 = Fan & Zhu method) (int) (Required)

Line 6: Ambient Pressure  $P_a$  (float, lbf./in<sup>2</sup>) (Required)

Line 7: Number of linked list chains (int) (Required)

= 1 – “standard” system configuration (such as shown in Figure 6.1)

= 2 – “standard” system plus secondary piping, such as a pressure transducer. Flows from the transducer enter the source cylinder of the “standard” system.

Line 8: Number of nodes in first chain (int) (Required)

The remaining lines describe the nodes representing system components. Pipe, sudden contraction and sudden expansion nodes may be repeated as necessary to sufficiently describe the physical system to ensure accurate discharge behavior predictions.

Line 9: node\_type of the first node (int). Select node\_type from the following Table:

Component	“Type”
TANK	1
TWO_TANK	6
START	0
PIPE	2
SUDDEN CONTRACTION	3
SUDDEN EXPANSION	4
NOZZLE THROAT	5



Following the configuration description in Figure 6.2:

- Line 9: node\_type for TANK (int) (here = 1, from above Table)
- Line 10: node\_number (int) – assigned by user – ID for each node – should  
be assigned in consecutive, ascending order.
- Tank volume (float, ft<sup>3</sup>)
- Tank initial pressure (float, PSIA)
- Tank initial temperature (°R)
- Line 11: node\_type for START (int) (= 0)
- Line 12: node\_number (int)
- Local inside diameter (float, inch)
- Discharge coefficient  $C_D$  (float)
- Line 13: node\_type for SUDDEN CONTRACTION (int) (= 3)
- Line 14: node\_number (int)
- Downstream inside diameter (float, inch)
- Discharge coefficient  $C_D$  (float)
- Line 15: node\_type for PIPE (int) (= 2)
- Line 16: node\_number (int)
- Pipe length (float, ft)
- Pipe internal diameter (float, inch)
- Inside wall roughness factor  $k_s/d$  (float)
- Line 17: Discharge coefficient  $C_D$  (float)
- Line 18: node\_type for NOZZLE THROAT (int) (= 5)

Line 19:      node\_number (int)

                  Throat internal diameter (float, inch)

                  Inlet – Throat length (float, inch)

                  Discharge coefficient  $C_D$  (float)

Figure 6.11 shows a typical input file allowing for predicting the response of a pressure transducer measuring source cylinder pressure.

Line Number	Data	Information
1	0.100	// timestep s
2	55.15,0.248,0.177	// gas constant R, cpg, cvg - Nitrogen
3	137.38,0.249,22.618	// solid density, c, mass lbm - Sod. Bicarb.
4	53.0	// solid particle average dia microns
5	0	// friction multiplier flag
6	14.7	// ambient pressure (psia)
7	1	// number of chains
8	5	// number of nodes in first chain
9	6	// TWO_TANK - first node, first chain
10	0,0.430,265.924,529.62	// node number, volume cu ft, press. PSIA, temp R
11	0	// START - second node, first chain
12	1,0.750,1.00	// node number, dia in, inlet Cd
13	3	// CONTRACTION - third node, first chain
14	2,0.5625,1.00	// node number, ds dia in, ds cd
15	2	// PIPE - fourth node, first chain
16	3,8.00,0.5625,0.00006	// node number, length ft, dia in, ks/d
17	1.000	// pipe ds cd
18	5	// THROAT - fifth node, first chain
19	4,0.1730,1.50,0.470	// node number, dia inch, length in, ds cd
20	3	// number of nodes in second chain list
21	1	// TANK - first node, second chain
22	5,0.0000811, 265.,529.6	// node number, volume cu ft, press. PSIA, temp R
23	0	// START - second node, second chain
24	6,0.125,1.0	// node number, dia in, inlet Cd
25	2	// PIPE - third node, second chain
26	7,0.461,0.125,0.00006	// node number, length ft, dia in, ks/d
27	0.71	// pipe ds cd

**Figure 6.11 Typical Input File - Dual Chains (Pressure Transducer).**

The entries are identical in nature to those described for Figure 6.2. The only differences are 1) the TWO\_TANK node\_type (= 6), which has entry parameters identical to those for a TANK, and 2) the second chain of nodes. The convention used in the model program is to represent the “main” system (tank/pipe/nozzle as appropriate) as

the first chain, and the chain representing the pressure transducer and its piping, etc..., as the second chain. Note that both chains may be configured with components as are necessary to accurately model the physical system. Flow out of the second chain feeds into the main tank (TWO\_TANK).

Note also that, while there are no SUDDEN EXPANSION nodes in the preceding examples, entries for SUDDEN EXPANSIONS are identical to those for SUDDEN CONTRACTIONS, except for having a node\_type of “4”.

## **7.0 Testing.**

As noted in Section 3.4, a search of the literature showed a singular lack of test data in flow regimes normally encountered by dry chemical fire suppression delivery systems. As a result, the original objectives of this research were modified. Instead of developing a complete theoretical model capable of analyzing all possible design configurations, a simpler theoretical model would be developed. The analytical model would have the aim of being able to predict the performance of simple systems, including a single source cylinder, piping system without branches, and single outlet. In lieu of the more extensive model, a series of discharge tests were performed, to gather performance data usable for comparison with predictions of the model. Where possible, the model would be adjusted to better reflect system performances observed in testing. Finally, test data would be compared to the final model, as a basis for critique of the developed model, to indicate improvements needed to make the model more reflective of actual system performance. Test plans were developed, system hardware and test equipment was acquired, and a series of tests were performed. These tests, their results, and comparisons with the predictive model, are described in this chapter.

### **7.1 *General Approach.***

The basic approach to system discharge testing was similar to that for development of the predictive model. Tests would first be done using simple configurations, with gas-only discharges. Modeling capabilities would be corrected and adjusted to match simple results. As experience with the test equipment increased,

testing would be extended to both more elaborate physical layouts, and include gas/powder mixtures. The ultimate intent was to gather performance data for discharges resembling, at least in source cylinder parameters, discharges experienced by systems implemented by manufacturers.

While the bulk of the testing was performed at Worcester Polytechnic Institute (WPI), some additional test data was also made available by Kidde-Fenwal. The tests performed at each location, test results, and comparisons with predictions of the model are described in the sections below.

## **7.2 Test Descriptions.**

Three series of tests were performed at WPI. The purposes of these tests were 1) to gather transient pressure data, and 2) to gather characteristic parameter information about individual components, in particular cylinder/valve discharge coefficient information. Little or no information exists in the literature about discharge coefficients for system valve assemblies. Since no hydraulic loss data exists in the literature for dry chemical nozzles, nozzle flow tests were also conducted at WPI.

### **7.2.1 WPI Tests.**

#### **7.2.1.1 Nozzle Flow Tests.**

The purpose of these tests was to gather performance data on typical nozzles used in dry chemical suppression delivery systems, with the intent of determining the discharge coefficient of the nozzles for gas-only flows. Nozzles that were to be used in testing are shown in Figure 4.6, and were donated to the project by Kidde-Fenwal.

A schematic of the test layout is shown in Figure 7.1.

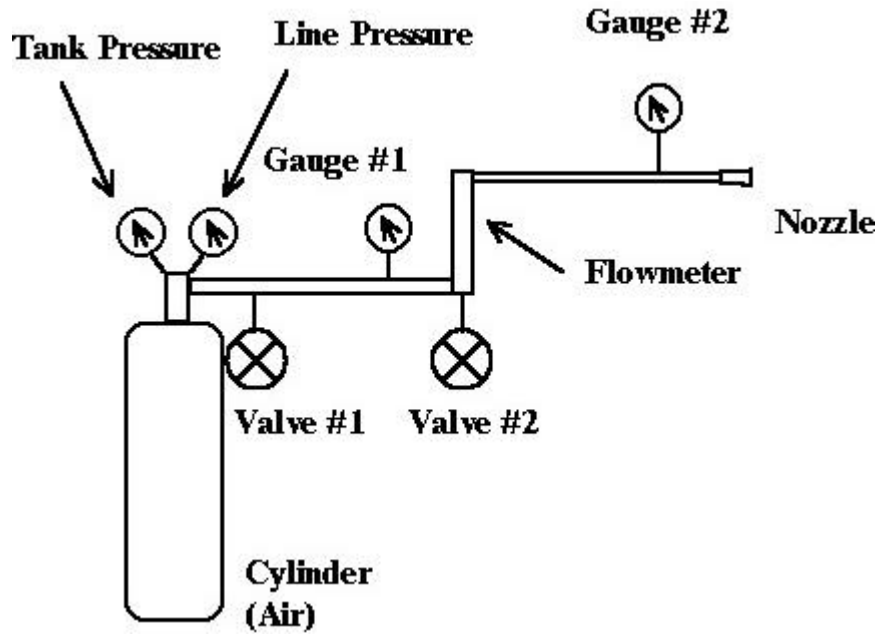


**Figure 7.1 Nozzle Flow Test - Configuration Schematic.**

The flowmeter used was a high-capacity Matheson FM-1127 rotameter, capable of measuring from 20 to 500 SLPM (“Standard” Liters Per Minute), with a maximum operating pressure of 200 PSIG, and ½” NPT female connectors on the back of the device. Note that valve #2 is on the inlet (at the base) of the flowmeter itself.

The testing procedure involved running air at a fixed line pressure through the piping, flowmeter, and nozzle. Valve #2 was used to control the amount of flow through the flowmeter and nozzle. Throughout the tests, Valve #2 was opened only far enough to achieve the desired amount of flow as measured by the flowmeter. Gauge #2 measured pressure for both the nozzle inlet, and since it was only a few inches downstream of the rotameter, the flowmeter itself. For several line pressure settings, and several mass flows (as controlled by valve #2), pressures were measured. Using pressure measurements, and the corresponding volumetric flows, mass flow through the line was calculated, and from that using equation (4.73), with the solids mass fraction  $\phi$  (and thus volume fraction  $\theta$ )

set to zero to simulate a gas-only discharge, the discharge coefficient of the nozzle being tested was determined.

Tests were run according to the following Table, using the nozzle shown in the top half of Figure 4.6(b). For each regulator pressure setting, readings of pressure in the #1 and #2 gauges were taken at various flow readings on the rotameter. The measured results, and calculated parameters, including discharge coefficient, are tabulated. The correction factors were supplied by the rotameter manufacturer. The rotameter used had been calibrated at 150 psig, and correction factors for the pressures encountered were interpolated from the table of correction factors.

	Test Sequence #1			Test Sequence #2			Test Sequence #3			
Tank Pressure (psig)	1820	1820	1820	2000	2000	2000	2000	2000	2000	2000
Regulator Pressure (psig)	100	100	100	145	145	145	170	170	170	170
Gauge #1 (psig)	58	54	54	100	95	89	134	130	125	120
Gauge #2 (psig)	10	12.2	15	15	16	19	14	15	16	19
Flowmeter (SLPM)	420	440	460	460	480	500	440	460	480	500
Flow (SCFM)	14.83	15.54	16.24	16.24	16.95	17.66	15.54	16.24	16.95	17.66
Correction Factor	0.491	0.507	0.522	0.520	0.528	0.543	0.516	0.522	0.528	0.545
Corrected mass flow (lbm/s)	0.0118	0.0134	0.0151	0.0151	0.0164	0.0182	0.0139	0.0151	0.0163	0.0183
Mass flow - Equation (4.73) (lbm/s)	0.0272	0.0300	0.0327	0.0327	0.0336	0.0368	0.0314	0.0325	0.0336	0.0368
Discharge Coefficient	0.433	0.448	0.463	0.461	0.487	0.493	0.443	0.465	0.487	0.496

**Table 7.1 Results of Nozzle Calibration Experiments**

The drop between gauge #1 and gauge #2 was caused by 1) a nearly 180° bend in the plastic piping between the end of the piping connected to the source cylinder,

including both gauge #1 and valve #1, and 2) valve #2 (a needle valve supplied by the rotameter manufacturer), which was used to control the amount of mass flow through the piping network. The large drop of pressure between the regulator and gauge #1, and between gauges #1 and #2, suggested that despite its placement ahead of the rotameter, using pressure gauge #1 as the local pressure in Equation (4.73) would not yield correct mass flows. Since gauge #2 was located just downstream of the rotameter, the pressure used in the calculations was the pressure reading at gauge #2. Calculation of  $C_d$  was based on a re-arrangement of equation (4.73) (with the mixture fraction  $\theta = 0$  for gas-only flow):

$$C_d = \frac{m_{dot}(t) \sqrt{T_{cyl}(t)}}{A_{nozzle\_throat} P_{cyl}(t)} \frac{1}{\sqrt{\frac{g}{R} \left( \frac{2}{g+1} \right)^{(g+1)/(g-1)}}$$

Based on the calculations as shown above, the discharge coefficient of the nozzle tested was between 0.430 and 0.500. A plot of calculated discharge coefficient versus corrected measured mass flow is shown in Figure 7.2. While the calculated discharge coefficient is over a relatively narrow range, the general trend is a coefficient that gradually increases with increasing mass flow.



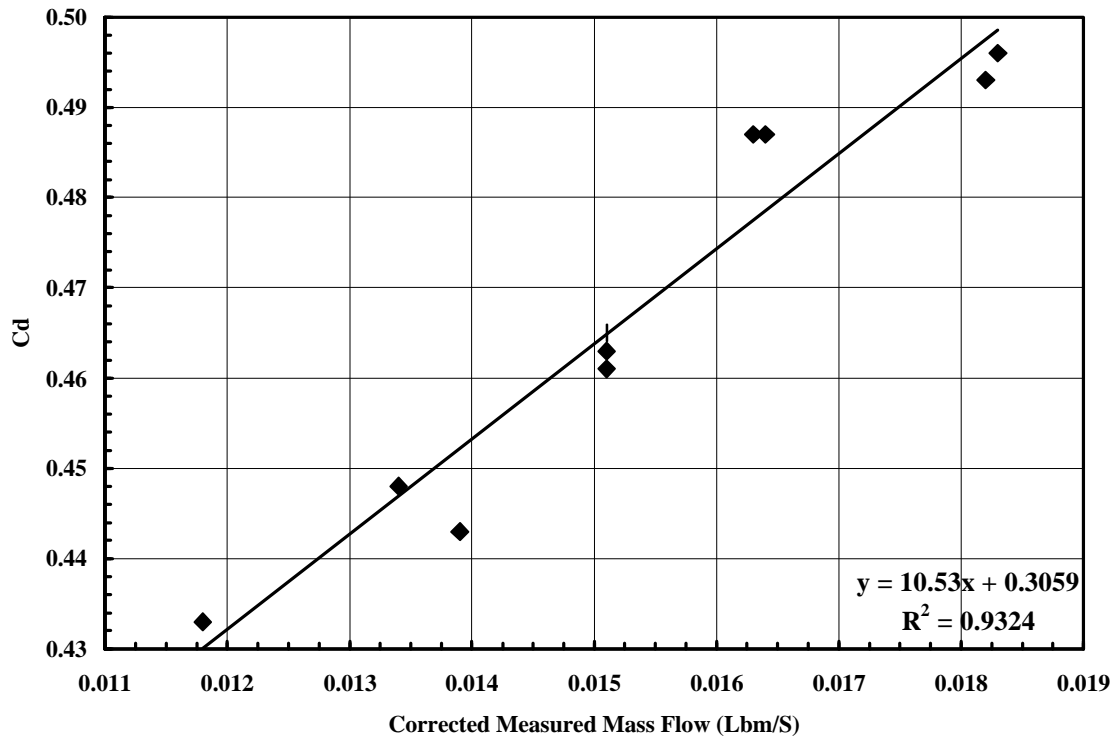


**Figure 7.2 Nozzle Discharge Coefficient Versus Corrected Measured Mass Flow**

The other nozzle shown in Figure 4.6 (b) was tested; however, the highest flows achievable with the test configuration shown in Figure 7.1 showed no rise in the pressure gauges. A configuration with higher volumetric flow capacity, and a larger scale rotameter, would be needed to determine the discharge coefficient of this nozzle.

### 7.2.1.2 Cylinder-Alone Tests.

The purpose of these tests was to gather performance data for discharges involving only the source cylinder assembly, both for gas-only and gas/agent discharges. Data from these tests was compared to cylinder/exit configurations of the model program. Data was also used to calculate the discharge coefficient of the cylinder valve assembly

consisting of the valve itself, an internal dip tube extending almost the full length of the cylinder, and a 90° turn in flow direction.

A schematic of the cylinder assembly is shown in Figure 7.3.

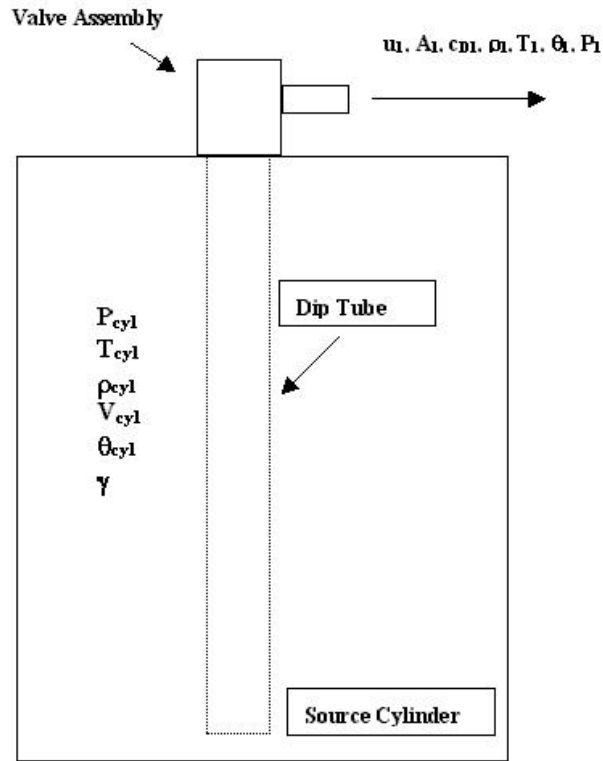


**Figure 7.3 Cylinder Assembly Tests – Schematic.**

The test procedure involves filling the cylinder with a desired amount of agent (or no agent if it is a gas-only test.) The cylinder is then pressurized using nitrogen to a target pressure. A pressure transducer tapping in through the cylinder exit valve assembly measures internal cylinder pressure, both for filling purposes, and during a discharge. A computer running a data acquisition program collects and records the signal from the pressure transducer, outputting a text file that can be imported into a spreadsheet program, or other appropriate program, for post-test processing.

The source cylinder is a standard Kidde-Fenwal IND-25 cylinder, with a volume of 0.430 ft<sup>3</sup>, and capacity of 25 pounds sodium bicarbonate agent (same as Kidde-Fenwal IND-21 cylinder, with a capacity of 21 pounds monoammonium phosphate.) The cylinder is shown in Figure 7.4.



**Figure 7.4 IND 25/21 Cylinder.**

Cylinder dimensions are shown in Figure 7.5.

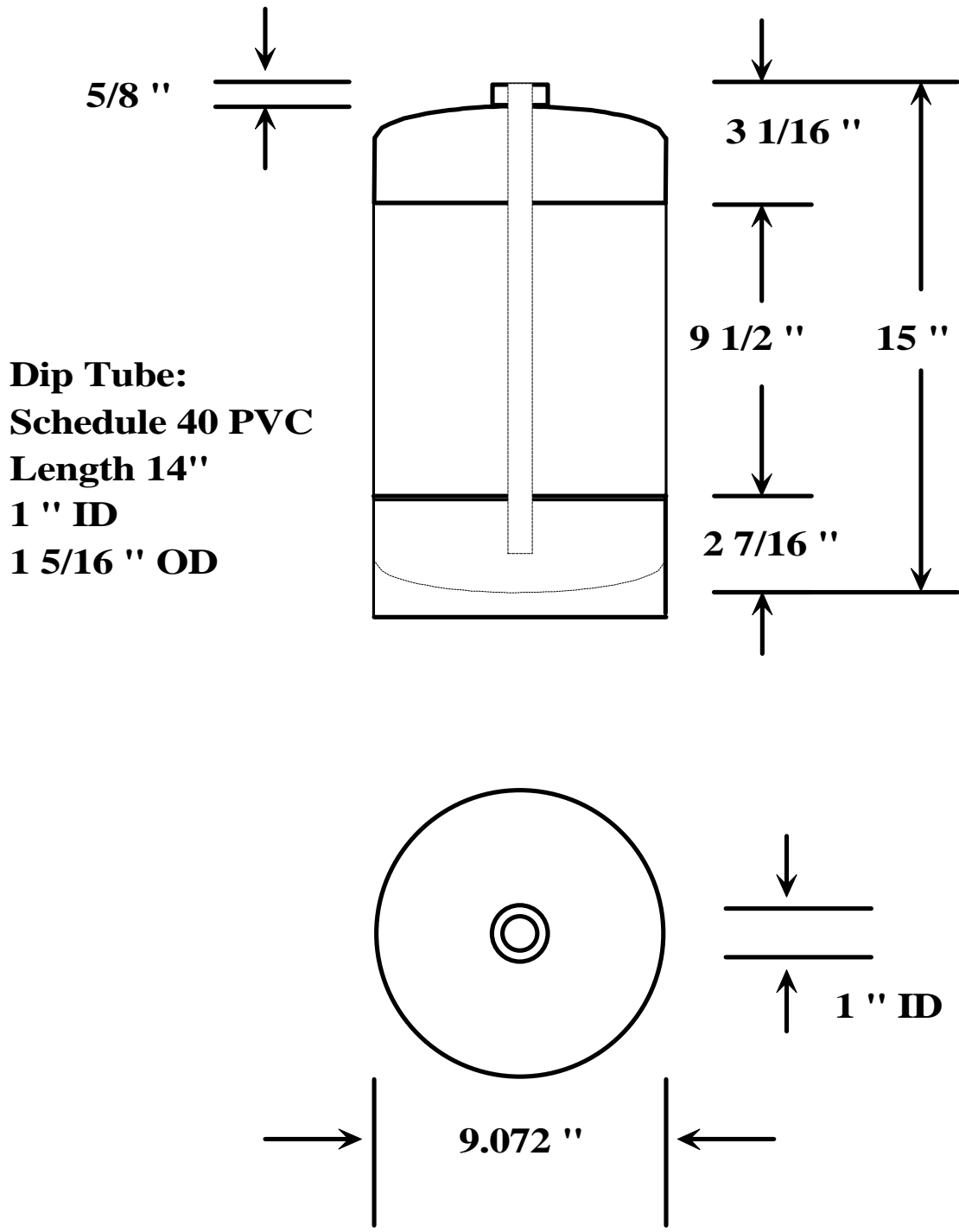


Figure 7.5 IND 25/21 Cylinder - Basic Dimensions.

The cylinder can be secured to a wall or other stable surface by means of a wall bracket and strap supplied by the manufacturer. In use, the cylinder is in the upright position, with the valve assembly on top.

The release valve assembly screws into the top of the cylinder, and is shown in Figure 7.6.



**Figure 7.6 Valve Assembly.**

The exit of the valve is a 0.75 inch ID exit, externally threaded to allow attachment of the delivery piping network to the tank. The valve itself is a spring-loaded plunger; once activated, the valve moves downwards less than 1 inch, opening the cylinder to discharge its contents. There are two taps through the body of the valve with access to the interior of the cylinder. One tap is normally used with a simple pressure gauge to monitor the charged cylinder pressure. The other is closed with a fusible bolt, which acts as a pressure relief in the event of heating of the cylinder to overpressurization. For test purposes, the relief bolt was removed from the one tap, which was fitted with a valve and used for filling the cylinder with carrier gas (air or nitrogen.) The simple gauge was removed from the other tap, and a pressure transducer installed, to measure cylinder pressure as a function of time, both for tank filling, and discharge testing.

A plastic dip tube, 0.75 Inch ID, extending almost to the bottom of the cylinder, screws into threads on the insides surface of the valve assembly. Typical dip tubes are shown in Figure 7.7.



**Figure 7.7 Dip Tubes.**

During discharge, a mixture of extinguishing agent and gas flows into the bottom of the dip tube, and upwards through the valve, through a 90° bend, and out of the cylinder assembly.

Several types of trigger mechanisms are available to initiate discharge. For the tests at WPI, a manual trigger assembly was used, and is shown in Figure 7.8. In the field, this mechanism is either triggered manually, or by fusible links connected by wiring to the mechanism.

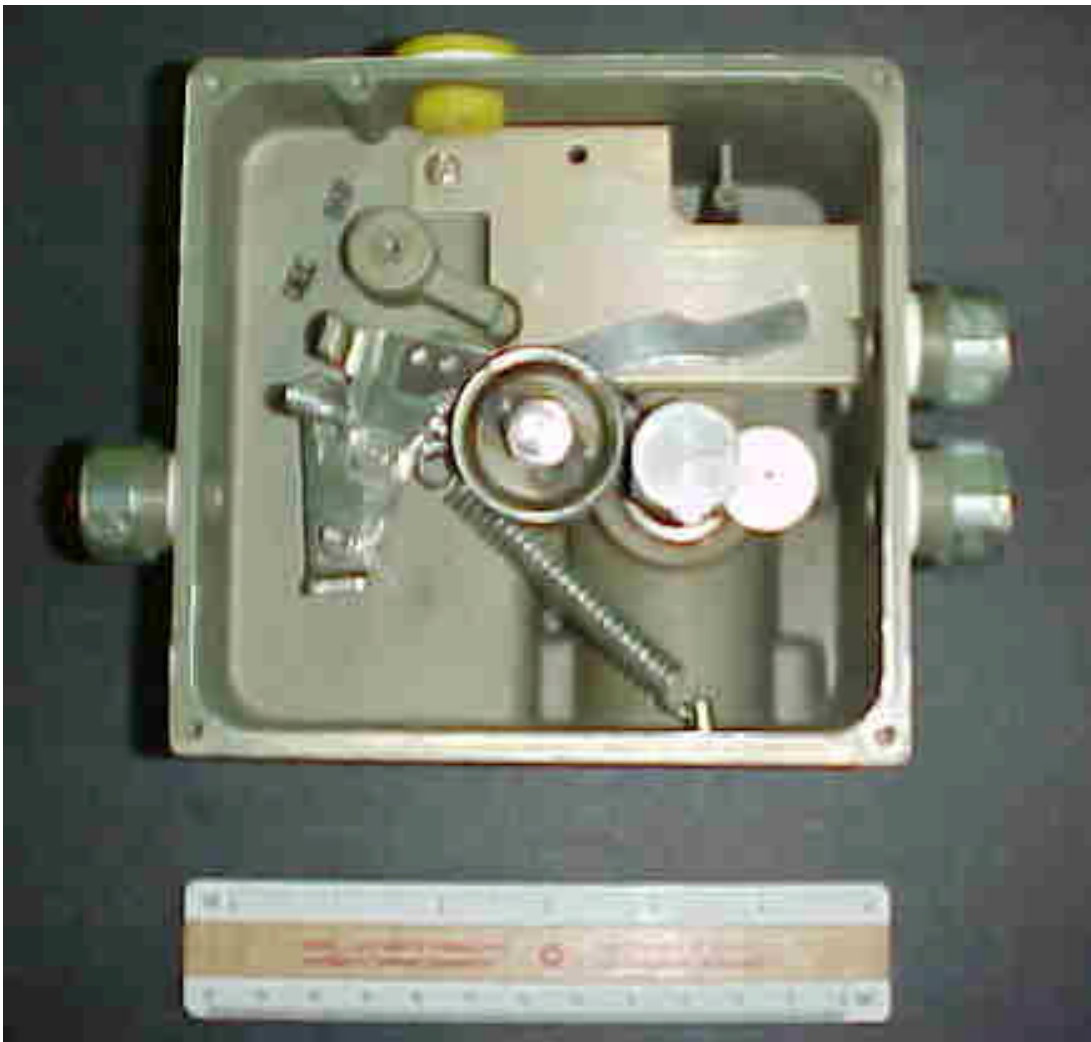


**Figure 7.8 Manual Trigger Mechanism.**

A particle deflector shield, and capture bags were also utilized; they are described in Section 7.2.1.4.

A fully assembled system is shown in Figure 7.9.



**Figure 7.9 WPI Dry Chemical Cylinder Alone Discharge Test Configuration.**

A series of discharge tests were run. The first tests were using gas only, either air or nitrogen; data from these tests was used to determine the valve assembly discharge coefficient (with dip tube, valve, and bend lumped together as one “component.”) A second series of tests were run discharging mixtures of nitrogen and sodium bicarbonate, and nitrogen and monoammonium phosphate. Details of the characteristics and properties of these materials are discussed in Section 7.3. A summary listing of the tests



is shown in Section 7.4.1.2; comparisons with model predictions are shown in Section 8.1.1.

### **7.2.1.3 Cylinder-Pipe-Nozzle Tests.**

The purpose of these tests was to gather transient pressure data for discharges involving a simple assembly, consisting of a single source cylinder assembly, piping, and nozzle, both for gas-only and gas/agent discharges. Pressure data from these tests was compared to cylinder/pipe/nozzle configurations of the model program.

A schematic of the configuration used in these tests is shown in Figure 6.1. The piping consisted of an 8-foot length of Lexan™ tubing, with an ID of 9/16 inch, with threaded connectors glued to the ends of the pipe with high-pressure epoxy. Off-the-shelf pipe fittings were used to connect the piping to the exit outlet of the cylinder, and the nozzle to the piping. A tee-joint installed between the downstream end of the pipe and the nozzle inlet allowed the use of a second pressure transducer, of the type described in Section 7.2.1.4, just upstream of the nozzle inlet. Teflon tape was used to seal the joints.

A particle deflector shield, and capture bags were also utilized; they are described in Section 7.2.1.4.

A fully assembled system is shown in Figure 7.10. The test procedure is similar to that for the tank-alone tests, except for measurement of the pressure just upstream of the system exit (usually a nozzle). A pressure transducer similar to that measuring cylinder pressure is connected to a channel of the computer's data acquisition system separate from that for the cylinder pressure, and pressures at both locations are measured

during discharge. Pressure in the cylinder during fill can also be monitored using the cylinder pressure transducer.



**Figure 7.10 Cylinder-Pipe-Nozzle Test Configuration.**

A series of discharge tests were run. The first tests discharged nitrogen only; data from these tests was used to determine discharge coefficients of the various components modeled. A second series of tests were run discharging mixtures of nitrogen and sodium bicarbonate, and nitrogen and monoammonium phosphate. Tests were also run using sodium bicarbonate without flow-enhancing additives, and with a shorter than normal dip tube. Details of the characteristics and properties of the agents are discussed in Section

7.3. A summary listing of the tests is shown in Section 7.4.1.3; comparisons with model predictions are shown in Section 8.1.2.

#### **7.2.1.4 Additional Equipment.**

In addition to the aforementioned equipment, a deflector was installed downstream of the delivery system exit; a deflector can be seen in Figure 7.11.

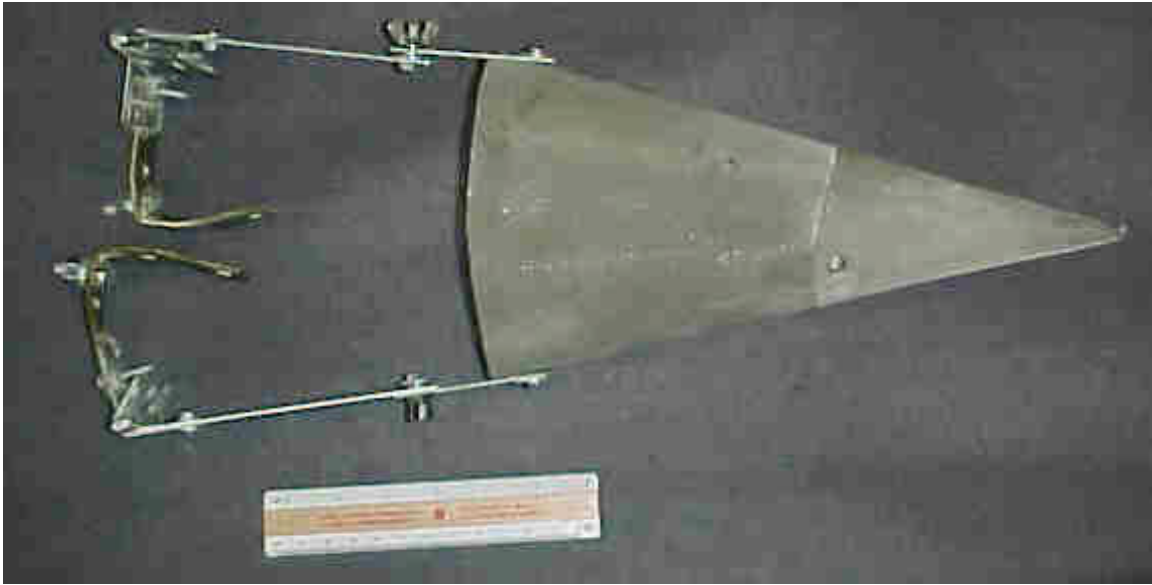


**Figure 7.11 Deflector Assembly.**

Also, as part of the agent/gas discharges, capture bags were utilized, attached just upstream of the cylinder exit. The purpose of these bags was to prevent spread of agent into the local laboratory environment. Capture of the agent kept hard-to-clean agent out of the local environment, and also allowed agent to be reused in subsequent tests, as well as allowed approximate weights of agent exiting through the cylinder exit to be measured. The deflector slowed the flow of agent once leaving the cylinder, so as to prevent potential perforation of the bag by agent particles during discharge. Capture bags were made of clear mylar, 3 mils thick, with capacities of 30, and later 60 gallons,

sufficient to capture the entire contents of the charged cylinder. Capture bags were used in pairs, with an interior bag with a pair of slits to allow for gas to exit the inner bag during discharge, and an outer bag tied so as to prevent agent leakage during discharge.

Two different types of strain gauge pressure transducers were used in testing. For most of the tests, the pressure transducers were manufactured by Lucas – Schaevitz, with a range of 0-500 psi, error range of 0.25% FS, and response time of 1 millisecond. The excitation was 10-30 VDC, with an output signal of 0-5 VDC. Near the end of testing, a transducer made by Omega was used, with a range of 0-3000 psig, error range of 0.25% FS, and response time of 1 millisecond. The excitation was 12-36 VDC, with an output signal of 0.5-5.5 VDC. Both transducers were threaded and screwed into mounts in the system. The transducers are shown in Figure 7.12.



(Lucas on Left, Omega on Right)

**Figure 7.12 Pressure Transducers.**

Signals from the pressure transducers were fed into a data acquisition (daq) system. For the early part of testing, LabView™ was programmed to acquire data from discharges. For information on LabView™, see **NI (1998a)** and **NI (1998b)**.

For the latter tests, a laptop computer using VirtualBench™ and a National Instruments DAQCard™-500 and CB-27 connector block was used to acquire data. Note that early tests sampled data at the rate of once per millisecond; to reduce the amount of data acquired, this was later reduced to the rate of once per five milliseconds.

### 7.2.2 Kidde International UK Tests.

In August 1997, work was undertaken by Kidde International similar in nature to the research described in this document. The purposes of these tests were to develop capabilities to model dry chemical fire suppression delivery systems, and to develop test equipment capable of measuring parameters of interest during dry chemical system discharge tests. A memorandum describing the test apparatus, basis for modeling, some test results, and comparisons with the developed model was written, and a copy donated by Kidde-Fenwal (**Spring (1998)**). A copy of the memorandum is in Appendix 10.7.

The test apparatus consisted of a hand-held extinguisher, charged with either gas alone, or gas and agent mixture, with a custom-made dip tube, cylinder head (in place of the normal manually-operated valve), and hose connecting to a ball valve controlling discharge.

Data was collected from tests using this apparatus, and included both gas (nitrogen) only discharges, and discharges of agent and gas. Discussions regarding results of the tests are presented in Section 7.4.2, and comparisons with WPI model predictions are presented in Section 8.2.

### 7.2.3 Corn Starch Tests.

Data was made available to the current research effort from researchers at Fenwal Safety Systems in Holliston, Massachusetts. The data obtained was from a series of discharge tests of explosion-suppression systems. The data provided showed pressure versus time information on the discharge of powdered corn starch, pressurized with

nitrogen. Source cylinders were identical to those described in Section 7.2.1, except for having only half the volume of the standard IND-25/21 cylinders.

Data was collected from tests using this apparatus for discharges of mixtures of corn starch and nitrogen. Discussions regarding results of the tests are presented in Section 7.4.3, and comparisons with WPI model predictions are presented in Section 8.3.

#### 7.2.4 Vendor System Tests.

Use was made of data from a representative sample of vendor pre-engineered test data in early model development, including discharge times, and residual powder mass information. One way to maximize system extinguishment effectiveness is to maximize the agent discharged from the system – residual powder can do nothing to put out a fire. Comparisons were made of predictions of residual powder in source cylinders, both for the program model, and for simple predictions of residual powder amounts, with amounts actually observed as a result of system discharge tests. The results of such comparisons are discussed in Sections 7.4.1.3, 8.1.2, 8.2 and 8.3.

### 7.3 **Test Materials.**

Two basic types of dry chemical fire suppressant agent are in general use. The sodium bicarbonate-base suppressant is intended for class B (flammable liquid) and class C (electrical equipment) fires. The exact size distribution of powder particles is proprietary. Typically, the majority of particles are smaller than 53  $\mu\text{m}$  in diameter. Published reports indicate that the maximum effectiveness of agents is generally achieved for particles of less than 100  $\mu\text{m}$  in diameter (**Ewing *et al* (1989, 1992, 1994, 1995), Hamins (1998)**).

The monoammonium phosphate-base agent is intended for class A (ordinary combustible materials) as well as class B and class C fires. The size distribution is similar to that for the BC powder, but with a slightly greater weighting of larger particles. Detailed size distributions are proprietary. Experiments to date at WPI have been performed with the ABC and BC powders and with gas-only discharges.

Samples of the two agents are shown in Figure 7.13. Characteristics of the materials are shown in Table 7.2.

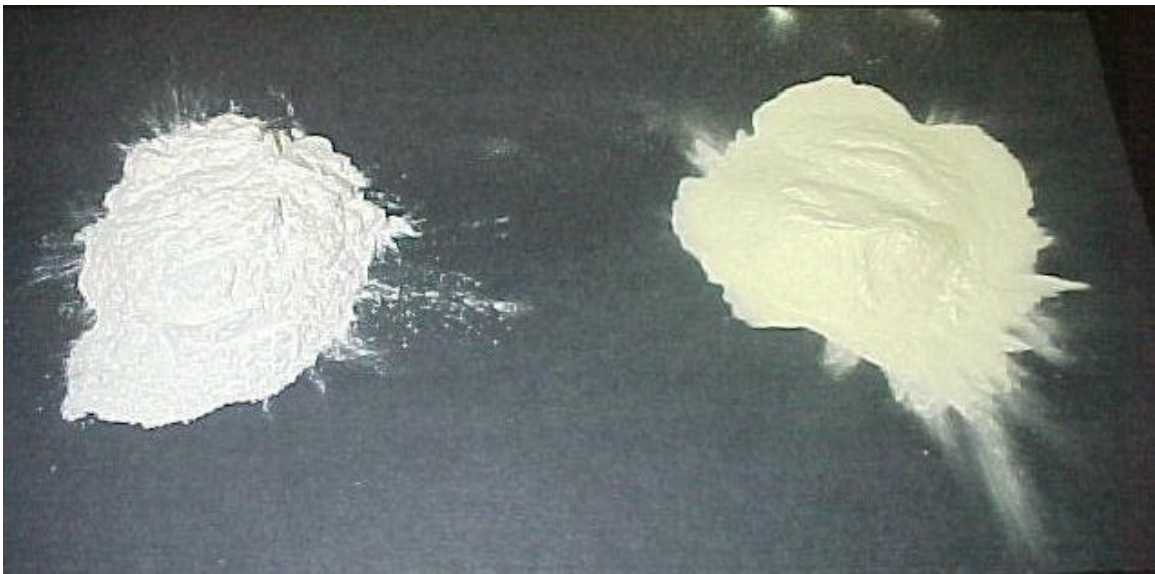


**Figure 7.13 Sodium Bicarbonate and Monoammonium Phosphate Agents.**

In addition to these agents, a variant of the sodium bicarbonate agent was also tested. This material consisted of 100% sodium bicarbonate, without the additives usually added to improve agent flow characteristics. No measurements of atmospheric humidity or moisture content were made during the experimentation with the pure sodium bicarbonate. However, prior to the running of discharge test PNS-3, the cylinder filled with the pure sodium bicarbonate was allowed to sit at rest, inside the closed



cylinder. A sample of this material is shown in Figure 7.14, with characteristics shown in Table 7.2.



**Figure 7.14 Sodium Bicarbonate Without Flow Additives.**

Material	Density (lbm/ft <sup>3</sup> )	Specific Heat (BTU/lbm-°R)
Sodium Bicarbonate	137.38	0.249
Monoammonium Phosphate	112.51	0.296
Corn Starch	96.00	0.594

**Table 7.2 Powder Material Properties.**

Visual observation of the three powders suggested strikingly different characteristics. The monoammonium phosphate was by far the most free-flowing, and the most likely to form dust clouds when poured from container to container. The sodium bicarbonate agent, was somewhat less free-flowing, although also likely to be suspended in air when moved between containers. The “pure” sodium bicarbonate was the least free flowing, and showed signs of caking in the cylinder after discharge and during transport between containers.

Note that Table 7.2 lists the solid densities; i.e., the densities of the powder materials for a solid piece of the material. As a powder, a free-flowing sample of material includes both solid powder particles and interstitial space between the particles. As an example, the fill of the cylinder at the start of test PNM-2 is shown in Figure 7.15. This test included a fill of 10 lbm of monoammonium phosphate. The fill level of MAP was measured after fill, before the valve assembly, with dip tube, was installed. As the Figure notes, the top level of the MAP agent was 5.125 inches from the inside base of the cylinder. With the dimensions given, the bulk density (lbm/ft<sup>3</sup>) is calculated from the formula

$$\mathbf{r}_{bulk} = \frac{m_{agent}}{V_{cyl}} \left( \frac{1}{1 - \frac{H_{fb}}{H_{cyl}}} \right) \quad (7.1)$$

where  $H_{fb}$  is the distance from the top measuring point of the cylinder to the free surface of the agent in the cylinder (inches),  $H_{cyl}$  is the total distance from the top to the bottom measuring point of the cylinder (inches),  $m_{agent}$  is the mass of agent in the cylinder before discharge (lbm), and  $V_{cyl}$  is the cylinder volume ( $\text{ft}^3$ ). As shown in Figure 7.15,  $H_{cyl} = 15$  inches, while  $H_{fb} = 9.875$  inches. With a cylinder volume of  $0.43 \text{ ft}^3$ , and 10 lbm of agent, the bulk density of the agent is  $68.07 \text{ lbm/ft}^3$ . Furthermore, as a result of this fill, a length of  $4 \frac{13}{16}$  inches of the 14-inch dip tube is immersed in the agent. The sodium bicarbonate agent would be expected to have a similar “fill” density.

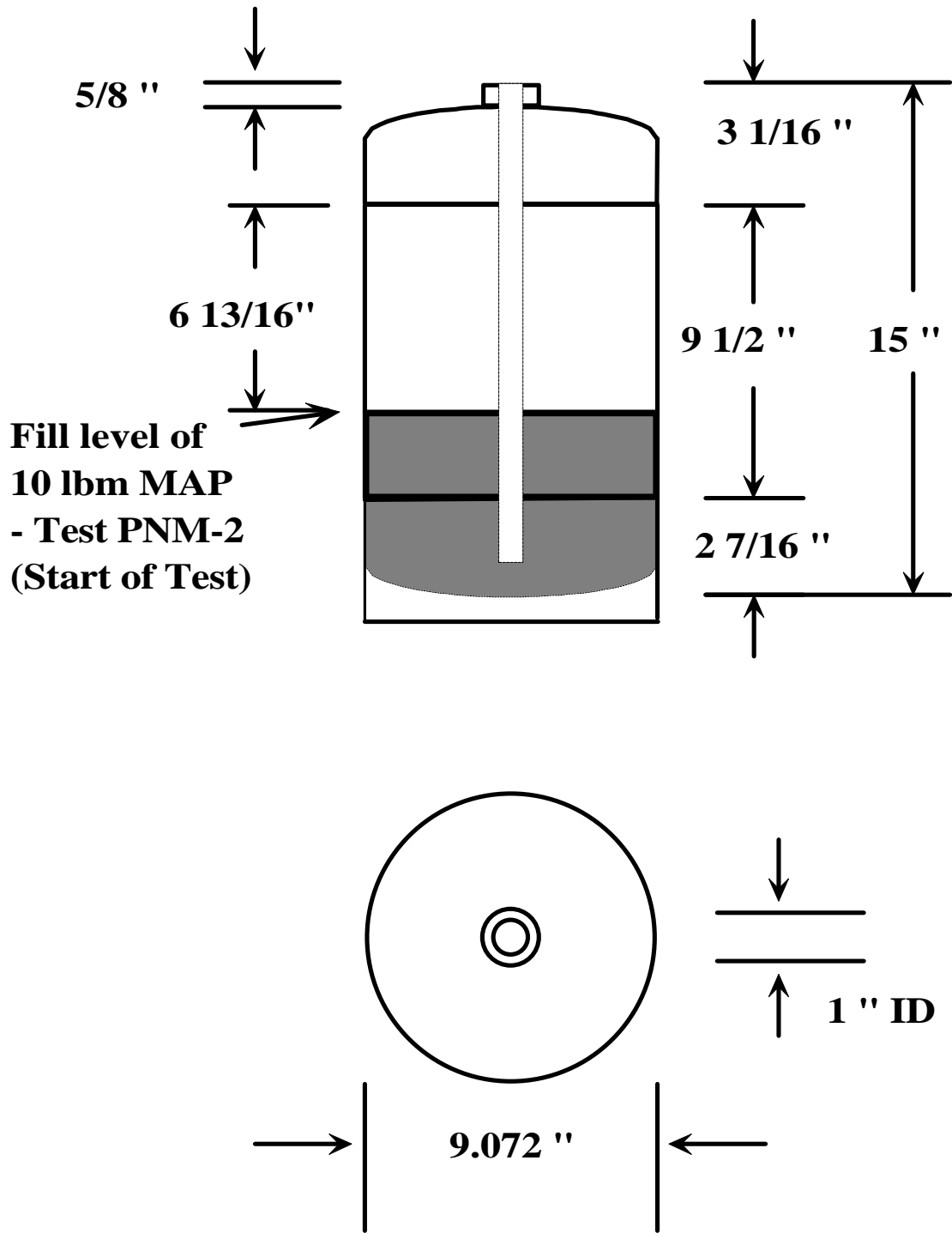


Figure 7.15 Fill Level of Cylinder - Test PNM-2.

Two gases were used in the tests. Air was used for most of the gas only tests, while, simulating actual system usage in the field, nitrogen was used to charge the source cylinder for most agent/gas mixture tests. Characteristics of these gases are shown in Table 7.3.

Material	Ideal Gas Constant R (ft-lbf/lbm-°R)	Specific Heat Constant Pressure (BTU/lbm-°R)	Specific Heat Constant Volume (BTU/lbm-°R)
Air	53.34	0.2396	0.171
Nitrogen	55.15	0.248	0.177

**Table 7.3 Gas Material Properties.**

Note that an dynamic viscosity of  $1.2 \times 10^{-5}$  lbf/ft-sec was used in the Reynolds number calculations used in determining friction factors for pipes, for both the gas-only and mixture Reynolds numbers.

#### **7.4 Test Results.**

Results of the various tests are presented in the following sections. Where appropriate, comparisons are also made between various tests. Comparisons of test results to analytical predictions are presented in Section 7.5.

##### **7.4.1 WPI Tests.**

##### **7.4.1.1 Cylinder-Alone Tests.**

A number of preliminary discharge tests, both with and without agent, were conducted prior to the listed discharges. However, it was discovered that the daq software, as configured at the time, had not been correctly recording measurement times during tests. Thus, while data was gathered for several discharges at various gas

pressures and agent loads, it was impossible to relate the data collected with the actual time during discharges. As a result, the data from these discharge tests was not retained in the test matrix.

Qualitatively, the results from these preliminary discharge tests were similar to the tests discussed below. The pressure measured in the cylinder, and the inflection points noted in the gas/agent mixture discharges were noted in the acquired data, although the timing was impossible to determine.

Cylinder-only test parameters for the fully successful discharges are shown in Table 7.4.

Test	Initial Pressure (psia)	Agent	Agent Mass (lbm)	Discharge Time (sec)	Carrier Gas	Mass Fraction
G-7	305.9	-	0	1.6	Air	0
P-6	307.2	Sodium Bicarbonate	25	5.2	Nitrogen	0.98521
P-7	314	Sodium Bicarbonate	10	3.0	Nitrogen	0.94764
M-1	314.6	Monoammonium Phosphate	10	3.1	Nitrogen	0.94979
M-2	312.5	Monoammonium Phosphate	21	4.9	Nitrogen	0.98250

Note: Discharge time: Start time approximately 0.014 seconds prior to first response pressure transducer; end time reached when pressure transducer response drops to within FS% Error region (0.25%, 16.2 psia).

**Table 7.4 Cylinder-Alone Discharge Tests.**

Cylinder pressure was measured during these discharge tests. Plots of the cylinder pressure as a function of time are presented in Figure 7.16 through Figure 7.20.

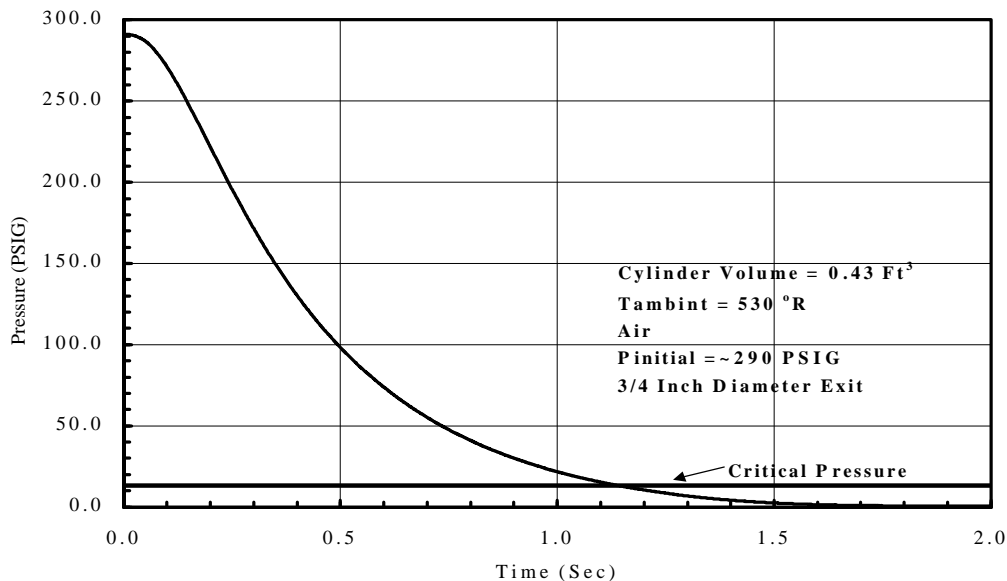


**Figure 7.16 Test G-7 - Pressure Vs Time.**

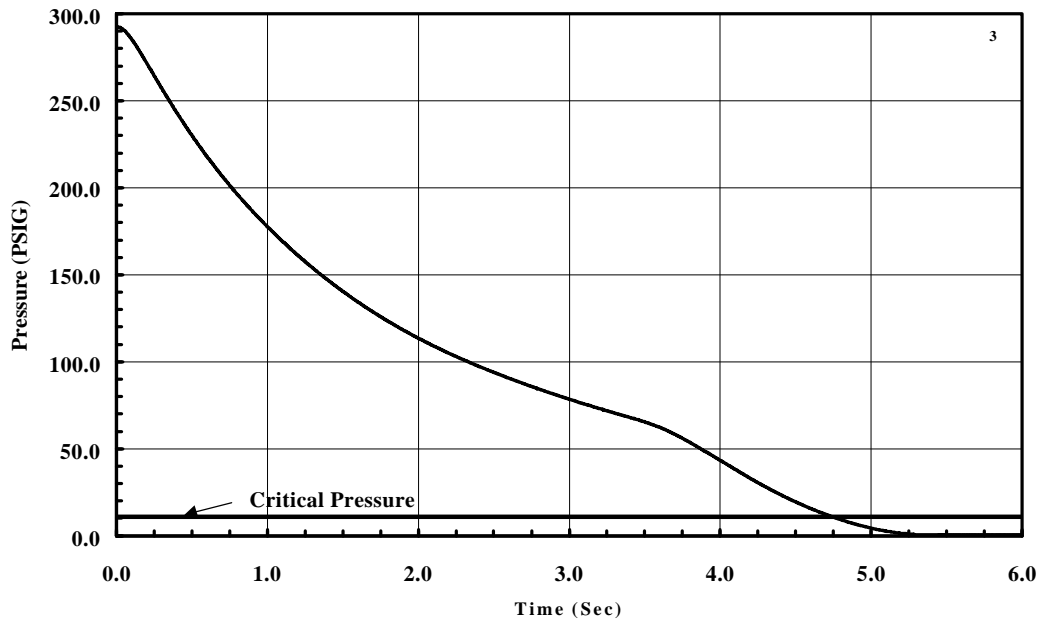


**Figure 7.17 Test P-6 - Pressure Vs Time.**

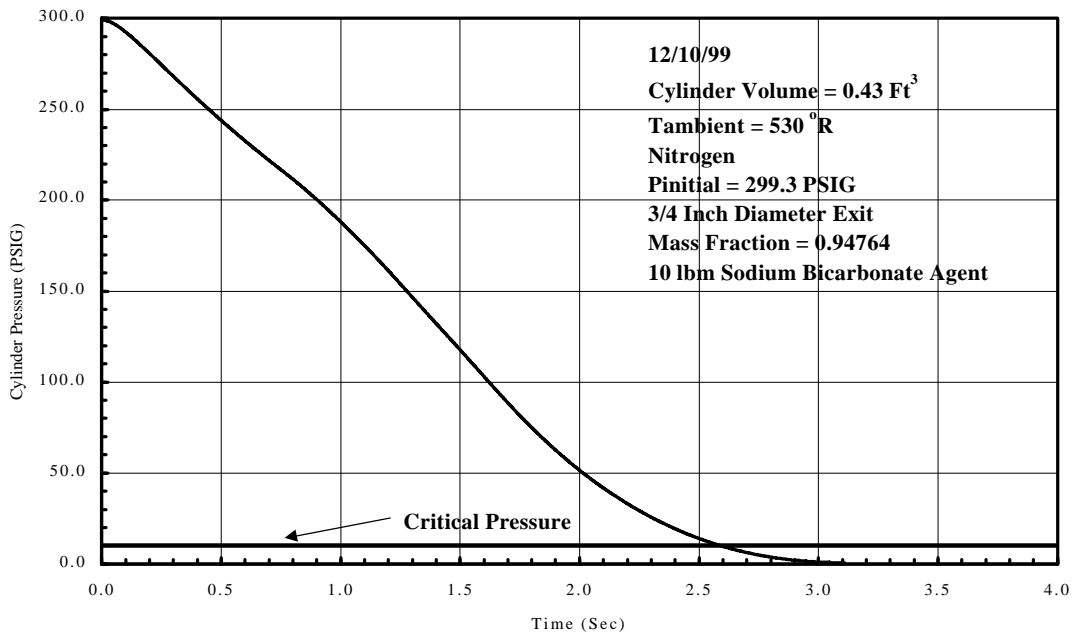


**Figure 7.18 Test P-7 - Pressure Vs Time.**



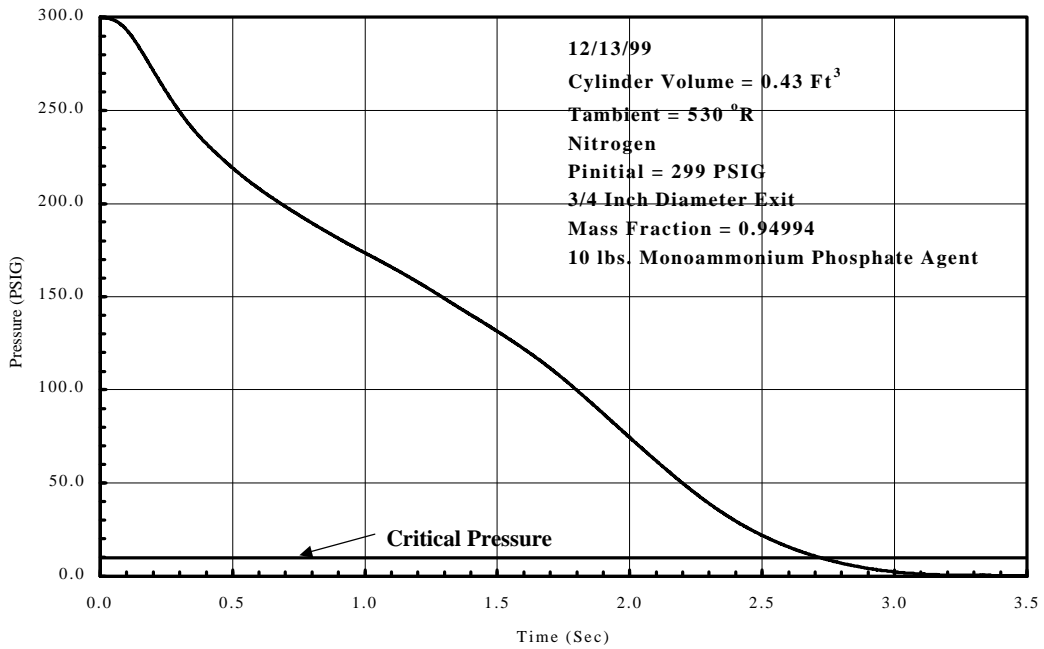


**Figure 7.19 Test M-1 - Pressure Vs. Time.**

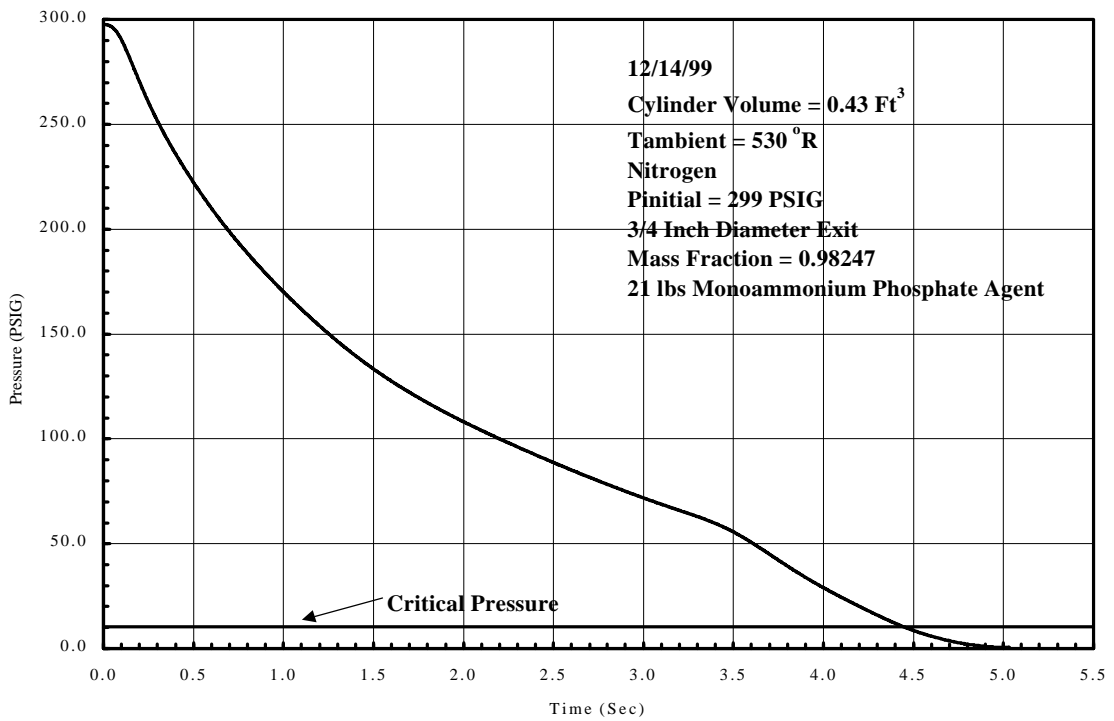


**Figure 7.20 Test M-2 - Pressure Vs Time.**

As can be seen in the Figures, there is an inflection point approximately 0.100 second after the initiation of discharge, caused by the opening of the cylinder valve. While the valve is opening, discharge of the cylinder's contents occurs at reduced flow levels, ramping up to full discharge flow once the valve is fully open.

In Figure 7.17 through Figure 7.20, a second inflection point can be seen, occurring within 2 seconds of the end of discharge. This second inflection point only occurs with agent-powder discharges. While the exact nature of this second inflection point is not fully understood, it is believed to be a result of varying of the mass fraction of agent in the cylinder discharge flow. The difference in pressure response of a blow down due to different amounts of agent in the cylinder can be seen in Figure 7.23 below. The 25 lbm load (test P-6) shows a definite second inflection point approximately 3.5 seconds after discharge initiation. The second inflection point for the 10 lbm load (test P-7) is almost impossible to locate, possibly occurring in the 0.8 to 0.9 second time frame. In the P-7 test, the level of agent in the cylinder at the start of blow down is much closer to the bottom of the dip tube than in the P-6 test; thus a reduction in agent mass fraction in the P-7 test would occur much sooner than in the P-6 test. Similar behavior can be seen in the cylinder-pipe-nozzle PNS-1 and PNS-4 tests (**Figure 7.36**). In these tests, identical 25 lbm loads of agent were used, with the same carrier gas initial pressure, but the PNS-4 dip tube was only half the length of the PNS-1 tube. As with the P-6 and P-7 tests, the agent level in the cylinder reaches the bottom of the shorter dip tube sooner than with the longer dip tube. As a result, interaction with the shorter dip tube occurs earlier in blow down for the PNS-4 test than for the PNS-1 test. Further, any second inflection point in

the PNS-4 test is almost impossible to detect, while the second inflection point is quite visible in the PNS-1 test.

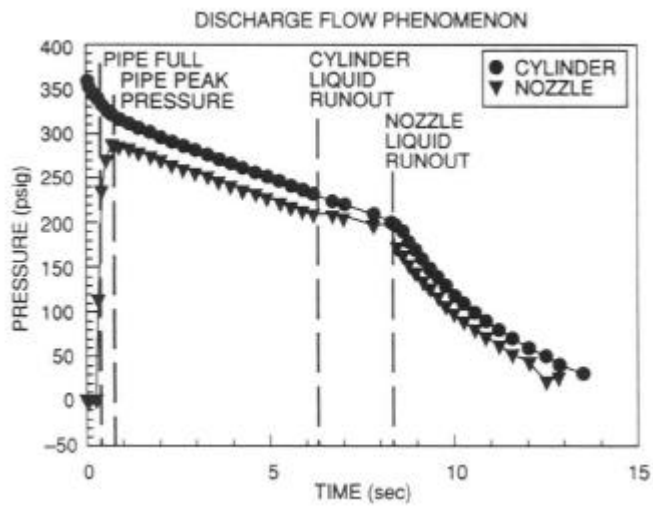
It has been noted by observation that, when filled with the manufacturer's specified amounts of agent (either sodium bicarbonate or monoammonium phosphate), the cylinder is not completely filled; usually the agent levels out 1-2 inches below the exit valve assembly threading on the cylinder. The general assumption has been that, during discharge, the agent and pressurized gas form a homogeneous mixture in the cylinder. If, however, the agent is entrained by high-velocity gases, and remains "settled out", and not in a homogeneous mixture, then movement of agent powder within the cylinder is much more complex. Agent close to the flow path of exiting gases is entrained into the gas flow, while agent powder somewhat removed from the dip tube bottom may exit in the manner of flowing powder in a hopper. As the angle of repose of the agent becomes sufficiently steep, powder flows "downhill". Once discharge begins, the free surface of the powder is no longer horizontal, but at an angle with the downwards-most end close to the dip tube. Eventually, enough powder is removed so that the downwards-most point of the powder surface (concave- or crater-shaped) reaches the cut-outs at the bottom of the dip tube. At this point, the gas in the cylinder now has a path out of the cylinder without having to entrain particles. As a result, while some powder entrainment continues, so long as there are entrainable particles close to the flow path of the gas, the amount of powder being entrained significantly drops. **Figure 8.15** shows the results of test PMS-2, charged with 10 lbm monoammonium phosphate. At the end of discharge, there is a residual amount of agent in the bottom of the cylinder. As the sketch suggests, sometime prior to the end of blow down, the level of agent in the cylinder reaches the

bottom of the dip tube. In fact, for either the predicted or actual amounts of residual agent, the level of agent can be seen to have clearly dropped below the bottom of the dip tube. It is at this point that the slope of the cylinder pressure trace in the mixture discharges increases dramatically. The amount of agent that can be entrained into the exiting gas flow is dramatically reduced from what it was when the agent level was above the bottom of the dip tube. As a result, the agent mass fraction in the mixture flow dramatically reduces. And, as comparisons of gas-only and mixture discharges shows, the lower the agent mass fraction, the more rapid the discharge.

As can be seen in Figure 7.22 below (and Figure 7.16 and Figure 7.17 above), gas-only discharges are significantly faster than mixture discharges. A rapid drop in the discharging mixture mass fraction, brought about by powder mass configuration changes in the cylinder towards the end of discharge, would readily cause a shift in the rate of pressure drop within the cylinder, resulting in an inflection point close to the end of discharge. The results of experiments described in Section 7.4.1.3 will discuss this issue further.

A comparison can be made between the behavior observed in the dry chemical discharges and similar discharges involving gas-liquid multi-phase flows. Comparison of Figure 7.21 with the results of dry chemical discharges shows a marked resemblance between the behaviors of the two mixtures. Both show the initial transient behavior in the cylinder, while the downstream pressure is rising as the piping fills and is pressurized. Both show the second inflection point – denoted in Figure 7.21 by the notation of “liquid runoff” in the 6-8 second time frame, and some transient behavior of the nozzle pressure just prior to the final drop off. Given the similarity of curve shapes of the gas-solids and

gas-liquids multiphase systems, it is most likely that the two systems are exhibiting similar behaviors during discharge, including a final drop off in the pressure curves due to depletion of liquid or solid agents, and the interaction of the agent with dip tubes in the discharge systems.



(Source: SFPE (1995), page 4-160)

**Figure 7.21 Typical Gas-Liquid Multi-Phase Cylinder Discharge.**

Figure 7.22 compares discharge times and characteristics of tests G-7 and P-6. Both tests are pressurized to 306 psia; however, test G-7 is a gas-alone test, while P-6 also includes 25 lbm of sodium bicarbonate agent. The discharge time for the agent/gas mixture, as expected, is significantly greater than for the gas-alone discharge. At the “critical pressure” (occurring for test P-6 at 11.7 psig = 26.4 psia), where the flow becomes unchoked, the discharge time for the mixture is approximately 3.5 times greater than that for the gas-only discharge. Furthermore, the difference in shapes of the two

curves is pronounced. While both exhibit the initial inflection point caused by the opening of the cylinder valve, only the mixture discharge exhibits the second inflection point.

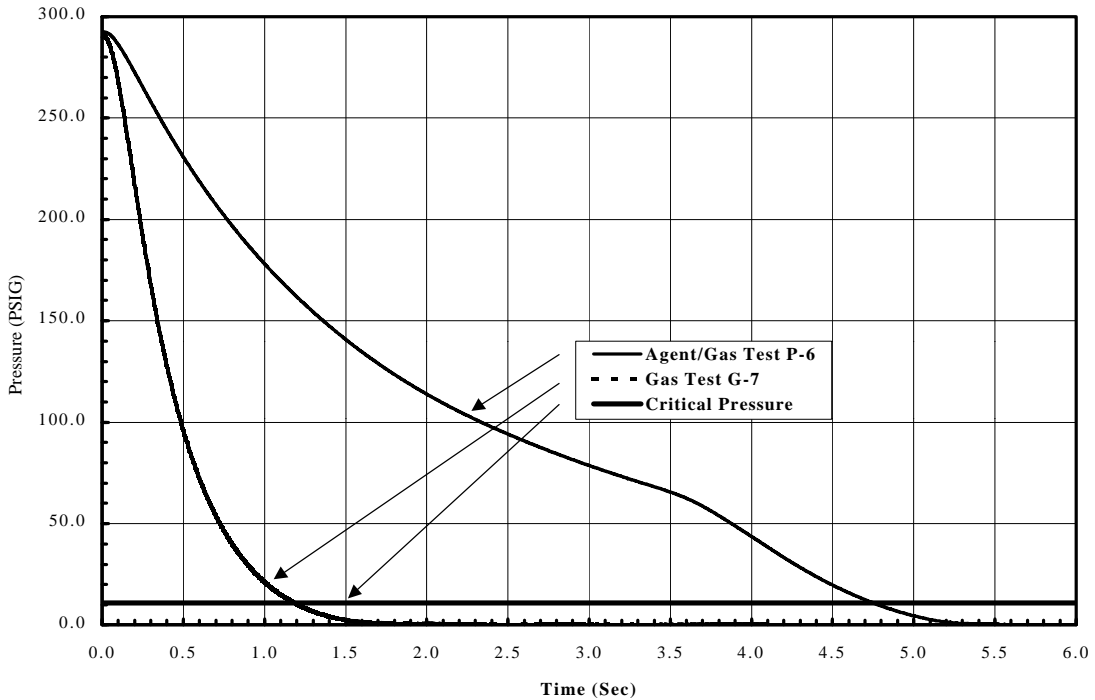
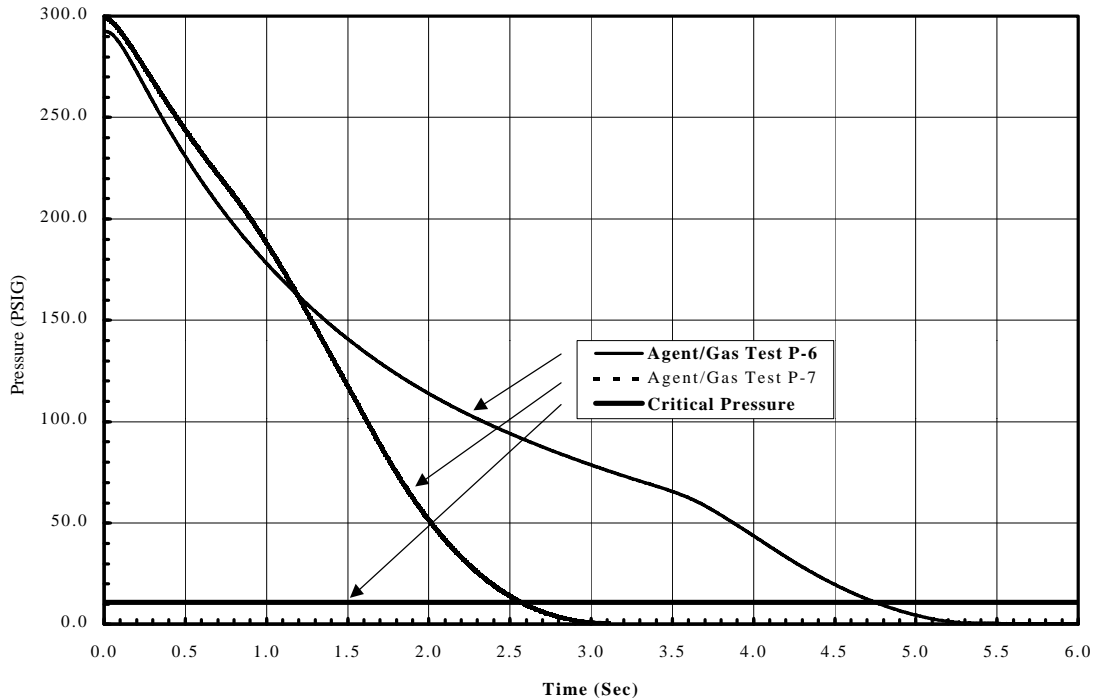


**Figure 7.22 Comparison of Discharge Tests G-7 and P-6.**

A comparison of the effect of the amount of agent on discharge is shown in Figure 7.23. The two discharges exhibit similar traces for the first 1.2 seconds of discharge; after that, test P-6, with 15 lbm sodium bicarbonate agent more than test P-7, diverges, taking almost twice as long to reach unchoking than test P-6. The critical pressure “curve” is the approximate pressure at which the discharge unchokes; because it is a function of the volume fraction  $\theta$ , the exact point at which unchoking occurs will

tend to vary somewhat. For the test discharges performed here, the critical pressure tended to be in the 11 psig (= 26 psia) range, based on equation (4.69).



Note: P-6: 25 lbm Sodium Bicarbonate  
P-7: 10 lbm Sodium Bicarbonate

**Figure 7.23 Comparison of Discharge Tests P-6 and P-7.**

While the second inflection point is fairly pronounced with test P-6, at approximately 3.7 seconds, the inflection point for test P-7 is a lot harder to detect, being faintly visible approximately 1 second into discharge. With less than half the agent present in test P-7, the level of agent in the tank reaches the lower end of the dip tube sooner than in test P-6. Also, with less agent, the suggested cratering effect as the level of agent reaches the bottom of the dip tube will be less; thus the less-pronounced second inflection point for test P-7. A similar effect is seen later, in comparison of tests PNS-1

and PNS-4 (the dip tube length in test PNS-4 is half the length of the “standard” length dip tube in PNS-1 (all other tests use dip tubes of the “standard” length.)

A comparison of the effect of the chemical composition of an agent on discharge is shown in

Figure 7.24.

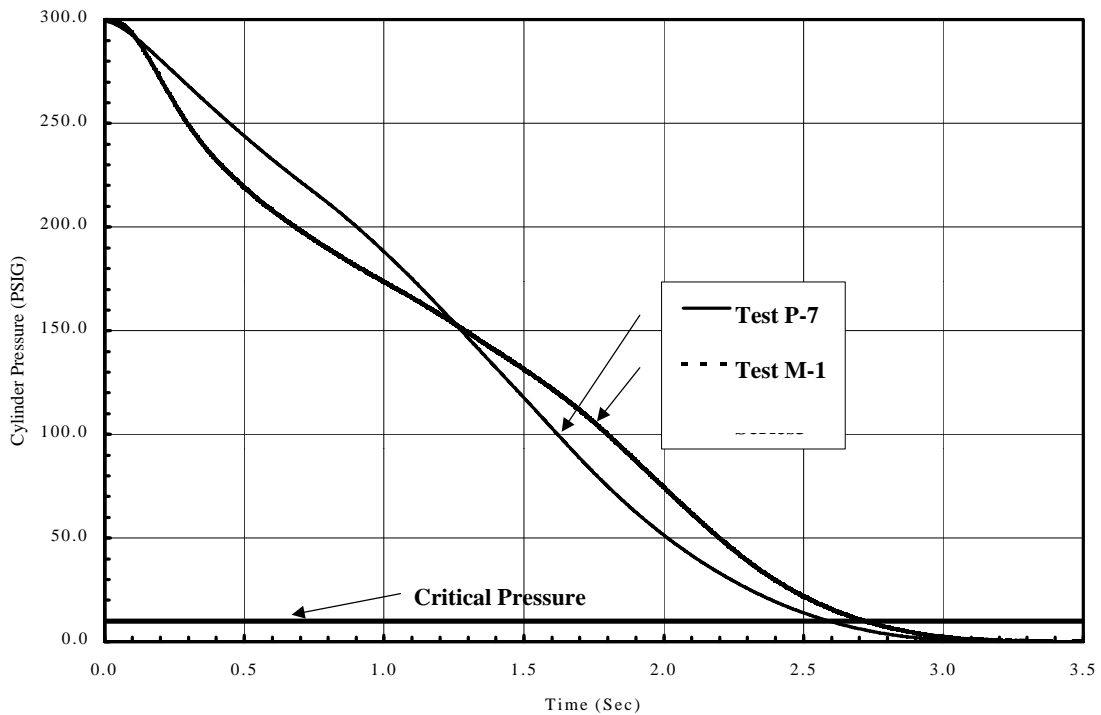


**Figure 7.24 Comparison of Discharge Tests P-7 and M-1.**

Test P-7 has 10 lbm of sodium bicarbonate agent, while test M-1 has 10 lbm of monoammonium phosphate. The particle size range and distribution is similar for both agents, although the composition of agent (proprietary to the manufacturer) differs between the two agents. Both discharges were pressurized to the same initial cylinder pressure, and the physical systems were identical for the two discharges. The results indicate close similarity to the performance behavior of the two agents, with the sodium



bicarbonate reaching the choking point slightly faster than the monoammonium phosphate (0.1 second difference). The shaping of the curves suggests somewhat different behavior of the two agents in the source cylinder, with the sodium bicarbonate discharge reaching a second inflection point somewhat before the monoammonium phosphate discharge. Test M-1 also shows a sharper initial pressure drop than Test P-7. Recall that both discharges are with agent loads less than half the manufacturer's typical loads (themselves not filling the cylinder to capacity.) As a result, the second inflection point is reached somewhat earlier in discharge than it would be for a full load of agent. Geometric effects of the cylinder interior, combined with flow and entrainment characteristics of the agents, clearly have an effect on the discharge time, and the amount of agent discharged from the cylinder.

#### **7.4.1.2 Cylinder-Pipe-Nozzle Tests.**

A table of cylinder-pipe-nozzle tests performed is shown in Table 7.5. This series of tests included a single source cylinder, 8 feet of clear Lexan™ piping, and (for all but one test), a single nozzle at the downstream end of the piping. All tests used nitrogen as the carrier gas. Note that two pressure measurements were made in these tests: one transducer measured pressure in the source cylinder, and the other measured static pressure at a location just upstream of the nozzle inlet (exit orifice for test PNS-2, without a nozzle.)

Test	Date	Initial Pressure (psia)	Agent	Mass Agent (lbm)	Exit Diameter (in)	Discharge Time (s)	Mass Fraction
PG-1	3/20/00	215.8	-	-	0.173	8.6	0
PG-2	3/20/00	325.7	-	-	0.173	10.4	0
PNS-1	3/28/00	314.7	SB	25	0.173	26.9	0.98485
PNS-2	3/30/00	314.7	SB	25	0.5625 (No nozzle)	7.5***	0.98485
PNS-3 #	5/30/00	319.7	SB*	27.4	0.173	28.0	0.98485
PNS-4 **, #	6/8/00	319.7	SB	25	0.173	13.4	0.98485
PNM-1 #	4/4/00	310.9	MAP	21	0.173	26.5	0.98261
PNM-2 #	4/27/00	122.7	MAP	10	0.173	17.1	0.97980

Notes:

\* - Off-the-shelf sodium bicarbonate, no flow additives present.

\*\* - Short dip tube, 7 inches long (regular tube 14 inches long).

\*\*\* - Time approximate – daq failure just prior to end of test.

# Omega 0-3000 psi pressure transducer used, due to failure of Lucas 0-500 psi transducer.

Discharge time: Start time approximately 0.072 seconds prior to first response of downstream pressure transducer; end time reached when pressure transducer response drops to within FS% Error region (0.25%, 16.2 psia).

**Table 7.5 Cylinder-Pipe-Nozzle Test Summary.**

Three series of tests were performed. The PG series established a baseline behavior of the test configuration by determining configuration performance when only gas was discharged through the piping and nozzle. The PNS series gathered performance data for discharges of sodium bicarbonate agent, and also looked at two variants – sodium bicarbonate without the additives normally used by the manufacturer to improve flow characteristics of the powder, and the effect of a shorter dip tube. The latter discharge was used to examine the validity of the supposition of powder behavior in the

cylinder during discharge influencing the characteristics of the discharge pressure trace, particularly the second inflection point.

Results of the individual discharge tests are shown in Figure 7.25 through Figure 7.32.

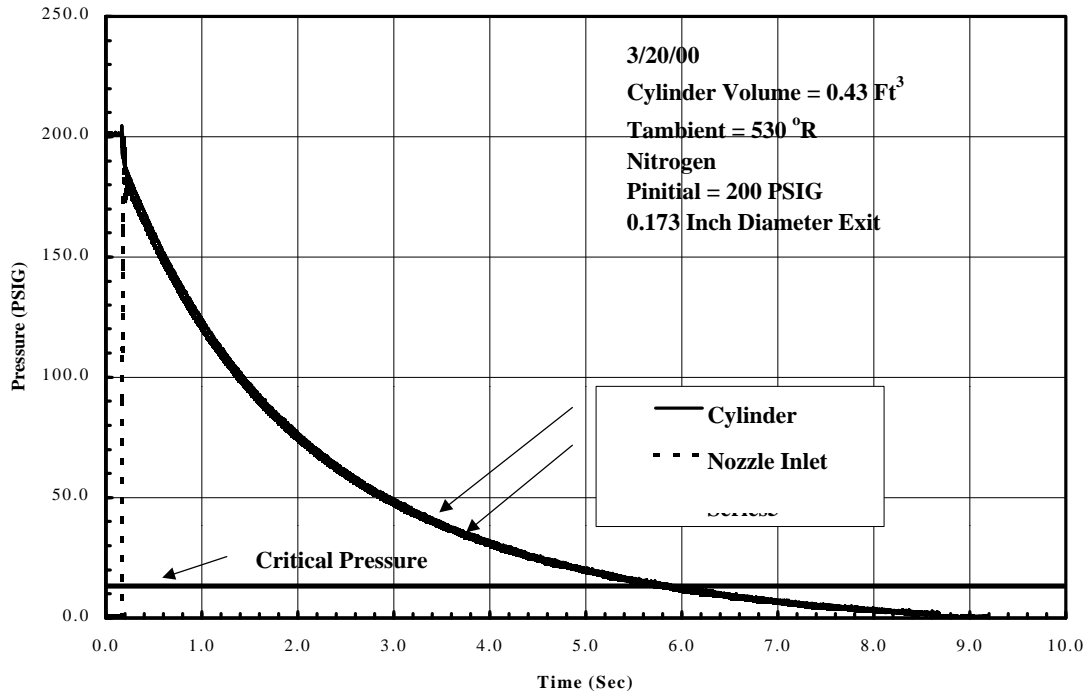


Figure 7.25 Test PG-1 - Pressure Vs Time.

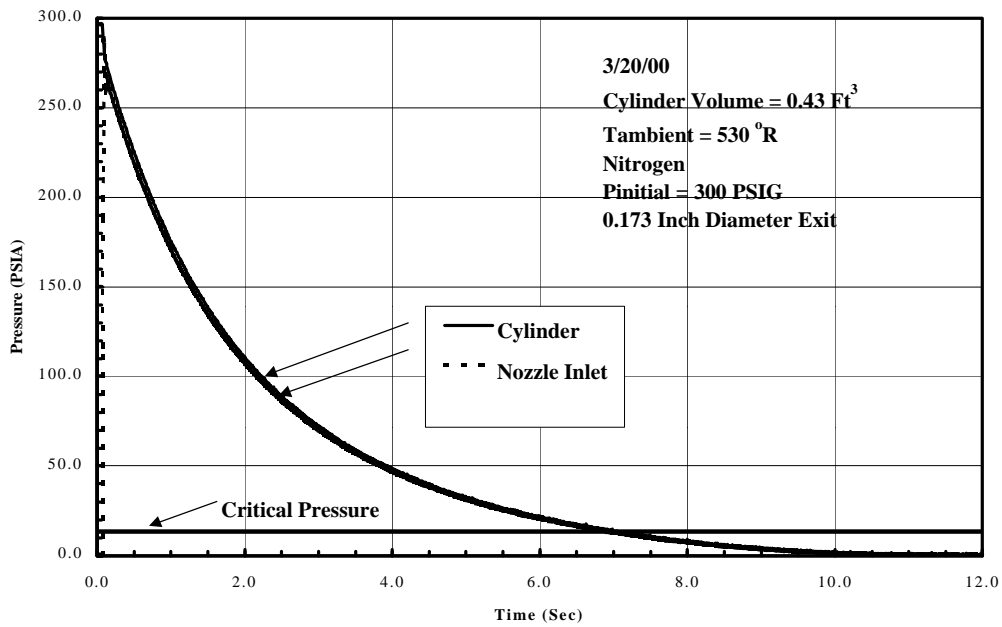


Figure 7.26 Test PG-2 - Pressure Vs Time.

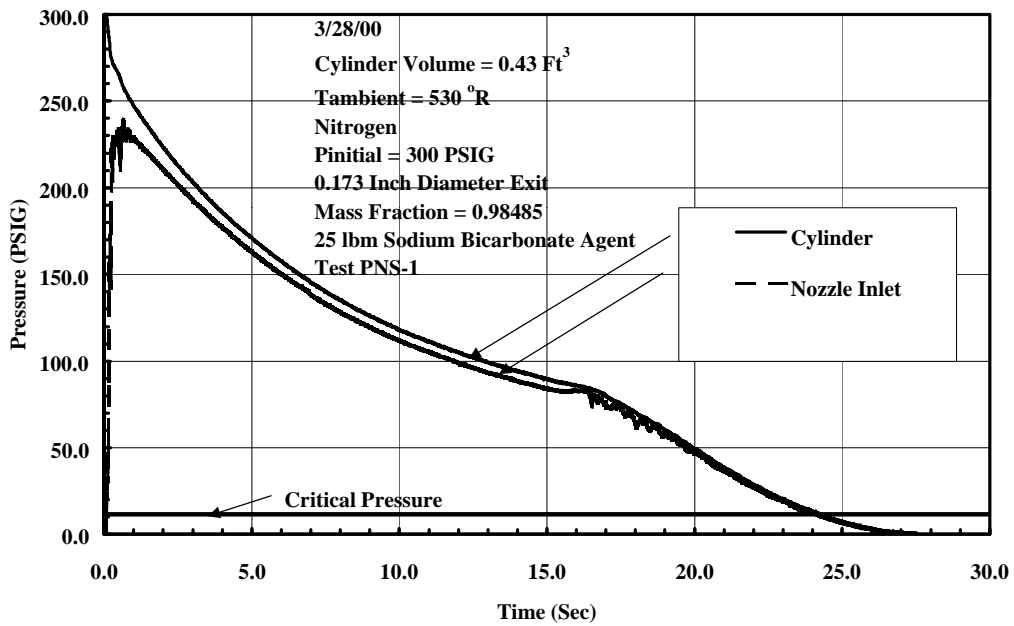


Figure 7.27 Test PNS-1 - Pressure Vs Time.

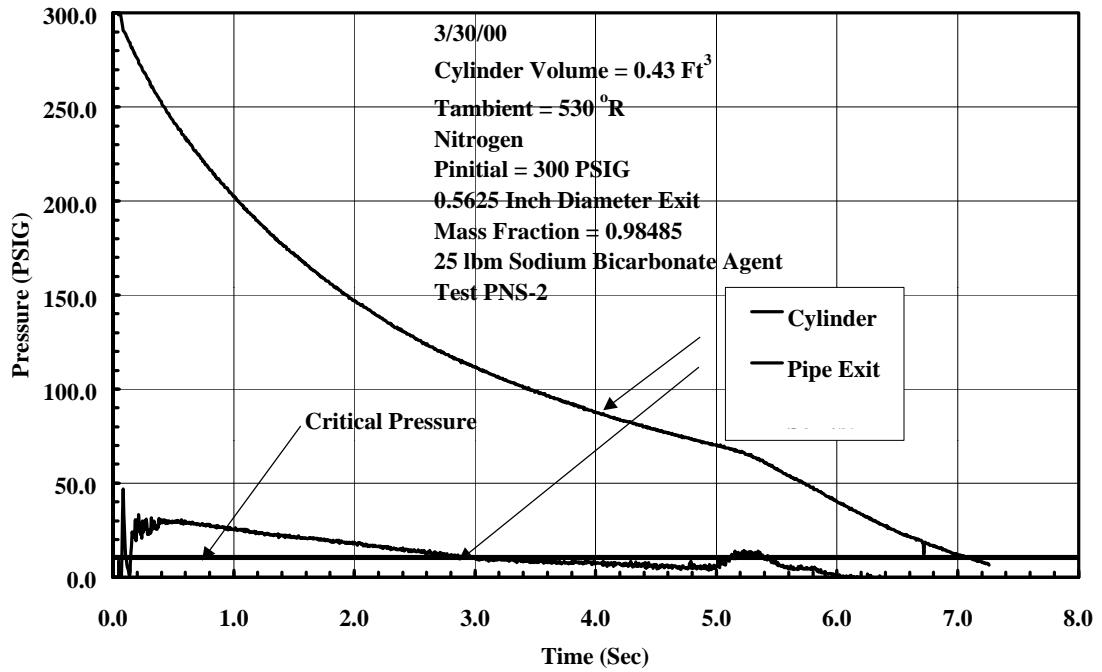


Figure 7.28 Test PNS-2 - Pressure Vs Time.

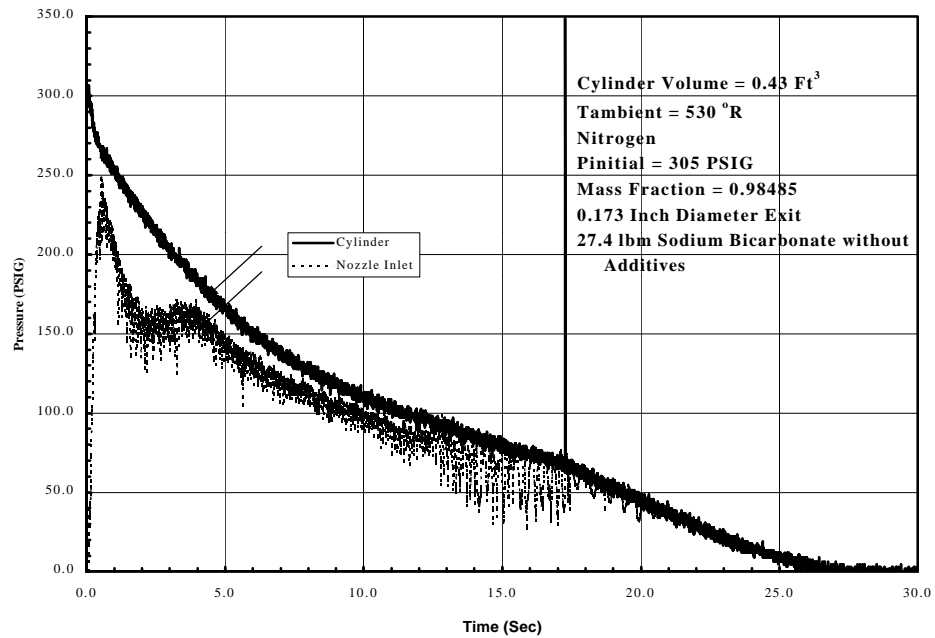


Figure 7.29 Test PNS-3 - Pressure Vs Time.

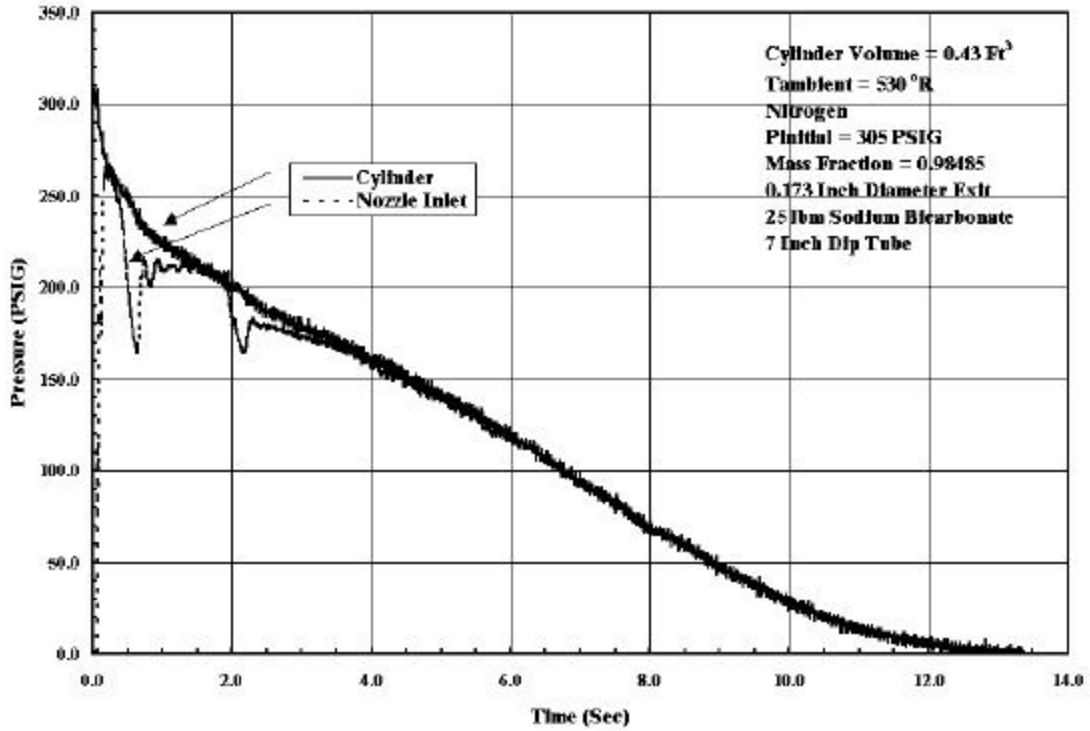


Figure 7.30 Test PNS-4 - Pressure Vs Time.

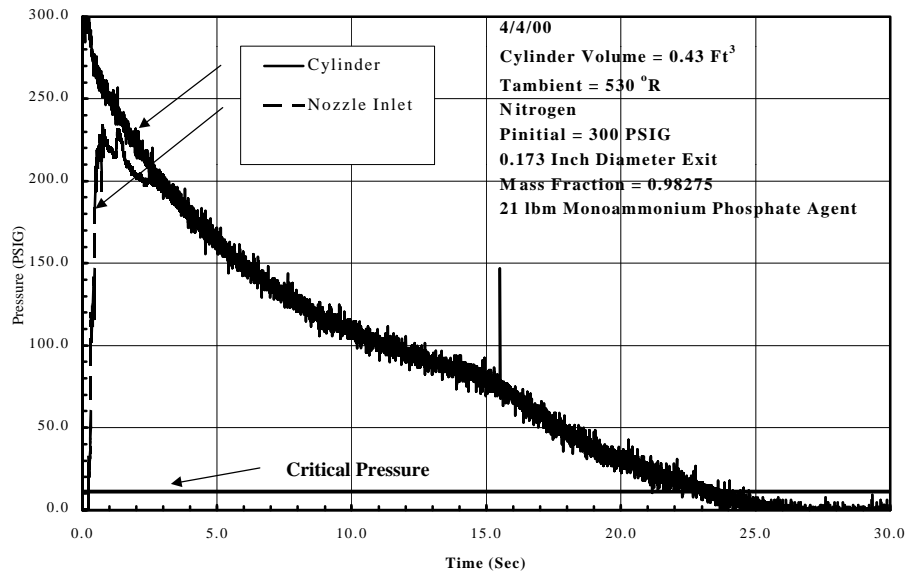
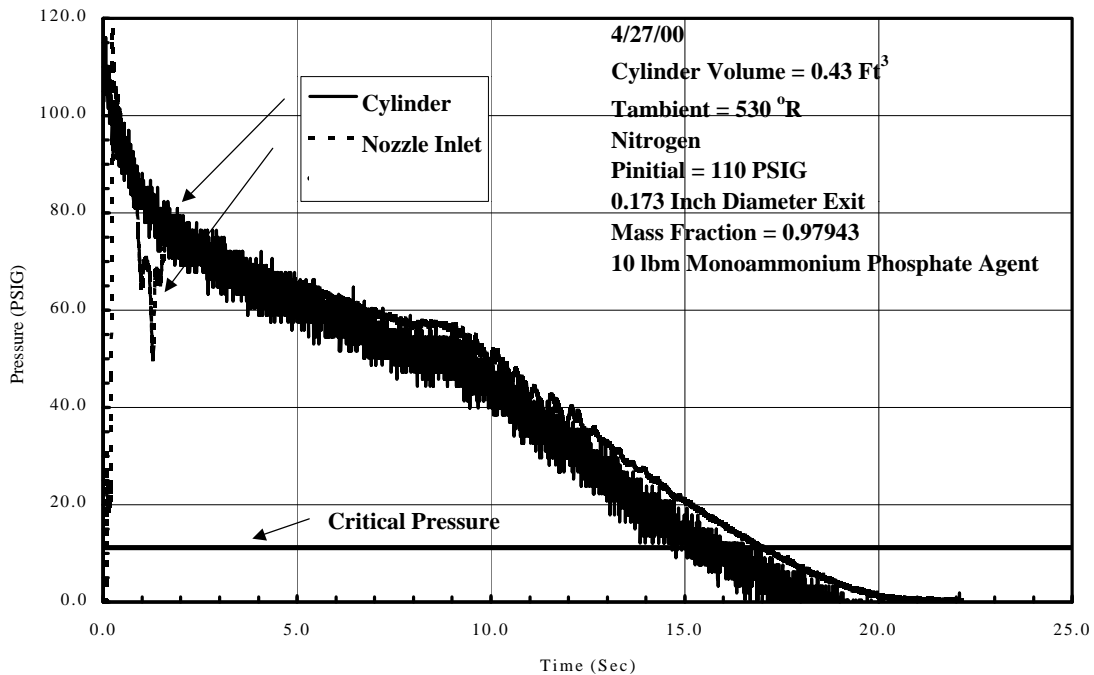


Figure 7.31 Test PNM-1 - Pressure Vs Time.



**Figure 7.32 Test PNM-2 - Pressure Vs Time.**

In all the figures, except for Figure 7.28 (Test PNS-2, without a nozzle), after the initial transients, the two pressure transducer traces are very close to each other, in some instances indistinguishable from each other. Given the locations of the two transducers, the results indicate that 1) there is a significant pressure drop across the nozzle, and 2), with the nozzle present, losses between component endpoints upstream of the nozzle are very small. As with the tank-only discharge tests, the second inflection point is only visible in powder/gas mixture discharge tests, re-affirming that the phenomena is a result of the presence of the powder in the cylinder. This is further affirmed by test PNS-2, in which demonstrates that the inflection occurs with or without the nozzle present, and by the fact that the inflection point occurred in the tank-only mixture discharges, without any downstream piping whatsoever. As before, the inflection occurs for both agents, and for

the sodium bicarbonate without flow additives (test PNS-3). For test PNS-4, with the half-length dip tube, there is a slight suggestion of an inflection point, occurring within the first second of discharge.

The greater scatter in the pressure trace of the cylinder pressure in tests PNS-3, PNS-4, PNM-1 and PNM-2 is due to the use of the Omega pressure transducer, in place of the Schaevitz transducer. The Omega transducer full scale range of 0-3000 psi, with a 0.25% FS error band, resulted in less precise cylinder pressure readings during cylinder fill and discharge.

Pressure traces in the PG test series showed little or no transient behavior during discharge (the longer time scale reduced the initial inflection due to the opening of the cylinder valve to insignificance). However, mixture tests showed several instances during discharge of significant transient response, particularly in the pressure transducer just upstream of the nozzle inlet (or exit). There are pressure fluctuations initially as the agent/gas mix enters the nozzle, suggesting that the flow “front” of the agent/gas mixture is not entirely homogenous, but takes some finite time to reach a uniform (or uniformly varying) mix. Pressure transience is also observable at the second inflection point. Shifts in the discharging mixture mass fraction as the cylinder powder reaches the bottom of the dip tube would account for the irregularity of the pressure trace.

In this test, there is a distinct initial peak in the downstream pressure, after which the flow plateaus in the interval of 2.0 - 3.5 seconds into discharge. This behavior in the pure sodium bicarbonate discharge may be due to temporary clogging and unclogging of the nozzle, as the solid material discharges. Without the additives present in the commercial agents, added to improve flow characteristics and reduce clumping due to



settling and moisture, the pure powder would not flow as freely as the commercial agents. This “spikiness” is observable in a initial portion of most of the tests, lasting as long as 2-4 seconds in tests PNS-2, PNS-4, and the PNM tests. It is of much shorter duration in test PNS-1.

Note also the fluctuations in the vicinity of the second inflection point for test PNS-3 (in the 12.5 to 17.5 second time frame.) Visual observations of flow behavior at this time show significant “chugging” occurring in the flow, indicated visually by rapid shifts in the agent mass fraction, and accompanied by considerable noise. Both flow irregularities and noise abruptly abated once the inflection point was passed. The “pure” sodium bicarbonate is hygroscopic, much more prone to absorb moisture than the commercial agent, and more likely to cake and clump. It is also more likely to be affected by prolonged periods of quiescence in the cylinder prior to discharge (in this case, a couple of weeks elapsed between filling of the cylinder, and the discharge test.)

The nozzle inlet pressure generally shows transience, for the full initial load of all three powders, for 4-6 seconds after reaching the second inflection point. This is due to changes in the mass fraction in the cylinder caused by the free surface of the agent reaching the end of the internal dip tube.

Videotape recordings were made of the flow through the Lexan™ piping for tests PNS-3, PNS-4, and PNM-2. Results of the videotaping are discussed at the end of this Section.

The measured residual powders collected after testing is shown in Table 7.6.

Test	Residual in Bag (g)	Residual In Tank (g)	Total Residual (g)	Starting Load (g)
P-6	11,116.8 (97.9%)	45.4 (0.4%)	11,162.2 (98.3%)	11,350.0
PNS-1	10,850.2 (95.6%)	290.2 (2.6%)	11,140.7 (98.2%)	11,350.0
PNS-2	11,148.0 (98.2)	105.4 (0.9%)	11,254.2 (99.1%)	11,350.0
PNS-3	10,745.0 (86.4%)	1,672.2 (13.4%)	12,417.5 (99.8%)	12,439.6
PNS-4	3,391.4 (29.9%)	7,840.6 (69.1%)	11,232.0 (99.0%)	11,350.0
PNM-1	9,052.9 (95.0%)	273.93 (2.9%)	9,326.8 (97.8%)	9,534.0
*PNM-2	4,425.7 (97.5%)	132.1 (2.9%)	4,557.8 (100%+)	4,541.4

\* weights approximate, may include minor errors.

**Table 7.6 Powder Weights and Their Distribution After Discharge Testing.**

One side result of the performed discharge tests was the high recovery rate of powder using double-bagging to contain the discharged powder. Total powder recovered was in the range of 98-100%. Generally the bulk of the powder after testing was found in the capture bags. PNS-3 was one exception; this test used sodium bicarbonate without the flow additives used by the manufacturer. The result was around 12 percent less agent in the capture bags – this agent was found in the source cylinder, reflected by the approximately 12 percent more agent measured in the cylinder, as indicated in the table. The other exception was PNS-4, in which a 7 inch dip tube, rather than the 14 inch tube normally used with this cylinder/valve system. The results of this test, with almost 70% of the original agent load still in the cylinder after discharge suggests that the dip tube is an important component in ensuring that as much agent as possible is discharged. It also suggests that flow of the agent within the cylinder, and its eventual entrainment,

constitutes an important portion of the discharge process, and should be included in any system model in order to accurately simulate system behaviors.

The influence of the piping network and nozzle on discharge time can be seen in Figure 7.33. The addition of piping and a nozzle significantly increases discharge time; in this instance the time to reach unchoking is increased by nearly a factor of 7. Similar increases in discharge time can also be seen for agent/gas mixtures resulting from the addition of piping and nozzles downstream of the source cylinder.

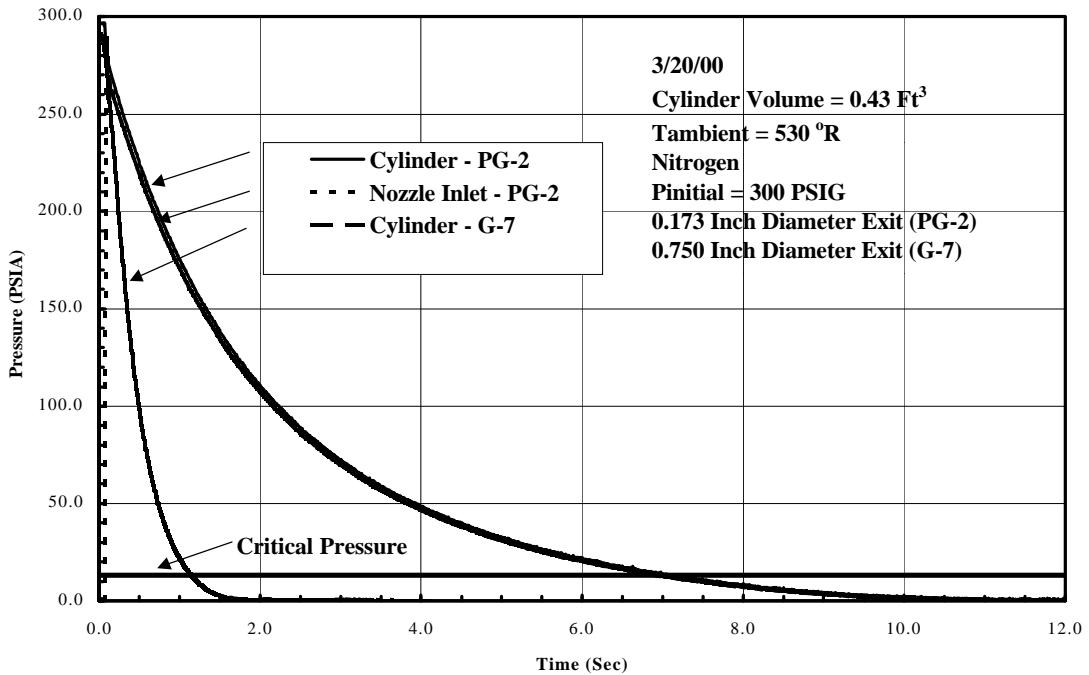


**Figure 7.33 Pipe/Nozzle Effects on Discharge Time (Gas Only Tests).**

The influence of initial pressure on discharge times can be seen in Figure 7.34. Increasing the cylinder initial pressure increases the depressurization time; in this instance, increasing in the initial pressure by 100 psi increased the time to reach

unchoking by approximately 1 second. Similar system responses to initial cylinder pressure changes can be expected for agent/gas mixtures.

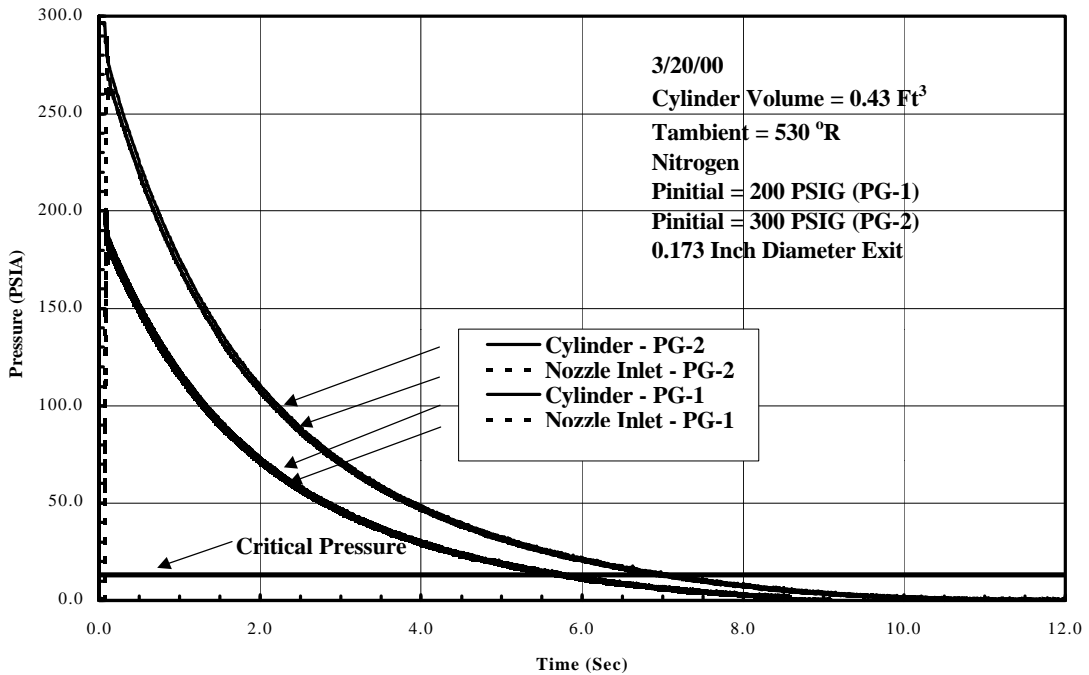


**Figure 7.34 Initial Cylinder Pressure Effects on Discharge Time (Tests PG-1 and PG-2 - Gas Only).**

The influence of piping/nozzle components on discharge time can be seen in Figure 7.35. The 8 foot Lexan™ piping has a small influence on the discharge time, extending the time to reach unchoking by approximately 2 seconds (note also that the piping is slightly smaller in diameter than the cylinder outlet.) The addition of the nozzle to the piping network significantly increases the discharge time. The discharge time increases by 17 seconds in going from the pipe to the pipe and nozzle configuration. As noted before, the nozzle also can be seen to influence the pipe pressurization and flow

conditions; when the nozzle constricts flow, upstream flows are also constricted, and the pipe plays only a minor role in influencing the discharge time. Without a nozzle, the downstream end of the pipe is at a much lower pressure than the upstream end. Without a nozzle, the discharge time of the system is not significantly influenced by the pipe, although flow conditions in the system are affected.

Also, as noted earlier, the second inflection point can be seen in all the pressure traces in Figure 7.35.

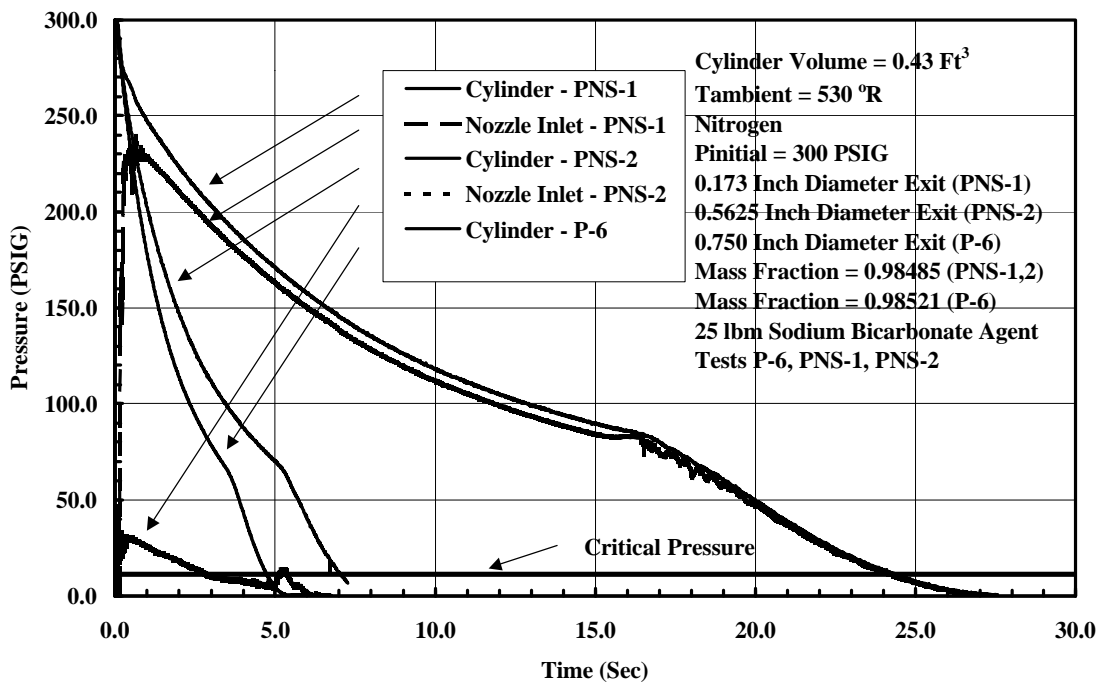


**Figure 7.35 Pipe Network Component Effects on Discharge (Tests P-6, PNS-1, PNS-2 - Sodium Bicarbonate Agent).**

A comparison of the influence of the length of the cylinder dip tube is shown in Figure 7.36. The discharge time was significantly shortened by the shorter discharge

tube. The free surface of the cylinder powder reaches the end of the dip tube earlier for the shorter tube, allowing for gas without agent to escape the cylinder earlier than for the full length dip tube. The residual agent left in the cylinder after discharge was greater for the shorter length dip tube as well, 17.3 lbm for the short tube, versus 0.6 lbm for the full length tube. Also note that the second inflection point is almost totally absent in the short dip tube discharge. However, the fluctuation in the nozzle inlet pressure trace for the short dip tube is significantly more pronounced than for the full length dip tube. The free surface of the agent in the cylinder reaches the lower end of the dip tube almost immediately after initiation of discharge; thus the initial transience is due to a combination of initialization of flow in the piping network, combined with changes in the flow mass fraction due to the interaction of the powder free surface with the end of the dip tube. Shifts in the time of the second inflection point can also be seen by comparing discharges with differing charges of agent – P-6 and P-7, for instance. The inflection for P-7 (25 lbm) is quite pronounced, while the inflection for P-6 occurs correspondingly earlier in discharge, and is much less pronounced. Tests M-2 and M-1 (21 lbm monoammonium phosphate and 10 lbm, respectively) show similar results.

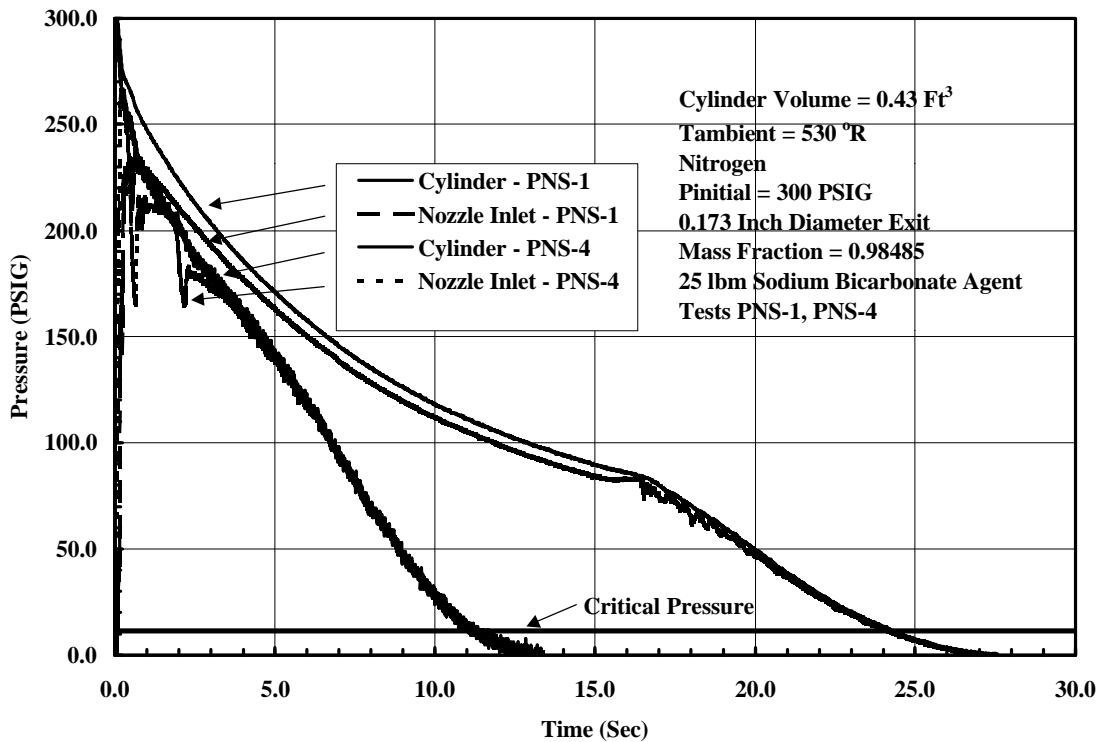


**Figure 7.36 Cylinder Dip Tube Length Effects on Discharge Time (Tests PNS-1, PNS-4).**

A comparison of the effects of the two extinguishing agents is shown in Figure 7.37. Despite the 4 lbm difference in the initial quantities of agent in the two tests, the results are strikingly similar, both in similarity of curve shapes, and similarity in total discharge times. Except for the sodium bicarbonate taking slightly longer in the 15-22 second time frame to discharge than the monoammonium phosphate, the two time traces at each location are almost identical, with the sodium bicarbonate taking no more than one second longer to reach unchoking than the monoammonium phosphate. As indicated earlier, the greater amount of scatter in test PNM-1 is due to use of a pressure transducer with wider full scale range, thus resulting in a larger full scale error, than that used in test PNS-1.

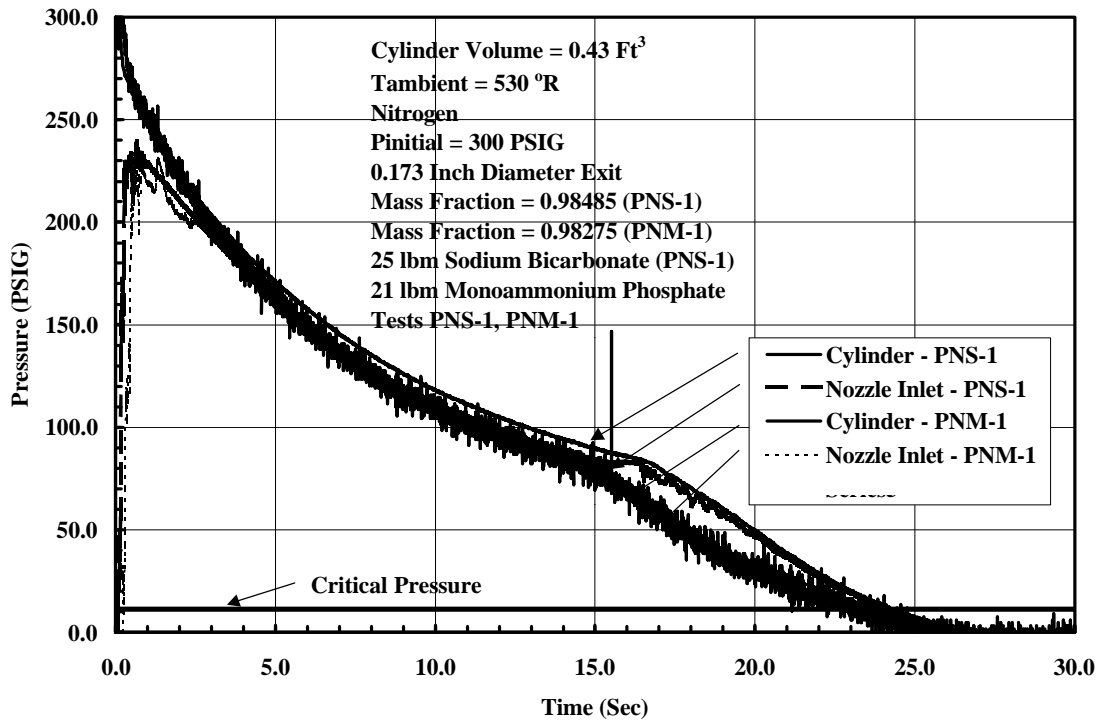


**Figure 7.37 Agent Effect on Discharge Time (Tests PNS-1, PNM-1).**

The influence of additives on agent performance is shown in Figure 7.38. In the early portion of discharge, the cylinder traces are virtually identical, with the untreated sodium bicarbonate no more than 1 second faster in discharging up to the second inflection point; after this point, the cylinder traces are again virtually identical. The nozzle inlet traces are significantly different, with the curve of the agent with additives smoothly following the cylinder trace throughout discharge. The trace of the untreated sodium bicarbonate shows a sharper initial peak, not recovering from initiation of discharge until almost 4 seconds, to follow the corresponding cylinder trace, though not as closely as the nozzle trace for the agent with additives follows its cylinder trace. The behavior of the untreated agent at the second inflection point, as indicated earlier, is



significantly more irregular than the behavior of the agent with additives, though the second inflection point takes place at approximately the same time into discharge for both powders.

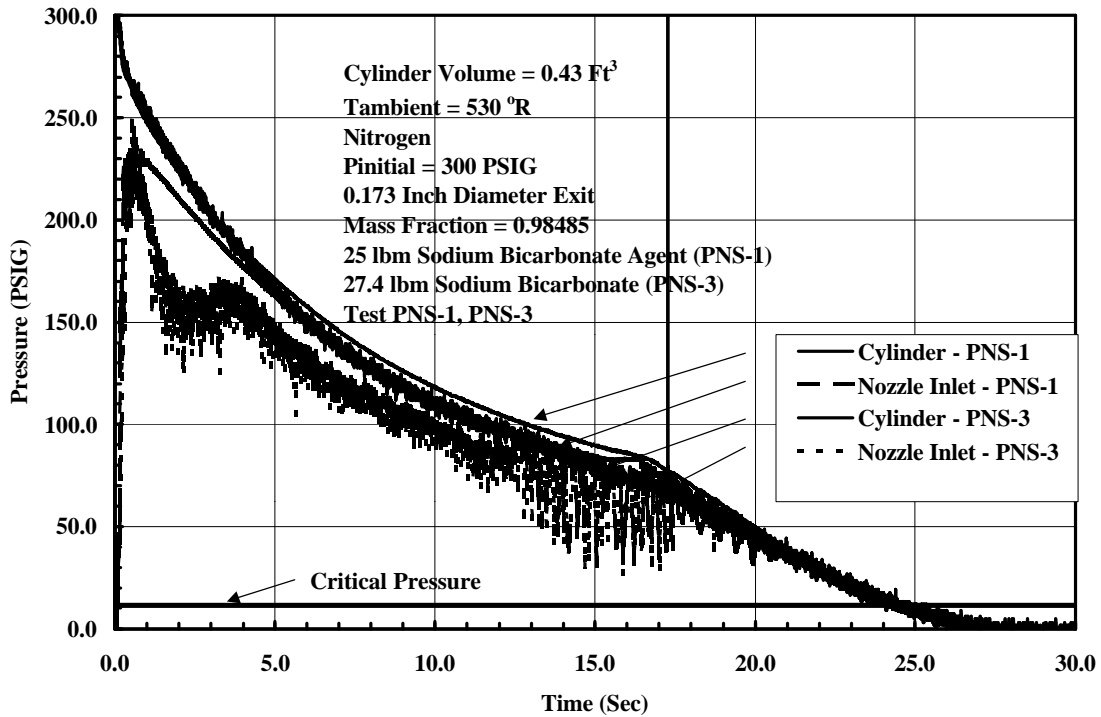


**Figure 7.38 Flow Additives Effect on Discharge (Tests PNS-1, PNS-3).**

Videotape recordings were made of several of the discharges, including tests PNS-3, PNS-4, and PNM-2. The focus of the camera was on the 8-foot clear Lexan™ tubing, to observe the onset of powder flow, and to note any changes in the characteristics of the flow during discharge, and when they occurred. Both the monoammonium phosphate tests and sodium bicarbonate agent tests generally showed uniform flow, with gradual thinning of the agent/gas mixture as the end of discharge was approached. Approximate correlation of the videotape frame speed with the time to fill

the pipe showed the powder flow to be traveling through the piping at a rate of 180 ft/sec in test PNS-4, and 120-240 ft/sec in test PNM-2. From the first appearance of agent through the piping, coordinated with timing events in the videotape, it was determined that the cylinder valve took approximately 0.067 seconds to fully open once triggered. The velocity of the powder through the piping can be calculated from the mass flow equation:

$$v_{\text{powder-average}} = \frac{m_{\text{powder-discharge}}}{t_{\text{discharge}} A_{\text{pipe}} \rho_{\text{powder}}}$$

For test PNS-1, similar in pressure and loading to the videotaped discharges, the predicted speed of sound in the pipe is approximately 204 ft/sec (based on the velocities and Mach numbers shown in the PNS-1 model output for the pipe, shown in Figure 6.6). Thus the mixture front traverses the pipe in 0.03 to 0.07 seconds, at a mixture velocity ranging from 0.6 to close to Mach 1.0. (Note that the gas-only speed of sound was predicted as 1144 ft/sec in this initial time frame.) Once the piping is pressurized, flow significantly slows down to a predicted Mach number of 0.08, as the nozzle restricts the flow.

Behavior of the “pure” sodium bicarbonate (PNS-3) was strikingly different from other discharges. The flow of agent in this discharge was observed to be more irregular in concentration than for other agents, with significant and rapid changes of solids concentrations in the time frame of the second inflection point. The videotape reveals a high level of “chugging” or slug flow at this point, accompanied by loud noise. Both the “chugging” and noise subsided once the second inflection point was passed, with gradual thinning of powder concentrations as the discharge came to an end.

#### 7.4.2 Kidde International UK Tests.

Results of the tests performed at Kidde International are reported in the memorandum in Appendix 10.7. The carrier gas was assumed to be nitrogen. The tests are summarized in Table 7.7.

Test	Date	Initial Pressure (psia)	Agent	Mass Agent (lbm)	Exit Diameter (in)	Discharge Time (s)	Mass Fraction
UK-F6	?	75.4	-	-	0.3125	5.0	0
UK-F7	?	87.0	Sodium Bicarbonate (?)	11.4	0.3125	~25.0	0.99001

\* Tank volume – 0.353 ft<sup>3</sup> – hand-held extinguisher cylinder.

**Table 7.7 Summary of Discharge Tests Performed at Kidde International (UK).**

As with the WPI tests, the results of these tests shows a significant increase in discharge time with the agent/gas mixture over the gas-only discharge. Note that, for test UK-F7, mass discharge as a function of time was measured, as well as cylinder pressure versus time. As noted in the memorandum, at about 80% of discharge, the flow of agent from the cylinder becomes significantly irregular, with “burping” observed in the mass flow trace, and by test observers during discharge. While the source of this phenomenon is not identified in the memorandum, it is most likely a result of interaction of the free surface of the agent still in the cylinder reacting with the bottom of the dip tube.

#### 7.4.3 Corn Starch Tests.

The summary of the tests supplied to WPI in support of these studies is shown in Table 7.8. The carrier gas for these tests was assumed to be air.

Test	Date	Initial Pressure (psia)	Agent	Mass Agent (lbm)	Exit Diameter (in)	Discharge Time (s)	Mass Fraction
F-9	?	113.7	Corn Starch	6	0.3703	?	0.98214
F-10	?	114.7	Corn Starch	6	0.3703	?	0.98142
F-11	?	115.3	Corn Starch	6	0.3703	?	0.98132

Test vessel volume 0.257 ft<sup>3</sup>

**Table 7.8 Summary of Available Corn Starch Tests.**

The results of these discharge tests are shown in Figure 7.39 through Figure 7.41.

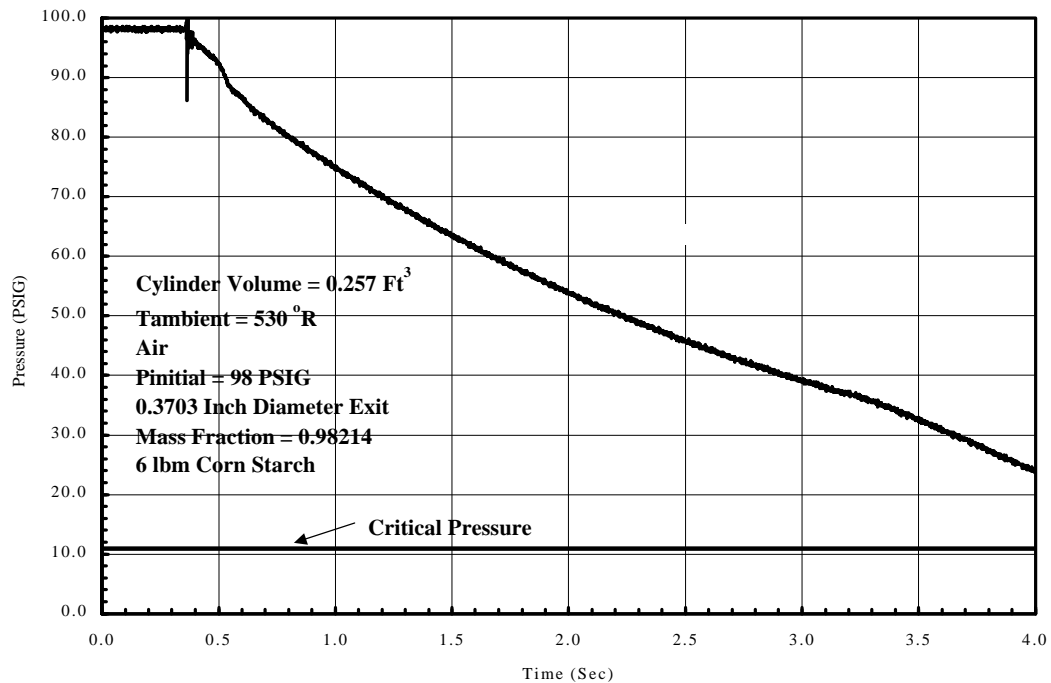


**Figure 7.39 Discharge Test F-9 - Pressure Vs Time.**

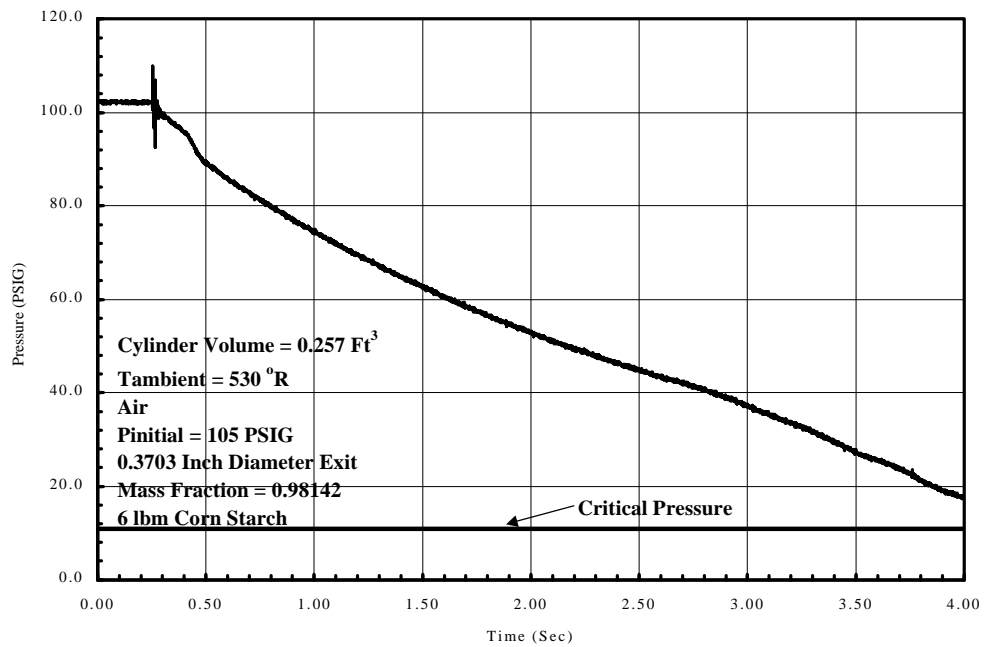


Figure 7.40 Discharge Test F-10 - Pressure Vs Time.

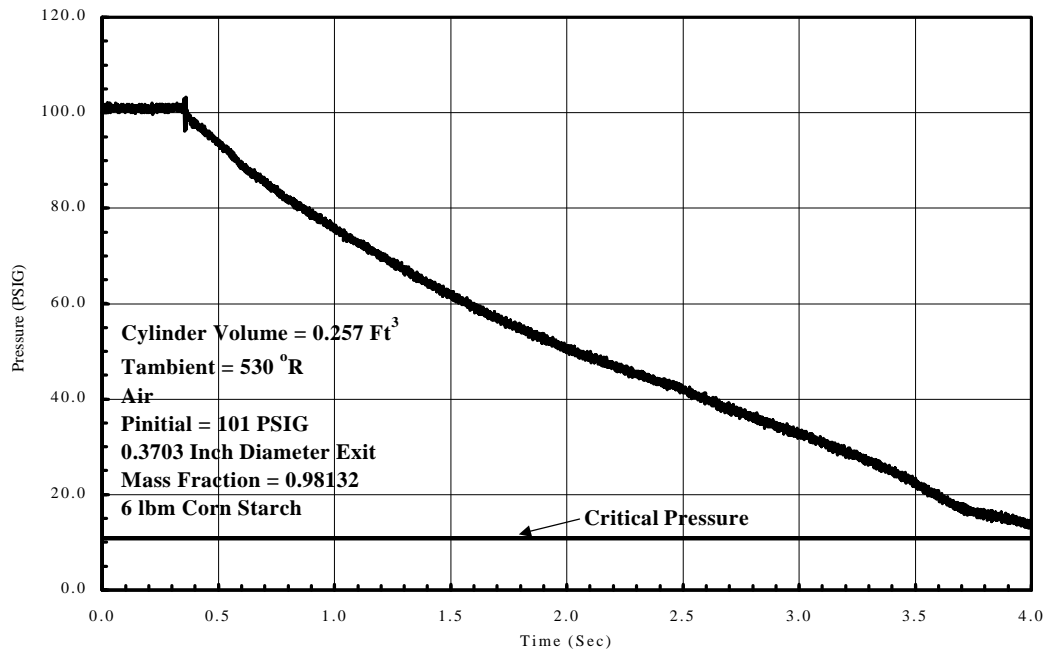


Figure 7.41 Discharge Test F-11 - Pressure Vs Time.

Measured cylinder residual powder levels were: 0.5 lbm for test F-9, 0.6 lbm for test F-10, and 1.6 lbm for test F-11. The physical geometry, materials, and starting conditions for all three discharges, as reported, were approximately the same; the cause of the apparently high residual level of corn starch in test F-11 is not clear.

Tests F-9 and 10 have an apparent inflection point approximately 0.2 seconds into discharge, although the inflection itself is slight. Test F-11 does not seem to exhibit an inflection point.

#### 7.4.4 Vendor System Tests.

Numerous tests are performed on various configurations of a proposed pre-engineered system. Most of the test data generated by these discharges are considered proprietary by a system's manufacturer, and are generally not available to the engineering community except as may occasionally occur through published papers. Data from these tests is generally of limited value in validating the model, since test records consist of details of the physical geometry of the discharge system to be tested, basic information about the agent and operating conditions, and a small amount of test results, including discharge times, and residual amounts of agents remaining within system components after discharge. A few of these tests were made available for validation purposes in the early portion of this research. Given the testing now available as a result of the documented research, the vendor system tests are primarily of help in 1) getting a feel for typical system design parameters, and 2) looking at the issues of residual agent and constancy of the solids mass fraction. Discussion of these comparisons occurs in Sections 8.1.1 and 8.1.2.

## 8.0 Comparison of Test Results To Model Predictions.

The ultimate purpose of gathering test data was to provide a means of validating the analytical program model. As part of these studies, the various test configurations were modeled, and performance predictions made using the computer model. The results of the analytical simulations of these test configurations are shown in the following Sections.

### 8.1 WPI Tests.

#### 8.1.1 Cylinder-Alone Tests.

A summary of the tank alone tests is shown in Table 7.4. Comparisons of the results of the analytical simulations to test discharge configurations for source cylinder only discharges are shown in Figure 8.1 through Figure 8.7.

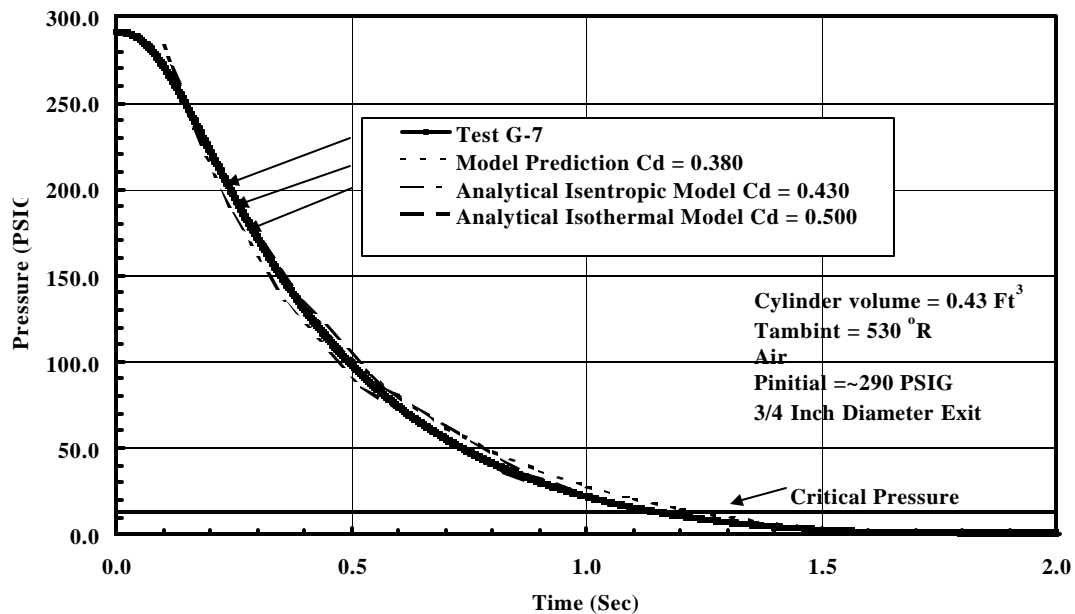


Figure 8.1 Test G-7 - Models Vs Discharge Test Response.

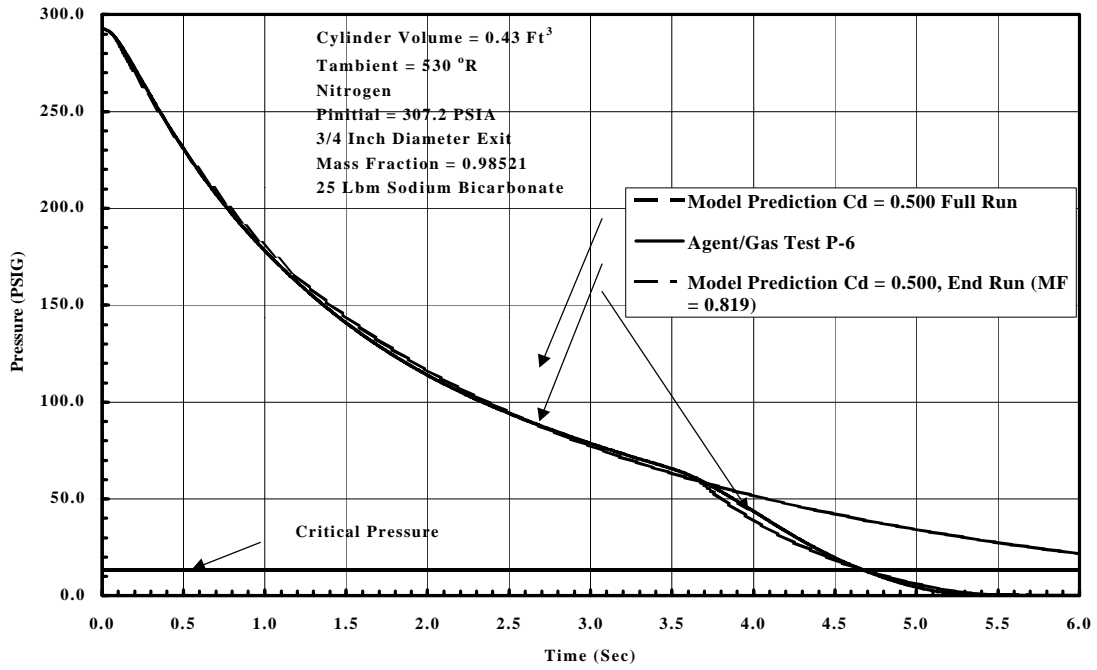


Figure 8.2 Test P-6 - Model Vs Discharge Test Response,  $C_d = 0.500$ .

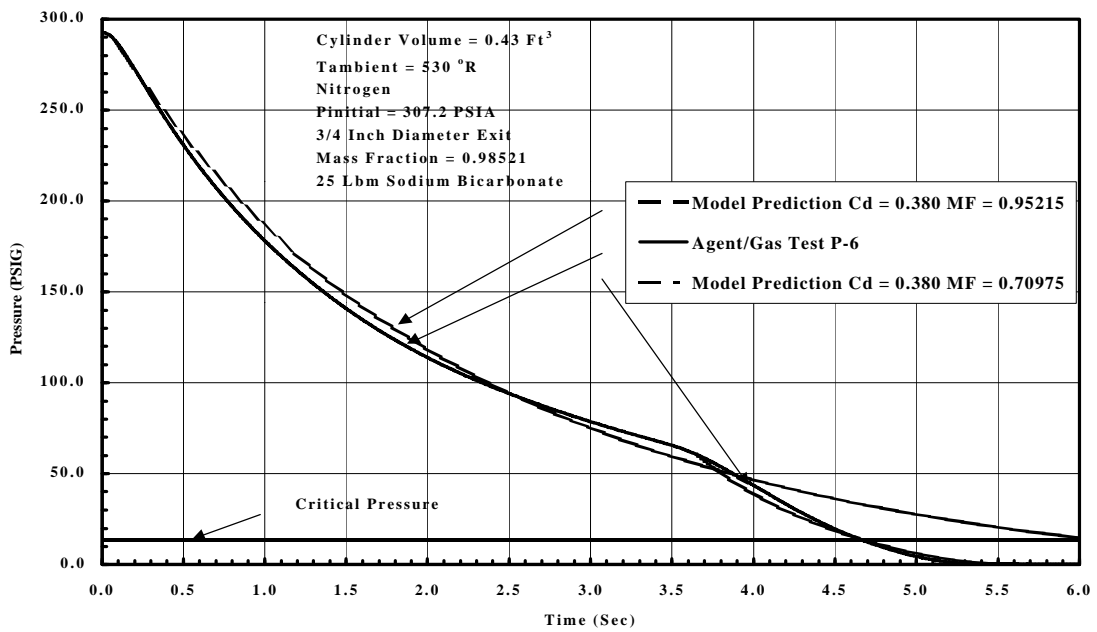
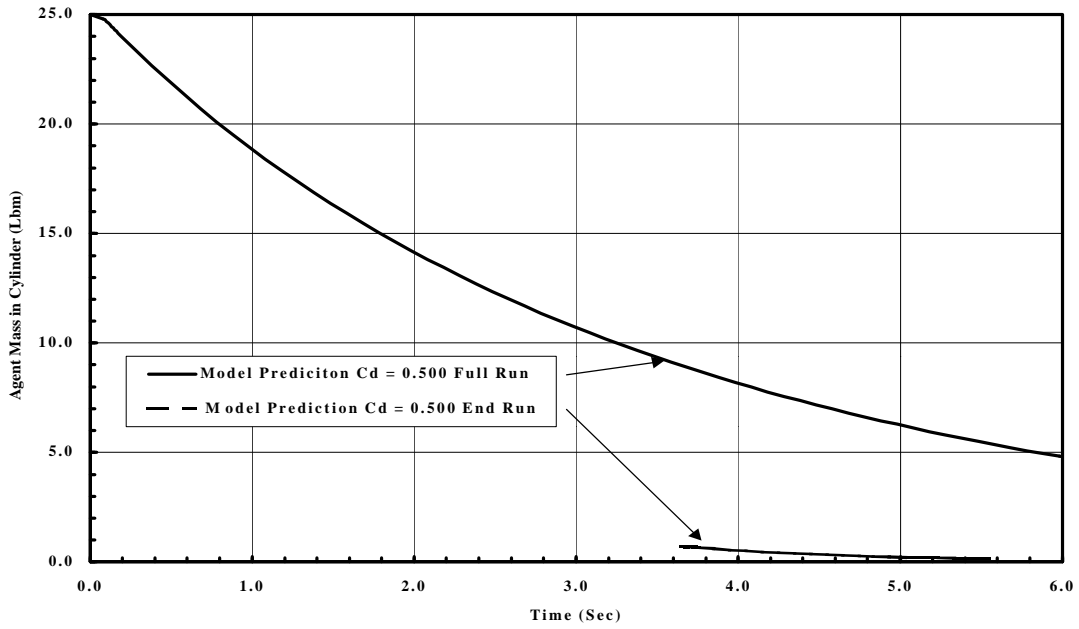
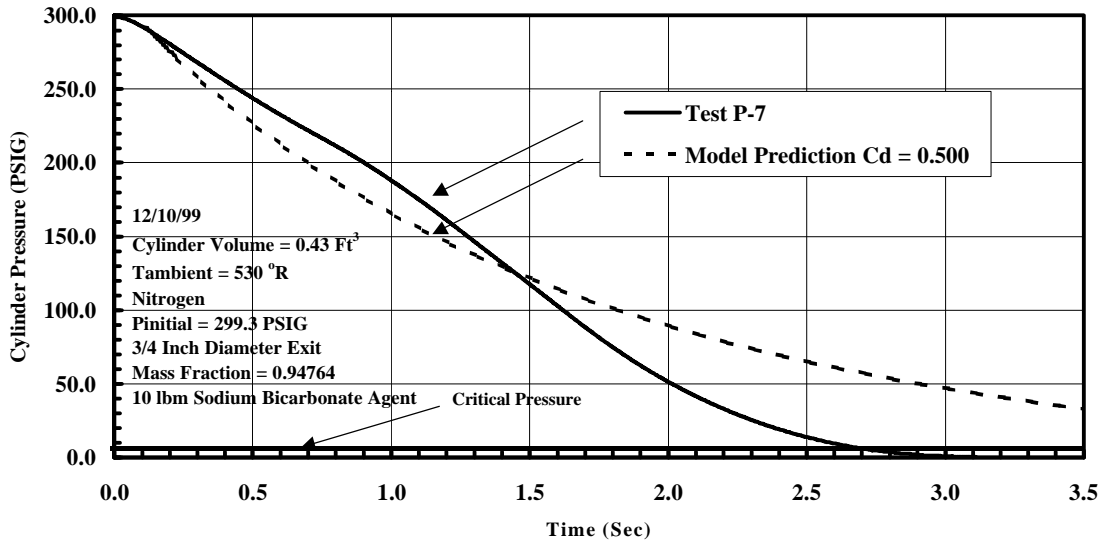


Figure 8.3 Test P-6 - Model Vs Discharge Test Response,  $C_d = 0.380$ .





**Figure 8.4 Test P-6 - Model - Mass Remaining in Cylinder.**



**Figure 8.5 Test P-7 - Model Vs Discharge Test Response.**

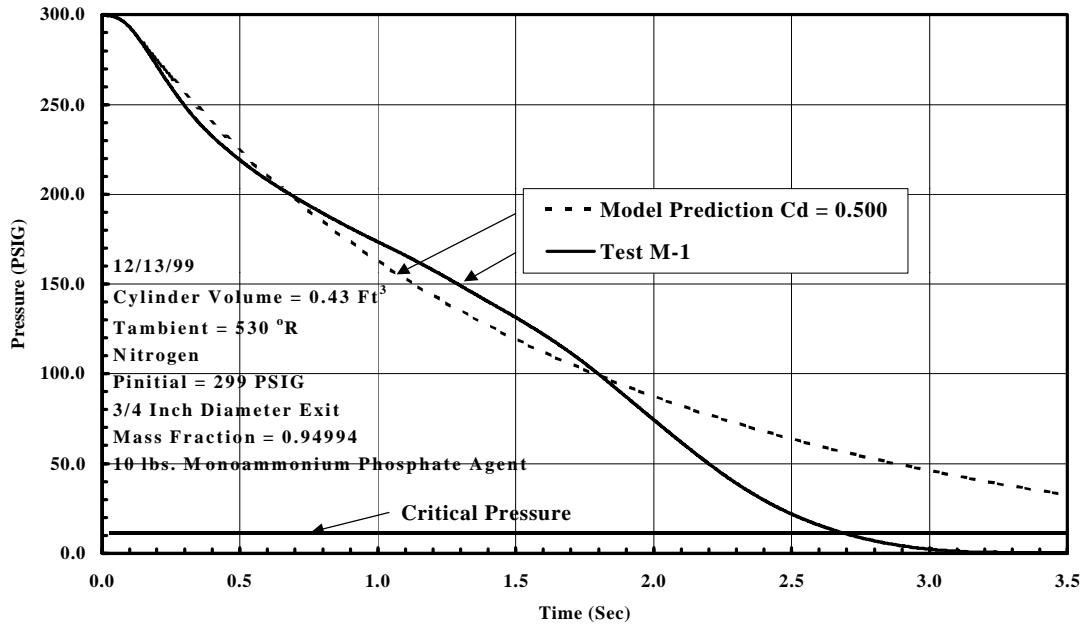


**Figure 8.6 Test M-1 - Model Vs Discharge Test Response.**

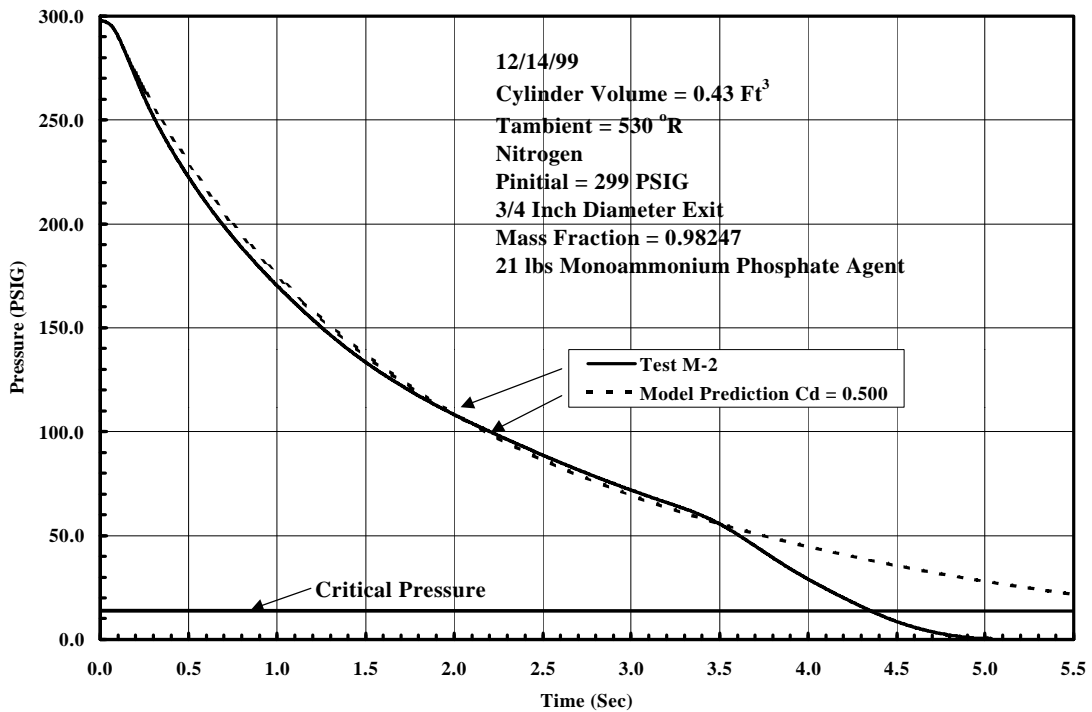


**Figure 8.7 Test M-2 - Model Vs Discharge Test Response.**

Figure 8.1 shows a very good match between the model and the test data. Note that, in order to avoid the initial inflection point caused by the opening of the cylinder valve, which is not included in the model, the initial time of the model was approximately 0.1 second after initiation of the discharge. The tight fit of model to data was achieved using a discharge coefficient for the valve/dip tube assembly of 0.380 (assuming a fully open valve.) A discharge coefficient of 0.430 worked well using the simplified tank discharge equation assuming isentropic flow conditions, equation (4.80). If the flow is assumed to be isothermal, a somewhat higher discharge coefficient of 0.500 successfully models the flow, using the simplified tank discharge equation assuming isothermal conditions, equation (4.88). On the average, for isentropic flow conditions, an average discharge coefficient of 0.400 should give satisfactory prediction results (assuming a dip tube of 14 inches length).

The modeling of test P-6 (Figure 8.2), shows good agreement between the model and the test data, up to the second inflection point, using a discharge coefficient of 0.500. The model tends to lag the test data by almost a full second at the time frame of the second inflection point. There is a divergence between the two pressure traces starting at the second inflection point, at approximately 3.7 seconds into discharge. As suggested earlier, the second inflection point is caused by events occurring within the source cylinder, events which are currently not modeled in the simulation program; thus the model does not duplicate all the events of relevance that occur during a mixture discharge. With a decreased mass fraction, a model calculation starting at the second inflection point closely matches the lattermost portion of the test data curve. In this

particular instance, the mass fraction of 0.819 (with a discharge coefficient of 0.500) was required to achieve these results. This would represent a decrease in mass fraction from its assumed constant value of 0.985. The mass fraction calculated based on the residual in the cylinder at the end of discharge was approximately 0.77.

An alternative approach is shown in Figure 8.3, in which the discharge coefficient of 0.380 derived from the gas-only discharges is used throughout the discharge simulation. However, the mass fraction was adjusted to improve the match of the model with the test data. As the Figure shows, a reduction of mass fraction from its initial value in the cylinder of 0.98521 to 0.95215 results in an excellent match of the model to the data, up to the second inflection point. After the second inflection point, a further reduction in mass fraction, to 0.70975, gives a good match between model and test data. In order to achieve a reduced mass fraction in the cylinder, the mass of agent flowing through the exit assembly must be increased; i.e., the mass fraction downstream of the cylinder would have to be higher than that in the cylinder in order to both match the pressure trace, and the amount of agent discharged (P-6 had a residual in the cylinder of approximately 0.1 lbm). In order to achieve all these goals, the model needs to be able to allow the mass fraction to not be constant, both as a function of discharge system physical location, and as a function of time,

Figure 8.4 shows the calculated mass remaining in the cylinder as a function of time, for a discharge coefficient of 0.500. The constant mass fraction results in an overprediction of the mass remaining in the cylinder (approximately 2 lbm) versus the 0.639 lbm actually observed. Starting from the second inflection point, the mass

remaining after discharge is much closer to the observed mass remaining, using the lower mass fraction in the calculations.

The modeling of test P-7 (Figure 8.5) starts approximately 0.2 seconds after discharge initiation. The model, using a discharge coefficient of 0.500 shows an good overall fit between the model and test data for the first 1.5 second of discharge. The test data diverges downwards after this, to reach the critical pressure in the source cylinder at least 2 seconds before the model trace.

Test M-1, with 10 lbm monoammonium phosphate, was modeled starting approximately 0.2 seconds after discharge initiation. As Figure 8.6 shows, the initial inflection point, when the cylinder valve opens, is not reflected in the model pressure trace. However, for most of the first 1.8 seconds, the match between model and test data is again good. The model diverges from the test data at approximately 1.8 seconds, a little later than the divergence seen by test P-7, charged with 10 lbm of sodium bicarbonate. The behaviors of the model and pressure data for tests P-7 and M-1 are quite similar – both models match the test data fairly well, up to the second inflection point; both tests have reduced loads of their respective agents. The reduced level of agreement between the test data and model for tests P-7 and M-1 reflects the lower level of agent in the cylinder for these tests. The agent powder reaches the bottom of the dip tube faster than for a full load of agent, and is affected by interaction with the bottom of the dip tube for a greater portion of discharge than the powder in the full load discharge tests.

Like tests M-1 and P-7, test M-2 (Figure 8.7) strongly resembles test P-6. Both tests (P-6 and M-2) have the manufacturer's recommended maximum agent loads. The

model prediction again shows good agreement with the pressure trace of M-2 (using a discharge coefficient of 0.500), up to the second inflection point.

The residual agent mass in the cylinder after discharge was measured only for test P-6, a mass of 0.1 lbm (see Table 7.6.) Assuming a constant solids mass fraction, the residual mass that should be left over can easily be calculated. By this calculation, the theory predicts a residual mass of 2.074 lbm for this discharge test, compared to the observed residual mass of 0.100 lbm (Table 8.1). Using the residual mass actually observed, the cylinder had an actual mass fraction of 0.770 at the end of discharge. As a result, a model properly reflecting actual behavior of a dry chemical system should allow for some variation in the mass fraction with time, if not also with location in a configuration. A tabulation of the predicted and observed cylinder residuals, and comparisons of mass fractions is shown in Table 8.1, with discussion of the consequences in Section 8.12.

### 8.1.2 Cylinder-Pipe-Nozzle Tests.

A summary of the cylinder-pipe-nozzle tests is shown in Table 7.5. Comparisons of the results of the model predictions to the test discharges are shown in Figure 8.8 through Figure 8.14.

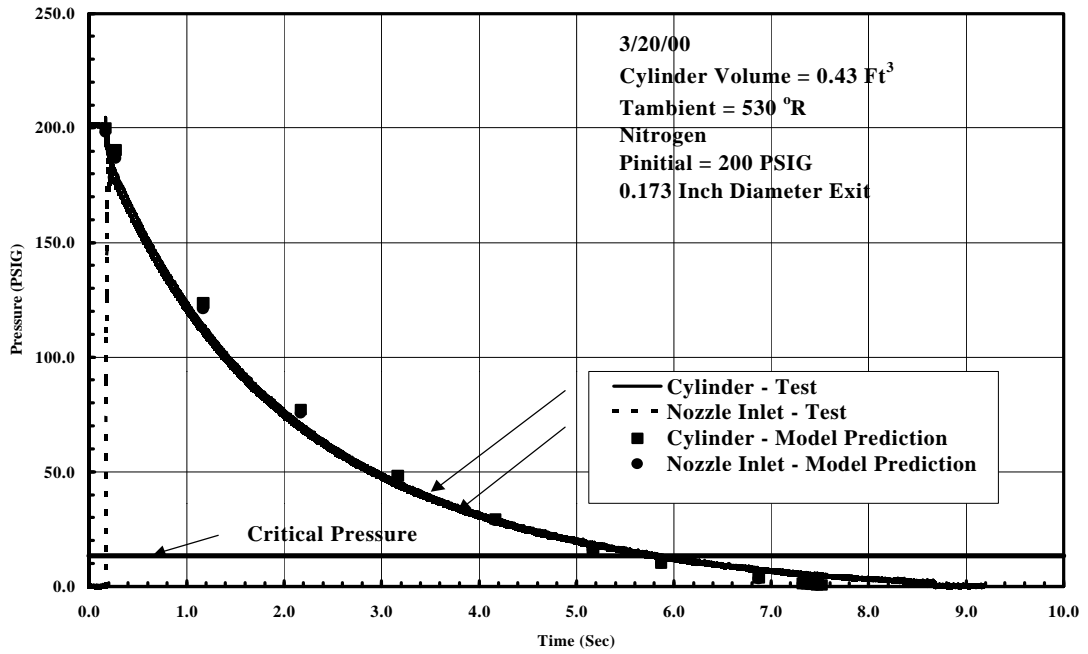


Figure 8.8 Test PG-1 - Comparison of Model Prediction and Test Data.

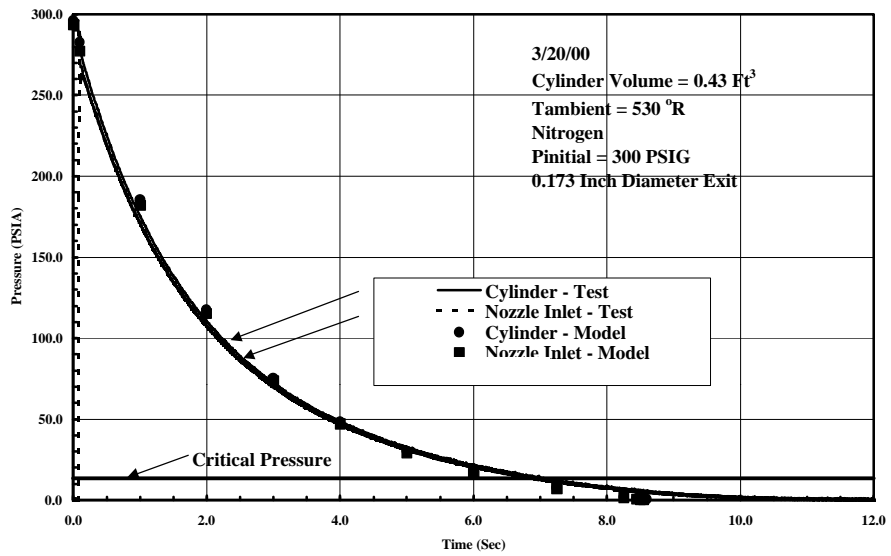


Figure 8.9 Test PG-2 - Comparison of Model Prediction and Test Data.

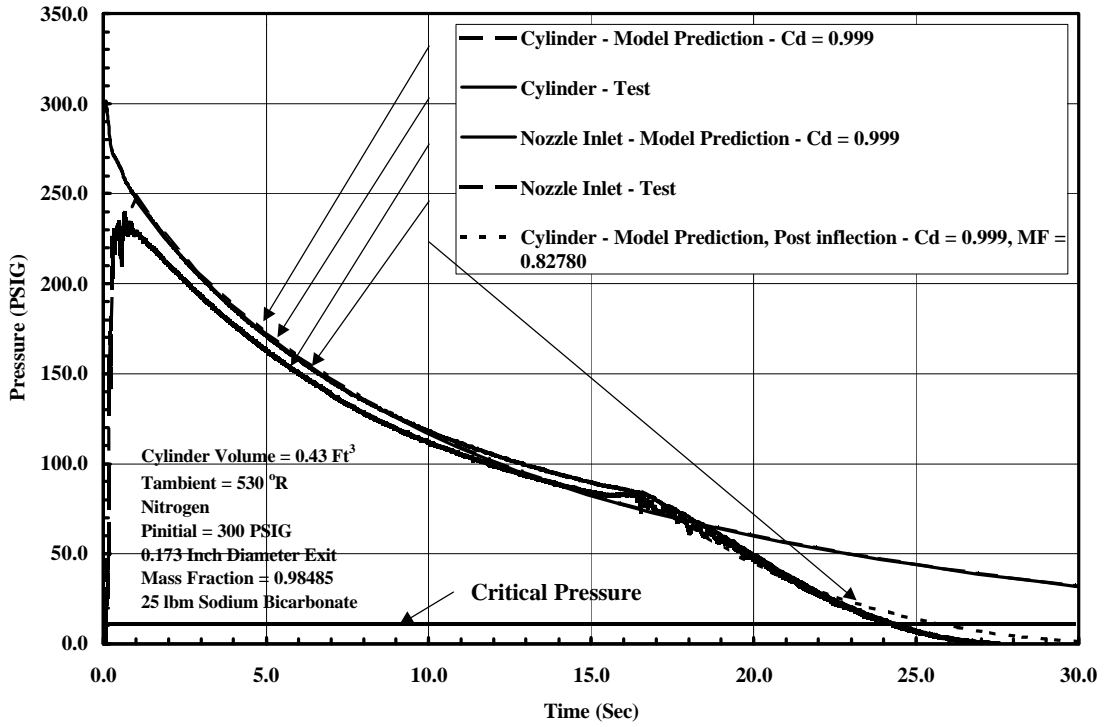


Figure 8.10 Test PNS-1 - Comparison of Model Prediction and Test Data.

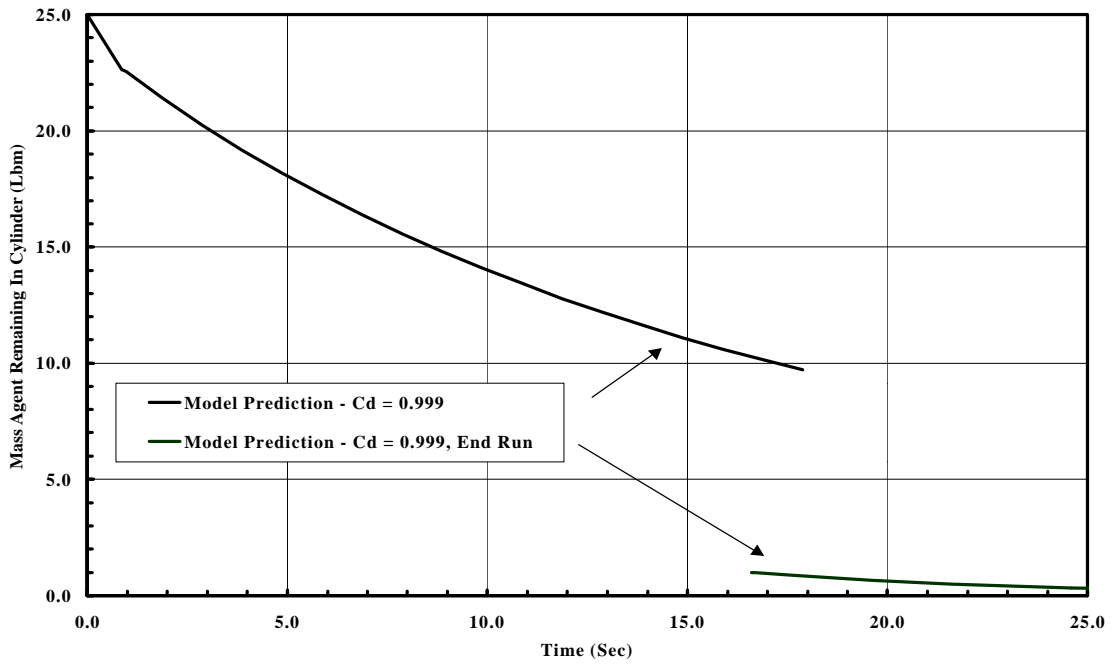


Figure 8.11 Test PNS-1 - Model - Mass Remaining in Cylinder.



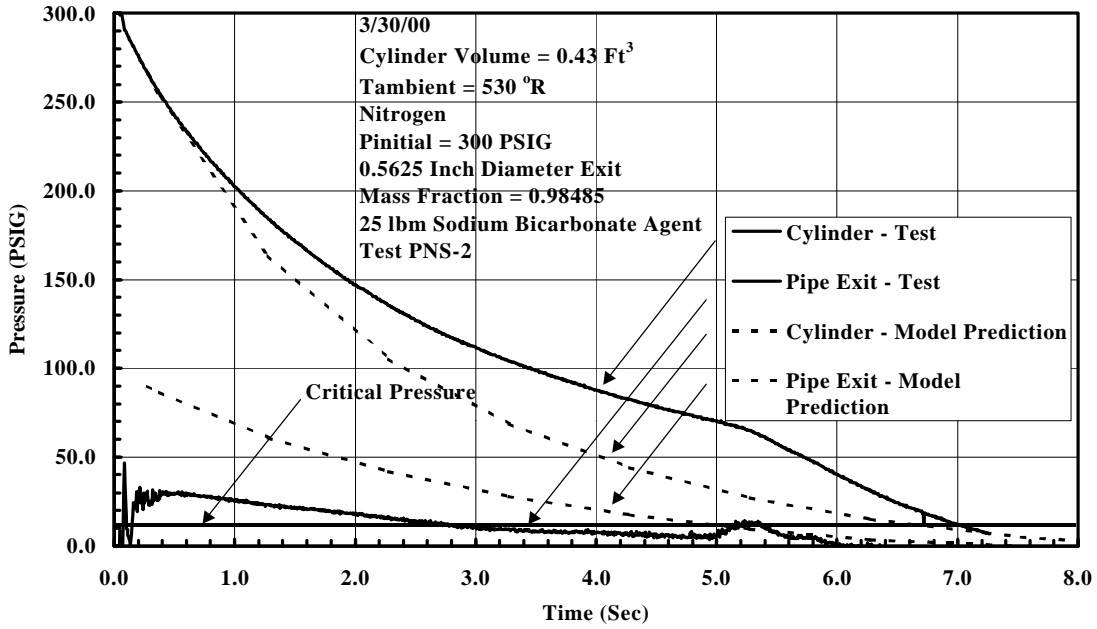


Figure 8.12 Test PNS-2 - Comparison of Model Prediction and Test Data.

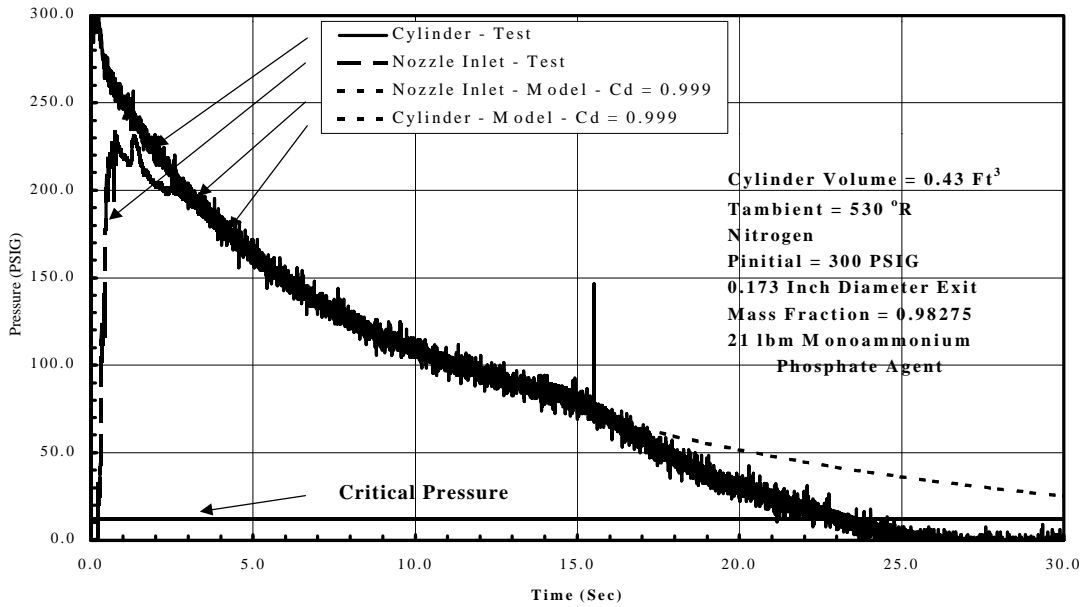
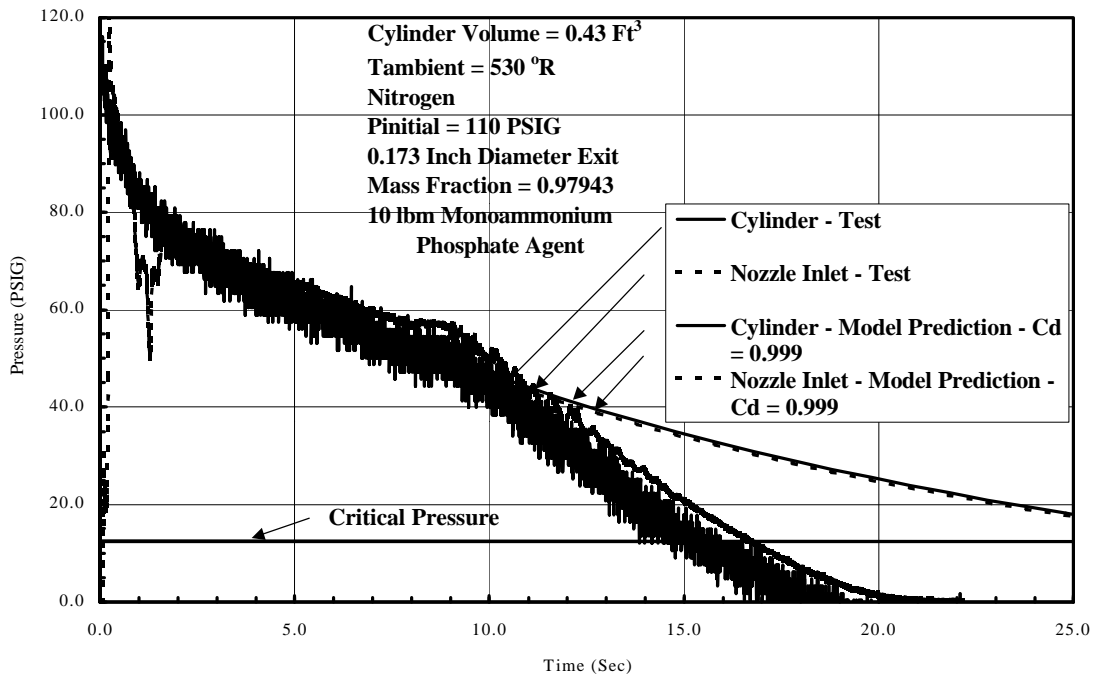


Figure 8.13 Test PNM-1 - Comparison of Model Prediction and Test Data.



**Figure 8.14 Test PNM-2 - Comparison of Model Prediction and Test Data.**

As with test G-7, the model predictions of tests PG-1 and PG-2 match very closely to the model test data, using a discharge coefficient of 0.999.

Predictions of the sodium bicarbonate discharges (PNS-1 and PNS-2) show good overall agreement between the model and test pressure traces, using a discharge coefficient of 0.999. The model prediction of PNS-1 correctly show that the pressure drop between the upstream and downstream ends of the 8-foot pipe are minimal with the nozzle downstream of the pipe. For test PNS-2, the model correctly shows the greater pressure drop occurring when there is no nozzle at the downstream end of the pipe. In PNS-2, the nozzle inlet pressure is predicted to be higher than actually observed, a reflection of the limited accuracy of the friction factor model implemented, as well as the use of a constant mass fraction in the model at all locations. As before, the second

inflection point is not reflected in the model predictions, again confirming that the event resulting in the inflection point occurs in the source cylinder, and not in the downstream piping network. For both PNS-1 and PNS-2, the model predictions were started approximately 1-2 seconds after discharge initiation, to avoid the effects of opening of the valve, and initial transience at the nozzle inlet caused by inflation of the piping network.

While the larger range of reported data in the source cylinder in the PNM-1 and PNM-2 traces makes judging the accuracy of the model predictions more difficult, it is clear from Figure 8.13 and Figure 8.14 that the model makes a good prediction of the test results, using a discharge coefficient of 0.999, up to the second inflection point. The models for both tests were started 1-2 seconds after discharge initiation, to avoid valve opening phenomena, and to avoid phenomena involved in inflation of the piping network. Both these tests included a nozzle; and as with the PNS tests, the model correctly indicates that the pressure drop from the source cylinder to the nozzle inlet is minimal with the nozzle present.

Residual agent masses in the cylinder after these tests are shown in Table 7.6. A comparison of the predicted and measured agent residual masses in the cylinder after discharge results in the following:

Test	Initial Mass Fraction (“Constant”)	Predicted Tank Residual Mass (lbm)	Actual Tank Residual Mass (lbm)	Termination Mass Fraction
P-6	0.98521	2.074	0.100	0.77000
PNS-1	0.98485	2.024	0.639	0.95516
PNS-2	0.98485	2.024	0.232	0.88516
PNM-1	0.98275	1.774	0.603	0.95287
PNM-2	0.97943	1.483	0.291	0.90651

**Table 8.1 Comparison of Predicted and Actual Cylinder Powder Residual Mass - WPI Tank-Pipe-Nozzle Tests.**

A comparison of the predicted and actual residual levels in the cylinder is shown in Figure 8.15, for test PNM-2. The level of residual agent in the cylinder, for both the predicted and actual residuals, was determined from the equation:

$$m_{residual} = m_{agent} \left( \frac{H_{cyl} - L_R}{H_{cyl} - H_{fb}} \right) \quad (8.1)$$

where  $m_{residual}$  is the residual agent in cylinder (lbm),  $m_{agent}$  is the original mass of agent in cylinder (lbm),  $H_{cyl}$  is the total length of cylinder, from top of flange to bottom of lower dome (inches),  $H_{fb}$  is the fill level of agent before discharge, from top of cylinder flange (inches), and  $L_R$  is the level of residual in cylinder after discharge, from top of cylinder flange (inches).

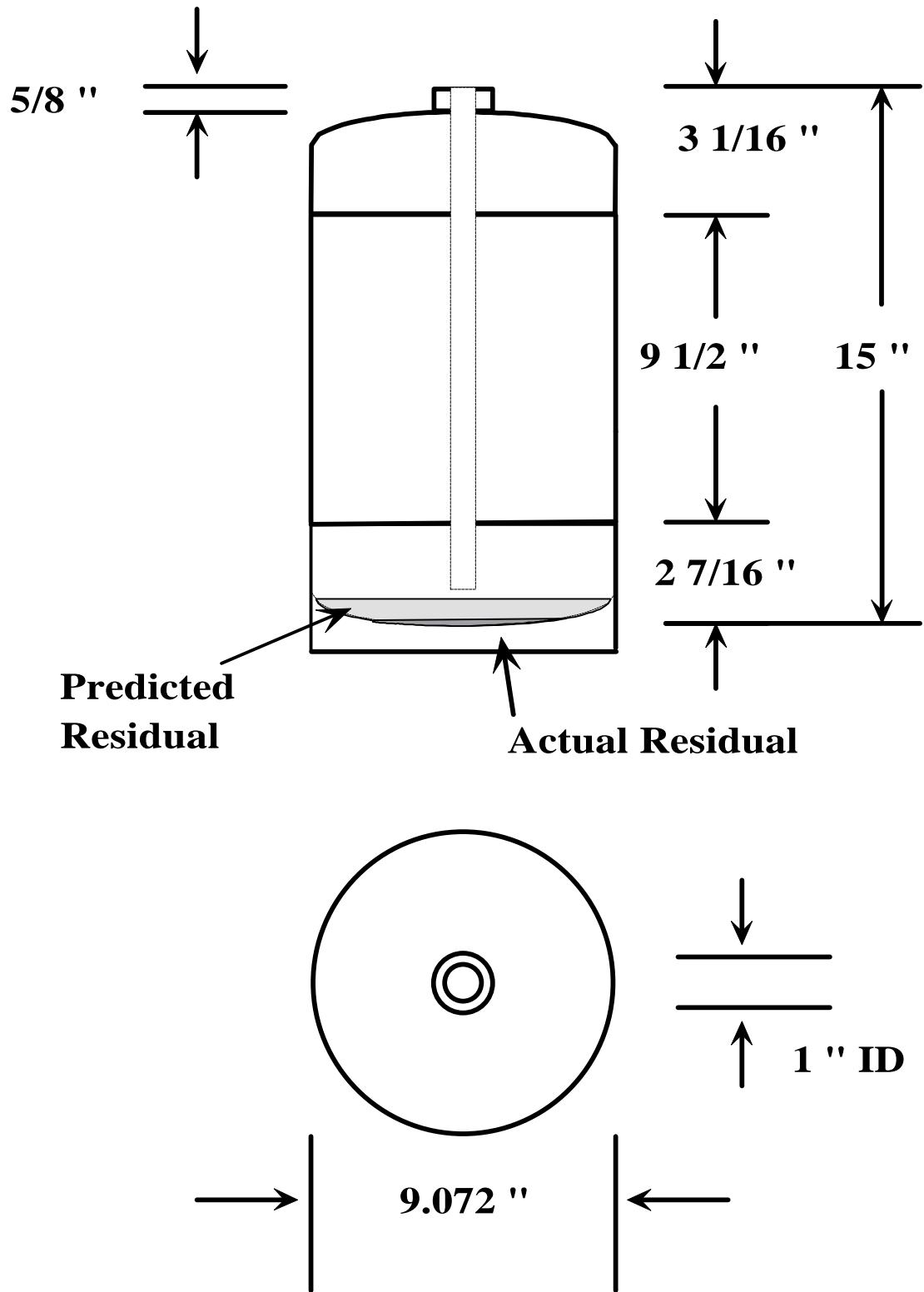


Figure 8.15 Test PNM-2 - Comparison of Predicted and Actual Residual Levels.

All of these tests included cylinders with full loads of agent (25 lbm sodium bicarbonate, 21 lbm monoammonium phosphate), except for PNM-2, with 10 lbm of agent. Test PNS-2 was run with cylinder and pipe only, and no nozzle. The constant mass fraction assumption resulted in consistent overprediction of the cylinder residual. This is due to the underlying assumption of a homogeneous mixture of agent and gas (at least during discharge, although how the agent in the cylinder is supposed to go into suspension in the gas, much less how it is supposed to remain in suspension for some unknown time prior to discharge is not specified). If the powder is carried from the cylinder as a result of entrainment, and generally acts approximately like a powder in a hopper, this, too, would result in residual amounts of agent after discharge, but with more complex behaviors in the cylinder, behaviors that would possibly result in different residuals. Calculation of the termination mass fraction based on the actual residuals shows mass fractions that are lower; in some cases dramatically lower, than the values predicted by the constant mass fraction assumption. Tests PNS-3 and PNS-4 were omitted; while both were found to have initial mass fractions of 0.98485, PNS-3 included sodium bicarbonate without additives, and PNS-4 had the half-length dip tube. The results were residuals significantly different from PNS-1, whose agent load and piping geometry was otherwise identical. Since these two tests, with only changes in the cylinder and its contents, had such different results from PNS-1, it is clear that while the constant mass fraction assumption may yield good predictions for some portions of a discharge, it clearly omits behaviors of the mixture in the cylinder that influence the discharge time and system behavior, as evidenced by the duration and shape of the pressure-time traces for agent/gas mixtures.

Tests PNS-3 and PNS-4 were not modeled with the program. Test PNS-3 was identical to test PNS-1, except for using a load of 25 lbm of sodium bicarbonate without the flow additives included in the powder mix by the manufacturer. In the current model there is no way to distinguish the two powders by the presence or absence of these additives, or their effects on material properties of the powders. As a result, the prediction for test PNS-1 would equally apply to this test. Test PNS-4 was identical to test PNS-1 except for the use of the 7-inch dip tube, instead of the standard 14-inch tube. The model currently has no means of distinguishing between dip tubes, at least without a more detailed modeling of the valve assembly. However, some idea of the impact of the shorter dip tube can be seen in comparing tests with the same dip tube, but different agent loads, such as tests PNM-1 and PNM-2 (21 lbm monoammonium phosphate, and 10 lbm, respectively.) Use of a reduced amount of agent, at a reduced pressure, could be used to approximately simulate a shorter dip tube scenario.

## **8.2 *Kidde International UK Tests.***

A summary of the discharge tests conducted by Kidde International included in these studies is shown in Table 7.7. Comparisons of the results of the analytical simulations to test discharge configurations for source cylinder only discharges are shown in Figures Figure 8.16 through Figure 8.17.

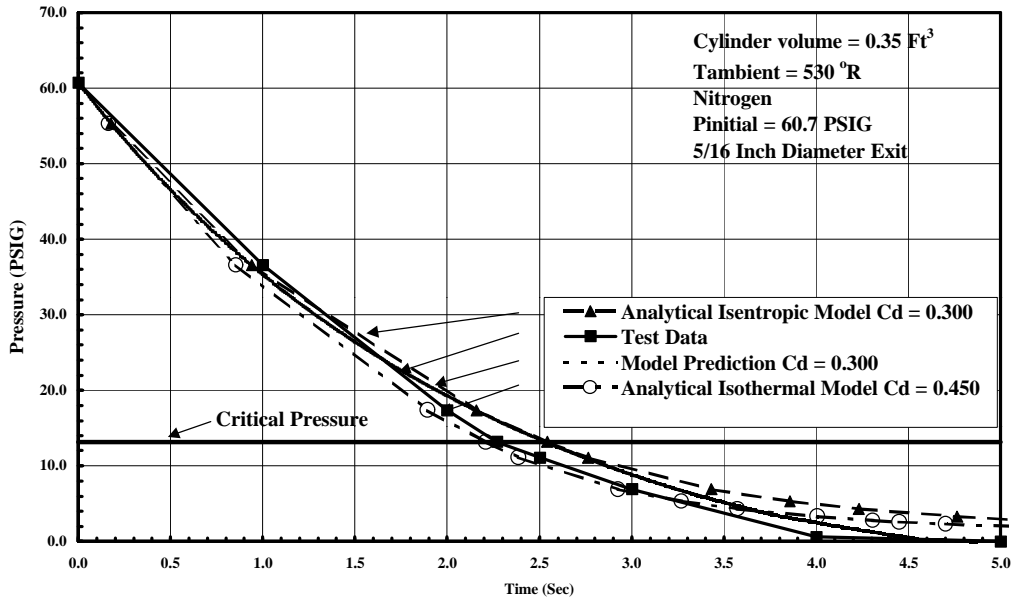


Figure 8.16 Test UK-F6 - Comparison of Model Prediction and Test Data.

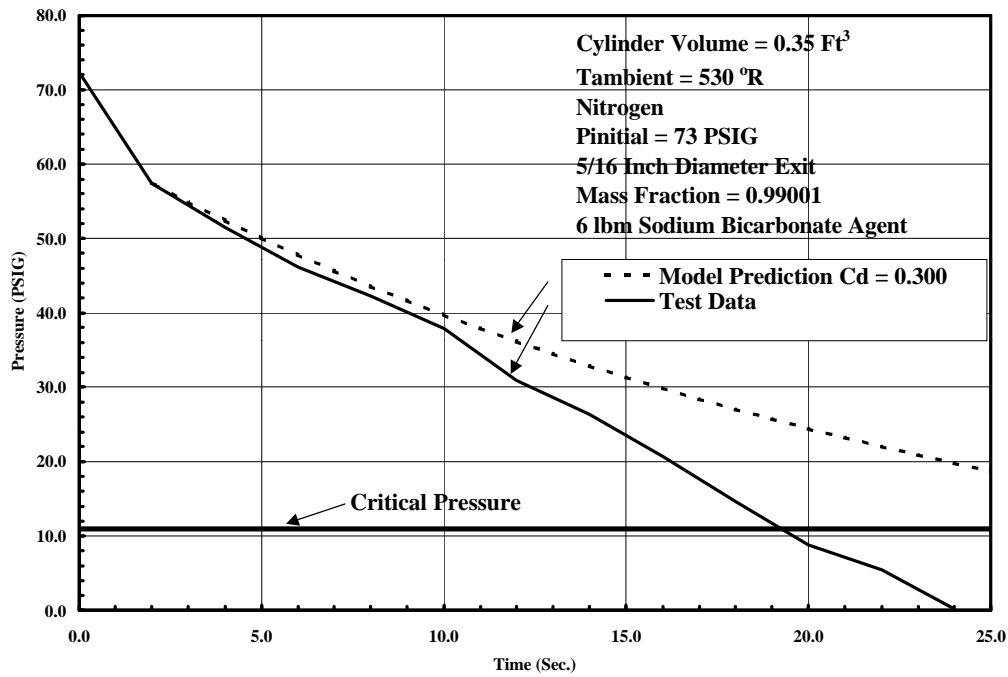


Figure 8.17 Test UK-F7 - Comparison of Model Prediction and Test Data.



Test UK-F6 is a gas-only discharge; as with the previous gas-only discharges, the model performs well, giving a good prediction of actual system performance. For this dip tube/exit assembly, a discharge coefficient of 0.300 for isentropic modeling, and 0.450 for isothermal modeling, gives a good match between prediction and test data.

Test UK-F7 included 6 lbm of agent; selecting a starting point for the modeling 2 seconds after initiation of the test discharge, a good modeling was achieved, using a discharge coefficient of 0.300, through the 10 second time frame. Note that an initial run was made to determine the mass fraction in the configuration, and the approximate mass in the cylinder at the 2-second time frame. An apparent inflection point in the test discharge occurs at this point, resulting in a divergence of the model prediction and discharge test curves.

Figure 8.18 shows a comparison of the mass measured in the cylinder during discharge compared to the model prediction of mass remaining in the cylinder.

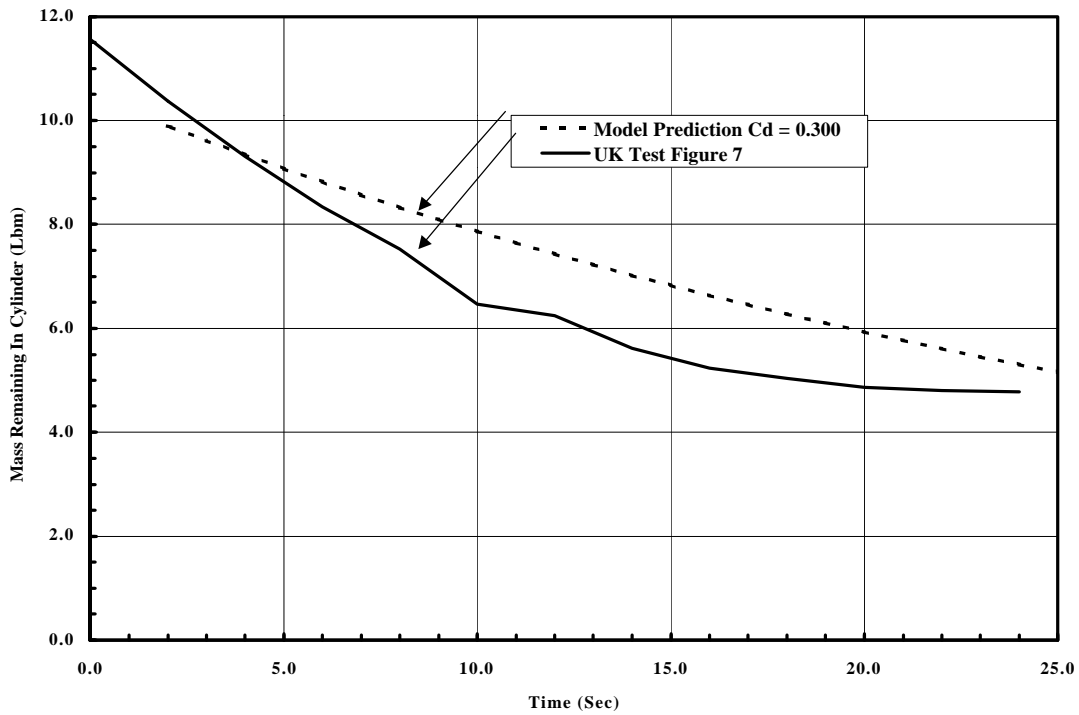


**Figure 8.18 Comparison of Predicted and Actual Agent Remaining in Cylinder, Kidde International - Test UK-F7.**

For the bulk of the discharge, the model, with the built-in assumption of a constant solids mass fraction, overpredicts the amount of mass remaining in the cylinder. “Forcing” the solids flow to be higher would require a higher mass fraction in the piping (at least in the cylinder exit) than allowed for by a constant mass fraction. Note that, at the apparent end of discharge (approximately 24 seconds), while the prediction and observed masses start to converge, the prediction is still higher than the actually observed residual agent mass.

### **8.3 Corn Starch Tests.**

A summary of the corn starch discharge tests conducted by Fenwal Safety Systems included in these studies is shown in Table 7.8. Comparisons of the results of the analytical simulations to test discharge configurations for source cylinder only discharges are shown in Figure 8.19 through Figure 8.21.

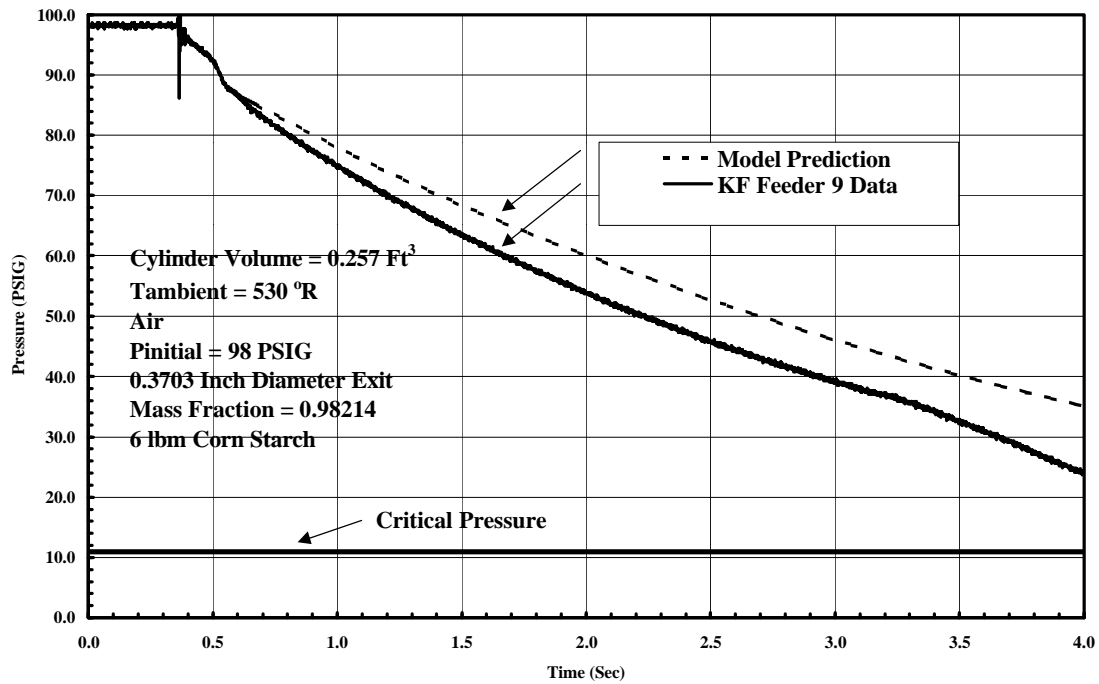


**Figure 8.19 Test F-9 - Comparison of Model Prediction and Test Data.**

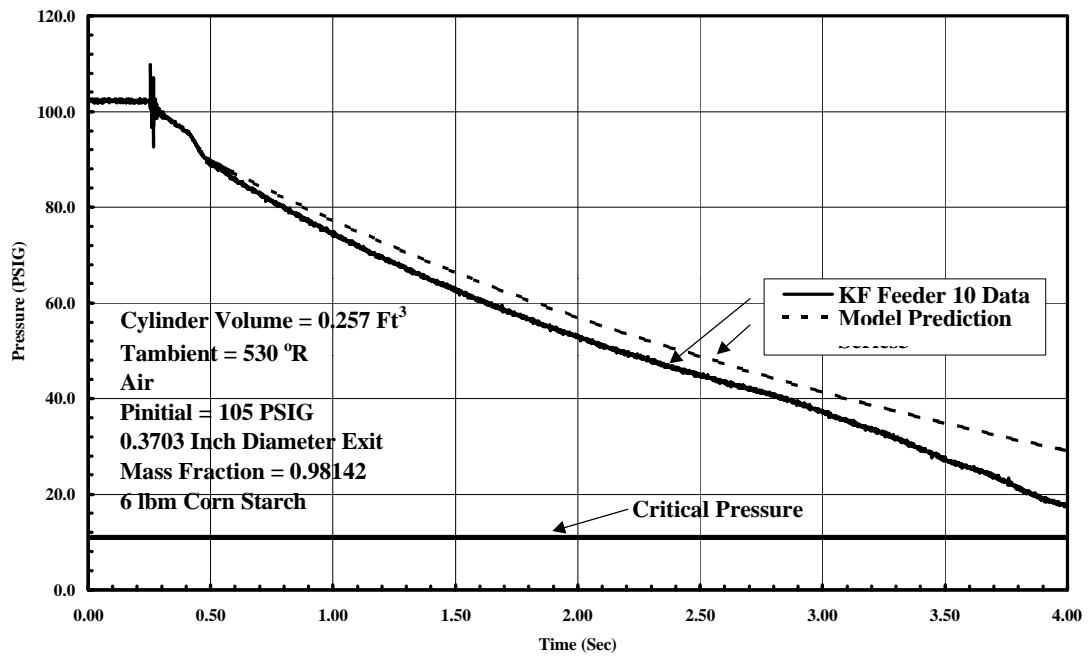


Figure 8.20 Test F-10 - Comparison of Model Prediction and Test Data.

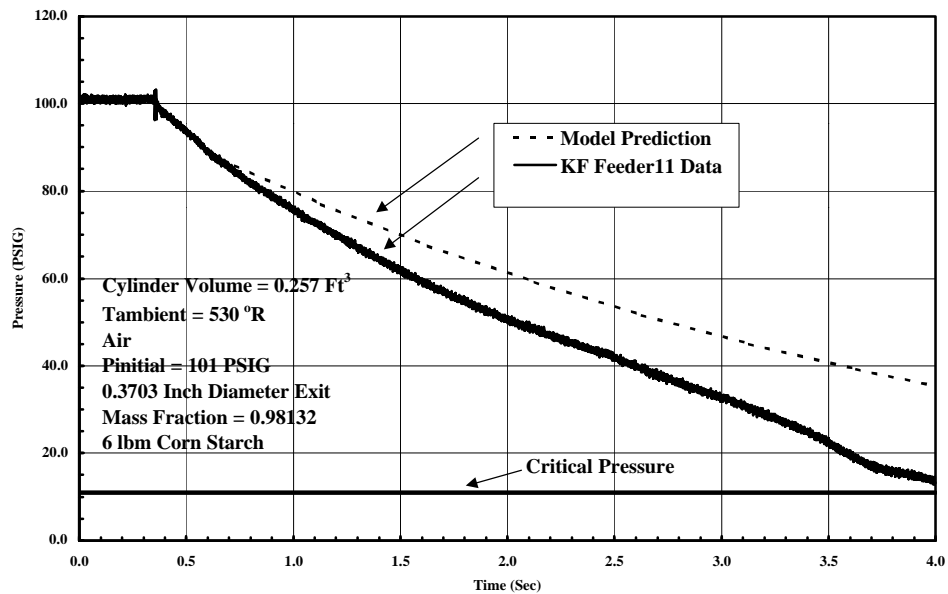


Figure 8.21 Test F-11 - Comparison of Model Prediction and Test Data.

A comparison of the model predictions to the test data suggests that, as for previous tests, the model prediction is conservative compared to discharge test data. The best prediction was for test F-10. Followed by test F-9, with the prediction for test F-11 lagging by as much as 1 second towards the end of the recorded data. The model predictions relative to the test data results are consistent with results observed in the previously discussed test results and comparisons.

Comparison of the predicted and actual cylinder residual mass at the end of discharge gives results as follows:

Test	Initial Mass Fraction (“Constant”)	Predicted Tank Residual Mass (lbm)	Actual Tank Residual Mass (lbm)	Termination Mass Fraction
F-9	0.98214	1.058	0.500	0.96442
F-10	0.98142	1.016	0.600	0.97012
F-11	0.98132	1.011	1.600	0.98858

**Table 8.2 Comparison of Predicted and Actual Cylinder Powder Residual Mass - Corn Starch Tests.**

As with the WPI tests (Table 8.1), the constant mass fraction assumption invariably seems to lead to incorrect predictions of residuals. Note that of all the documented tests, only test F-11 shows a slight increase in the termination mass fraction, whose calculation is based on the observed residual – it is not clear why this slight increase occurred. The general result is that while the assumptions of a constant mass fraction, and homogeneous mixture in the cylinder results in the presence of a termination residual, and good predictions for some portions of a discharge, they do poorly in

modeling the actual flow of mass out of the cylinder, and poorly predict the amount of residual agent at termination of discharge.

#### **8.4 Vendor System Tests.**

Comparisons of the vendor tests to model predictions are limited due to the proprietary nature of the system tests, and the data generated. Also, the limited nature of the data gathered, primarily discharge times and powder mass distribution, make using the data of limited value in validating the behavior of the predictive model. Predictions with early versions of the model were compared to vendor testing with a discharge system consisting of 25 lbm sodium bicarbonate mixture pressurized to 360 psia with nitrogen. For a pipe network with an equivalent length of 110 feet of 1 inch ID pipe, tee split, followed by 11 equivalent feet of  $\frac{3}{4}$  inch ID pipe and nozzles, the early version of the model predicted a discharge time of 7 seconds, compared to an actual discharge time of 10 seconds. A test discharge using 21 lbm monoammonium phosphate agent, 66.5 equivalent feet of  $\frac{3}{4}$  inch ID pipe and a nozzle, the early model predicted a discharge time of 22 seconds, compared to an measured discharge time of 28 seconds. The early model predictions showed no inflection points, as events occurring in the system during discharge were not included in this version of the model.

Examining the source cylinder residual powder data reveals that, like the previously discussed tests, the residuals predicted assuming a constant solids mass fraction do not compare well with the powder residuals actually observed after discharge. Observed cylinder residuals showed 0.200 to 0.400 lbm of agent remaining after discharge. Predicted residual levels were significantly greater, on the order of 2 lbm.

These inconsistencies are consistent with residual discrepancies observed in the

previously discussed test results. Discharge times for the system data available, when modeled, show similar behaviors to the results observed earlier.

### **8.5 Assessment of Model Sensitivities and Accuracy.**

The ability of a program to accurately predict phenomena depends in part on how well the implemented model reflects the phenomena being modeled. It also depends on the accuracy of variable parameters, both those entered by the program user, and any parameters programmed in by the program developer. For example, if material properties are inexact, there will be some distortion in the predicted results, the extent of the distortion depending on the sensitivity of the calculations to the variance of the inputs from correctness.

The sensitivity of a program's response to variations in inputs is in part a function of the developed model. The equations describing the phenomena may show a sensitivity of the model to small changes in one parameter, while gross changes in another may only result in minor variations in the output. These sensitivities represent the relative importance of various input parameters to the model describing the phenomena. They tell the designer which design parameters must be strictly specified, with tight tolerances, to obtain the desired results, and which parameters are more flexible, and possibly amenable to modifications meeting other design criteria (example: whether a wall is load-bearing or not in part determines the design constraints that must be used to design that structure).

Sensitivities of the dry chemical fire suppression delivery system simulation program were examined. Results are broken down into three categories: material properties, which are linked to each other; physical properties, as in the cylinder, which

again cannot be independently changed; and parameters describing the rest of the piping network, which can be (more or less) independently changed. Finally, several parameters not fitting in any other category are examined separately.

Parameter sensitivities were analyzed using the tank-pipe-nozzle configuration shown in Figure 6.1, used in the previously described system discharge tests. Baseline input parameters, and their variable values for this configuration, are shown in Section 6.0.

#### 8.5.1 Material Parameters.

Parameters in this category include the gas Ideal Gas Law Constant, specific heat at constant pressure, specific heat at constant volume, and solids density and specific heat. For a given gas or solid, these are properties of the material, and while there may be some variance in the accuracy of the numerical values, the user cannot arbitrarily raise or lower the numerical values of any one parameter. In essence, the user selects the material to be analyzed, and enters specific values for the properties, based on testing, research, or some other reference source.

As a result, examination of program accuracy and sensitivities for these parameters is limited to the impact of inexactness of data entry upon the predicted performance. For example, if the user enters, for the Ideal Gas Law constant “55.0” rather than “55.15”, what is the impact upon the results? In essence, how does the inaccuracy of the entered parameter distort the predicted performance?

Plots of percent change in predicted time to reach unchoking as a function of percent changes in input parameters are shown in Figure 8.22 for the carrier gas, and Figure 8.23 for the solid powder. Figure 8.22 shows variance for the Ideal Gas Law



constant, specific heat at constant pressure, and specific heat at constant volume. Figure 8.23 shows variance for solids density and specific heat.

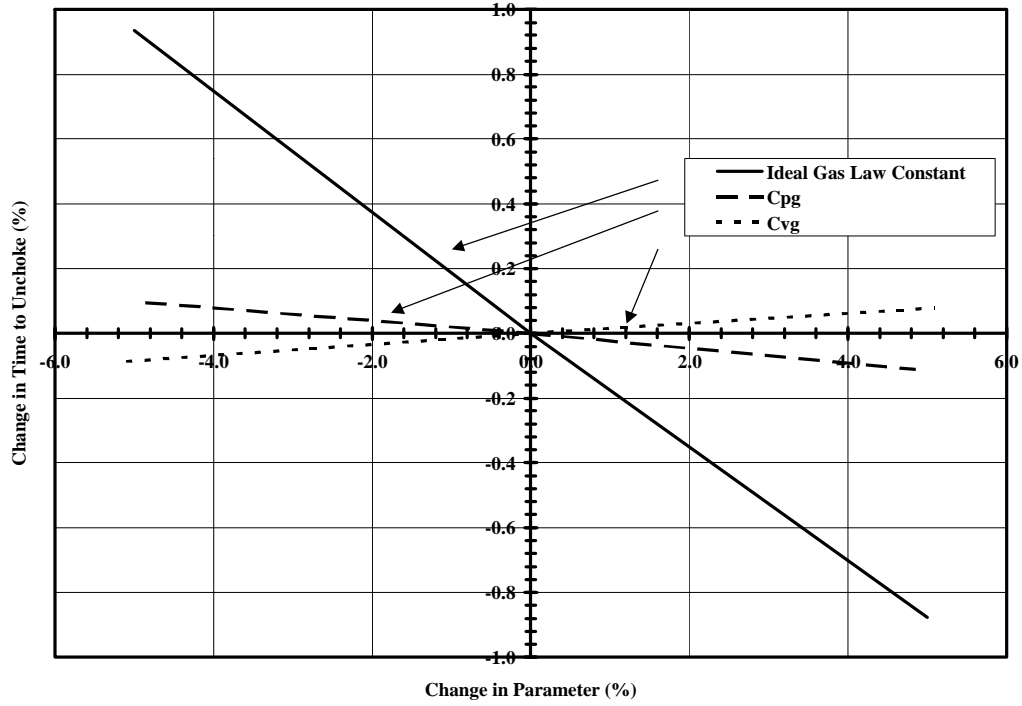


**Figure 8.22 Variance in Time to Unchoke as a Function of Gas Parameter Changes.**

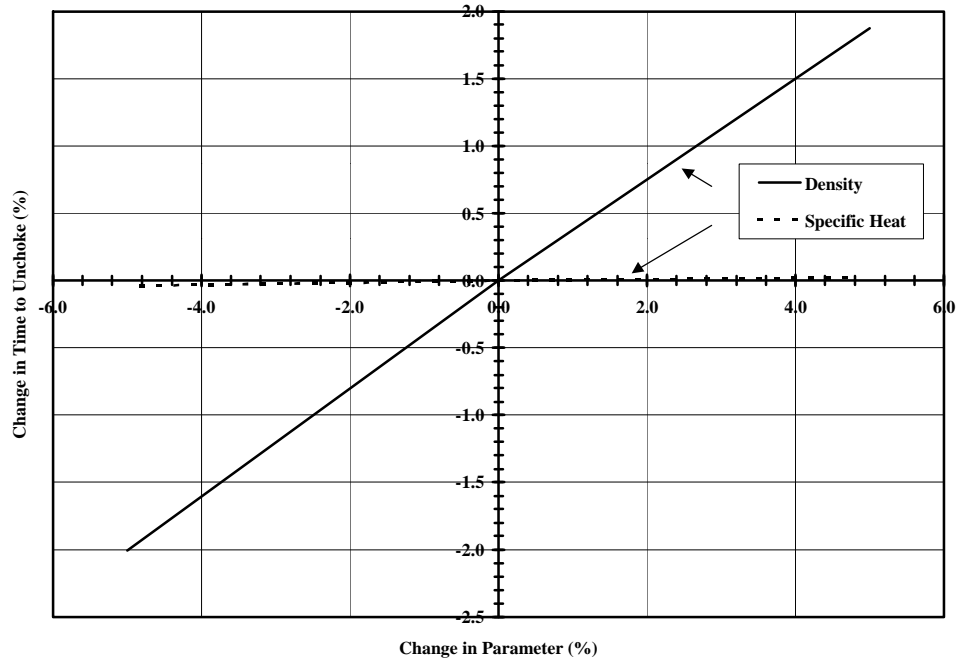


**Figure 8.23 Variance in Time to Unchoke as a Function of Solids Parameter Changes.**

As Figure 8.22 shows, the time to unchoke is relatively insensitive to variations in the specific heats. These gas parameters are part of the basis of the gas specific heat ratio  $\gamma_G$ , which in turn is part of the basis of the mixture specific heat ratio  $\gamma$ . The Ideal Gas Law constant  $R_G$  is used more directly, in Ideal Gas Law (both gas and mixture) calculations, as well as in speed of sound manipulations. As a result, the program is relatively more sensitive to inaccuracies in the Ideal Gas Law constant than to inaccuracies in either of the specific heats.

As Figure 8.23 shows, the time to unchoke is fairly sensitive to changes in the powder density, and almost completely insensitive to changes in the powder specific heat. As with the gas specific heats, the powder specific heat is a component of the calculation of the mixture specific heat ratio  $\gamma$ . The powder density is used extensively in the calculations, as part of the mass fraction and volume fraction, and in determination of the

mixture density. Also note that the percentage change in time to unchoke is affected almost twice as much by changes in the powder density as by changes in the gas Ideal Gas Law constant.

### 8.5.2 Cylinder Parameters.

Parameters in this category include cylinder initial pressure, temperature and cylinder volume. For this particular category, the mass of the agent and gas in the cylinder were held constant for changes in the parameters. Since these parameters are related through the Ideal Gas Law, it is impossible to change one without simultaneously affecting at least one of the others. For example, if the agent and gas masses and cylinder volume are held constant, a rise in pressure must also result in a rise in temperature. Throughout the analyses of these parameters, the mass of the agent and gas were forced to remain constant, since the intent was to investigate the impact of changes of the other cylinder parameters on discharge times of a presumably unchanging mass of agent and gas. For changes in the tank volume, material masses and temperature were held constant; thus changes in volume were accompanied by corresponding changes in initial pressure. For cylinder pressure and temperature, masses and volume were held constant, so that a change in pressure resulted in a change in corresponding change in temperature, and vice versa.

The results of the sensitivity studies for cylinder parameters are shown in Figure 8.24.

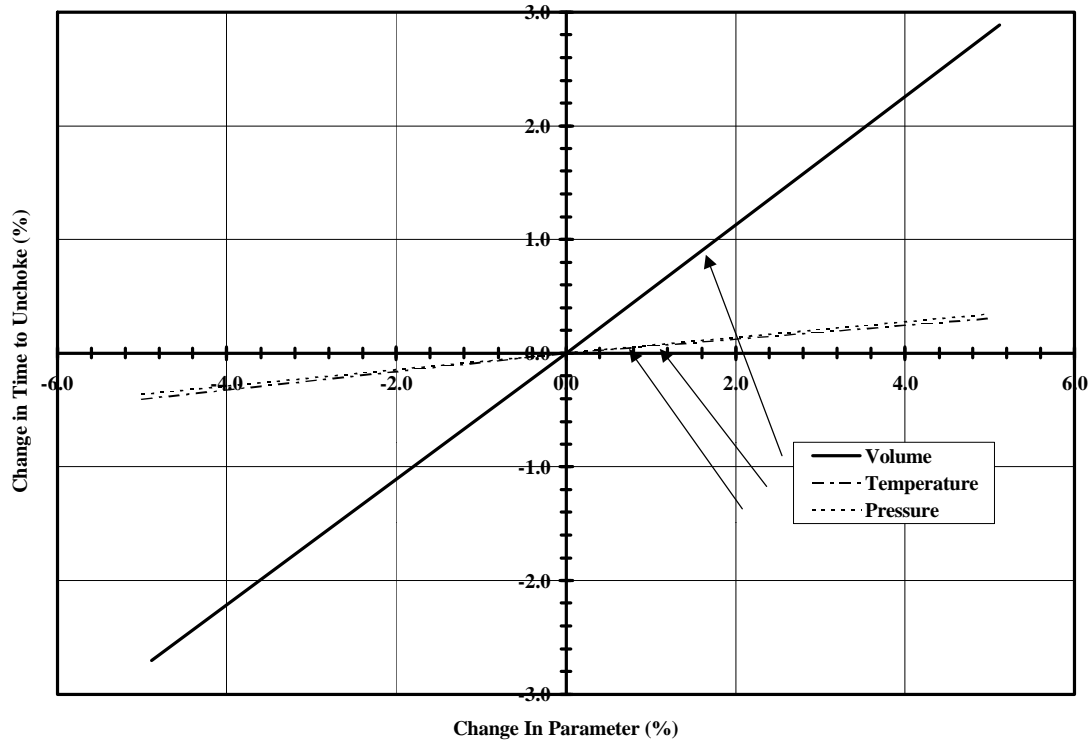


**Figure 8.24 Variance in Time to Unchoke as a Function of Cylinder Parameter Changes.**

As the Figure shows, for a fixed mass of agent and gas, the cylinder volume has a significant impact on discharge time. For the same mass of gas and agent, a larger cylinder means more volume, which is taken up by the gas, thus reducing gas pressure. The model, in this instance, predicts a somewhat longer discharge time for an increase in volume. For fixed material masses and volume, the pressure and temperature are linked closely together, thus resulting in almost no difference in variations of time to reach unchoking as a result of variations in these parameters. The results of the studies show a relatively large sensitivity (masses constant) of the program to cylinder volume, and relatively little sensitivity to small changes in pressure or temperature.

Note that as a part of these sensitivity studies, the influence of these parameters on the amount of mass of agent discharged was examined. The results indicated that increasing pressure, either by decreasing the cylinder volume, or increasing temperature, resulted in small but definite increases in the amount of mass discharged. Note that for manufactured systems in use in the field, the amount of mass discharged is already relatively high, >>90%, and the amounts of residual relatively small. As a result, large increases in the amount of mass discharged will probably not be possible (at least by adjustment of parameters available to the analyst in this program), although small improvements may be made.

### 8.5.3 Network Component Parameters.

This category includes input parameters describing the various network piping components, and the impact of their variation on model results. Most of these parameters can be varied independently of each other (exception: sudden contractions and expansions – if a parameter for these components changes – downstream diameter for instance, a component connected to that changing location must also change it's dimension, as well.)

The results of these sensitivity studies are shown in Figure 8.25 through Figure 8.28.

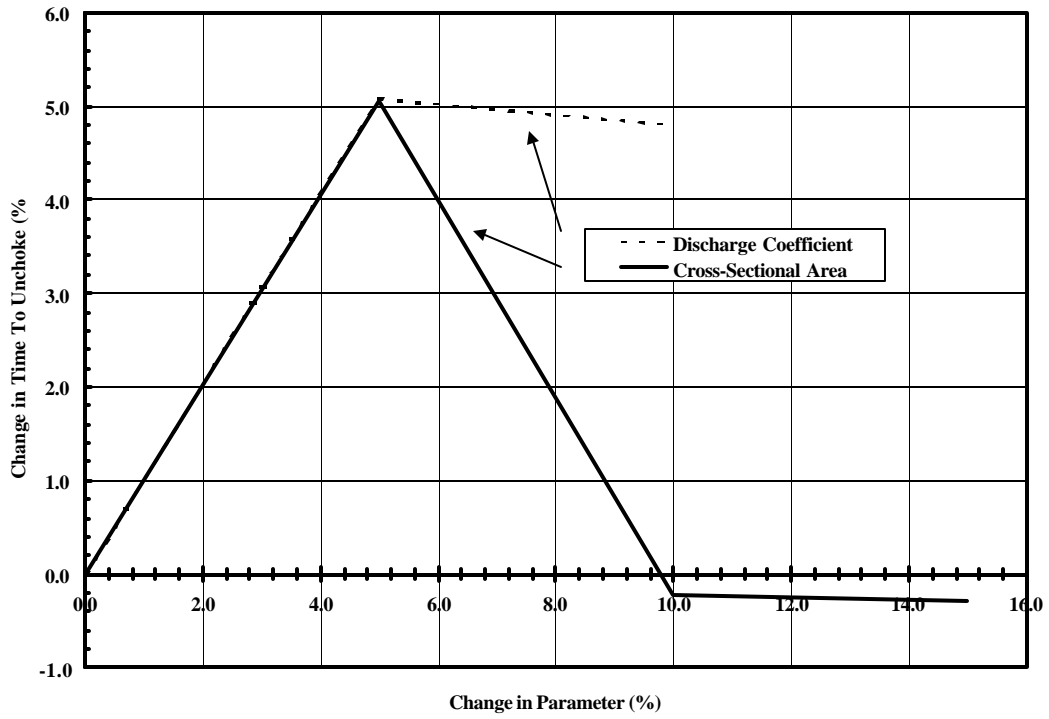


**Figure 8.25 Variance in Time to Unchoke as a Function of START Parameter Changes.**

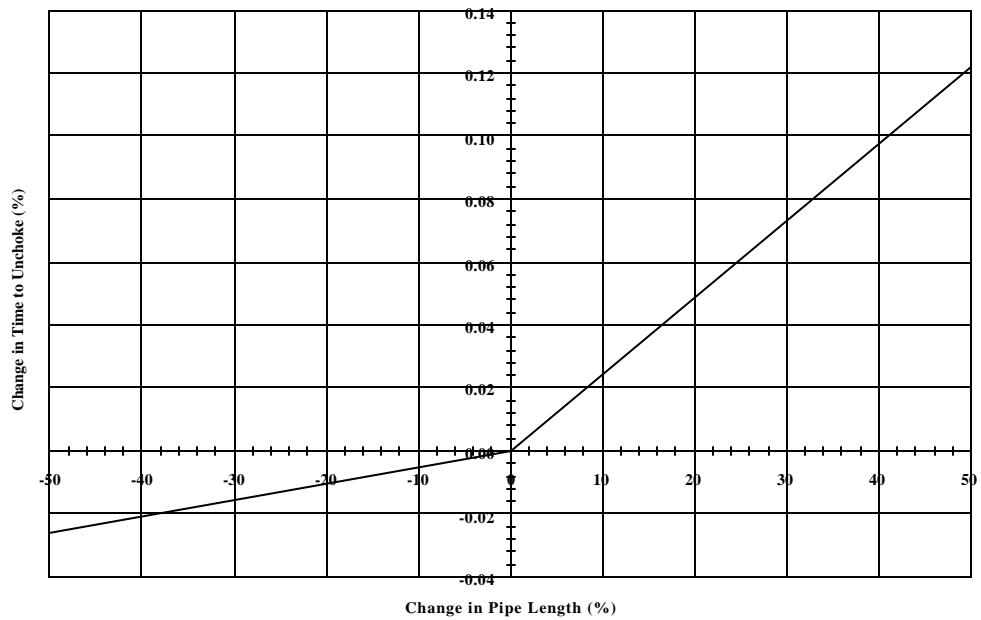


**Figure 8.26 Variance in Time to Unchoke as a Function of Pipe Length Change.**

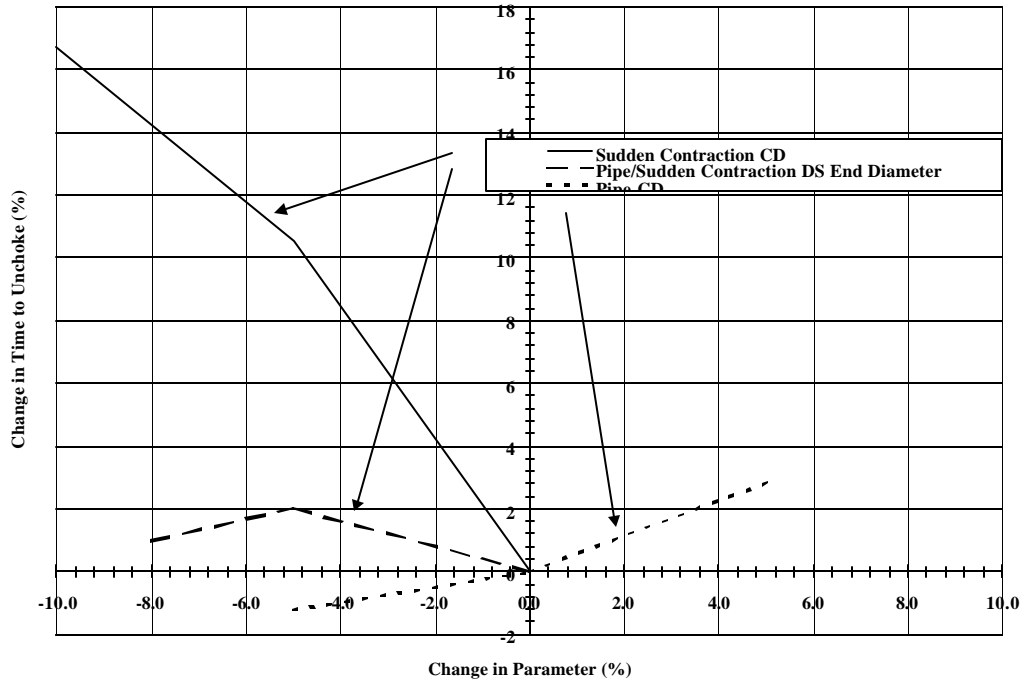


**Figure 8.27 Variance in Time to Unchoke as a Function of Pipe and Sudden Contraction Changes.**

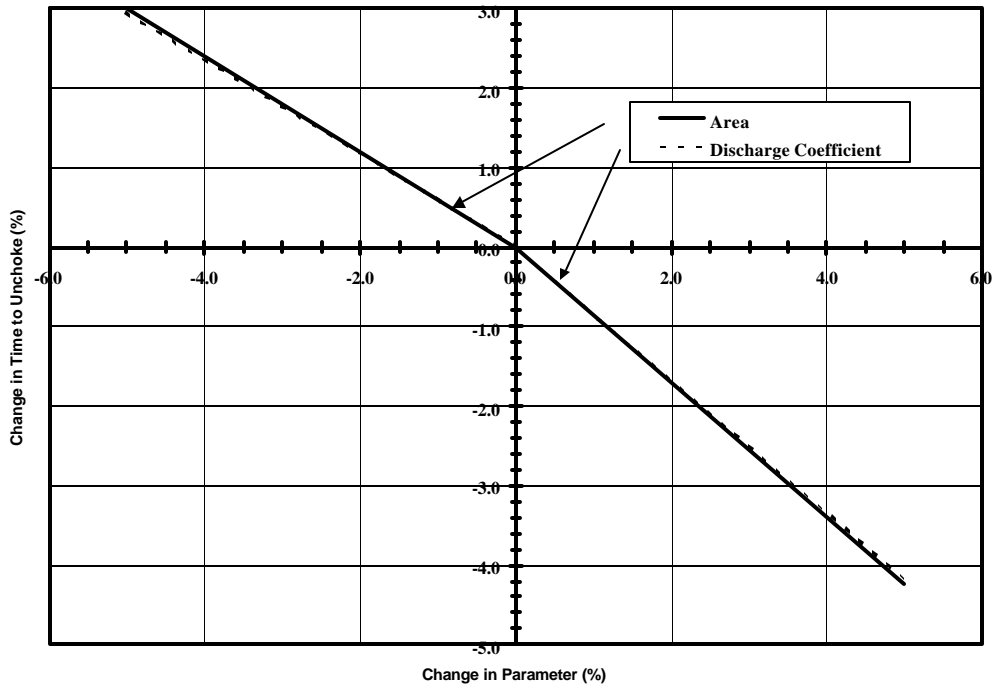


**Figure 8.28 Variance in Time to Unchoke as a Function of Nozzle Changes.**

Note that, in some instances, geometric constraints built into the program prevent certain variations in a parameter. For instance, it makes no sense to have a sudden contraction in a model, and allow the downstream diameter to equal or exceed the upstream diameter. The design can be changed that way, but the simulation model should be likewise changed. In estimation of upstream Mach numbers using the isentropic flow tables, an area ratio outside the range available in tables published in most standard texts will also cause a halt in program execution, should the cross sectional areas, or areas times discharge coefficients, exceed limits.

The results show a mixed bag of sensitivities. Figure 8.25 shows sensitivities for the exit node (“START”). The analyzed configuration includes a START node, followed by a sudden contraction, so reductions in the upstream cross-sectional area were not allowable. The expansion of the upstream area showed mixed results – small percent increases in area resulted in increases in time to reach unchoking by as much as 5%, while large percent increases resulted in slight decreases in time, almost negligible. The discharge coefficient, over the range examined, showed a more consistent increase in time to reach unchoking, although the effect of increasing the discharge coefficient seemed to diminish for percent increases greater than 6%.

Because of the need for large percent changes in length in order to see any appreciable changes in time, pipe length was plotted separately, over a range of  $\pm 50\%$ . Figure 8.26 shows a small, but definite trend towards increasing time to reach unchoking as pipe length is allowed to grow. The small percent changes suggest that small changes in pipe lengths in a system design will have little significant impact on system



performance. Short length changes can be safely be allowed without impacting overall system operations. Long lengths of pipe, on the order of tens of feet, will start to impact discharge times, but the impact will only be on the order of a few seconds. Note that the current model implementation does not distinguish between horizontal and vertical pipes; vendor test results suggest that there are small but significant flow differences between the two, particularly as to whether the vertical flow is upwards or downwards. The results show in differences in delivered agent at the nozzles. These differences are not reflected in the model, or in the sensitivity studies.

Pipe and sudden contraction sensitivities are shown in Figure 8.27. As noted earlier, sizing restrictions for the components have limited the kinds of variations that could be applied to a parameter. Since the pipe diameter and downstream diameter of the sudden contraction are identical in this configuration, sensitivities for the two components were combined into one plot. The results show a relatively strong dependence of time to reach unchoking on decreases in the sudden contraction discharge coefficient. The pipe discharge coefficient shows a small, but definite trend towards increasing discharge time as the coefficient increases, while the sudden contraction downstream / pipe diameter shows almost no trend as the diameter decreases. Note that while the roughness coefficient  $k_s/d$  is entered in the inputs, it had zero impact on the time to reach unchoking.

Figure 8.28 shows nozzle parameter influences on time to reach unchoking. The area and discharge coefficient are multiplied together, so that the impact of changes of the two on discharge time is not surprising. As with gas-alone flows, there is a distinctive trend towards decreases in the discharge time as the throat area is allowed to increase.

This is also reflected in discharge tests PNS-1 and PNS-2, where the removal of the nozzle in test PNS-2 resulted in a shorter discharge time, and larger pressure differential along the length of the pipe.

As part of these sensitivity studies, the effect of these changes on the amount of agent discharged was also examined. For the piping network, variations of the program input parameters for the piping network had zero impact on the amount of mass discharged.

The results of the studies suggest that the greatest impact on discharge time results from variations in the cross-sectional areas of piping network components, and less impact from pipe lengths. The largest impacts are in the nozzle throat, and to some extent, the sudden contraction discharge coefficient. There was limited impact by varying the START area and discharge coefficient. The user must exercise some caution in applying variations, in that the program will fail to run if a change results in an impossible combination of parameters, such as a “sudden contraction” with downstream area larger than the upstream area. In these cases, appropriate changes to the model configuration (and the system design, as well) should be made before continuing the analysis.

#### 8.5.4 Other Parameters.

The parameters examined here either do not fit readily into any of the other categories previously examined, or are parameters that do not affect discharge system performance, but do affect accuracy of the program outputs. The results of these studies are shown in Figure 8.29 through Figure 8.30.

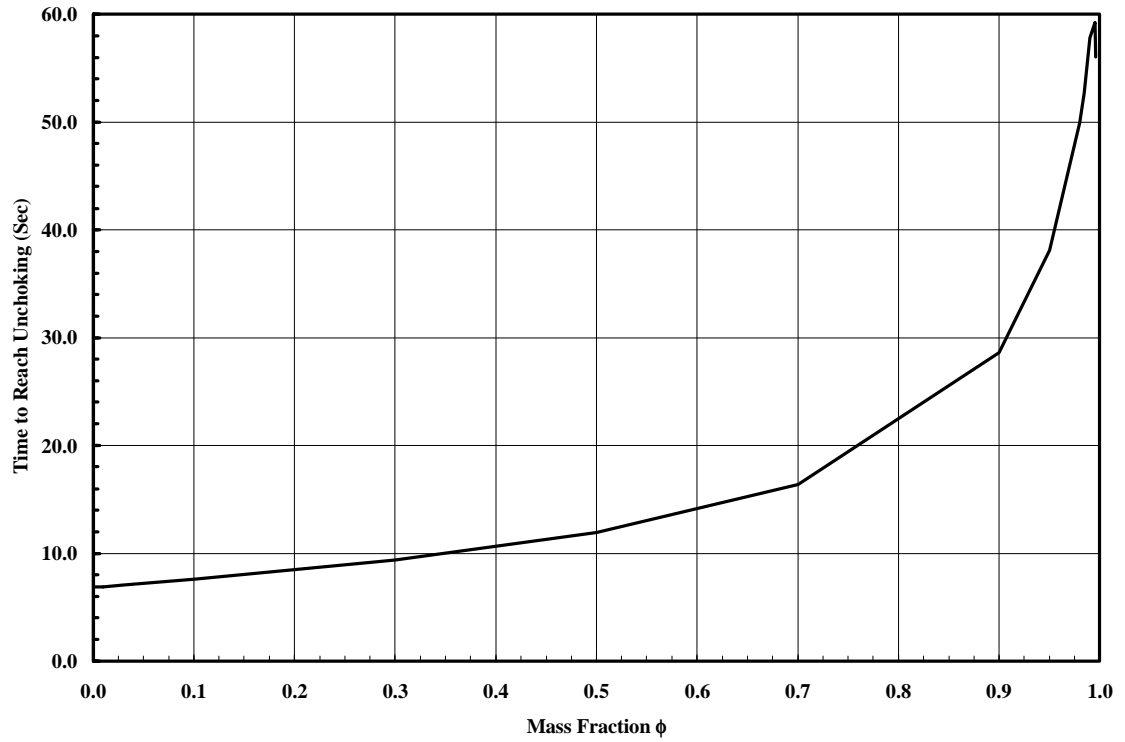


**Figure 8.29 Variance in Time to Unchoke as a Function of Mass Fraction Changes.**

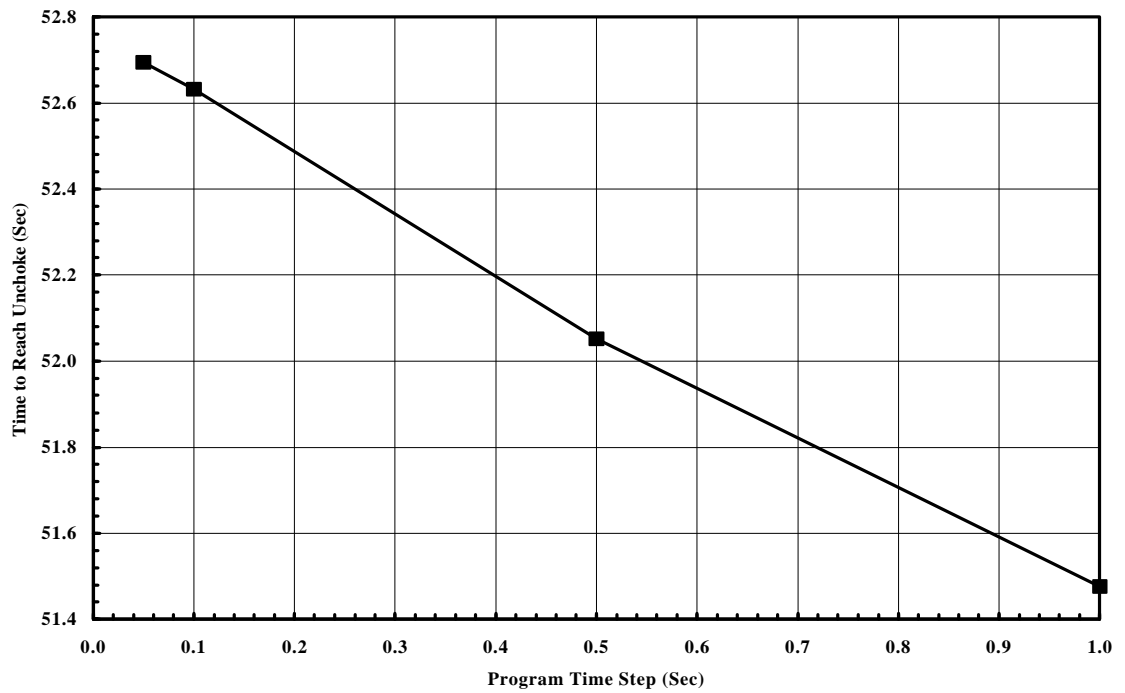


**Figure 8.30 Variance in Time to Unchoke as a Function of Program Time Step Changes.**

Figure 8.29 shows the variation of discharge time with mass fraction. The program cannot run with a mass fraction of zero because of mathematical considerations (a mass fraction of zero results in division by zero errors.) However, it can run with a low fraction; a fraction of 0.001 results in discharges that are almost equal to those predicted by isentropic theory for gas-only discharges (for this configuration, the gas-alone discharge was found to be approximately 7.5 seconds; with an agent mass sufficient to achieve a mass fraction of 0.001, a discharge time of 7.54 seconds was found). Thus gas-only discharges can be simulated, by using a negligible mass fraction. Mass fractions below 0.7 show relatively low discharge time sensitivities. Above 0.70, and particularly above 0.90, the sensitivity is extreme, with variations in the third decimal place of the mass fraction having a significant effect on discharge time and mass discharged. Note that for mass fractions greater than 0.995, the discharge time actually starts to decrease. This is an artifact of how discharge time is being determined. The program judges discharge time as the time for the source cylinder pressure to be equal to ambient pressure. Above 0.995, the amount of carrier gas in the cylinder is reduced to the point where the pressure during a discharge simulation reaches ambient before all the powder is discharged. Perhaps a better measure of system performance would be the time for the system to discharge a certain amount of agent. In a plot of this type, as the mass fraction approached 1.0, the time to discharge would asymptotically go to infinity, rather than peak out.

The time step of the program is an artifact of the program, and has no influence on actual system performance. However, as Figure 8.30 shows, the selection of a time step can have a significant impact on the user's ability to estimate events such as the time

to unchoke. While unchoking is recognized in the program, the precise moment when it occurs is not recognized formally – the user has to interpolate cylinder output data to determine the moment when unchoking occurs.

There are practical limits to what time step can be selected. The current implementation of the model limits the maximum number of time steps the program can execute before quitting. This maximum time step count prevents an infinite loop of some sort from making it difficult to stop the program without interrupting execution (which usually loses all output data), particularly if, for some reason, nothing is happening between loops. If the time step is too small (0.050 second in this example), this limitation can be encountered. In any event, the time step should be set as large as is comfortable for the user, and compatible with the expected discharge time of the real system. One liability of too large a time step is increasing relative inaccuracy in pin-pointing specific events, such as unchoking. As Figure 8.30 shows there is some variation in the calculated time to unchoke as the time step is increased. A time step of 0.100 was used in the baseline calculations; time steps as large as 1.0 second allowed for as much as a 2% decrease in the calculated discharge time. Given that a large time step for a discharge simulation that lasts a second or less is pointless, the user has to balance the need for some precision in being able to use output results to pin-point events, with the need to not generate large amounts of output data that does not enhance understanding of the discharge being modeled.

#### 8.5.5 Model Accuracy.

The accuracy of the model to predict discharges depends on a number of factors, and on precisely what is being modeled. As Figure 8.1, Figure 8.8, Figure 8.9 and Figure

8.16 show, for gas-only discharges, the model gives an extremely close match to the data. Note that no gas-only tests were run with a pipe and no nozzle, so the quality of the fit to pipes may be difficult to properly assess. The only exception to the otherwise excellent fit is in the initial inflection point. Since the opening of the cylinder valve is not in the current model, attempting to predict gas-only discharges without accounting for the valve opening will result in inaccuracies. But overall, the fit to gas-only data is superb.

The fit of the model to test data, as reflected in the other comparisons in Section 7.5, varies, with the relatively good fits show in tests P-7, M-1, PNM-1, PNM-2, UK-F7, F-9 and F-10. Note that these tests a) show a good fit if the initial transients are bypassed, and b) show a good fit up to the point of the second inflection, when all tests diverge significantly from the predictions. All the simulations predict longer depressurization times than actually experienced by the hardware. Also, as shown in Section 7.5, with the exception of test F-11, the model overpredicts the amount of residual agent after termination – this overprediction is also reflected in the computer model predictions. The modeling of pipe flow, as a result of the data generated in test PNS-2, must be held somewhat in suspect, as well. This should not be surprising, since the only empirical formulas for adjusting the interior wall friction factor for multiphase gas/solids flow were developed from experimentation on “dilute” flows – the adjustments necessary to account for high density, high velocity flows are undoubtedly different, and currently unknown.

As a result of the aforementioned points, the model is somewhat at the mercy of events not included in the theoretical model that occur as powder is discharged or as the cylinder valve opens. Except for the initial valve opening, the model predicts gas-only

discharges well; but overpredicts mixture depressurization time, and underpredicts the amount of mass discharged. Experimental studies allowing the mass fraction to vary with time and location suggest that a better fit of the model to the data is possible with a mass fraction that varies with both time and location in the discharge configuration. The mathematics of a such a variable mass fraction are significantly more complicated than for a constant mass fraction, and require a mathematically adequate definition of the mass fraction to be derivable. However, as demonstrated in the modeling of tests P-6 and PNS-1, reducing the mass fraction after the second inflection point resulted in a cylinder pressure prediction very close in accuracy to the observed test data. This reduced mass fraction is caused by the agent in the cylinder reaching the bottom of the dip tube, resulting in lesser amounts of agent entrained into the exiting mixture flow, and thus a lower mass fraction in the exiting flow. Based on the observed tests and analytical results, a model that reflects the behavior of the solid powder agent in the cylinder during discharge, and the opening of the cylinder valve would more correctly predict the pressure performance in the cylinder. Measurement of mass loss during discharge, and mass fraction in selected locations within a piping configuration would help to confirm that the mass fraction should not be treated as constant at all locations, and for all times during a discharge.

The good fit in the comparisons is due in part to precise selection of starting parameters, selected at a moment in early discharge to avoid the initial transients experienced by the system. Given the apparent importance of events occurring within the source cylinder involving the interplay of agent and carrier gas, the easiest course for future development and improvement would seem to lie in the better understanding and

proper modeling of cylinder events, with implementation of more complex mathematics put off until an assessment of the accuracy of a model more accurately modeling the system can be made.

The model, as currently implemented, seems to model most of the discharge well, using an appropriate, empirically-determined discharge coefficient. The model simulates gas discharges very well, and comes close to modeling mixture discharges, up to and including the second inflection point.



## 9.0 Conclusions and Recommendations.

### 9.1 *Conclusions.*

- A high density, high velocity gas/solids two-phase mixture model has been developed using mixture properties and thermodynamics based on the assumption of a constant solids mass fraction. This formulation has been applied to the quasi-steady conservation equations describing the flow out of the cylinder and through the various piping components.
- The object-oriented computer code is intended to allow maximum flexibility in suppression system component simulation. The result is a model program that should be easy to modify and maintain, with code less prone to error.
- The model agrees well with gas-only blow down tests of cylinders without downstream piping networks when a discharge coefficient of 0.380 is used for the cylinder dip tube / valve assembly.
- Testing of a cylinder without downstream piping network, with a 21-25 lbm of agent pressurized to 300 psig, shows an increase in discharge time of four to five times the 1.2 second-duration of a gas-only discharge. This is consistent with the theoretical model, which shows a significant reduction in the speed of sound as a result of addition of the solid agent particles to the carrier gas.
- Testing with cylinder, pipe, and nozzle, shows a substantially longer duration discharge time than for the cylinder alone. As an example, for a gas-only discharge, the piping network increased the time to reach unchoking from 1 second (for a tank assembly alone) to 7 seconds (tests G-7 and PG-2). As a further example, for a gas-

solids mixture, addition of the pipe increased the time to reach unchoking from 5 seconds (for a tank assembly alone) to 7 seconds (tests P-6 and PNS-2). Addition of a nozzle to the pipe increased the discharge time from 5 seconds (for a tank assembly alone) to 25 seconds (tests P-6 and PNS-1). Almost all the additional time is due to the nozzle; the 8-ft length pipe effect is negligible.

- Tests with gas and powder showed a significantly longer discharge time than tests with only gas. A second inflection point was observed, close to the end of discharge, but while flow in the system was still choked, resulting in a more rapid depressurization of the cylinder than predicted by the current model. This second inflection point is apparently due to the agent powder within the cylinder reaching the lower end of the dip tube. Tests using a reduced amount of agent (P-7, 10 lbm sodium bicarbonate versus P-6, 25 lbm) or a shorter dip tube (PNS-4, 7 inches versus PNS-1, 14 inches) show either a “mild” inflection point close to the start of discharge, or no inflection point at all. In these instances, the agent level in the cylinder reaches the dip tube shortly after the initiation of discharge.
- Gas-only discharges are reproduced by the model exceptionally well; for example, cylinder-only test G-7 reached unchoking in 1.15 seconds; the model predicted 1.20 seconds (using a discharge coefficient of 0.380 for the cylinder valve assembly.) For a cylinder-pipe-nozzle assembly, the model correctly predicted the gas-only discharge time of 10 seconds, with a cylinder pressurized to 300 psig, a nozzle with throat diameter of 0.173 inches, and a discharge coefficient of 0.470. For two-phase mixtures, good agreement can be achieved using a discharge coefficient accounting for changes in the mass fraction during discharge. In test P-6 (cylinder-only), using a

- discharge coefficient of 0.500 for the valve assembly, the model successfully modeled the test cylinder pressure trace, predicting the observed 60-psig pressure at the second inflection point at 3.65 seconds, the time observed. However, the model predicted a time to unchoke of greater than 6 seconds, versus the observed 4.68 seconds. For a cylinder-pipe-nozzle assembly, data from test PNS-1 was matched well using a discharge coefficient of 0.999, up to the inflection point, which was correctly predicted to be at approximately 90 psig. However, the model predicts a time to unchoke of greater than 30 seconds, versus the observed 24 seconds.
- Good agreement can be achieved between the model and test data for mixture discharges, up to the time frame of the second inflection point. Modeling the reduction in mass of agent in the cylinder during discharge, and reducing the mass fraction when the bottom of the dip tube is reached, would allow more accuracy in modeling the pressure response in the cylinder. Running the model with a reduced mass fraction from the starting point of the second inflection point resulted in a good match between the model and test data. Similar results were observed comparing other tests to model predictions, such as test PNS-1. Inclusion of system events, such as the opening of the cylinder valve, and agent mass level reaching the bottom of the dip tube, would improve model accuracy.
  - Observed agent residual masses in the cylinder after blow down were between 0.1 and 0.6 lbm, compared to model-predicted residuals using the constant mass fraction assumption of 2.0 lbm or more. As a result of this discrepancy, and the inability of the constant mass fraction assumption to predict the second inflection point, the

assumption must be considered inappropriate to accurately model two-phase blow downs.

- The current “simple” model, with its assumption of a constant mass fraction, is of limited value in modeling gas-solids two-phase blow downs. Empirically-determined discharge coefficients can be used to compensate for the constant mass fraction to match pressure in the cylinder during blow down, but the mass removal of agent from a system during blow down would still not be correctly modeled. Extension of the model to allow for the mass fraction to vary with location and time is necessary to make the model usable in engineering design.

## **9.2        *Recommendations.***

- The reduction in agent mass in the cylinder as discharge progresses needs to be added to the model. This will allow for determination of a time at which the agent reaches the bottom of the dip tube, and reduction by some means of the solids mass fraction, to model the appearance of the second inflection point observed in two-phase blow downs.
- The model needs to be extended to eliminate the assumption of a constant mass fraction. This is necessary to improve model predictions of agent discharge during a blow down.
- Tee-joints need to be added to the model. This will allow for the modeling of most configurations of interest. Part of this effort should include the phenomena of phase separation occurring in elbows, and the modeling of remixing if the physical

geometry of the system permits it; otherwise, the possibility of flows in branches becoming completely separated by phase needs to be considered for modeling.

- The opening of the cylinder valve needs to be added to the model. This will allow the user to start modeling a blow down from when the valve first opens, rather than having to approximate state conditions in the cylinder after the valve has opened.

Further items for long-range investigation and implementation:

- Phenomena, such as particle-particle collisions, particle drag effects, and gravitational effects, should be examined for their impact on blow downs. These effects should be added to the model only if their inclusion is sufficient to alter the pressure and mass flow characteristics of the two-phase mixture.
- Friction factor studies should be done for dry chemical flow regimes (high Reynolds number, high loading flows). Model predictions for test PNS-2 (tank, pipe, and no nozzle) showed the model predicting piping pressures twice as high as observed at the nozzle inlet pressure. Empirical formulations as currently reported in the literature to calculate mixture friction factors were not successful in matching test data and model predictions.
- Changes in particle mass fraction in a system during discharge should be experimentally quantified.
- To improve maintainability and downstream implementation of additional modeling capabilities, and to improve model user-friendliness, the entire model should be rewritten to more rigorously implement OOD principles and features. C++ should be exploited more fully to simplify source code, and increase speed and efficiency of execution.

- Additional user-oriented features should be implemented, including:
  - A graphical user interface (GUI) to allow for on-screen configuration design, and more rapid post-processing of simulation data.
  - More error checking so that the user:
    - Is limited in the entry of incorrect or inconsistent input data.
    - Can spot physically unworkable or impossible designs.
- A better iterative solver than the “zero” routine should be implemented in the model. The zero routine requires that an equation to be solved be continuous over an almost infinite range. Since most of the solutions sought involved subsonic Mach numbers, the mapping of guesses outside this range has resulted in relatively complex coding. While some re-mappings of these guesses are now implemented, a more rigorous solver might better handle these situations. A “better” solver could also improve the speed and efficiency of the program.

## 10.0 Appendices

### 10.1 “Zero” Code.

A full description of the zero routine, its development, and usage can be found in **Van Zandt (1994)**.

### 10.2 *Pipe Cross-Sectional Integrations.*

As part of the development of the pipe flow model, one-dimensional gas/solids mixture momentum equation for pipe flow was derived from the momentum balance proposed by **Ahmadi & Ma (1990a)** and **Cao & Ahmadi (1995)**, from a momentum balance equation derived by **Ural (1993)**, and compared to the one-dimensional gas-only adiabatic momentum equation as derived for pipe flow in standard fluids dynamics textbooks such as **Streeter & Wylie (1985)**, **John & Haberman (1988)** and **Shapiro (1953)**. The goal was to compare the resulting derived equations with each other and to determine by observation what additional terms over those found in a fluid-only derivation occur in a two-phase gas-solids model. The Ahmadi derivation describes the inclusion of phenomena such as interparticle collisions, mixture/wall interactions, and particle drag; these phenomena must be represented mathematically by terms and factors not included in fluid-only models. While these phenomena have to date not been formally included in the model, the results of the analyses show that, indirectly, many of the effects mentioned can be accounted for by empirical determination of the friction factor multiplier. Furthermore, while the current model was derived only for quasi-steady state conditions, Ural’s work suggests that expansion of the model to include simple unsteady-flow modeling can be achieved by inclusion of velocity time derivatives.

The results of these studies also suggest that the primary difference in the pipe flow momentum equation derived using Ahmadi's analyses and the equations developed for fluid-only conditions is in the addition of an eddy viscosity term to the viscous term in the equation. Ahmadi used this term to account for interparticle collisions and mixture / wall stresses. If the velocity fields of the solids and gaseous phases are assumed identical (or nearly so), the additional viscous terms can be accounted for in a friction factor accounting for both phases. Thus this functional form of the eddy viscosity term is important in helping to select a suitable empirical friction factor.

### 10.2.1 Fluid-Only Momentum Equation Derivation.

The situation being analyzed can be found in most standard fluid mechanics textbooks, such as **Streeter & Wylie (1985)**. Most texts present both incompressible AND compressible analyses; the analyses here is for compressible flow. A sketch of the situation being modeled is shown below.

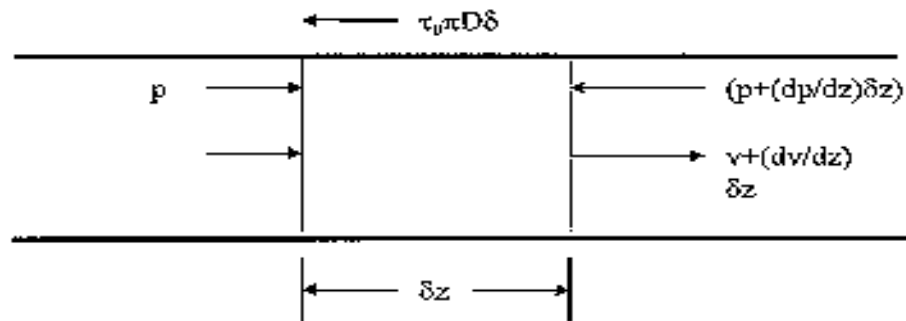


**Figure 10.1 Standard Text Book Pipe Momentum Conservation – Schematic.**

The assumptions of the standard analyses include:

- Perfect gas (constant specific heats)



- Steady, one-dimensional flow (not time dependent)
- Adiabatic flow
- Constant friction factor over the length of pipe considered
- Effective diameter  $D$  equal to four times the hydraulic radius (defined as the cross-sectional area divided by the perimeter)
- No significant elevation changes
- No work added to or extracted from the flow.

While not explicitly stated in standard texts, the velocity is assumed to be averaged over the cross-sectional area of the pipe.

Writing the momentum balance equation for this situation results in:

$$pA - \left( p + \frac{dp}{dz} \delta z \right) A - \tau_0 \pi D \delta z = \rho v A \left( v + \frac{dv}{dz} \delta z - v \right) \quad (10.1)$$

which simplifies to:

$$\rho v dv + dp + \frac{4 \tau_0}{D} dz = 0 \quad (10.2)$$

The wall shear stress is defined as:

$$\tau_0 = \frac{\rho f v^2}{8} \quad (10.3)$$

Substituting equation (10.3) into equation (10.2) yields:

$$\rho v dz + dp + \frac{f \rho v^2}{2D} dz = 0 \quad (10.4)$$

Dividing through by  $dz$  yields the differential form:

$$\rho v \frac{dv}{dz} + \frac{dp}{dz} + \frac{\rho f v^2}{2D} = 0 \quad (10.5)$$

By use of the energy and mass balance equations, ideal gas law and definition of speed of sound, this is ultimately converted to:

$$\frac{(1 - M^2)dM}{\gamma M^3 \left\{ \left[ (\gamma - 1) / 2 \right] M^2 + 1 \right\}} = \frac{f}{2D} dz \quad (10.6)$$

Equation (10.6) can, with a little manipulation, be integrated.

### 10.2.2 Ural Momentum Equation Derivation

The momentum balance equation derived in **Ural (1993)** was developed as part of an analysis of duct gas flow resulting from explosions. Treating the flow as one-dimensional, the momentum balance used by Ural is:

$$\frac{\partial v}{\partial t} + v \frac{\partial v}{\partial z} = -\frac{1}{\rho} \frac{\partial p}{\partial z} + v \frac{\partial^2 v}{\partial r^2} \quad (10.7)$$

Multiplying through by  $\rho$  yields:

$$\rho \frac{\partial v}{\partial t} + \rho v \frac{\partial v}{\partial z} = -\frac{\partial p}{\partial z} + \mu \frac{\partial^2 v}{\partial r^2} \quad (10.8)$$

Assuming radial symmetry, integrating across the cross-sectional area from 0 to the pipe ID of  $R_0$ , the results of integration of each term are:

$$\int_0^{R_0} \mathbf{r} \frac{\mathbf{f}v}{\mathbf{f}t} dr = \mathbf{r} \frac{d}{dt} \int_0^{R_0} v(dr)^2 = \mathbf{r} \frac{d}{dt} \bar{v} R_0^2 = \mathbf{r} \frac{d\bar{v}}{dt} R_0^2 \quad (10.9)$$

$$v \frac{\partial v}{\partial z} = \frac{1}{2} \frac{\partial v^2}{\partial z} \quad (10.10)$$

$$\int_0^{R_0} \frac{\mathbf{r}}{2} \frac{\mathbf{f}v^2}{\mathbf{f}z} (dr)^2 = \frac{\mathbf{r}}{2} \frac{\mathbf{f}}{\mathbf{f}z} \int_0^{R_0} v^2 (dr)^2 = \frac{\mathbf{r}}{2} \frac{\mathbf{f}}{\mathbf{f}z} \bar{v}^2 R_0^2 = \frac{\mathbf{r} R_0^2}{2} \frac{\mathbf{f} \bar{v}^2}{\mathbf{f}z} = \mathbf{r} R_0^2 \bar{v} \frac{\mathbf{f} \bar{v}}{\mathbf{f}z} \quad (10.11)$$

$$\int_0^{R_0} \mathbf{m} \frac{\mathbf{f}^2 v}{\mathbf{f} r^2} r dr = \mathbf{m} \int_0^{R_0} \frac{\mathbf{f}^2 v}{\mathbf{f} r^2} r dr = \mathbf{m} \frac{\mathbf{f}v}{\mathbf{f}r} \Big|_0^{R_0} = \mathbf{t}_w \quad (10.12)$$

Replacing the terms in equation (10.8) with the results of equations (10.9), (10.10), (10.11), and (10.12), and dividing by  $R_0$ , the results are:

$$\rho \frac{\partial \bar{v}}{\partial t} + \rho v \frac{\partial \bar{v}}{\partial z} = -\frac{\partial p}{\partial z} + \frac{1}{R_0} \tau_w \quad (10.13)$$

Ural assumes that  $\partial v/\partial t \ll v\partial v/\partial z$  at the inlet and outlet of the duct, and  $\partial v/\partial t \gg v\partial v/\partial z$  between stations in the duct. Thus, within a pipe, the equation would be:

$$\rho \frac{\partial \bar{v}}{\partial t} = -\frac{\partial p}{\partial z} + \frac{1}{R_0} \tau_w \quad (10.14)$$

### 10.2.3 Ahmadi Momentum Equation Derivation

Derivation of the Ahmadi form of the momentum conservation equation first required derivation of the basic equations from **Ahmadi & Ma (1990a)**, expansion and collection of terms, and adding of equations together to arrive at an equation for a “composite” fluid, such as is considered in the model. Note that Ahmadi’s equations are all in terms of cartesian coordinates, they must be converted to cylindrical coordinates in order to be compared to Ural’s and the fluid-only momentum equations.

In the axial direction, the basic momentum equation (from **Ahmadi & Ma (1990a)**) is:

$$\rho \frac{D v_z}{Dt} = \bar{\rho} f_z + \frac{\partial \tilde{\tau}_{jz}}{\partial x_j} + \frac{\partial \hat{t}_{jz}}{\partial x_j} + \bar{P}_z \quad (10.15)$$

This may be rewritten (See **Sabersky et al (1971)**, p. 20-21, for notation equivalences)

as:

$$\rho \frac{D v_z}{Dt} = \bar{\rho} f_z + \nabla \cdot \tilde{\tau}_{jz} + \nabla \cdot \hat{t}_{jz} + \bar{P}_z \quad (10.16)$$

where  $j = r, \theta, z$  (cylindrical coordinate directions), and  $\bar{P}$  is defined as the interaction momentum supply. For a composite “fluid”, this term is zero.

Assume that flows are only in the axial direction (i.e.;  $v_\theta, v_r = 0$ ). Also, assume that flows in the pipe are only a function of time and axial location  $z$ . (See also **Hughes & Brighton (1991)**, p. 324). Symmetry requires that  $\partial v_z / \partial r = 0$  at the center line of the pipe. Equation (10.16) becomes:

$$\bar{\mathbf{r}} \frac{\mathcal{I} v_z}{\mathcal{I} t} + \bar{\mathbf{r}} v_z \frac{\mathcal{I} v_z}{\mathcal{I} z} = \bar{\mathbf{r}} f_z + \frac{1}{r} \frac{\mathcal{I}}{\mathcal{I} r} \left( r \tilde{\mathbf{t}}_{rz} \right) + \frac{1}{r} \frac{\mathcal{I}}{\mathcal{I} q} \tilde{\mathbf{t}}_{qz} + \frac{\mathcal{I}}{\mathcal{I} z} \tilde{\mathbf{t}}_{zz} + \frac{1}{r} \frac{\mathcal{I}}{\mathcal{I} r} \left( r \tilde{\mathbf{t}}_{rz} \right) + \frac{1}{r} \frac{\mathcal{I}}{\mathcal{I} q} \tilde{\mathbf{t}}_{qz} + \frac{\mathcal{I}}{\mathcal{I} z} \tilde{\mathbf{t}}_{zz} \quad (10.17)$$

The momentum equation in the radial direction is:

$$0 = \bar{\mathbf{r}} f_r + \nabla \cdot \tilde{\mathbf{t}}_{jr} + \nabla \cdot \tilde{\mathbf{t}}_{jr} \quad (10.18)$$

and, with the aforementioned assumptions, equation (10.18) becomes

$$0 = \bar{\mathbf{r}} f_r + \frac{1}{r} \frac{\mathcal{I}}{\mathcal{I} r} \left( r \tilde{\mathbf{t}}_{rr} \right) + \frac{1}{r} \frac{\mathcal{I}}{\mathcal{I} q} \tilde{\mathbf{t}}_{qr} + \frac{\mathcal{I}}{\mathcal{I} z} \tilde{\mathbf{t}}_{zr} + \frac{1}{r} \frac{\mathcal{I}}{\mathcal{I} r} \left( r \tilde{\mathbf{t}}_{rr} \right) + \frac{1}{r} \frac{\mathcal{I}}{\mathcal{I} q} \tilde{\mathbf{t}}_{qr} + \frac{\mathcal{I}}{\mathcal{I} z} \tilde{\mathbf{t}}_{zr} \quad (10.19)$$

Assuming axisymmetric conditions (i.e.; no variation in the  $\theta$ -direction), equations

(10.17) and (10.19) become:

$$\bar{\mathbf{r}} \frac{\mathcal{I} v_z}{\mathcal{I} t} + \bar{\mathbf{r}} v_z \frac{\mathcal{I} v_z}{\mathcal{I} z} = \bar{\mathbf{r}} f_z + \frac{1}{r} \frac{\mathcal{I}}{\mathcal{I} r} \left( r \tilde{\mathbf{t}}_{rz} \right) + \frac{\mathcal{I}}{\mathcal{I} z} \tilde{\mathbf{t}}_{zz} + \frac{1}{r} \frac{\mathcal{I}}{\mathcal{I} r} \left( r \tilde{\mathbf{t}}_{rz} \right) + \frac{\mathcal{I}}{\mathcal{I} z} \tilde{\mathbf{t}}_{zz} \quad (10.20)$$

and

$$0 = \bar{\mathbf{r}} f_r + \frac{1}{r} \frac{\mathcal{I}}{\mathcal{I} r} \left( r \tilde{\mathbf{t}}_{rr} \right) + \frac{\mathcal{I}}{\mathcal{I} z} \tilde{\mathbf{t}}_{zr} + \frac{1}{r} \frac{\mathcal{I}}{\mathcal{I} r} \left( r \tilde{\mathbf{t}}_{rr} \right) + \frac{\mathcal{I}}{\mathcal{I} z} \tilde{\mathbf{t}}_{zr} \quad (10.21)$$

The stress tensors, in cylindrical coordinates (based on **Ahmadi & Ma (1990a)** (equation 71), and **Shames (1992)**, p. 441) with all  $\tau$ 's multiplied by  $1/2$ , are:

$$\tilde{\mathbf{t}}_{rz} = \mathbf{m}^T \left( \frac{\mathbf{f} v_r}{\mathbf{f} z} + \frac{\mathbf{f} v_z}{\mathbf{f} r} \right) = \mathbf{m}^T \frac{\mathbf{f} v_z}{\mathbf{f} r} \quad (10.22)$$

$$\tilde{\tau}_{zr} = \tilde{\tau}_{rz} \quad (10.23)$$

$$\tilde{\tau}_{zz} = - \left( \gamma \bar{\rho} k + \frac{2}{3} \mu^T \frac{\partial v_z}{\partial z} \right) + \mu^T \frac{\partial v_z}{\partial z} \quad (v_r = v_\theta = 0) \quad (10.24)$$

$$\tilde{\tau}_{rr} = - \left( \gamma \bar{\rho} k + \frac{2}{3} \mu^T \frac{\partial v_r}{\partial r} \right) + \mu^T \frac{\partial v_r}{\partial r} = -(\gamma \bar{\rho} k) \quad (10.25)$$

$$\hat{\mathbf{t}}_{rz} = \mu \frac{\partial v_z}{\partial r} \quad (10.26)$$

$$\hat{\mathbf{t}}_{zr} = \hat{\mathbf{t}}_{rz} \quad (10.27)$$

$$\hat{\mathbf{t}}_{zz} = \left( -p + \frac{2}{3} \mu \frac{\partial v_z}{\partial z} \right) + \mu \frac{\partial v_z}{\partial z} \quad (10.28)$$

$$\hat{\mathbf{t}}_{rr} = \left( -p + \frac{2}{3} \mu \frac{\partial v_r}{\partial r} \right) + \mu \frac{\partial v_r}{\partial r} = -p \quad (10.29)$$

Applying the stress tensors to equations (10.20) and (10.21) results in:

$$\begin{aligned} \bar{\mathbf{r}} \frac{\mathbf{f} v_z}{\mathbf{f} t} + v_z \frac{\mathbf{f} v_z}{\mathbf{f} z} &= \bar{\mathbf{r}} f_z + \frac{1}{r} \frac{\mathbf{f}}{\mathbf{f} r} \left( r \mathbf{m}^T \frac{\mathbf{f} v_z}{\mathbf{f} r} \right) - \frac{\mathbf{f}}{\mathbf{f} z} (\mathbf{g} \bar{\mathbf{r}} k) + \frac{\mathbf{f}}{\mathbf{f} z} \left( \frac{2}{3} \mathbf{m}^T \frac{\mathbf{f} v_z}{\mathbf{f} z} \right) \\ &+ \frac{\mathbf{f}}{\mathbf{f} z} \left( \mathbf{m}^T \frac{\mathbf{f} v_z}{\mathbf{f} z} \right) + \frac{1}{r} \frac{\mathbf{f}}{\mathbf{f} r} \left( r \mathbf{m} \frac{\mathbf{f} v_z}{\mathbf{f} r} \right) - \frac{\mathbf{f} p}{\mathbf{f} z} + \frac{\mathbf{f}}{\mathbf{f} z} \left( \frac{2}{3} \mathbf{m} \frac{\mathbf{f} v_z}{\mathbf{f} z} \right) + \frac{\mathbf{f}}{\mathbf{f} z} \left( \mathbf{m} \frac{\mathbf{f} v_z}{\mathbf{f} z} \right) \end{aligned} \quad (10.30)$$

and

$$0 = \bar{\mathbf{r}} f_r - \frac{1}{r} \frac{\mathbf{f}}{\mathbf{f} r} (r \mathbf{g} \bar{\mathbf{r}} k) + \frac{\mathbf{f}}{\mathbf{f} z} \left( \mathbf{m}^T \frac{\mathbf{f} v_z}{\mathbf{f} r} \right) - \frac{1}{r} \frac{\mathbf{f}}{\mathbf{f} r} (r p) + \frac{\mathbf{f}}{\mathbf{f} z} \left( \mathbf{m} \frac{\mathbf{f} v_z}{\mathbf{f} r} \right) \quad (10.31)$$

Collect like terms in the two equations:

$$\begin{aligned} \bar{\mathbf{r}} \frac{\mathcal{I} v_z}{\mathcal{I} t} + v_z \frac{\mathcal{I} v_z}{\mathcal{I} z} = \bar{\mathbf{r}} f_z + \frac{1}{r} \frac{\mathcal{I}}{\mathcal{I} r} \left( r(\mathbf{m} + \mathbf{m}^T) \frac{\mathcal{I} v_z}{\mathcal{I} r} \right) + \frac{\mathcal{I}}{\mathcal{I} z} \left( \frac{2}{3} (\mathbf{m} + \mathbf{m}^T) \frac{\mathcal{I} v_z}{\mathcal{I} z} \right) + \frac{\mathcal{I}}{\mathcal{I} z} \left( (\mathbf{m} + \mathbf{m}^T) \frac{\mathcal{I} v_z}{\mathcal{I} z} \right) \\ - \frac{\mathcal{I}}{\mathcal{I} z} (p + \mathbf{g} \bar{\mathbf{r}} k) \end{aligned} \quad (10.32)$$

$$0 = \bar{\mathbf{r}} f_r - \frac{1}{r} \frac{\mathcal{I}}{\mathcal{I} r} \left( r(p + \mathbf{g} \bar{\mathbf{r}} k) \right) + \frac{\mathcal{I}}{\mathcal{I} z} \left( (\mathbf{m} + \mathbf{m}^T) \frac{\mathcal{I} v_z}{\mathcal{I} r} \right) \quad (10.33)$$

Assuming that the analysis is being applied to a horizontal pipe, the mass of the mixture will neither add to nor detract from the motion of the mixture. (If the flow were in a vertical pipe, body forces would have to be included in the analysis, at least until it could be demonstrated that body forces could be safely neglected.) Thus, assuming no body forces, the result is:

$$\bar{\mathbf{r}} \frac{D v_z}{\mathcal{I} t} = \frac{1}{r} \frac{\mathcal{I}}{\mathcal{I} r} \left( r(\mathbf{m} + \mathbf{m}^T) \frac{\mathcal{I} v_z}{\mathcal{I} r} \right) + \frac{\mathcal{I}}{\mathcal{I} z} \left( \frac{5}{3} (\mathbf{m} + \mathbf{m}^T) \frac{\mathcal{I} v_z}{\mathcal{I} z} \right) - \frac{\mathcal{I} p}{\mathcal{I} z} - \frac{\mathcal{I}}{\mathcal{I} z} (\mathbf{g} \bar{\mathbf{r}} k) \quad (10.34)$$

$$0 = -\frac{1}{r} \frac{\mathcal{I}}{\mathcal{I} r} (r p) - \frac{1}{r} \frac{\mathcal{I}}{\mathcal{I} r} (r \mathbf{g} \bar{\mathbf{r}} k) + \frac{\mathcal{I}}{\mathcal{I} z} \left( (\mathbf{m} + \mathbf{m}^T) \frac{\mathcal{I} v_z}{\mathcal{I} r} \right) \quad (10.35)$$

Expanding the equations for the  $1/r$  parameters:

$$\bar{\mathbf{r}} \frac{D v_z}{\mathcal{I} t} = -\frac{\mathcal{I} p}{\mathcal{I} z} + \frac{(\mathbf{m} + \mathbf{m}^T) \mathcal{I} v_z}{r \mathcal{I} r} + \frac{\partial}{\partial r} \left( (\mathbf{m} + \mathbf{m}^T) \frac{\mathcal{I} v_z}{\mathcal{I} r} \right) + \frac{\mathcal{I}}{\mathcal{I} z} \left( \frac{5}{3} (\mathbf{m} + \mathbf{m}^T) \frac{\mathcal{I} v_z}{\mathcal{I} z} \right) - \frac{\partial}{\partial z} (\mathbf{g} \bar{\mathbf{r}} k) \quad (10.36)$$

$$0 = -\frac{p}{r} - \frac{\mathbf{g} \bar{\mathbf{r}} k}{r} - \frac{\mathcal{I} p}{\mathcal{I} r} - \frac{\mathcal{I} (\mathbf{g} \bar{\mathbf{r}} k)}{\mathcal{I} r} + \frac{\partial}{\partial z} \left( (\mathbf{m} + \mathbf{m}^T) \frac{\partial v_z}{\partial r} \right) \quad (10.37)$$

Integrating each term of equation (10.36) across the cross-sectional area with respect to  $r$ :

$$2\mathbf{p} \int_0^{R_0} \bar{\mathbf{r}} \frac{\mathcal{I} v_z}{\mathcal{I} t} dr = 2\mathbf{p} \bar{\mathbf{r}} \frac{d}{dt} \int_0^{R_0} v_z \frac{d(r^2)}{2} = \mathbf{p} \bar{\mathbf{r}} \frac{d}{dt} v_z R_0^2 \quad (10.38)$$

$$2\mathbf{p} \int_0^{R_0} \frac{\bar{\mathbf{r}}}{2} \frac{\mathcal{I}(v_z^2)}{\mathcal{I}_z} r dr = 2\mathbf{p} \int_0^{R_0} \frac{\bar{\mathbf{r}}}{2} \frac{\mathcal{I}(v_z^2)}{\mathcal{I}_z} \frac{\partial(r^2)}{2} = \frac{\mathbf{p} \bar{\mathbf{r}}}{2} \frac{\mathcal{I}}{\mathcal{I}_z} \int_0^{R_0} (v_z^2) d(r^2) = \frac{\mathbf{p} \bar{\mathbf{r}}}{2} \frac{\mathcal{I}(\overline{v^2})}{\mathcal{I}_z} R_0^2 \quad (10.39)$$

$$2\mathbf{p} \int_0^{R_0} \frac{\partial p}{\partial z} r dr = 2\mathbf{p} \frac{\partial}{\partial z} \int_0^{R_0} p \frac{d(r^2)}{2} = \mathbf{p} \left( \frac{\partial p}{\partial z} \right) R_0^2 \quad (10.40)$$

$$2\mathbf{p} \int_0^{R_0} \frac{(\mathbf{m} + \mathbf{m}^T)}{r} \frac{\partial v_z}{\partial r} r dr = 2\mathbf{p} \int_0^{R_0} (\mathbf{m} + \mathbf{m}^T) \frac{\partial v_z}{\partial r} dr = 2\mathbf{p} \left( \overline{(\mathbf{m} + \mathbf{m}^T) \frac{\partial v_z}{\partial r}} \right) \frac{R_0^2}{R_0} \quad (10.41)$$

$$2\mathbf{p} \int_0^{R_0} \frac{\partial}{\partial r} \left( (\mathbf{m} + \mathbf{m}^T) \frac{\partial v_z}{\partial r} \right) r dr = 2\mathbf{p} \int_0^{R_0} \left( (\mathbf{m} + \mathbf{m}^T) \frac{\partial v_z}{\partial r} \right) dr = 2\mathbf{p} \left( \overline{(\mathbf{m} + \mathbf{m}^T) \frac{\partial v_z}{\partial r}} \right) \frac{R_0^2}{R_0} \quad (10.42)$$

$$2\mathbf{p} \int_0^{R_0} \frac{\partial}{\partial z} \left( \frac{5}{3} (\mathbf{m} + \mathbf{m}^T) \frac{\partial v_z}{\partial z} \right) r dr = 2\mathbf{p} \frac{\partial}{\partial z} \int_0^{R_0} \left( \frac{5}{3} (\mathbf{m} + \mathbf{m}^T) \frac{\partial v_z}{\partial z} \right) \frac{d(r^2)}{2} = \mathbf{p} \frac{\partial}{\partial z} \left( \frac{5}{3} (\mathbf{m} + \mathbf{m}^T) \frac{\partial v_z}{\partial z} \right) R_0^2 \quad (10.43)$$

$$2\mathbf{p} \int_0^{R_0} (\mathbf{g} \bar{\mathbf{r}} k) r dr = 2\mathbf{p} \bar{\mathbf{r}} \int_0^{R_0} (\mathbf{g} k) \frac{d(r^2)}{2} = \mathbf{p} \bar{\mathbf{r}} (\bar{\mathbf{g}} k) R_0^2 \quad (10.44)$$

The resulting equation, after applying the integrated terms to equation (10.36), and dividing by  $R_0$ , is:

$$\bar{\mathbf{r}} \frac{Dv_z}{Dt} = -\frac{\partial p}{\partial z} + \frac{4}{R_0} (\mathbf{t}_w + \mathbf{t}_{wT}) + \frac{5}{3} \left( \overline{(\mathbf{m} + \mathbf{m}^T) \frac{\partial v_z}{\partial z}} \right) - \bar{\mathbf{r}} (\bar{\mathbf{g}} k) \quad (10.45)$$

where  $\tau_{wT}$  represents the force imposed on the mixture due to turbulence, and includes solid particle-related phenomena. Mixture compressibility, and energy losses due to mixture turbulence, are also represented in the equation.

## 10.2.4 Summary

The resulting momentum equations, integrated across the cross-sectional area of the pipe, are:

**Textbook** (with some rearrangement of signs):

$$\rho v \frac{dv}{dz} = -\frac{dp}{dz} + \frac{\rho f v^2}{2D} \quad (10.6)$$

**Ural:**

$$\rho \frac{\partial \bar{v}}{\partial t} = -\frac{\partial \bar{p}}{\partial z} + \frac{1}{R_0} \tau_w \quad (10.14)$$

**Ahmadi:**

$$\bar{r} \frac{D \bar{v}_z}{Dt} = -\frac{\partial \bar{p}}{\partial z} + \frac{4}{R_0} (\bar{t}_w + \bar{t}_{wT}) + \frac{5}{3} \left( \overline{(m + m_t) \frac{\partial v_z}{\partial z}} \right) - \bar{r}(\bar{g}) \quad (10.45)$$

The primary changes introduced by the multiphase Ahmadi analysis are 1) the viscous stress term including the eddy viscosity, 2) an additional term for the mixture compressibility stresses, and 3) a loss term resulting from the turbulence of the flow. The combination of the laminar and turbulent viscous stresses may be converted directly to wall stress terms which can be accounted for in calculations by a friction factor augmented for the inclusion of the agent in the flowing material. As a result, many of the viscous stress terms resulting from the two phases may be accounted for by an empirically determined friction factor for mixture flow.

### **10.3 Particle Acceleration to Gas Velocity**

The objectives of these calculations were to determine 1) the time it would take a single particle of dry chemical agent to reach the top of a typical storage tank, and 2), the time for a particle to reach at least 99% of the velocity of the carrier gas. The analysis has bearing on how important particle entrainment is in the source tank, and how



important such phenomena as interparticle collisions and particle drag are to the modeling of a gas/solids multiphase flow with particles less than 100 microns in size.

The analysis proceeds in a manner nearly identical to that described in **Crowe et al (1977)**, with the only difference for this analysis in the placing of the gravitational force opposite to the drag force seeking to accelerate a particle. The analysis in **Crowe et al (1977)** aligned gravitation and particle drag in the same direction. In any event, the analysis showd mathematically that gravitation plays but a minor role in the acceleration of the particle.

The equation of motion for a particle being accelerated upwards is:

$$m \frac{dv}{dt} = c_d \rho_g (u - v) |u - v| \frac{A}{2} - mg \quad (10.46)$$

where

- m = mass of particle
- v = particle velocity
- c<sub>d</sub> = particle drag coefficient
- ρ<sub>g</sub> = gas density
- u = gas velocity
- A = projected area of particle
- G = gravitational acceleration

Dividing through by m (= ρV, where V = particle volume), and resolving for the formulas for area and volume (assuming spherical particles), the result is:

$$\frac{dv}{dt} = \frac{3c_d \rho_g (u - v) |u - v|}{4\rho_d d_p} - g \quad (10.47)$$

where

- ρ<sub>d</sub> = particle density
- d<sub>p</sub> = particle diameter

The Reynolds number for a particle depends on the gas-particle relative velocity:

$$\text{Re} = \frac{\rho_g |u - v| d_p}{\mu_g} \quad (10.48)$$

where

$\mu_g$  = gas viscosity

Rearranging yields:

$$|u - v| = \frac{\text{Re} \mu_g}{\rho_g d_p} \quad (10.49)$$

Substituting (10.49) into (10.47) results in:

$$\frac{dv}{dt} = \frac{3c_d \text{Re} \mu_g}{4\rho_d d_p^2} (u - v) - g = \frac{18\mu_g f}{\rho_d d_p^2} (u - v) - g \quad (10.50)$$

where

$$f = \frac{\text{Re} c_d}{24} \quad (10.51)$$

Let

$$\tau = \frac{\rho_d d_p^2}{18\mu_g f} \quad (10.52)$$

Substituting (10.52) into (10.50) yields:

$$\frac{dv}{dt} = \frac{1}{\tau} (u - v) - g \quad (10.53)$$

After some manipulation, integration by separation of variables, and further manipulation, the final form of the equation is:

$$v = u - (u - v_0)e^{-t/\tau} - g\tau(1 - e^{-t/\tau}) \quad (10.54)$$

The following numerical inputs were used, assuming a sodium bicarbonate particle in a nitrogen gas carrier, at standard temperature, and approximately 360 psig pressure:

$$\begin{aligned} v_0 &= 0 \\ u &= 146.4 \text{ ft/sec} \\ g &= 32.174 \text{ ft/sec}^2 \\ \mu_g &\approx 2 \times 10^{-5} \text{ lbm/ft-sec} \\ \rho_d &= 137.3 \text{ lbm/ft}^3 \\ d_p &= 1.64 \times 10^{-4} \text{ ft} \\ \rho_g &= 1.774 \text{ lbm/ft}^3 \end{aligned}$$

The results of the calculations show that the time for a particle to travel 17 inches - the inside height of a 25 pound cylinder of agent and carrier gas - even for a slow gas velocity, are short, on the order of 0.10 second or less. The maximum distance for a particle to reach 99% of the carrier gas velocity is less than 2 inches. Given this information, it would be expected that particles of the size, shape, and type considered accelerate rapidly to the velocity of the carrier gas. Furthermore, these particles rapidly recover from events such as bends or tees in a piping system.

Note that in the calculations performed, the gravitational term was calculated to be four orders of magnitude smaller than the drag forces, on the average. As a result of this, the gravitational term in the equation could be safely neglected for calculations with these sorts of inputs.

#### **10.4 Influence Coefficients**

A comparison of influence coefficients between the coefficients for mixtures and coefficients for gas-only fluids is shown below. Parameters as shown in Table 4.2 were

calculated for an instance of a typical dry chemical fire suppression system, and compared to the calculated values of a fluid with no solid phase. The tables as shown below were generated for  $dP/P$ ,  $d\rho/\rho$ ,  $dT/T$ ,  $da/a$ ,  $dM^2/M^2$ , and  $dv^2/v^2$ . A calculation was mathematically not possible at  $\theta = 1$ ; however calculations were performed at a volume fraction close to 1.0. The bottom three rows of each table show the influence coefficients for a gas-only fluid at conditions otherwise identical to those for the mixture.

As can be seen in the tables, for the most part, the trends and values calculated for the mixture were similar to those for the gas-only fluid, except at values of Mach number and volume fraction close to 1.0. As can be seen in the equations, the derivatives tend to change rapidly for the mixture, as they do for the gas-only fluid. While there are some changes in signs for volume fractions close to 1.0, in the vicinity where most dry chemical fire suppression systems start discharging from, with a volume fraction in the cylinder of approximately 0.5, trends in the influence coefficients are the same for the mixture and gas-only fluid. As a result, for the regimes of interest, while the behaviors of a gas-solids mixture and gas-only fluid may differ somewhat, their basic behaviors, such as, subsonically, increasing Mach number with decreasing cross-sectional area, are the same. Thus, the general behavior of fluids may be successfully used in the modeling of the gas-solids mixture.

Input Parameters (Based on test P-6, with sodium bicarbonate agent, nitrogen

gas):

$$P_{0\text{-tank}} = 307.211 \text{ psia}$$

$$T_{0\text{-tank}} = 530 \text{ }^{\circ}\text{R}$$

$$V_{\text{tank}} = 0.43 \text{ ft}^3$$

$$R_{\text{G-N}_2} = 55.15 \text{ ft-lbf/lbm-}^{\circ}\text{R}$$

$$\gamma_{\text{G}} = 1.4034$$

$$C_d = 0.38$$

$$\rho_{\text{D}} = 137.38 \text{ lbm/ft}^3$$

$$\phi = 0.98521$$

$$C = 0.249 \text{ BTU/lbm-}^{\circ}\text{R}$$

$$C_{\text{pg}} = 0.2477 \text{ BTU/lbm-}^{\circ}\text{R}$$

$$C_{\text{vg}} = 0.177 \text{ BTUY/lbm-}^{\circ}\text{R}$$

$$A_{\text{n}} = 0.00307 \text{ ft}^2$$

dP/P:

$\theta$	Mach Number	dA/A	fdx/2D
0.25	0.25	0.08945	-0.00895
	0.50	0.44701	-0.44798
	0.75	1.72064	-1.72902
	1.00	619.38462	-624.75262
0.50	0.25	0.13414	-0.13425
	0.50	0.66955	-0.67173
	0.75	2.56669	-2.58546
	1.00	309.69231	-313.71831
0.75	0.25	0.26805	-0.26849
	0.50	1.33333	-1.34200
	0.75	5.04968	-5.12353
	1.00	206.46154	-211.82954
0.999	0.25	46.82811	-65.85203
	0.50	106.01991	-278.30226
	0.75	138.42134	-644.52436
	1.00	155.00116	-1162.50866
0.0	0.25	0.06710	-0.06713
	0.50	0.33550	-0.33605
	0.75	1.29407	-1.29880

dp/p:

$\theta$	Mach Number	dA/A	fdx/2D
0.25	0.25	0.06651	-0.06709
	0.50	0.33237	-0.33526
	0.75	1.27936	-1.29048
	1.00	460.53846	-464.53847
0.50	0.25	0.06620	-0.06707
	0.50	0.33045	-0.33447
	0.75	1.26677	-1.28335
	1.00	152.84615	-154.84615
0.75	0.25	0.06528	-0.06701
	0.50	0.32472	-0.33333
	0.75	1.22981	-1.76242
	1.00	50.28205	-51.61538
0.999	0.25	-0.25559	-0.04683
	0.50	-0.57866	-0.10602
	0.75	-0.75551	-0.13842
	1.00	-0.84600	-0.15500
0.0	0.25	0.06667	-0.06710
	0.50	0.33333	-0.33550
	0.75	1.28571	-1.29407

dT/T:

$\theta$	Mach Number	dA/A	fdx/2D
0.25	0.25	0.00077	$4.8541 \times 10^{-5}$
	0.50	0.00385	0.00097
	0.75	0.01482	0.00839
	1.00	5.33333	5.36800
0.50	0.25	0.00173	0.00011
	0.50	0.00865	0.00218
	0.75	0.03315	0.01877
	1.00	4.00000	4.02600
0.75	0.25	0.00692	0.00044
	0.50	0.03247	0.00867
	0.75	0.13044	0.07385
	1.00	5.33333	5.36800
0.999	0.25	302.41701	19.02392
	0.50	684.67899	172.28235
	0.75	893.92816	506.10302
	1.00	1001.00100	1007.50751
0.0	0.25	0.00004	$2.72594 \times 10^{-5}$
	0.50	0.00217	0.00055
	0.75	0.00836	0.00473



da/a:

$\theta$	Mach Number	dA/A	fdx/2D
0.25	0.25	0.02256	-0.02239
	0.50	0.11271	-0.11237
	0.75	0.43386	-0.43435
	1.00	156.17949	-157.53015
0.50	0.25	0.06707	-0.06713
	0.50	0.33477	-0.33586
	0.75	1.28335	-1.29273
	1.00	154.84615	-156.85915
0.75	0.25	0.19931	-0.20126
	0.50	0.99139	-1.00433
	0.75	3.75465	-3.82419
	1.00	153.51282	-157.53015
0.999	0.25	-104.12486	-56.29324
	0.50	-275.74093	-192.05506
	0.75	-307.78724	-391.33443
	1.00	-344.65335	-658.59991
0.0	0.25	0.00002	-1.36297x10 <sup>-5</sup>
	0.50	0.00108	-0.00027
	0.75	0.00418	-0.00237

$dM^2/M^2$ :

$\theta$	Mach Number	dA/A	fdx/2D
0.25	0.25	-2.26759	0.17896
	0.50	-3.37182	0.89499
	0.75	-7.14709	3.44966
	1.00	-1854.82051	1244.13723
0.50	0.25	-2.40069	0.26839
	0.50	-4.00000	1.34127
	0.75	-9.66927	5.15215
	1.00	-927.07692	623.41062
0.75	0.25	-2.79723	0.53654
	0.50	-5.96556	2.67533
	0.75	-17.01860	10.17322
	1.00	-616.05129	418.29108
0.999	0.25	159.93268	112.68014
	0.50	364.61927	384.32217
	0.75	476.66415	782.94569
	1.00	533.99754	1317.50982
0.0	0.25	-2.20087	0.13423
	0.50	-3.00433	0.61755
	0.75	-5.87386	2.59287

$dv^2/v^2$ :

$\theta$	Mach Number	dA/A	fdx/2D
0.25	0.25	-2.13303	0.13418
	0.50	-2.66474	0.67052
	0.75	-4.55873	2.58095
	1.00	-923.07692	929.07692
0.50	0.25	-2.13241	0.13414
	0.50	-2.66090	0.66955
	0.75	-4.53354	2.56669
	1.00	-307.69231	309.69231
0.75	0.25	-2.13056	0.13403
	0.50	-2.69445	0.66667
	0.75	-4.45962	2.52484
	1.00	-102.56410	103.23077
0.999	0.25	-1.48882	0.09366
	0.50	-0.84268	0.21204
	0.75	-0.48899	0.27684
	1.00	-0.30800	0.31000
0.0	0.25	-2.13333	0.13420
	0.50	-2.66667	0.67100
	0.75	-4.57143	2.58814

## 10.5 *Station\_list, Station\_list\_node Classes Listing (classes.h).*

```
////////////////////////////////////
// classes.h - class header file for dry chem program - project5
// R.M. Eber
// 9/8/00
//
// Notes:  class station_list acts as a header to a node chain.
//         Also, calls to manipulations are done from there.
//         class station_list_node provides stations at which
//         calculations are performed, and data for comparisons
//         and outputs are stored.  Calculation procedures for
//         state variables are kept here.
////////////////////////////////////
#ifndef STDIO_H
#include <stdio.h>
#define STDIO_H
#endif /* stdio.h */

#ifndef STDLIB_H
#include <stdlib.h>
#define STDLIB_H
#endif /* stdlib.h */

#ifndef MATH_H
#include <math.h>
#define MATH_H
#endif /* math.h */

#ifndef ZERO_H
#include "zero.h"
#define ZERO_H
#endif /* zero.h */
// canned routine for finding new values (as roots) of mach numbers
//         and densities.

#ifndef DATA1_H
#include "data1.h"
#define DATA1_H
#endif /* data1.h */

#define DELTA_MAX 0.001
#define NUMBER 22
#define NUMBER_2 22

// enumeration of component "type"

enum Component { START, TANK, PIPE, CONTRACTION, EXPANSION, THROAT,
                TWO_TANK };

enum { FALSE, TRUE };

// forward declaration required for mention of class station_list in
//         declaration of class station_list_node.
```

```

class station_list;

class station_list_node
{
    private:
        Component type; // type of pipe/fitting upstream of node
        FILE *out; // file pointer for outputting data

    // node state data
    double pl_old; // local static pressure (PSIA)
    double pt_old; // local total pressure (PSIA)
    double rho1; // local static density (lbs/cu. ft)
    double rho_t; // local total density (lbs/cu. ft)
    double temp1; // local static temperature (R)
    double temp_t; // local total temperature (R)
    double theta; // local theta
    double mach_old; // local mach number
    double T0bar; // tank value corrected to T0 at time = 0
    double p0bar; // tank value corrected to p0 at time = 0
    double theta0bar; // tank value corrected to theta0 at time = 0

    double rho_g1; // local gas density (lbm/cu. ft.)
    double a; // local speed of sound (ft./sec.)
    double a_g; // local gas speed of sound (ft./sec.)
    double u; // local velocity (ft./sec.)

    double Reg; // gas-only Reynolds number
    double Rem; // mixture Reynolds number
    double f; // gas-only friction factor(based on mixture
    // Re)
    double fprime_f; // mix/gas-only friction factor ratio
    double fl_d; // fL/D factor for sc, se nodes
    double fz_fprime_f; // mix/gas-only friction factor (Fan & Zhu
    // p 471)

    // geometric data
    double length; // length of upstream fitting (pipe)(if any)
    // (ft.)
    double local_dia; // diameter at local station (ft.)
    double ksd; // roughness factor for pipes
    double area; // cross-sectional area at node (sq. ft)
    double mass_flow; // mass flow (lbm/cu. ft.) at node
    double vol_flow; // volume flow (cu. ft./sec.) at node
    double tank_volume; // tank volume (cu. ft.)
    double solid_mass; // mass of powder in cylinder (lbm)

    int node_number; // label applied when node constructed
    int choke_flag; // temporary label marking a possibly choked
    // node
    int choke_pt_flag; // permanently marked node for choking
    // candidacy
    int throat_choke; // used by throat_rho() to force convergence
    // when unchoked flow (end game) - 1 if in
    // choked flow, 0 if in unchoked flow.

```

```

double cd;           // inlet discharge coefficient
double rho10;       // source tank local density at time = 0
double templ0;      // source tank temperature at time = 0
double pl_old0;     // source tank local pressure at time = 0
double theta00;     // source tank volume fraction at time = 0

double prat_crit;   // critical pressure ratio using ptotal at
                    // given node
double rhot0;       // source tank stagnation density at time = 0
double noz_length;  // distance from nozzle inlet to throat (ft.)

double prat_critical; // used in choking check.
double prat_original; // also used in choking check.

station_list_node *next; // next station in system
station_list_node *prev; // previous station in system

public:

// constructors and member functions

// constructor, no data inputs
station_list_node()
{
    // make sure pointers are initialized
    next = NULL;
    prev = NULL;
}

// constructor, component type and
// mach number inputs only
station_list_node(Component typ, int n_number, FILE *fp,
                  double diameter, double leng = 0.0)
: type(typ), out(fp), local_dia(diameter), length(leng),
  node_number(n_number)
{
    // make sure pointers are initialized
    // Default length = 0 for "non-pipes"
    next = NULL;
    prev = NULL;
    choke_flag = 0;
    choke_pt_flag = 0;
}

// constructor with all state variables set -
// - set pointers
station_list_node(Component typ, int n_number,
                  FILE *fp, double pl, double rho1,
                  double templ, double theta, double diameter, double leng = 0.0)
: type(typ), out(fp), pl_old(pl), pt_old(pl),
  rho1(rho1), rhot(rho1), templ(templ), tempt(templ),
  theta(theta), local_dia(diameter), length(leng),
  node_number(n_number), rho10(rho1), templ0(templ), pl_old0(pl),
  theta00(theta), rhot0(rho1)
{

```

```

    // make sure pointers are initialized
    // Default length = 0 for "non-pipes"
    next = NULL;
    prev = NULL;
    choke_flag = 0;
    choke_pt_flag = 0;
    if((typ == TANK) || (typ == TWO_TANK))
    {
        T0bar = 1.0;
        p0bar = 1.0;
        theta0bar = 1.0;
    }
}

// functions....

// set source tank outlet discharge pressure
void set_cd(double value) { cd = value; }

// set nozzle length (from entrance to throat)
void set_noz_length(double value) { noz_length = value; }

// set source tank gas density
void set_rhogl(double pl, double tl)
    { rhogl = (pl*144.0)/(55.15*tl); }

// set cross-sectional area at node
void set_area(double value) { area = value; }

// set volume (for tank node(s))
void set_volume(double value) { tank_volume = value; }

// set initial powder mass in cylinder
void set_mass(double value) { solid_mass = value; }

// set throat_choke flag in throat node
void set_throat_choke(double value) { throat_choke = value; }

// set initial mixture and gas speeds of sound.
void set_speeds(double gamma, double gc, double R, double t0tank,
    double gamma_mix, double phi, double theta0)
    {
        ag = sqrt(gamma * gc * R * t0tank);
        a = (sqrt(gamma_mix * gc * R * (1.0 - phi) * t0tank))
            / (1.0 - theta0);
    }

// set gas-only friction factor for pipe nodes
void set_f(double value) { f = value; }

// set fL/D value for sc and se nodes
void set_floss(double value) { fl_d = value; }

// set f_prime/f augmentation factor for pipe nodes
void set_fprime_f(double value) { fprime_f = value; }

```

```

// return file handle
FILE *get_fp() { return out; }

station_list_node *get_next() { return next; }

station_list_node *get_prev() { return prev; }

// return number label of node
int get_number() { return node_number; }

// return throat_choke flag in throat node
int get_throat_choke() { return throat_choke; }

// return Component type
enum Component get_type() { return type; }

// return area
double get_area() { return area; }

// return discharge coefficient
double get_cd() { return cd; }

// set choke_flag
void set_choke_flag(int value) { choke_flag = value; }

// set choke_point_flag
void set_choke_pt_flag() { choke_pt_flag = 1; }

// set the pipe roughness value, if required
void set_ksd(double value) { ksd = value; }

// set mach number (zero in tank) for tank nodes
void set_mach(double value) { mach_old = value; }

// give station_list full access to variables, member
// functions
friend class station_list;

}; // end of class station_list_node declaration

struct element {
    int node_number;
    double node_area;
    station_list_node *aptr;
};

class station_list
{
private:
    station_list_node *head; // marks start of node chain
    station_list_node *tail; // marks end of node chain
    station_list_node *lead; // "current" node marker
    station_list_node *lag; // "previous" node marker

```



```

station_list_node *current; // indicates current node for some
                           // member functions
station_list_node *next_head; // used by PT chain to point to
                              // TWO_TANK (for PT chain choking).
station_list_node *prev_tail; // used in tank/PT stuff.

public:

// constructor with no inputs
station_list() : head(NULL), tail(NULL), lead(NULL), lag(NULL)
{ }

// constructor with single node input
station_list(station_list_node *n) :
    head(n), tail(n), lead(n), lag(n) { }

// destructor - gets rid of any attached list
~station_list()
{
    if (head)
    {
        lead = head->next;
        lag = head;

        while (lead)
        {
            delete lag; // delete station_list_nodes;
            lag = lead;
            lead = lead->next;
        } // end of while()

        delete lag; // delete last (or perhaps only) node
    } // end of if()
} // end of ~station_list()

// double-linked list building functions

// adds a node to the chain
void insert(station_list_node *n);

// add a node whether or not node chain is empty.
void add_node(station_list_node *n);

// other functions
// find and return pointer to the(a) START node
station_list_node * find_start();

void set_next_head(station_list_node *n)
{ next_head = n; }

void set_prev_tail(station_list_node *n)
{ prev_tail = n; }

// iteratively generate gas-only friction factor
double friction_factor(struct data1 *user1,

```

```

    station_list_node *ptr);

double get_tank_pr() { return head->pt_old; }

double get_tail_pr() { return tail->pl_old; }

double get_tail_theta() { return tail->theta; }

double get_tail_mach() { return tail->mach_old; }

double get_prat_critical() { return head->prat_critical; }

double get_prat_original() { return head->prat_original; }

station_list_node * get_tail_ptr() { return tail; }

// this will need re-doing with multiple tanks, head locations,
// etc....
station_list_node * get_tank_ptr() { return head; }

// for testing purposes
// print out basic list information - verify double-linked list
void show_list(FILE *fp, int h);
void backwards_list(FILE *fp, int h);

// calculation for density iterations
// double con_rho(struct data1 *user1, station_list_node *ptr);

double con_rho(struct data1 *user1, station_list_node *ptr);
double expansion_rho(struct data1 *user1, station_list_node *ptr);
double new_density(double guess, struct data1 *user1,
    station_list_node *ptr);
double pipe_rho_func(struct data1 *user1, double m0,
    double rho0, double m1, station_list_node *ptr);
double throat_rho(struct data1 *user1, station_list_node *ptr);

// calculate state vectors at each non-tank node

// compressible flow model
void do_compressible_state(struct data1 *user1,
    station_list_node *ptr);

// incompressible flow models
void do_pipe_incompressible(struct data1 *user1,
    station_list_node *ptr);
void do_sc_incompressible(struct data1 *user1,
    station_list_node *ptr);
void do_se_incompressible(struct data1 *user1,
    station_list_node *ptr);
void do_start_incompressible(struct data1 *user1,
    station_list_node *ptr);

// state parameter calculations in common in node calculations
void rest_of_calcs(struct data1 *user1, station_list_node *ptr);

```

```

void tank_calc(double timestep, station_list_node *ptr,
               struct data1 *user1, int h);

void print_out_results(double time, struct data1 *user1);
    // for temporary checks of data
void print_out_tank_results(double time, station_list_node *ptr,
                            struct data1 *user1);

int is_choked(struct data1 *user1, station_list_node *ptr, int h);

// new functions for recursive solution trials....

void calc(struct data1 *user1, station_list_node *ptr,
          double mach_guess);

void scan(station_list_node *ptr, int pass);
void reset_ptrs();
void bubble(struct element *ptr, int counter, int sort_flag);

double calc_us_from_th1(struct data1 *user1, station_list_node *ptr,
                       double in_mach, int tag);
double calc_throat_mach(struct data1 *user1, station_list_node
                       *ptr);

double estimate(double fl_d_pipe);
double est_mach(double a_ratio, station_list_node *ptr);

double pipe_lint_calc(struct data1 *user1, double m0, double rho0,
                     double rho1, station_list_node *ptr);

double pipe_lint_iter(struct data1 *user1, double rho0,
                     double length, station_list_node *ptr);
double pipe_rho_iter(struct data1 *user1, double m0, double rho0,
                     double rho1, station_list_node *ptr);

// change flag from 1 (choked flow) to 0 (unchoked flow) in THROAT
// node ONLY.
void reset_throat_choke(station_list_node *ptr);

}; // end of class station_list declaration

struct carrier {
    double lint; // variables for choking answer for pipes
    double mach;
    double density;
};

struct friction {
    double mach;
    double fl_d;
};

struct m_area {
    double area_ratio;
    double mach;
};

```

```
};
```

## 10.6 Data Structure Listing (data1.h).

```
////////////////////////////////////  
// data1.h  
//  
// data structure declaration  
//  
// program project5  
// 9/30/00  
// R. M. Eber  
//  
////////////////////////////////////  
  
struct data1 {  
    double gc;           // gravitational conversion constant  
                        // (lbm-ft/lbf-sec2)  
    double gamma;       // Gas specific heat ratio  
    double pambient;    // Ambient air pressure (PSIA)  
    double R;           // Gas ideal gas constant (ft-lbf/lbm R)  
  
    double phi;         // Mixture mass fraction  
    double pcritical;  // critical choking ratio at nozzle throat  
  
    double tank_vol;    // tank volume (cu. ft.)  
    double p0_initial;  // initial tank pressure (PSIA)  
    double t0_initial;  // initial tank temperature (R)  
    double rhog0_initial; // initial tank gas density (lbm/cu. ft)  
    double rhod;        // density of particle material (lbm/cu. ft)  
    double dia_particle; // average solids particle diameter (ft.)  
    double massd0;      // total mass of agent at start (lbm)  
    double vg0;         // initial volume of gas in tank (cu. ft.)  
  
    double cpg;         // gas constant pressure specific heat  
                        // (btu/lbm R)  
    double cvg;         // gas constant volume specific heat  
                        // (btu/lbm R)  
    double c;           // particle material specific heat  
                        // (btu/lbm R)  
    double apipe;       // pipe area (sq. ft)  
  
    double cd;          // tank pipe inlet discharge coefficient  
    double l_pipe;      // outside pipe equivalent length (ft)  
    double dia_pipe;    // outside pipe diameter (ft)  
    double ksd;         // pipe roughness factor  
    double dia_noz_th;  // nozzle throat diameter (ft)  
  
    double dia_tank_orif; // tank orifice diameter (ft)  
    double dia_noz_fwd;  // nozzle forward end diameter (ft)  
    double dia_noz_hole; // nozzle holes diameter (ft)  
    double loading;      // solids/gas loading ratio  
    double l_tank_pipe;  // tank pipe length (ft)
```

```

double dia_tank_pipe; // tank pipe diameter (ft)
double rho_mix_tank; // initial tank mixture density (lbm/cu. ft)
double delta; // tank properties factor
// (Chenoweth/Paolucci)
double gamma_mix; // mixture specific heat ratio
double noz_fwd_end_rat; // nozzle fwd end area/throat area

double noz_throat_rat; // nozzle throat area/fwd end area
double theta0; // tank initial volume ratio

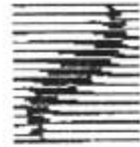
double time; // carries current time for some calcs (sec)
// int choke_flag; // 1 = choked, 0 = unchoked
// // probably should be enumerated TRUE_FALSE
int cut_flag; // for se/sc iterations
int master_counter; // for diagnostics only.
int pressure_calc_flag; // =1 if compressible START, PIPE, THROAT
// pl calculated - need final correction
// in rest_of_calcs().
// =0 otherwise (different component,
// incompressible, etc....)

int fprime_flag; // 0 = Pfeffer mixture friction multiplier.
// 1 = Fan & Zhu mixture friction
// multiplier.

double time_old1; // used in remaining powder mass
// calculation.
double mass_flow_old1; // used in remaining powder mass
// calculation.
};

```

## 10.7 *Kidde International (UK) Memo (Spring).*



Kidde International

### **Memorandum**

Date: 7<sup>th</sup> August 1997

From: P G Togher

To: R J Strople, E J Ortiz, G Meikle, D J Spring, B D Powell

cc:

---

### **Re: Update on the powder discharge modelling**

#### **Overview**

The work carried out to date consists of two main areas. These are the creation of measurement apparatus to collect data for validation of the model, and the actual modelling of the suppressant discharge. The first phase has been completed, with the creation of a discharge test rig and the collection of discharge data. Although work has started on the model, it is still in its early stages and no theoretical powder discharge data has yet been produced. The model has however shown reasonable performance when predicting gas only discharge. This could be an important step, depending on the modelling approach that is finally selected.

This memo will consist of two main sections, the first will describe the new discharge test rig, the second will examine the data collected with this equipment, along with comparison with the model were possible. This will be followed by a brief discussion on the next stage of the model development. Finally, an appendix will provide a summary of the theory used in the model.

#### **The discharge test equipment**

To enable the creation and validation of any model, data on discharge parameters is required. The two most crucial parameters are mass discharge and vessel pressure. To allow these parameters to be measured an experimental discharge measurement rig was created. The discharge test equipment can be seen in figure 1.

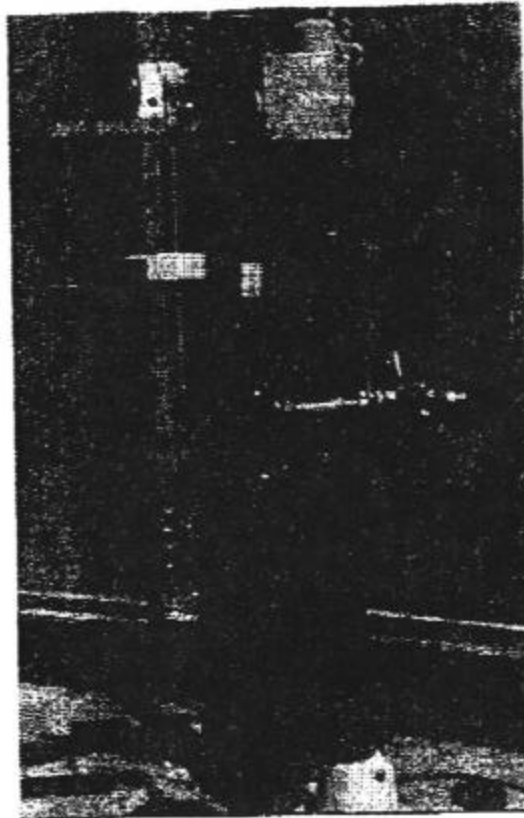


**Figure 1.** The discharge test rig.

The rig uses an old modified WKP powder extinguisher for the tests. The dip tube, head and hose have been custom made, and a transducer port has been added. The bottle has a total mass of 7.83 kg when empty, a volume of  $\approx 10$  litres and a maximum safe working pressure of 10 bar(g). The measurements are based around a 20 bar pressure transducer (figure 3) mounted on the vessel, and a 20kg load cell (figure 2) from which the vessel is suspended during firing.

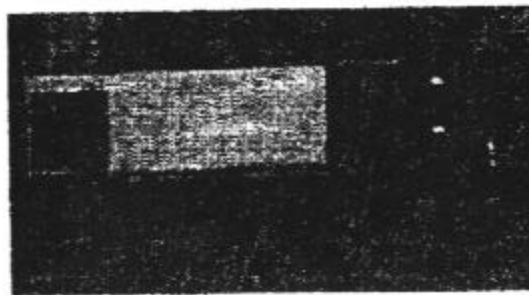


**Figure 2.** The 20 kg load cell used to weigh the extinguisher.

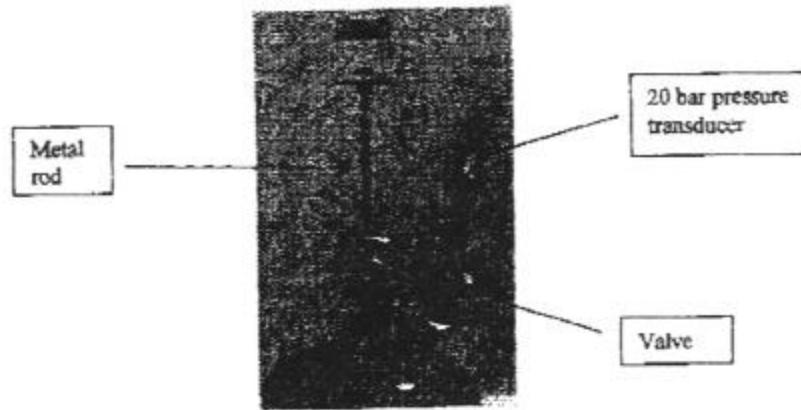


**Figure 3.** This shows the mounting assembly and pressure transducer. The valve below the pressure transducer allows the bottle to be charged in-situ.

The main difficulty with the measurement system is ensuring that the reaction force from the discharge does not perturb the mass measurement. To prevent the reaction force affecting the mass measurement the extinguisher is discharged through a horizontal hose. The hose is clamped at the end, where it is attached to a pneumatic ball valve (see figure 4). This valve is also clamped so that the extinguisher can be fired quickly, but without affecting the mass measurement of the cylinder.

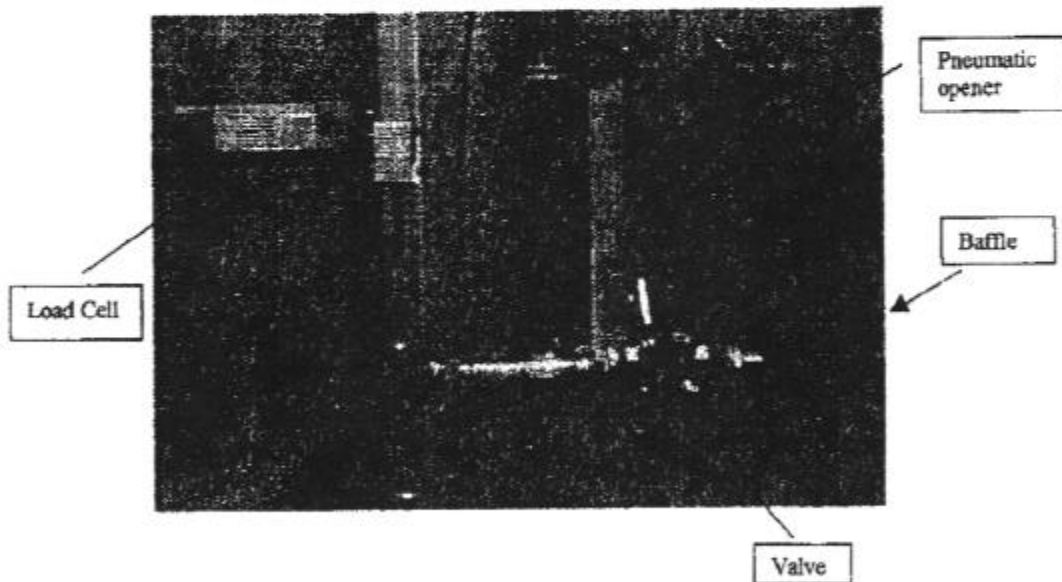


**Figure 4.** The pneumatic opening system, showing how the valve is clamped to prevent any effect on the load cell, while the hose is horizontal to eliminate reaction forces.

The extinguisher is suspended from the load cell via a rod (see figure 3). This is intended to minimise low frequency vibration. A basket is also available for tests using standard extinguishers, although this is not currently utilised.



The output from the load cell and the pressure transducer are fed back to a data logger. The data logger is triggered by a switch, which also opens the pneumatic ball valve. This starts the data logging process and fires the extinguisher.

The pneumatic ball valve can be fitted with various orifice sizes in order to measure to effect of the orifice diameter. It will also be used to attach different nozzles when required. The baffle fitted over the exit orifice is used to break up the flow of powder so that it can be collected without blowing a hole through the container. This does not affect the measurement in any way.

### The Discharge Test Data

This section provides examples of the data collected from discharge tests. The first examples will show the pressure drop for a cylinder discharge using nitrogen only. This data will also show examples of the fit provided by the model for this case. The final example shows the data collected for the powder discharge tests.

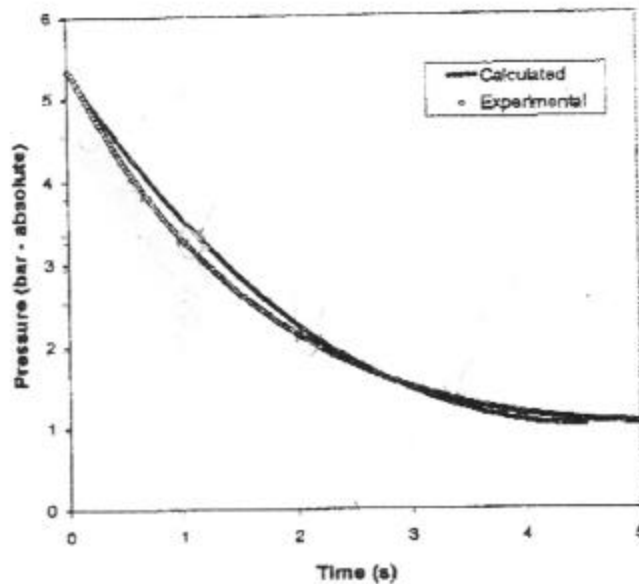


Figure 5. Graph showing the experimental pressure decay for nitrogen discharge with a nominal 5 bar initial pressure, along with the calculated pressure decay.

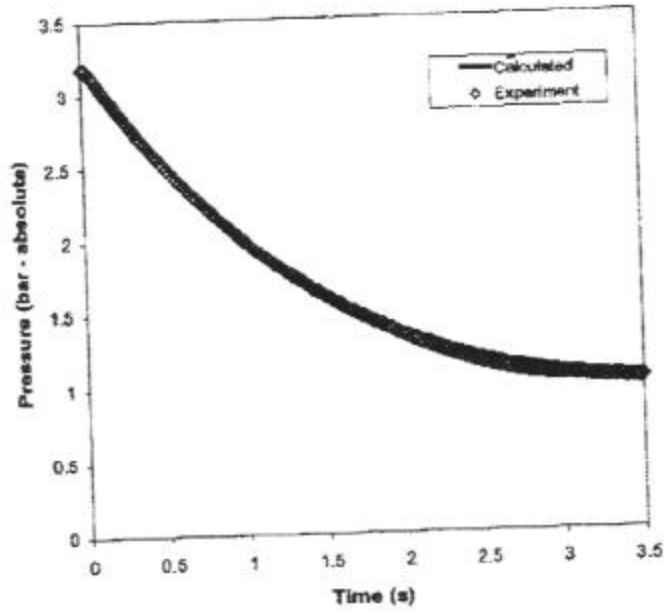


Figure 6. Graph showing the experimental pressure decay for nitrogen discharge with a nominal 3 bar initial pressure, along with the calculated pressure decay.

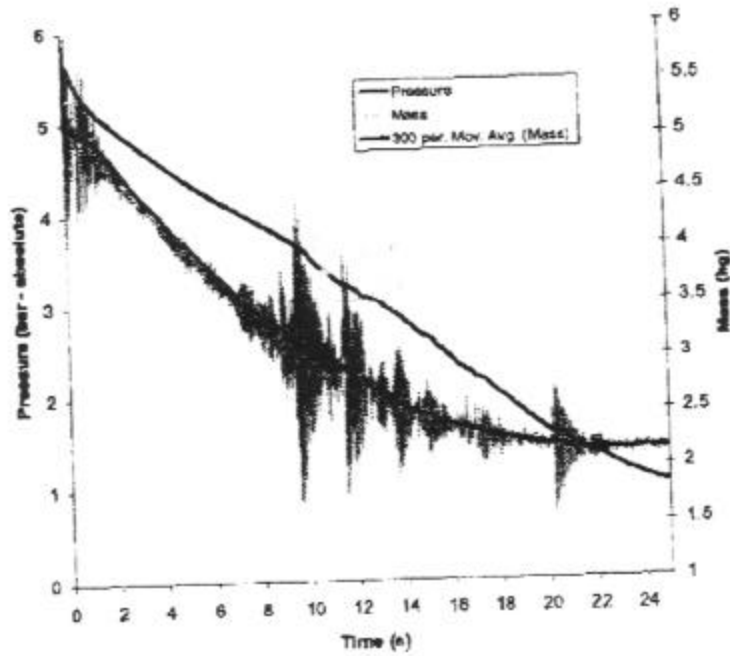


Figure 7. Graph showing pressure decay and mass discharge for a powder extinguisher with a 6 bar initial pressure.

It can be seen in figure 7 that the pressure characteristics are well behaved, along with the mass discharge, until  $\approx 80\%$  of the powder that will be discharged has been expelled. The amount of powder left can depend on many features, and further tests will be carried out to examine at what point the flow changes. The sudden change in the discharge character should be linked to the onset of "burps". It is hoped that enough powder will have been discharged before the onset of this phenomenon that the model will be able to effectively ignore this phase of the discharge. It is also expected that optimisation of the pressure, orifice size and the dip tube design will delay the onset of this effect.

### Future Work

The current model successfully predicts the nitrogen discharge characteristics of the test extinguisher. This is an important first step. This model will, according the homogeneous fluid mixture theory (see appendix A), predict the powder discharge characteristics using a modified equation of state. Although this is not difficult to implement, several other obstacles have yet to be dealt with. These concern the transition from an adiabatic gas system to an isothermal powder-gas mixture. Although the homogeneous mixture method allows the use of standard fluid flow equations, there are not any standard equations to describe certain isothermal conditions (i.e. isothermal flow through an orifice). Another factor that has yet to be implemented is the inclusion of terms that, although negligible in a gas system, can be significant in a powder-gas mixture. These factors include the potential energy change and kinetic energy and momentum changes. Also, small changes in the quasi steady state routines will be required to model the effect of the gas and gas-powder volumes with-in the cylinder.

I am currently in the process of implementing these features in order to assess the accuracy of the homogeneous mixture method.



**P G Togher**

## Appendix A

### Theory

This appendix outlines the theoretical approach used to model the powder discharge from an extinguisher.

#### Modelling Powder Flow

It is intended that the powder flow will be modelled, initially, as a homogeneous mixture using the steady state equations for pipe flow in a quasi steady state computer model. The homogenous mixture method, as suggested by Rudinger<sup>1</sup> and Wallis<sup>2</sup>, is the simplest method of calculating the powder flow in this situation. The method works by using the standard equations for compressible fluid flow, but introduces a modified equation of state to account for the effects of the powder. The modified equation of state is given by

$$PV_M = \frac{(1-\phi)}{(1-\xi)} RT \quad (1)$$

Where P is the pressure,  $V_M$  is the mixture specific volume, R is the gas constant, T is the mixture temperature while  $\phi$  is the mass fraction and  $\xi$  is the volume fraction of the powder in the mixture.

There is a limit to the accuracy of this approach, and the validity of the assumptions will break down under extreme conditions. It is hoped that this will not be the case in this situation, although this will not be known until more work has been completed.

For this approach to work, the model must first demonstrate that it is capable of modelling the compressible gas flows within the extinguisher. It can be seen from figure 5 and figure 6 that this has been achieved and that the equations governing single-phase compressible flow have been implemented.

The model uses a combination of standard derivations of the Navier-Stokes equation to model the pipe flow and orifice discharge. The equation governing adiabatic flow along a pipe is

$$\int \frac{dP}{V} + G^2 \left[ \ln \left( \frac{V_2}{V_1} \right) + \frac{2fL}{d} \right] = 0 \quad (2)$$

Where P is pressure, V is specific volume, G is mass flux, f is the fanning friction factor (assume  $f=0.005$  for this type of flow), L is the pipe length and d is the internal diameter of the pipe. There is a similar equation for isothermal flow.

<sup>1</sup> Handbook of Powder Technology (Vol 2) "Fundamentals of Gas-Particle Flow". G Rudinger, Elsevier 1980

<sup>2</sup> One-dimensional Two-phase Flow. G B Wallis, McGraw-Hill Book Company 1969

For sonic flow:-

$$M = A \sqrt{P_H \rho_H k \left( \frac{2}{k+1} \right)^{\frac{(k+1)}{(k-1)}}} = \text{shapiro eqn (choked flow)} = A \sqrt{\frac{k}{k-1} \left( \frac{2}{k+1} \right)^{\frac{k+1}{k-1}} \frac{P}{T_0}} \quad (4)$$

Where  $A$  is the orifice cross-sectional area,  $M$  is the mass flow rate,  $k$  is the specific heat ratio,  $\rho_H$  is the density of the higher pressure gas,  $P_H$  is the higher pressure and  $P_1$  is the lower pressure. The model automatically switches equations depending on the pressure.

Unfortunately, I have not found any equations that describe isothermal flow through an orifice. The reason that the isothermal equations are required is that the powder provides a large heat reservoir, ensuring that all flows are isothermal. It is therefore my intention to re-derive or modify these equations if required.

Another important factor will be the "minor losses" within the system. These losses include entrance and exit pressure losses for bends, valves and fittings within the extinguisher. These losses, although known as "minor losses", can in fact represent the major loss contributions in systems with high pressure differentials and short pipe lengths. They are generally modelled as

$$\Delta P = C \cdot v^2 \quad (5)$$

Where  $\Delta P$  is the pressure loss,  $C$  is an experimentally determined constant and  $v$  is the fluid velocity.

The value of  $C$  is the only fitting parameter within the model. In order to optimise the accuracy of this constant, the losses are broken down into values for the dip tube,  $C_{DT}$ , the head,  $C_H$ , and the hose,  $C_{Hose}$ . These values can be established experimentally by measuring the pressure decay after each section has been added. The model can then be used to fit these results and the effect of each section can be determined. The values of  $C_{DT}$ ,  $C_H$ , and  $C_{Hose}$  can then be used to calculate the losses for the whole system.

It can be seen from figures 5 and 6 that these equations give acceptable results when used in conjunction with a quasi steady state approach. At present, there are no results for the powder discharge. This is because effects that are negligible for a gas discharge must be considered for a powder-gas mixture. The main terms that need to

<sup>3</sup> Fluid Mechanics with Engineering Application. R.L. Daugherty, J.B. Franzini, E.J. Finnemore McGraw-Hill Book Company. 1989 (SI Metric Edition.) P.274-275.

In the case of adiabatic flow through an orifice, the following equations can be used<sup>3</sup>.

For subsonic flow:-

$$M = A \sqrt{2 \rho_H P_H \frac{k}{k-1} \left[ \left( \frac{P_1}{P_H} \right)^{\frac{2}{k}} - \left( \frac{P_1}{P_H} \right)^{\frac{(k+1)}{k}} \right]} \quad (3)$$

## 11.0 Bibliography.

**Abrahamson (1977)** – Abrahamson, J., “Collision rates of small particles in a vigorously turbulent fluid,” *Chem. Engng Sci*, **30**, 1975, pp. 1371-1379. Referenced in **Williams & Crane (1983)**.

**Abramovich (1971)** – Abramovich, G. N., “The Effect of Admixture of Solid Particles or Droplets on the Structure of a Turbulent Gas Jet,” *Int. J Heat and Mass Transfer*, Vol. 14, 1971, p. 1039. Referenced in **Choi & Chung (1983)**.

**Acton (1970)** – Acton, Forman S., *Numerical Methods That Work*, 1970, NYC, Harper & Row.

**Ahmadi & Ma (1990a)** - Ahmadi, G., Ma, D., “A Thermodynamical Formulation for Dispersed Multiphase Turbulent Flows - I,” *International Journal of Multiphase Flows*, 1990, Vol. 16, No. 2, pp. 323-340.

**Ahmadi & Ma (1990b)** - Ahmadi, G., Ma, D., “A Thermodynamical Formulation for Dispersed Multiphase Turbulent Flows - II,” *International Journal of Multiphase Flow*, 1990, Vol. 16, No. 2, pp. 341-351.

**Ansul (1995)** - Ansul Corporation, *Ind-X Industrial Fire Suppression System - Installation, Operation, Recharge, Inspection, and Maintenance Manual*, August 1, 1995, UL EX 1727.

**Arnold et al (1990)** - Arnold, G. S., Drew, D. A., Lahey, Jr., R. T., “An Assessment of Multiphase Flow Models Using the Second Law of Thermodynamics,” *International Journal of Multiphase Flow*, 1990, Vol. 16, No. 3, pp. 481-494.

**Babcock & Wilcox** - Babcock & Wilcox Co. (USA), *Reports B.A.W.* 1159, 1181, 1194, 1201, and 1207, Babcock and Wilcox Co., NYC. Referred to in **Boothroyd (1966)**.

**Barth (1962)** – Barth, W., “Flow Problems with Mixtures of Gaseous and Entrained Solid Particles,” *Engr. Digest*, Vol. 23, 1962, p. 81. Referenced in **Choi & Chung (1983)**.

**Bird et al** - Bird, Edward B., Giesecke, Hans D., Hillaert, John A., Friderichs, Tom J., Sheinson, Ronald S., *Development of a Computer Model to Predict the Transient Discharge Characteristics of Halon Alternatives*, MPR Associates, Inc/Naval Research Laboratory.

**Boothroyd (1966)** - Boothroyd, R. G., “Pressure Drop in Duct Flow of Gaseous Suspensions of Fine Particles,” *Trans. Instn Chem. Engrs*, Vol. 44, 1966, pp. T306-T313.

**Boothroyd (1969)** - Boothroyd, R. G., “Similarity in Gas-Borne Flowing Particulate Suspensions,” *Journal of Engineering for Industry*, May, 1969, pp. 303-314.

**Cao & Ahmadi (1995)** - Cao, J., Ahmadi, G., “Gas-Particle Two-Phase Turbulent Flow in a Vertical Duct,” *International Journal of Multiphase Flow*, Vol. 21, No. 6, pp. 1203-1228.

**Chenoweth & Paolucci (1990)** - Chenoweth, D. R., Paolucci, S., "Compressible Flow of a Two-Phase Fluid Between Finite Vessels - I," 1990, *International Journal of Multiphase Flow*, Vol. 16, No. 6, pp. 1047-1069.

**Choi & Chung (1983)** - Choi, Y. D., Chung, M. K., “Analysis of Turbulent Gas-Solid Suspension Flow in a Pipe,” *Journal of Fluids Engineering*, September 1983, Vol. 105, pp. 329-334.

- Cholin (1969)** - Cholin, Roger, "The Development of the Safety First Automatic System," *Fire Journal*, September 1969, pp. 14-19.
- Chung et al (1986)** - Chung, M. K., Sung, H. J., Lee, K. B., "Computational Study of a Turbulent Gas-Particle Flow in a Venturi," *Journal of Fluids Engineering*, June 1986, Vol. 108, pp. 248-253.
- Crowe et al (1977)** - Crowe, C. T., Sharma, M. P., Stock, D. E., "The Particle-Source-in-Cell Method for Gas Droplet Flow," *Journal of Fluids Engineering*, 1977, Vol. 99, pp. 325-332.
- Depew (1960)** - Depew, C. A., "Heat Transfer to Flowing Gas-Solids Mixtures in a Vertical Circular Duct," Ph.D. Thesis, 1960, University of California, Berkeley, USA.. Referenced in **Ozbelge (1983)**.
- Doss (1985)** - Doss, Ezzat D., "Analysis and Application of Solid-Gas Flow Inside a Venturi With Particle Interaction," *International Journal of Multiphase Flow*, 1985, Vol. 11, No. 4, pp. 445-458.
- Doss & Srinivasan (1986)** - Doss, E. D., Srinivasan, M. G., "Modeling of Wall Friction for Multispecies Solid-Gas Flows," *Journal of Fluids Engineering*, December 1986, Vol. 108, pp. 486-488.
- Drew (1971)** - Drew, D. A., "Averaged Field Equations for Two-Phase Flow," *Studies in Applied Mechanics*, June 1971, Vol. L, No. 2. Referenced in **Sharma & Crowe (1978)**.
- Durst et al (1984)** - Durst, F., Milojevic, D., Schönung, B., "Eulerian and Lagrangian Predictions of Particulate Two-Phase Flows: A Numerical Study," *Applied Mathematical Modeling*, April 1984, Vol. 8, pp. 101-115.
- Eckel (1989)** - Eckel, Bruce, *Using C++*. 1989, NYC, Osborne McGraw-Hill.



**Elghobashi & Abou-Arab (1983)** – Elghobashi, S. E., Abou-Arab, T. W., “A Two-Equation Turbulence Model for Two-Phase Flows,” *Phys. Of Fluids*, Vol. 26, April 1983, pp. 931-938. Referenced in **Chung et al (1986)**.

**Emanuel (1986)** – Emanuel, George, *Gasdynamics: Theory and Application*, 1986, NYC, American Institute of Aeronautics and Astronautics, Inc.

**Ewing et al (1989)** - Ewing, Curtis T., Faith, Francis R., Hughes, J. Thomas, Cathart, Homer W., “Flame Extinguishment Properties of Dry Chemicals: Extinction Concentrations for Small Diffusion Pan Fires,” *Fire Technology*, May 1989, Vol. 25, No. 2, pp. 134-149.

**Ewing et al (1992)** - Ewing, Curtis T., Faith, Francis R., Romans, James B., Hughes, J. Thomas, “Flame Extinguishment Properties of Dry Chemicals: Extinction Weights for Small Diffusion Pan Fires and Additional Evidence for Flame Extinguishment by Thermal Mechanisms,” *J. of Fire Prot. Engr.*, 4 (2), 1992, pp. 35-52.

**Ewing et al (1994)** - Ewing, Curtis T., Beyler, Craig L., Cathart, Homer W., “Extinguishment of Class B Flames by Thermal Mechanisms; Principles Underlying a Comprehensive Theory; Prediction of Flame Extinguishing Effectiveness,” *J. of Fire Prot. Engr.*, 6 (1), 1994, pp. 23-54.

**Ewing et al (1995)** - Ewing, Curtis T., Faith, Francis R., Romans, James B., Siegmann, Charles W., Ouellete, Ralph J., Hughes, J. Thomas, Cathart, Homer W., “Extinguishing Class B Fires with Dry Chemicals: Scaling Studies,” 1995, *Fire Technology*, First Quarter 1995, Vol. 31, No. 1, pp. 17-43.

**Fan & Zhu (1998)** – Fan, Liang-Shih, Zhu, Chao, *Principles of Gas-Solid Flows*, 1998, NYC, Cambridge University Press.

- Farber (1953)** – Farber, L., “The Venturi as a Meter for Gas-Solids Mixtures,” *Trans. ASME*, July 1953, pp. 943-951. Referenced in **Chung *et al* (1986)**.
- Forssell *et al* (1995)** - Forssell, Eric W., DiNenno, Philip J., *Discharge Flow Model for Gaseous Total Flooding Fire Protection Systems - Users Guide (DRAFT)*, March 1995, Hughes Associates, Inc., Columbia, MD.
- Hairu & Molstad (1949)** - Hairu, O. H., Molstad, M. C., “Pressure Drop in Vertical Tubes in Transport of Solids by Gases,” *Ind. Engng. Chem.*, 1949, **41**, pp. 1148-1160. Referenced in **Ozbelge (1983)**.
- Hamins (1998)** – Hamins, Anthony, “Flame Extinction by Sodium Bicarbonate Powder in a Cup Burner,” *Twenty-Seventh Symposium (International) on Combustion*, The Combustion Institute, 1998, pp. 2857-2864.
- Han *et al* (1991)** - Han, K. S., Chung, M. K., Sung, H. J., “Application of Lumley’s Drag Reduction Model to Two-Phase Gas-Particle Flow in a Pipe,” *Journal of Fluids Engineering*, March 1991, Vol. 113, pp. 130-136.
- Hawes *et al* (1964)** - Hawes, R. I., Holland, E., Kirby, G. T., Wallar, P. R., *AEW-R244/1964*. (Winfrith: Atomic Energy Research Establishment). Referred to in **Boothroyd (1966)**.
- Heinrich (1942)** - Heinrich, G., "Über strömungen von schäumen", 1942, *Z. angew. Math. Mech.*, **22**, pp. 117-118. Referenced in **Chenoweth & Paolucci (1990)**.
- Hestroni (1989)** - Hestroni, G., “Particles-Turbulence Interaction,” *International Journal of Multiphase Flow*, 1989, Vol. 15, No. 5, pp. 735-746.

**Hishida et al (1992)** - Hishida, K., Ando, A., Maeda, M., “Experiments on Particle Dispersion in a Turbulent Mixing Layer,” *International Journal of Multiphase Flow*, 1992, Vol. 18, No. 2, pp. 181-194.

**Hughes & Brighton (1991)** – Hughes, William F., Brighton, John A., *Theory and Problems of Fluid Dynamics* (2<sup>nd</sup> Edition), 1991, NYC, McGraw-Hill.

**Ito (1960)** – Ito, H., “Pressure losses in smooth pipe bends,” *Trans. Am. Soc. Mech. Engrs (J. Bas. Engng)* **82D**, pp. 131-143. Referenced in **Morikawa et al (1978a)**.

**John & Haberman (1988)** – John, James E. A., Haberman, William L., *Introduction to Fluid Mechanics* (Third Edition),” 1988, Englewood Cliffs, NJ, Prentice-Hall, Inc..

**Julian & Dukler (1965)** – Julian, F. M., Dukler, A. E., “An Eddy Viscosity Model for Friction in Gas-Solids Flow,” *AIChE Journal*, Vol. 11, No. 5, Sept. 1965, pp. 853-858. Referenced in **Doss & Srinivasan (1986)**.

**Kidde-Fenwal (1994)** - Kidde-Fenwal, Inc., *Industrial Dry Chemical Fire Suppression System - Installation, Operation, and Maintenance Manual*, November, 1994, P/N 220423, UL EX-2153.

**Lee & Crowe (1982)** – Lee, J., Crowe, C. T., “Scaling Laws for Metering the Flow of Gas-Particle Suspensions through Venturis,” *ASME Journal of Fluids Engineering*, Vol. 104, Mar. 1982, pp. 88-91. Referenced in **Chung et al (1986)**.

**Lempp (1966)** – Lempp, M., “Die Strömungsverhältnisse von Gas-Feststoff-Gemischen,” *Verzweigungen pneumatischer Förderanlagen. Aufbereitungs-Techn.* **7**, pp. 81-91. Referenced in **Morikawa et al (1978b)**.

**Lumley (1976)** - Lumley, J. L., *Topics in Applied Physics*, Vol. 12, *Turbulence*, Edited by Bradshaw, P., Springer-Verlag, Berlin, Heidelberg, and New York, pp. 289-324.

Reference in **Han et al (1991)**.

**Maeda & Ikai (1976)** – Maeda, M., Iaki, S., “Distributions of solid particles transported by air in branched lines,” *Chem. Engng. Ronbunshu* **2**, pp. 25-30 (in Japanese).

Referenced in **Morikawa et al (1978b)**.

**Marble (1970)** – Marble, F. E., “Dynamics of dusty gases,” *A. Rev. Fluid Mech.* **2**, 1970, pp. 397-446. Referenced in **Chenoweth & Paolucci (1990)**.

**Melville & Bray (1979)** - Melville, W. K., Bray, K. N., “A Model of the Two-Phase Turbulent Jet,” *Journal of Heat and Mass Transfer*, 1979, Vol. 22, pp. 647-656.

**Michaelides (1984)** - Michaelides, Efstathios E., “A Model for the Flow of Solid Particles in Gases,” *International Journal of Multiphase Flow*, 1984, Vol. 10, No. 1, pp. 61-77.

**Miller & Gidaspow (1992)** - Miller, A., Gidaspow, D., “Dense, Vertical Gas-Solid Flow in a Pipe,” *AIChE Journal*, 1992, 38, pp. 1801-1815.

**Morikawa et al (1978a)** - Morikawa, Y., Tsuji, T., Matsui, K., Jittani, Y., “Pressure Drops Due To Pipe Bends in Air-Solids Two-Phase Flows, Circular and Elliptical Bends,” *International Journal of Multiphase Flow*, 1978, Vol. 4, pp. 575-583.

**Morikawa et al (1978b)** - Morikawa, Y., Kondo, T., Hiramoto, T., “Pressure Drops and Solids Distribution of Air-Solids Mixture in Horizontal Unsymmetric Branches,” *International Journal of Multiphase Flow*, 1978, Vol. 4, pp. 397-404.

**NFPA 10 (1998)** - NFPA 10, *Standard for Portable Fire Extinguishers*, 1998, National Fire Protection Association, Quincy, MA.

**NFPA 17 (1998)** - NFPA 17, *Standard for Dry Chemical Fire Extinguishing Systems*, 1998, National Fire Protection Association, Quincy, MA.

**NI (1998a)** – “LabView™ User Manual,” 1998, National Instruments Corporation, Austin, TX.

**NI (1998b)** – “LabView™ Function and VI Reference Manual,” 1998, National Instruments Corporation, Austin, TX.

**Özbelge (1983)** - Özbelge, Tülay A., “An Algorithm for Hydrodynamics of Turbulent Upward Flowing Dilute Gas-Solids Suspensions,” *International Journal of Multiphase Flow*, 1983, Vol. 7, pp. 437-446.

**Özbelge & Somer (1982)** - Özbelge, T. A., Somer, T. G., “Heat Transfer to Gas-Solid Suspensions Flowing Turbulently in a Vertical Pipe,” *Proc. 16th Southeastern Seminar on Thermal Sciences*, 1982, Ann Arbor, Michigan, USA. Referenced in Hairu & Molstad (1949).

**Paolucci (1985)** - Paolucci, S., "Heat Transfer During the Early Expansion of Gas in Pressurized Vessels," 1985, *International Journal of Heat and Mass Transfer*, Vol. 28, No. 8, pp. 1525-1537.

**Patankar & Spalding (1967)** - Patankar, S. V., Spalding, D.B., *Heat and Mass Transfer in Boundary Layers*, Int. Ed., Intertext Books, London, 1967. Referenced in **Chung et al (1986)**.

**Pfeffer et al (1966)** - Pfeffer, R., Rosetti, S., Lieblein, S., *Analysis and Correlation of Heat-Transfer Coefficient and Friction Factor Data for Dilute Gas-Solid Suspensions*, 1966, NASA Technical Note, NASA TN D-3603.

**Roberson & Crowe (1993)** - Roberson, John A., Crowe, Clayton T., *Engineering Fluid Mechanics* (5th Edition), 1993, Boston, MA, Houghton Mifflin Company.

**Rose & Barnach (1957)** – Rose, H. E., Barnach, E., “Flow of Suspensions of Non-Cohesive Spherical Particles in Pipes,” *Engineer*, June 14 – pp. 880-901, June 21 – pp. 939-941, 1957.

**Ross (1964)** – Ross, Shepley L., *Differential Equations*; 1964, Waltham, MA, Ginn & Company.

**Ruck & Makiola (1989)** - Ruck, B., Makiola, B., “Particle Dispersion in a Single-Sided Backward-Facing Step Flow,” *International Journal of Multiphase Flow*, 14, pp. 787-800.

**Rudinger (1965)** – Rudinger, George, “Some Effects of Finite Particle Volume on the Dynamics of Gas-Particle Mixtures,” *AIAA Journal*, 1965, Vol. 3, No. 7, pp. 1217-1222.

**Sabersky et al (1971)** - Sabersky, Rolf. H., Acosta, Allan J., Hauptmann, Edward G., *Fluid Flow: A First Course in Fluid Mechanics* (2nd Edition), 1971, NYC, Macmillian Company.

**Saffman & Turner (1956)** – Saffman, P. G., Turner, J. S., “On the collision of drops in turbulent clouds,” *J. Fluid Mech.*, **1**, 1956, pp. 16-30. Referenced in **Williams & Crane (1983)**.

**Schuchart (1968)** – Schuchart, P., “Widerstandsgesetze beim pneumatischen Transport in Rohrkrümmern,” *Chemie-Ing.-Tech.*, **40**(21/22), 1968, pp. 1060-1067. Referenced in **Morikawa et al (1978a)**.

- Schumacher (1994)** – Schumacher, Dale (Ed.), *Software Solutions in C*, 1994, NYC, Academic Press, Inc.
- SFPE (1995)** – Society of Fire Protection Engineers, *SFPE Handbook of Fire Protection Engineering* (2<sup>nd</sup> Ed.), 1995, Society of Fire Protection Engineers, Quincy, MA & National Fire Protection Association, Boston, MA.
- Shames (1992)** – Shames, Irving H., *Mechanics of Fluids* (3<sup>rd</sup> Edition), 1992, NYC, McGraw-Hill.
- Shammas (1995)** – Shammas, Namir Clement, *C/C++ Mathematical Algorithms for Scientists and Engineers*, 1995, NYC, McGraw Hill.
- Sharma & Crowe (1978)** - Sharma, M. P., Crowe, C. T. “A Novel Physico-Computational Model for Quasi One-Dimensional Gas-Particle Flows,” *Journal of Fluids Engineering*, September 1978, Vol. 100, pp. 343-349.
- Sheinson (1996)** - Sheinson, Ron, Private conversation with Professor R. Zalosh, November, 1996.
- Soo (1989)** - Soo. S. L., *Particulates and Continuum: Multiphase Fluid Dynamics*, 1989, NYC, Hemisphere Publishing Corporation.
- Streeter & Wylie (1985)** – Streeter, Victor L., Wylie, E. Benjamin, *Fluid Mechanics* (8<sup>th</sup> Edition), 1985, NYC, McGraw-Hill.
- Swan (1992)** - Swan, Tom, *Mastering Borland C++*, 1992, Carmel, Indiana, Sams Publishing.
- Tangren et al (1949)** - Tangren, R. F., Dodge, C. H., Seifert, H. S., "Compressibility effects in two-phase flow," 1949, *J. appl. Phys.*, **20**, pp. 637-645.

**Tanenbaum & Augenstein (1986)** – Tanenbaum, Aaron M., Augenstein, Moshe J., *Data Structures Using PASCAL* (2<sup>nd</sup> edition), 1986, Englewood Cliffs, NJ, Prentice-Hall, Inc..

**Tsuji & Morikawa (1982)** – Tsuji, Y., Morikawa, Y., “LDV measurements of an air-solid two-phase flow in a horizontal pipe,” 1982, *J. Fluid Mech.*, **120**, pp. 385-409.

Referenced in **Hestroni (1989)**.

**Tsuji & Shiomi (1984)** – Tsuji, Y., Shiomi, H., “LDV measurements of an air-solid two-phase flow in a vertical pipe,” 1984, *J. Fluid Mech.*, **139**, pp. 417-434. Referenced in **Hestroni (1989)**.

**Tsuji et al (1989)** - Tsuji, Y., Shen, N., Morikawa, Y., “Numerical Simulation of Gas-Solid Flows Part 1 - Particle-to-Wall Collisions,” *Technol. Rep. Osaka Univ. Jap.*, 39, pp. 233-241. Referenced in **Cao & Ahmadi (1995)**.

**UL (1999)** - *Fire Protection Equipment Directory* , 1999, Underwriters Laboratories, Inc., Northbrook, IL.

**UL 299 (2000)** - UL 299, *UL Standard for Dry Chemical Fire Extinguishers*, 2000, Underwriters Laboratories, Inc., Northbrook, IL.

**UL 711 (2000)** - UL 711, *UL Standard for Rating and Testing of Fire Extinguishers*, 2000, Underwriters Laboratories, Inc., Northbrook, IL.

**UL 1254 (1999)** - UL 1254, *UL Standard for Pre-Engineered Dry Chemical Extinguishing System Units*, 1999, Underwriters Laboratories, Inc., Northbrook, IL.

**Ural (1989)** - Ural, Erdem A., "Experimental Measurement of the aerodynamic Entrainability of Dust Deposits", Factory Mutual Research Corporation, Norwood, MA, Presented at the *12th International Colloquium on Dynamics of Explosions and Reactive Systems*, Ann Arbor Michigan, July 24-28, 1989.



**Van Zandt (1994)** – Van Zandt, James R., “Root Finding,” 1994, NYC, Academic Press, Inc. Chapter 16 of **Schumacher (1994)**.

**Williams & Crane (1983)** - Williams, J. J., Crane, R. I., “Particle Collision Rate in Turbulent Flow,” *International Journal of Multiphase Flow*, 1983, Vol. 9, No. 4, pp. 421-435.